Expanding the scope of Next Generation Maleimides for Antibody Conjugation

Yanbo Zhao

A thesis submitted in partial fulfilment of the requirements for the degree of Doctor of Philosophy

Supervisor: Prof. James R. Baker

July 2023

Declaration

I, Yanbo Zhao, confirm that the work presented in this thesis is my own. Where information has been derived from other sources, I confirm that this has been indicated in the thesis.

Yanbo Zhao

April 2023

Abstract

Antibody drug conjugates (ADCs) are increasingly promising targeted therapies for cancer treatments, due to the combination of antibodies with tumour selectivity and cytotoxic drugs. Current strategies to construct ADCs suffer from heterogeneity, complexity, and high costs. Dibromomaleimides (DBMs), a class of next generation maleimides (NGMs), have shown ability to site-selectively bridge antibody disulfide bonds, delivering robustly stable conjugates following maleimide hydrolysis. This work expands DBM scope by developing trifunctional DBMs built around a lysine core, introducing multiple functionalities (such as fluorophores) onto an antibody, which would be of significant interest for treatments of complex diseases.

However, a problem associated with DBM-based disulfide bridging arises as disulfide scrambling where incorrectly bridged disulfides observed in antibody hinge region, thus forming two antibody isomers with limited homogeneity. To resolve this issue, *in situ* NGM-based bioconjugation has been conducted to enable simultaneous disulfide reduction and bridging. A variety of dithiomaleimides (DTMs) has been explored to attempt to minimise cross-reactivity to TCEP, a typical disulfide reducing agent. Compared to highly reactive DBMs, these DTMs have attenuated reactivity, and thus can be applied during the reduction. Upon disulfide reduction, the presence of these DTMs enables an efficient bridging and leads to a reduction in scrambled disulfide bonds compared to conventional DBM-based bioconjugation. However, the resultant conjugates also involve mis-bridged antibody species, therefore, NGM-based *in situ* bioconjugation still needs optimisation.

Lastly, investigations on benzeneselenols as novel antibody reducing agents have been conducted. Traditional benzeneselenols show good reducing ability but suffer from the poor aqueous solubility and malodour. A new generation of benzeneselenols with improved bioconjugation properties have been developed, through the synthesis of substituted aryl derivatives with improved solubility for better compatibility with biological conditions.

Overall, this work expands the scope of DBMs and explores methods to generate more homogeneous antibody conjugates using DBMs and related reagents.

Impact statement

Cancer is one of the biggest challenges in clinical research, and is responsible for many deaths worldwide, leading to a significant loss in the quality of life too. Cancer tumours can also be heterogeneous, which makes cancer treatments more complex. Chemotherapy and radiotherapy are two front-line treatments, where the former uses potent cytotoxic drugs, and the latter uses high-energy X-rays. However, both approaches do not sufficiently discriminate cancer cells from healthy cells, resulting in off-site toxicities and side-effects. To selectively kill cancer cells, targeted drug delivery is of increasing importance and interest.

Antibody drug conjugates (ADCs), as a class of targeted therapy, consist of the monoclonal antibody, chemical linker, and anti-cancer drug. By specifically binding to target antigens *via* the antibody moiety, ADCs can undergo cell internalisation to release drugs specifically to cancer cells. To build the ADC, the chemical linker plays a key role in conjugating the cytotoxic payload to the antibody. Dibromomaleimides (DBMs) have been developed as a promising reagent class for disulfide bridging that can deliver robust site-specific antibody conjugation, maintaining the integrity of antibody structure.

However, most of the current ADC linker technologies have limited scope that they only attach one moiety to the antibody. The first aim of this project was to expand the scope of DBM reagents by developing trifunctional DBM linkers derived from a lysine scaffold. These trifunctional reagents involve two clickable handles that enable the incorporation of two different functionalities to the antibody. The resultant dual-modality antibody conjugates have promising applications in cancer treatments, such as traceable targeted therapy or drug-resistant cancer therapy.

Furthermore, the homogeneity of ADCs critically impacts their therapeutic efficacy, and many antibody modification techniques generate heterogeneous products. Disulfide bridging aims to overcome this by delivering site-specific modification, however, disulfide scrambling is possible to occur in antibody hinge region, forming 'half-antibody' conjugates. The second aim of this project was to optimise disulfide bridging by exploring novel reducing agents and DBM-related bridging reagents that can be applied in *in situ* antibody bioconjugation. The optimised *in situ* disulfide bridging could potentially generate antibody conjugates with enhanced homogeneity, providing more opportunities for the development of ADCs.

For my mum and dad

给我最爱的爸爸妈妈

Acknowledgements

First of all, I would like to thank Prof. Jamie Baker for being a wonderful supervisor, who is always happy to help, patient and supportive. Jamie and his enthusiasm for research encouraged me all the time during the past few years. No matter how many failed experiments I met, Jamie was always positive and calm, guiding me towards next steps. I also appreciate Jamie's sense of humour as his jokes provided more entertainment for all of us. I would also like to thank Prof. Vijay Chudasama for being my secondary supervisor, who always brings up valuable ideas for my project and warm conversations in life. I'm proud that we are both from Slytherin!

Thanks to Dr Abil Aliev for providing the NMR support, Dr Kersti Karu for helping me with the MS, and Prof. Tom Sheppard for his guidance in organic chemistry. I am also grateful to Dr Jon Wilden for conducting my first year and upgrade viva examinations, Prof. Alethea Tabor and Prof. David Spring, for taking the time to read my thesis and carry out my PhD viva examination.

KLB is the best lab ever, my PhD could not be so enjoyable without being surrounded by the greatest people. I would like to thank Nafsika, Archie, Roshni, Lula, Alina, Muhammed, Mikesh and Charlie in Baker's group; Antoine, Andre, Calise, Peter, Marcos, Richard, Faiza, Steven, Fabien, Alex, Nehaal, Lea, Ioanna, Chapman, Cliona and Toby in Chudasama's group; Dave, Rachel, Matt, Sahra, Richard, Usman, Phyllida and Will in Sheppard's group.

Alina, my dearest Dr Chrzastek, as well as the funniest girl, thanks for guiding me in both work and life, sharing all the stories with me and cracking the best jokes. When people were pranking me, you always stayed on my side by sneakily helping me and telling me all the truth. I would still chuckle if I thought about your reaction when I first told you to be nice! I love the way that we can always go crazy together when we shared that sour orange in Barcelona, when we hiked on that mountain without taking the train. I always miss the days when I came in, and you were there ready to gossip with me, all the golden memories!

Muhammed, the most handsome and meanest boy, thanks for listening to all my rants, proofreading my writing, calling me granny, and cleaning my laptop screen all the time. Even though you mocked me running like a duck, told me to shut up 10 times per day, and put my

pictures everywhere in the lab, I know you still see me as your best friend, so do I. I'm glad to have you around during these years, I will miss this halal boy very much in the future.

Siyao, my 'spinach' girl, thanks for always patiently listening to me, emotionally supporting me, sharing your life with me, and being the greatest friend ever. It was my best luck to know you since my first year of PhD, I will always miss every moment we spent together. Your happiness is always my biggest wish.

Mikesh, the smartest boy, my lab brother, little Miki, I love your sense of humour so much! Even though you never appreciated my jokes, singing <Attention> and playing kpop songs - all your loss. I still cherish every moment staying together with you. I always find work more entertaining because of your company, I will miss our coffee breaks and taking selfies together.

Roshni, RMfH, Roshini Mouldy, my sweetest young lady, thanks for helping me with work, thanks for all the sweet messages, thanks for coming into my life and being my bestie! You were one of the people who talked to me every day with all the patience at the beginning. When I met problems, you were always the first one that I wanted to ask since you could explain everything so clearly. It was amazing to have you around me especially when I was so stressed, but until I saw you, I felt relaxed.

Lula, as known as Luigia, the coolest kitty girl, thanks for taking care of me at the very beginning, thanks for supporting me all over these years, thanks for always being patient and sweet. I was stressed when I just started lab work, it was you and your big smile that comforted me every single day.

Charlie, the cutest boy, the baby Baker, who spotted me on World ADC website. Thanks for listening to my nonsense talking, thanks for teaching me London slangs, thanks for sharing your life and gossips with me.

Nafsika, my dear Dr Forte, thanks for showing me everything in details especially bioconjugation - I would not be able to learn so quicky without you. Thanks for always being helpful in research and bringing up all the good ideas.

Archie, who finished his four-year PhD but still has a shocking amount of hair! Thanks for cheering me up when I met problems, thanks for helping me a lot with work. Your jokes used to make me chuckle a lot, I miss them!

问渠那得清如许，为有源头活水来   *--朱熹*

路漫漫其修远兮，吾将上下而求索   *--屈原*

Table of Contents

Abbreviations

ADC	Antibody drug conjugate
ADPN	Arylenedipropiolonitrile
AF488	Azide-Fluor 488
Ala	Alanine
aq.	Aqueous
BBS	Borate buffered saline
BCN	Bicyclononyne
BCN-Fluor	5-carboxyfluorescein-PEG_3-bicyclononyne
BME	β-mercaptoethanol
Boc	Tert-butoxycarbonyl
bsAbs	Bispecific antibodies
CDC	Complement-dependent cytotoxicity
CDRs	Complementary-determining regions
CEA	Carcinoembryonic antigen
C_H	Constant domain of heavy chain
C_L	Constant domain of light chain
CLT	Cysteine-to-lysine transfer
COSY	Correlated spectroscopy
CuAAC	Copper-catalysed azide-alkyne cycloaddition
Cy5.5-azide	Sulfo-Cy5.5-azide
DAR	Drug-to-antibody ratio
DBM	Dibromomaleimide
DCM	Dichloromethane
DEP	Diethynyl phosphinate

DEPT	Distortionless enhancement by polarization transfer
DFO	Desferrioxamine B
DIPEA	*N,N*-Diisopropylethylamine
diBrPD	Dibromopyridazinedione
DIM	Diiodomaleimide
DMAP	4-Dimethylaminopyridine
DMF	*N,N*-Dimethylformamide
DMSO	Dimethyl sulfoxide
DNA	Deoxyribonucleic acid
DOX	Doxorubicin
DTM	Dithiomaleimide
DTNB	5,5'-dithio-bis-(2-nitrobenzoic acid)
DTT	Dithiothreitol
DVP	Divinylpyrimidine
DVT	Divinyltriazine
EDC	1-Ethyl-3-(3-dimethylaminopropyl)carbodiimide
EEDQ	2-Ethoxy-1-ethoxycarbonyl-1,2-dihydroquinoline
EDG	Electron-donating group
EDTA	Ethylenediaminetetraacetic acid
EI	Electron ionisation
ELISA	Enzyme-linked immunosorbent assay
eq.	Equivalents
ESI	Electrospray Ionisation
EWG	Electron-withdrawing group
Fab	Antigen-binding fragment

FAR	Fluorophore-to-antibody ratio
Fc	Crystallisable fragment
FcRn	Neonatal Fc receptor
FDA	Food and drug administration
FGE	Formylglycine-generating enzyme
GFP	Green fluorescent protein
Grb2	Growth factor receptor-bound protein 2
GSH	Glutathione
HC	Heavy chain
HER2	Human epidermal growth factor receptor 2
His	Histidine
HIPS	Hydrazino-iso-Pictet-Spengler
HL	Heavy light
HMBC	Heteronuclear multiple bond correlation
HOBt	Hydroxybenzotrazole
HPLC	High-performance liquid chromatography
HRMS	High resolution mass spectrometry
HRP	Horseradish peroxidase
HSA	Human serum albumin
HSQC	Heteronuclear single quantum coherence
IC_{50}	Half-maximal inhibitory concentration
IEDDA	Inverse electron-demand Diels-Alder cycloaddition
Ig	Immunoglobulin
IR	Infrared
LC	Light chain

LC-MS	Liquid chromatography-mass spectrometry
LC-MS/MS	Liquid chromatography tandem mass spectrometry
LRMS	Low resolution mass spectrometry
Lys	Lysine
mAb	Monoclonal antibody
MALDI-TOF	Matrix assisted laser desorption ionisation-time of flight mass spectrometry
MBM	Monobromomaleimide
MESNa	2-Mercaptoethanesulfonate sodium salt
MMAE	Monomethyl auristatin E
MMAF	Monomethyl auristatin F
mp	Melting Point
MPAA	4-Mercaptophenylacetic acid
MS	Mass spectrometry
MTM	Monothiomaleimide
MW	Molecular weight
MWCO	Molecular weight cut-off
m/z	Mass-to-charge ratio
NCL	Native chemical ligation
NGM	Next generation maleimide
NHS	N-hydroxysuccinimide
NMR	Nuclear magnetic resonance
NOESY	Nuclear overhauser effect spectroscopy
QTOF	Quadrupole time-of-flight
PABC	*para*-aminobenzyl carbamate
PB	Phosphate buffer

PBS	Phosphate buffer saline
PBD	Pyrrolobenzodiazepine
PEG	Polyethylene glycol
PET	Positron emission tomography
PD	Pyridazinedione
pKa	Acid dissociation constants
PNGase F	Peptide:*N*-glycosidase F
PROTAC	Proteolysis targeting chimera
RNA	Ribonucleic Acid
Rpm	Revolutions per minute
RS	RNA synthetase
RT	Room Temperature
sat.	Saturated
scFv	Single-chain fragment variable
SDS-PAGE	Sodium dodecyl sulphate-polyacrylamide gel electrophoresis
SMCC	Succinimidyl 4-(*N*-maleimidolmethyl) cyclohexane-1-carboxylate
SPAAC	Strain promoted azide-alkyne cycloaddition
SPIEDDA	Strain-promoted inverse electron demand Diels−Alder cycloaddition
TCEP	Tris(2-carboxyethyl)phosphine
TCO	Trans-cyclooctene
TDC	THIOMAB-drug conjugate
TFA	Trifluoroacetic acid
TG	Transglutaminase
THF	Tetrahydrofuran
THPTA	Tris-hydroxypropyltriazolylmethylamine

TLC	Thin layer chromatography
Tris	Tris(hydroxymethyl)aminomethane
tRNA	Transfer ribonucleic acid
UAA	Unnatural amino acid
UV-Vis	Ultraviolet visible spectroscopy
VC-PABC	Valine-citrulline-p-aminocarbamate
V_H	Variable domain of heavy chain
V_L	Variable domain of light chain

Chapter 1: Introduction

1.1 Antibody

Antibodies, also known as immunoglobulins (Igs), are produced by the immune system to protect the human body from infections *via* selectively and specifically binding to antigens on pathogens. Antibodies are divided into 5 classes: IgM, IgD, IgG, IgE, and IgA. The IgG, commonly applied in therapeutics, is the most abundant class in human serum, accounting for roughly 10-20% of plasma protein.[1] Based on different disulfide bond structures, IgGs are further divided into 4 subclasses: IgG1, IgG2, IgG3 and IgG4, named in order of their abundance in serum. IgG1 is of significant therapeutic interest and widely studied in antibody-based therapies (**Figure 1**).[2,3]
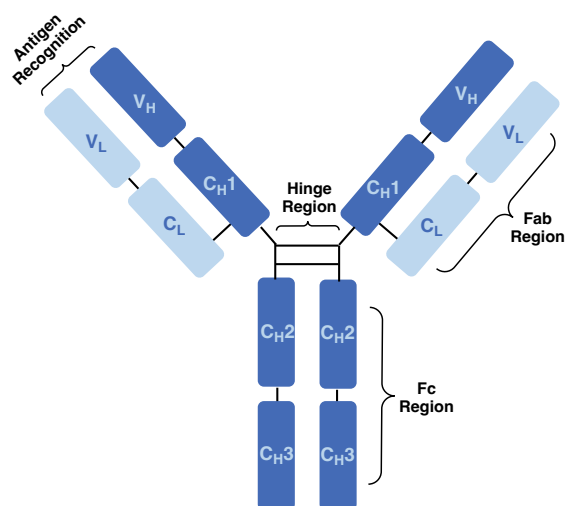
Figure 1– Two-dimensional structure of IgG1.[2]

1.1.1 Antibody structure

The antibody IgG1 (**Figure 1**), a roughly Y-shaped protein, contains two identical heavy chains (HC) and two identical light chains (LC). Each HC is composed of three constant domains (C_H1, C_H2 and C_H3) and one *N*-terminal variable domain (V_H). Each LC is composed of one constant domain (C_L) and one variable domain (V_L).[2] Each LC associates with the V_H and C_H1 domains to form fragment antigen-binding (Fab) region. The V_H and V_L domains, consisting of three hypervariable complementarity-determining regions (CDRs), contribute to two antigen-recognition sites located at each Y arm, whilst the hinge region between C_H1 and C_H2 domains

provides flexibility for antibodies upon antigen binding. The fragment crystallisable (Fc) region, formed by lower hinge region and C_H2/C_H3 domains, bind to Fc receptors and complement proteins by initiating complement-dependent cytotoxicity (CDC). For example, Fc region can prolong serum half-lives of IgG antibodies *via* interaction with the neonatal Fc receptor (FcRn).[4] Furthermore, antibody glycosylation at conserved positions in constant domains is a key regulator of humoral immune activity.[5] For example, there is an *N*-glycosylation site at the conserved *N*297 residue in Fc region, which can restrict protein conformation and tune binding affinity.[6]

1.1.2 Antibody fragments

IgG antibodies bind to antigens through Fab regions and communicate with Fc receptors *via* Fc regions. However, when Fc-mediated effects are unnecessary or undesirable, Fc regions can be removed from antibodies *via* enzymatic proteolysis. For example, the prolonged serum half-life might lead to a poor contrast in imaging applications and the inappropriate release of cytotoxic payloads to some Fc receptor-expressing cells. Upon the removal of Fc, monovalent (Fab, scFv, single variable V_H and V_L domains) and divalent ((Fab')$_2$, diabodies, minibodies) antibody fragments could be further generated (**Figure 2**).[7] Widely used as a model for initial antibody modification, the Fab fragment can be separated from IgGs using pepsin and papain digestion.[8] Fab contains a single disulfide bond and such Fab conjugates are of clinical interest due to the potential for enhanced tumour penetration and tunable half-lives for drug delivery.[9,10,11]
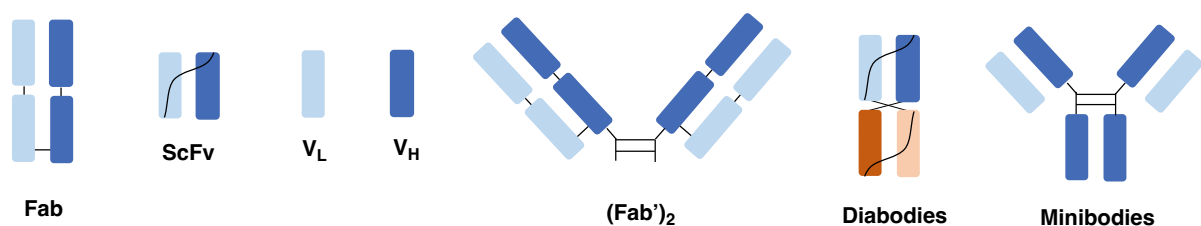
Figure 2 – A variety of antibody fragments.[7]

1.1.3 Antibody application

Cancer is a notorious challenge to human health because of the uncontrollable growth and reproduction of cancer cells, which cannot be easily distinguished by the immune system

from healthy cells. Cancer cells also have the potential to spread from one specific part to other parts of the body, which makes the development of cancer treatments more challenging. Although chemotherapy has been successful in some cases of oncological treatments, it attacks both cancer cells and healthy cells, leading to side-effects such as fatigue, hair loss, nausea and vomiting. Therefore, a concept of targeted therapy was elucidated to give an alternative approach to cancer therapy.[12]

Targeted therapy was first proposed by Paul Ehrlich at the beginning of the 20th century. He postulated that if a compound could selectively target a disease-causing organism, then a toxin could be delivered to the organism selectively.[13,14] Antibodies can be applied as targeted therapy due to their specificity and sensitivity towards antigens. To develop the highly tailored treatment, monoclonal antibodies (mAbs) were produced using hybridomas with monovalent affinity to antigens by Georges Köhler and César Milstein in 1970s.[15] Since then, there has been significant investment and development in antibody technology, leading to over 500 mAbs approved and applied in research study, such as trastuzumab[16] and rituximab[17], both of which have anti-cancer properties. Although mAbs have high specificity and affinity towards specific antigens, they are less stable than small molecules, hence they require relatively high doses for ideal efficacy.[18] To overcome suboptimal therapeutic efficacy and drug resistance, modified mAbs[19] such as antibody drug conjugates (ADCs) were developed.[20]

1.2 Antibody drug conjugates

An ADC is a monoclonal antibody (mAb) equipped with a cytotoxic drug *via* a chemical linker, combining the potency of the drug and the selectivity of an antibody (**Figure 3**).[21] Till December 2021, a total of 11 ADCs: Mylotarg®,[22,23,24,25] Adcetris®,[26,27,28] Kadcyla®,[29,30] Besponsa®,[31,32,33] Polivy™,[31,32,33] Enhertu®,[34,35,36] Padcev™,[37] Trodelvy®,[38,39] Blenrep®,[40,41] Zynlonta™,[42] and Tivdak®[43] have been approved by the US Food and Drug Administration (FDA).[44]
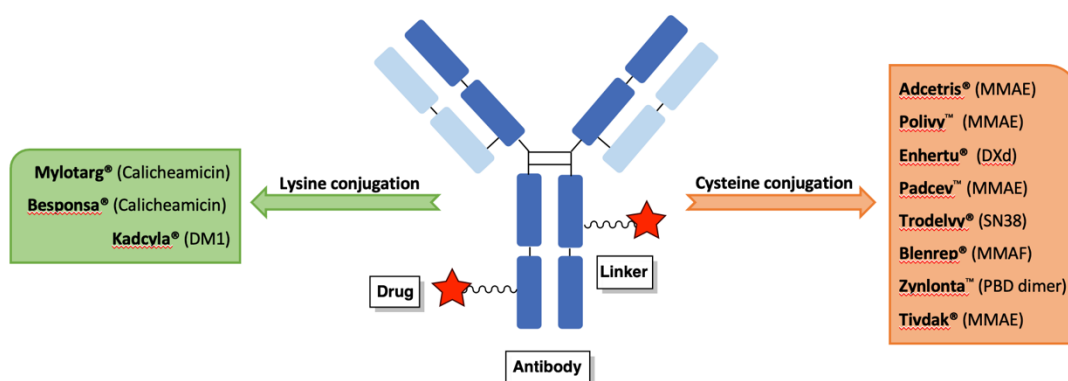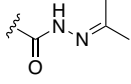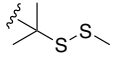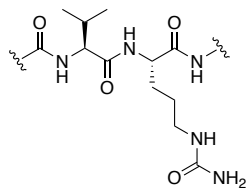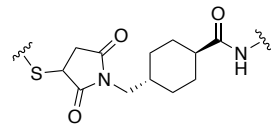
Figure 3 – Approved ADCs (drugs).

1.2.1 Linkers

The linker is crucial in an ADC - it must demonstrate good stability in circulation, as this can prevent premature release of payloads and result in more efficient delivery of payloads to the target site, whilst preventing off-site toxicities. The design of linkers also needs to consider the conjugation site and the number of attachments on the antibody, as drug-to-antibody ratio (DAR) affects drug distribution and pharmacokinetics.[45]

The chemical linkers of ADCs are classified as cleavable and non-cleavable. Cleavable linkers liberate payloads when the *in vivo* environment changes, whilst non-cleavable linkers only release payloads during the lysosomal degradation of ADCs.[46] Cleavable linkers include acid-labile, reducible and enzyme-labile variants. Acid-labile linkers break when pH lowers, reducible linkers decompose when the concentration of reduced glutathione increases, and enzyme-labile variants cleave when in contact with hydrolytic enzymes.[47] The type of cleavable linkers can be designed according to the properties of the targeted tumour microenvironment. Cleavable linkers usually possess plasma stability, however, they may degrade in circulation over time. Whilst non-cleavable linkers often have prolonged half-lives and increased plasma stability, the lysosomal digestion releases payloads with charged amino-acids attached. The charged catabolites are hydrophilic and are confined to the target cell, which would limit the bystander effect. Bystander effect is when the released payloads are hydrophobic enough to diffuse across cell membranes and then kill the cells surrounding the target tumour cell.[48,49] Examples of cleavable linkers and non-cleavable linkers are listed (**Table 1**).[50]

Table 1 – Cleavable and non-cleavable linkers.[50]
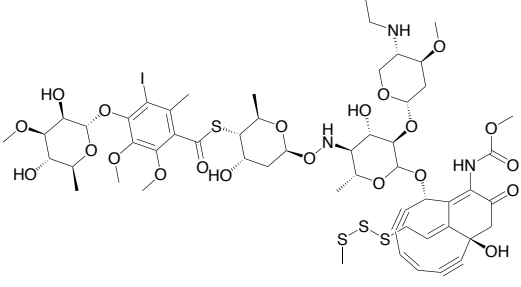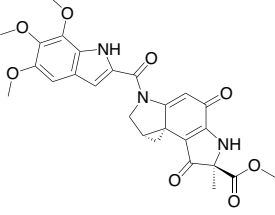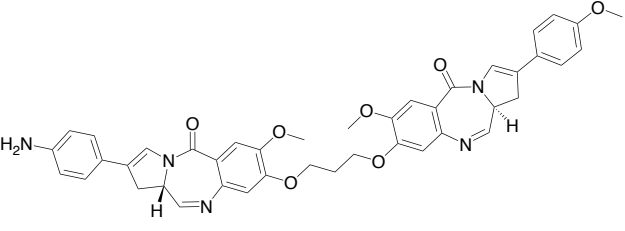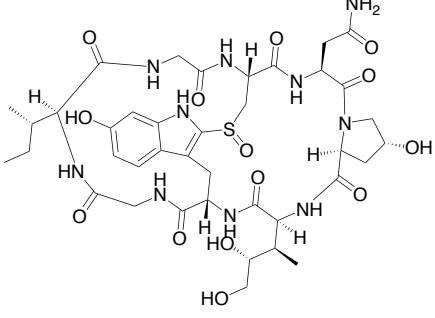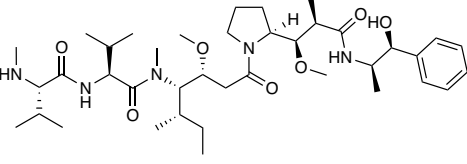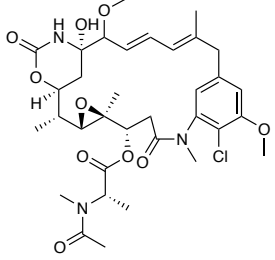
ADC linkers	Cleavable linkers			Non-cleavable linkers
	Acid-labile	**Reducible**	**Enzyme-labile**	
Examples	Hydrazone[51]	Disulfide[52]	Val-Cit[53]	Maleimide-based[54]
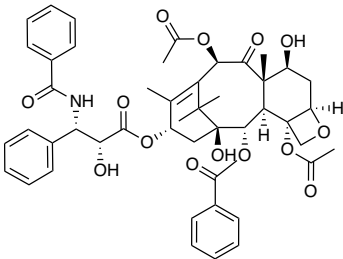
1.2.2 Payload selection

The payloads used in ADCs are highly potent cytotoxic drugs with half maximal inhibitory concentration (IC_{50}) usually in the nanomolar and picomolar range.[45,55,56] The property of attached payloads is crucial for ADC efficacy. For example, the hydrophobic drugs can diffuse across cellular membranes.[57] However, the covalent attachment of these drugs leads to hydrophobic patches on the hydrophilic surface of mAb.[58] Furthermore, ADCs loaded with hydrophobic drugs are vulnerable to non-specific binding and uptake by phagocytic cells.[59,60] The average amount of attached payloads on mAb, as known as DAR, is also important for ADC potency. ADCs with higher DARs are more potent as well as more likely to undergo aggregation.[58]

The payloads of currently approved ADCs usually target these cellular structures: DNA, RNA polymerase, or tubulin filaments (**Table 2**). The drugs targeting DNA usually induce double-strand DNA break (calicheamicins),[61] alkylate DNA (duocarmycins)[62] or crosslink DNA (pyrrolobenzodiazepine dimers, PBDs).[63] Some drugs are RNA polymerase inhibitors (amanitins) and some are microtubule inhibitors such as auristatins (MMAE, MMAF), maytansines (DM1, DM4) and taxol derivatives (paclitaxel).[56,64,65]

Table 2 – Payloads of approved ADCs.

Target	Drug Name	Structure
DNA	Calicheamicin	
	Duocarmycin	
	PBD	
RNA polymerase	Amanitin	
Microtubule	MMAE	
	Maytansine	

	Paclitaxel	

1.2.3 ADC mechanism of action

Once ADCs reach the target site, they can bind to the cell-surface antigens. Following the binding, the ADC-receptor complex is formed, which is then internalised *via* antigen-mediated endocytosis. As the pH decreases, linker cleavage and antibody degradation further occur during endo-lysosomal pathways, which releases the cytotoxic payloads. These free payloads can travel in the cytoplasm to reach their intended targets and initiate their mechanisms of action - DNA or microtubule disruption - and this results in cellular death (**Figure 4**).[56] If the cytotoxic metabolites are uncharged and can pass through the cellular membrane, they may also enter neighbouring cells to result in bystander effect.[66]
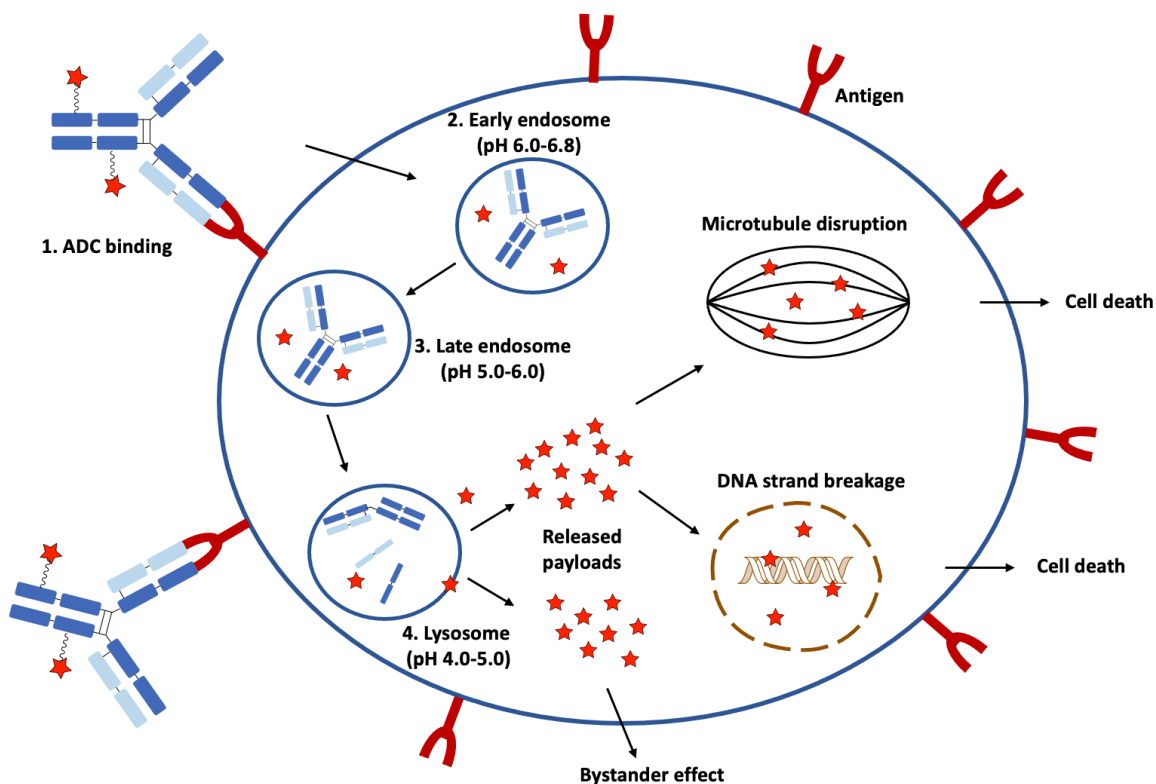
Figure 4 – General ADC mechanism of action.[56]

1.3 Antibody modification

ADCs can be constructed by the modification of accessible amino acid residues on antibodies, resulting in native antibody modification. However, since there are multiple reactive residues, it is difficult to control the conjugation site and the number of attached payloads, leading to a heterogeneous mixture of ADCs with different drug-to-antibody ratios (DARs), or conjugation sites. This impacts the pharmacokinetics of ADCs and can result in a loss of efficacy. To achieve residue-selective antibody modification, lysine and cysteine residues are commonly targeted, due to their solvent accessibility and high nucleophilicity. Among the current FDA-approved ADCs, three use lysine conjugation whilst the rest use cysteine conjugation. Other than lysine and cysteine residues, amino acids like tyrosine[67], tryptophan[68] and methionine[69] have also been explored. Alternative ways to obtain selective antibody modification is antibody engineering, where antibodies are armed with artificial amino acids or unnatural amino acids (UAA).[70]

1.3.1 Native antibody modification

1.3.1.1 Lysine conjugation

Lysine conjugation is a common approach for protein and antibody modification, resulting in stable amide bonds. Lysine residues (side-chain amine pKa 10.5) are abundant, and randomly distributed on the antibody. There are over 80 lysine residues in a typical IgG1 antibody and at least 20 of them are solvent accessible for modification.[71] Therefore, lysine conjugation inevitably yields a heterogeneous mixture of antibody conjugates, which includes the antibody attached with different numbers of payloads, and the antibody attached with payloads at different conjugation sites.[72] The antigen-binding efficacy of the antibody might be reduced if the lysine residues adjacent to the CDRs are modified. In addition, the clinical dosage of ADCs given to patients may be more difficult to effectively determine if the amount of attached payloads is unknown.[73] Consequently, lysine modification may be an unfavourable strategy if site-selectivity is desired (**Figure 5**).[74]
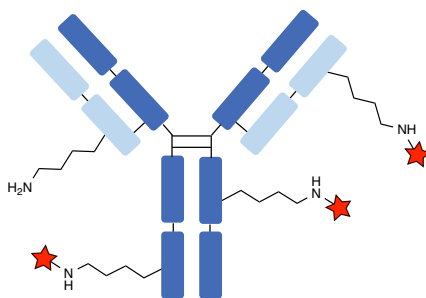
Figure 5 – ADCs *via* lysine conjugation.

Activated esters, such as *N*-hydroxysuccinimide (NHS) esters, are common reagents for the modification of lysine residues to generate stable amide bonds (**Figure 6a**).[75,76] These reagents are highly lysine reactive and commercially available. However, NHS esters can also react with other amino acids, for example serine, tyrosine and threonine, leading to limited chemoselectivity.[77,78] Alternatively, some other reagents including aldehydes,[79] iminoboronates,[80,81] isothiocyanates,[82] sulfonyl halides[76,83,84] and diazonium salts[85] have been explored to deliver selective lysine modification (**Figure 6b-6f**).
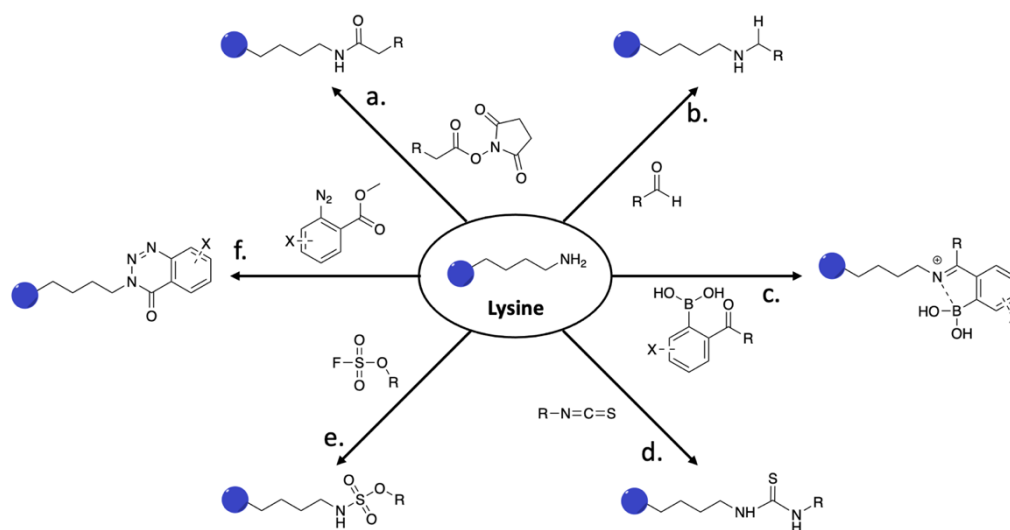
Figure 6 – Lysine conjugation reagents: a. NHS esters,[75,76] b. aldehydes,[79] c. iminoboronates,[80,81] d. isothiocyanates,[82] e. sulfonyl fluorides,[83,84] f. diazonium salts.[85]

In summary, lysines are highly reactive and have the potential to form stable chemical linkages upon reaction with electrophilic reagents, hence lysine conjugation is a dominant strategy for antibody modification. There are notable reviews of interest that further cover

lysine modification.[86] However, the issue is that lysine conjugation might lead to heterogeneity due to high abundance of lysines, and may result in reduced ADC solubility due to removal of previously charged residues.[87]

1.3.1.2 Cysteine conjugation

Due to the low relative abundance and high nucleophilicity at physiological pH, cysteine residues (thiol pKa 8.6) have become an additional target for antibody modification. The reduction of interchain disulfide bonds is required to release up to 8 free cysteine residues on IgG1 for further modification, therefore, cysteine conjugation might generate a mixture of antibody conjugates with DARs of 0-8 (**Figure 7**). Hence, despite cysteines showing less native abundance, cysteine conjugation could still result in heterogeneous antibody conjugates due to incomplete conjugation of one or more cysteine sites. The loss of disulfide bonds could also be limiting, as they are important for protein tertiary structure and biological activities.[88,89] ADCs with high DARs could also lead to rapid *in vivo* clearance, due to increased hydrophobicity and aggregation of ADCs, lowering tumour-killing effects, and it may be difficult to control drug loading extent with cysteine modification.[74]
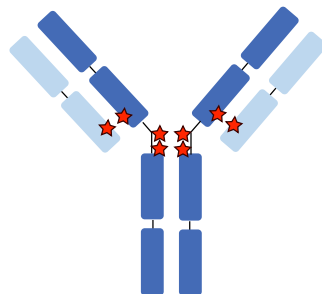
Figure 7 – ADCs *via* cysteine conjugation.

Multiple reagents including pyridyl disulfides,[90,91] alkyl halides,[92] vinyl sulfones,[93,94] iodoacetamides[95] and α,β-unsaturated carbonyl compounds (maleimides and pyridazinediones)[96] can react with cysteines (**Figure 8**).[76] Pyridyl disulfides are capable of capping the free cysteines under mild conditions, releasing 2-pyridinethione. Cysteines react with alkyl halides, substituting the halide to enable *S*-alkylation. Vinyl sulfones efficiently trap cysteine thiols at alkaline pH under mild aqueous conditions, generating stable β-thiosulfonyl linkages.[97] Vinyl sulfones can also be applied as PEGylation reagents,[98] probes, chelating

reagents or fluorescent tags.[99] Iodoacetamide derivatives, iodoacetamide-alkyne, were demonstrated as cysteine-reactive probes for reactive-cysteine profiling.[100] Maleimides and pyridazinediones[96] also react with cysteine residues, where maleimide outperforms other reagents for rapid reaction and selectivity.[101] The maleimide participates in a rapid reaction due to the high electrophilicity of the alkene that is caused by the neighbouring carbonyl groups and the maleimide ring strain (**Figure 8e**).[102] The maleimide, first discovered by Friedmann *et al.*,[103] is one of the most popular reagents for cysteine conjugation, due to its high chemoselectivity towards the cysteine thiols at the physiological pH.[104] However, the resulting maleimide conjugates are prone to retro-Michael deconjugation, leading to payload loss and reduced efficacy. Self-hydrolysing maleimides, developed to improve the stability of maleimide conjugates, participate in rapid hydrolysis to give the corresponding succinamic acids, thus the hydrolysed conjugates no longer undergo retro-Michael reaction.[105]
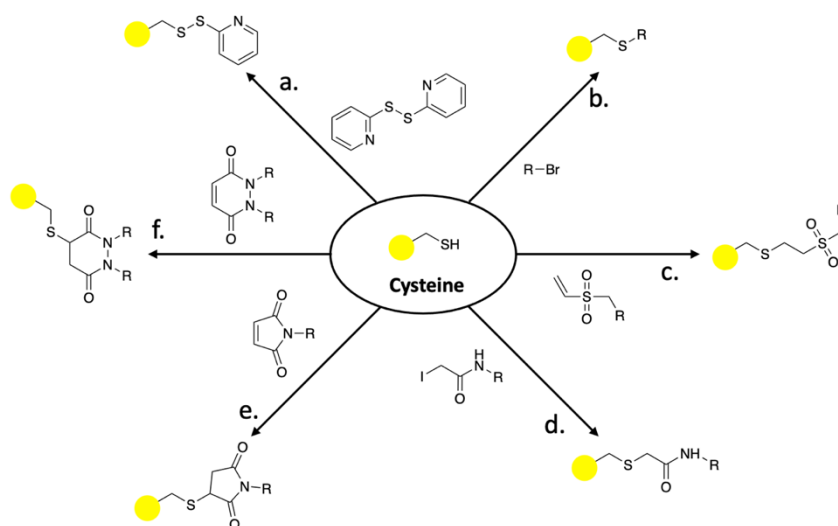
Figure 8 – Cysteine conjugation reagents: a. pyridyl disulfides,[90,91] b. alkyl halides,[92] c. vinyl sulfones,[93,94] d. iodoacetamides,[95] e. maleimides,[96] f. pyridazinediones.[96]

In summary, cysteine modification is another popular strategy for antibody modification. Cysteines have lower abundance than lysines in native antibodies, however, cysteine conjugation could still result in heterogeneous ADCs. The loss of intact disulfide bonds of antibodies is another concern in cysteine conjugation, which can potentially affect their biological activities.

1.3.1.3 Disulfide bridging

To obtain more site-specific and homogeneous ADCs, an alternative approach is desired. By covalently bridging two cysteines, one drug is loaded on each disulfide where a DAR of 4 in IgG1s can be achieved and the stabilising effect of the disulfide bond can be maintained. Since the modification on disulfide is distal from the antigen binding sites, the insertion of carbon bridges is minor to antibody biological activities. The developed disulfide bridging reagents include next generation maleimides (NGMs),[106,107,108] pyridazinediones (PDs),[109,110,111] bis-sulfones,[112,113,114] divinylpyrimidines (DVP),[115,116] divinyltriazines (DVT),[116,117] arylenedipropiolonitriles (ADPN),[118] dichlorotetrazines,[119] and others (**Figure 9**).[120,121,122,123] NGMs will be discussed separately in **Chapter 1.4** as they are the focus of this project.
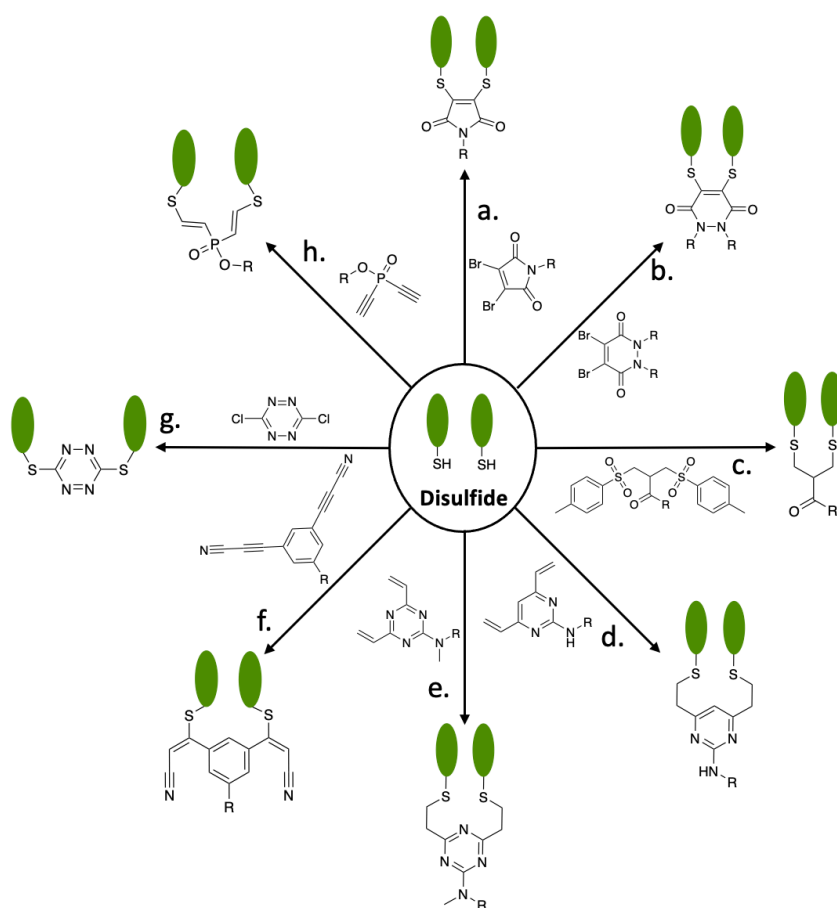
Figure 9 – Disulfide bridging reagents: a. (NGMs),[106,107,108] b. pyridazinediones (PDs),[109,110,110,111] c. bis-sulfones,[112,113,114] d. divinylpyrimidines (DVP),[115,116] e. divinyltriazines (DVT),[116,117] f. arylenedipropiolonitriles (ADPN),[118] g. dichlorotetrazines,[119] h. diethynyl phosphinates (DEP).[122]

As next generation PDs, the dibromopyridazinediones (diBrPDs) in disulfide bridging were first reported by Chudasama *et al.* by generating thio-cleavable and hydrolytically stable conjugates on peptides or proteins.[124] Maruani *et al.* developed a dual-clickable diBrPD with two reactive handles and applied it on trastuzumab Fab and full antibody to give dual-modality ADCs (**Figure 10a**).[125] They also utilised trifunctional diBrPDs to generate bispecifics *via* a strain-promoted inverse electron demand Diels-Alder cycloaddition (SPIEDDA) (**Figure 10b**).[126] The diBrPD platform was further explored as the all-in-one reagent, which can both reduce and bridge the Fab disulfide bond (**Figure 10c**).[127] More examples have exhibited high flexibility of PD reagents including diBrPDs as *in situ* bridging reagents,[128] bis-diBrPDs,[129] and nanoparticles covered with diBrPD-bridged Fab conjugates.[130]

a.
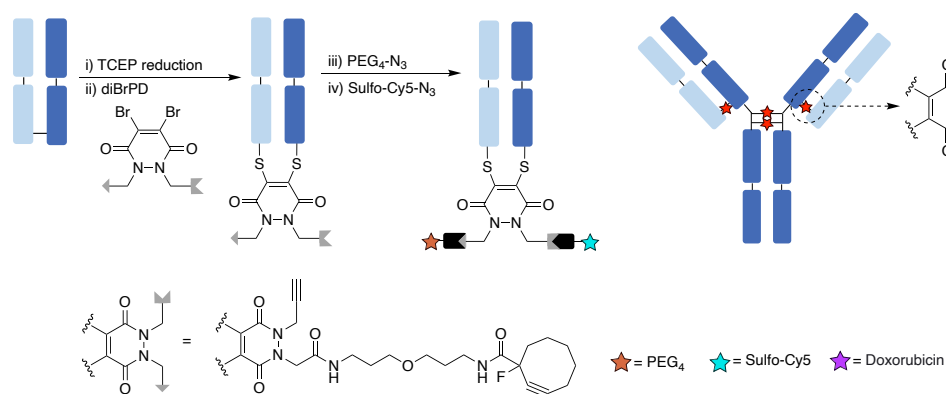
b.
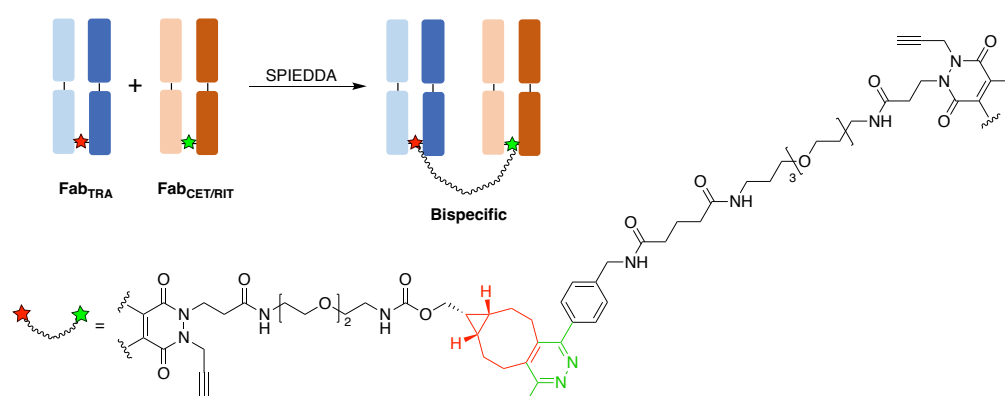
c.
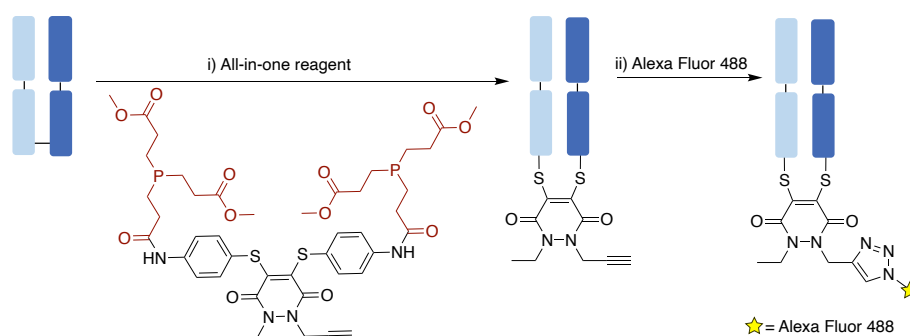
Figure 9 – Application of diBrPDs: a. preparation of dual-modality Fab and full antibody conjugates,[125] b. preparation of bispecifics,[126] c. Fab disulfide reduction and bridging using the all-in-one reagent.[127]

Liberatore *et al.* first reported bis-sulfones as disulfide bridging reagents by inserting a sulfone reagent into a disulfide bond through bis-alkylation.[131] The PEGylated bis-sulfone underwent a sequential addition-elimination-addition reaction with the reduced disulfide bond (**Scheme 1**).[132,133] The bis-alkylation attempts on disulfides, including somatostatin, glutathione, interferon α-2b and an anti-CD4 antibody fragment demonstrated that fundamental tertiary structures could be maintained. Therapeutic proteins with extended *in vivo* half-life were generated *via* a three-carbon PEGylated bridge.[134,135] A bis-sulfone with MMAE as a payload was applied on both trastuzumab Fab and full antibody. This reagent incorporated a long PEG spacer, an enzymatically cleavable valine-citrulline-*p*-aminocarbamate (VC-PABC) linker and the MMAE payload.[136] The generated Fab and antibody conjugates have a DAR of 1 and a DAR of ~4 respectively. They both displayed high yield, high homogeneity, good serum stability, whilst also retaining antigen-binding capability, *in vitro* cytotoxicity and *in vivo* potency.[137]
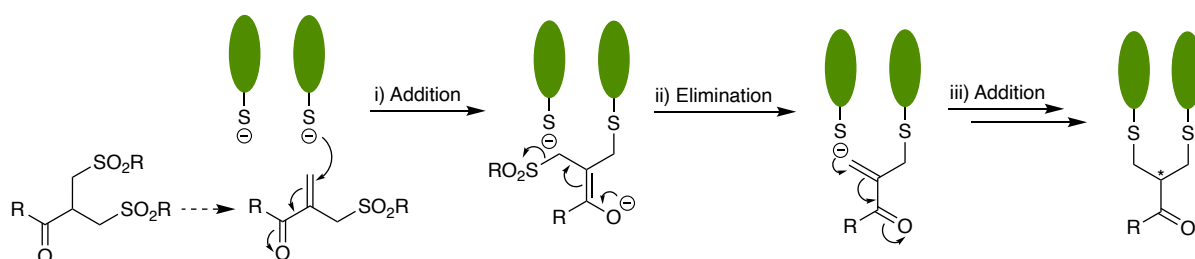
Scheme 1 – Disulfide bridging *via* a three-carbon bridge in peptides and proteins.[132,133]

The divinylpyrimidine (DVP) motif was designed for creating homogeneous ADCs *via* selective disulfide bridging (**Figure 9d**).[115] DVP motifs were further explored as a tetra-DVP platform to all-in-one bridge 4 disulfide bonds in IgG1.[116] Divinyltriazines (DVT) can chemoselectively and efficiently bridge antibody disulfide bonds, since the equivalents of DVT required for a rapid antibody conjugation can be reduced to a near stoichiometric ratio (**Figure 9e**).[117] The arylene-dipropiolonitrile (ADPN) motif delivering selective antibody disulfide bridging was loaded with a MMAE generated ADCs with controlled DAR of ~4 (**Figure 9f**).[118] Dichlorotetrazines also enabled site-specific labelling on two cysteine residues where the tetrazine moiety is available for the incorporation of functionalities *via* tetrazine ligations (**Figure 9g**).[119] Other reagents for disulfide bridging like diethynyl phosphinates (DEP) were also demonstrated with disulfide bridging ability where the electron-deficient triple bond can be attacked by thiols subsequently (**Figure 9h**).[122]

Disulfide bridging can generate site-specific antibody conjugates, however, this methodology also has drawbacks. Since there are only 4 solvent accessible disulfide bonds in IgG1, the DAR of prepared ADCs is limited up to 4, which may be undesirable for some targets which require higher concentrations of payload delivery. In addition, the two disulfide bonds located in hinge region are very close to each other. Therefore, disulfide scrambling is possible to occur, resulting in the formation of 'half-antibodies' where two thiols on the same heavy chain are bridged (**Figure 11a**).[138] The half-antibody species lower homogeneity of the prepared ADCs and affect secondary antibody interactions such as antibody-dependant cell-mediated cytotoxicity.[139]
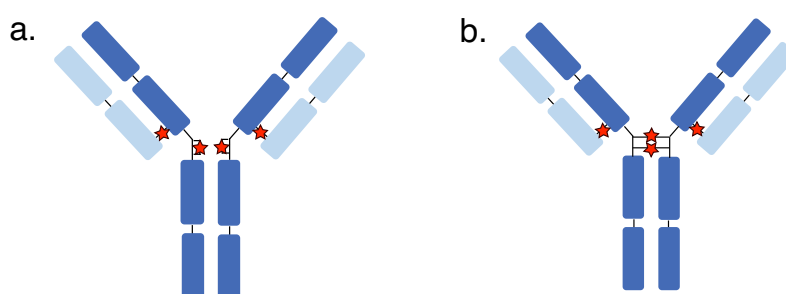
Figure 10 – Structure of ADCs: a. half-antibody conjugate b. full-antibody conjugate.*[138]*

1.3.2 Antibody engineering

Other than native antibody modification, antibody engineering is an alternative way to yield site-specific and homogeneous antibody conjugates. Engineered antibody modification includes the preparation of cysteine mutants like THIOMABs, the incorporation of unnatural amino acids (UAA) or enzyme-directed modification.

1.3.2.1 THIOMABs

Antibodies with engineered cysteine residues at specific sites, known as THIOMABs, have been developed by Junutula *et al.* initially. These sites have been designed to be distal from the antigen-binding region to ensure no disturbance to antibody biological activities as well as the maximum of cysteine reaction availability in bioconjugation.[140] The prepared THIOMABs were shown to load drugs with near-uniform DARs of 2 at defined sites, during which homogeneous THIOMAB-drug conjugates (TDCs) were yielded. TDCs are superior to conventional ADCs as they exhibit uniform distribution of payloads and being equivalently efficacious.[140,141] The monobromomaleimides (MBMs) platform was applied on THIOMAB to generate a highly stable, potent and homogeneous TDC with a controlled DAR of 2 (**Figure 12a**). The prepared TDC proved to have retained antigen-binding ability and efficient cell-killing ability.[142] A homogeneous TDC with a high DAR (up to 18) has been developed with XTEN polypeptides conjugated where each XTEN polypeptide moiety contains 9 cysteines and is further loaded with cytotoxic payloads (**Figure 12b**). Across two different cytotoxic payloads, a microtubule and DNA damaging agent, improved anti-tumour efficacy of the prepared TDCs with high DARs compared to the controls with low DARs was observed, even when the total payload dose for each was equivalent.[143] Another example is a THIO-SELENOMAB that the scFv-Fc was engineered with two cysteines and one selenocysteine, which further generated a dual-labelled TDC (**Figure 12c**). The dual-labelled TDC displayed excellent stability in human plasma as a proof of a robust strategy for site-specific attachments of two different drugs to the antibody.[144] Consequently, THIOMAB technology has improved the homogeneity of ADCs by retaining the native disulfide bonds and directing the attachment of drugs at defined sites and with near-uniform stoichiometry.
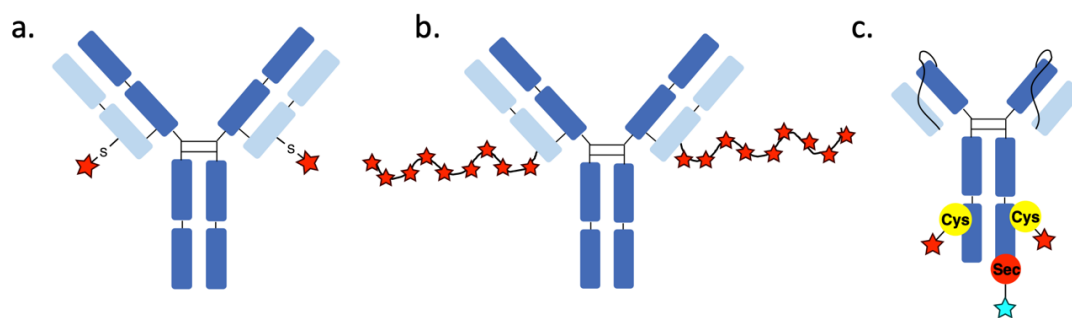
Figure 11 – Example of THIOMAB conjugates: a. the TDC with MBM conjugated,[142] b. the TDC with XTEN polypeptide conjugated,[143] c. the dual-labelled TDC yielded from a THIO-SELENOMAB.[144]

1.3.2.2 Unnatural amino acids

Unnatural amino acids (UAAs) usually have special chemical reactivity, which helps to build selective reactivity at the site of insertion. The biological pathway to generate the mutated antibody fragment with incorporated UAAs was displayed (**Figure 13**). The cell-permeable UAA is added to the culture medium where it works as a substrate for a tRNA synthetase (RS). The RS is engineered to only recognise the UAA and acylate an orthogonal engineered tRNA. For incorporation into the antibody, the RS/tRNA and antibody genes are recombinantly expressed.[145,146] For example, the azidophenylalanine was inserted into yeast proteins where the azide further reacted with a PEG-alkyne to deliver site-specific PEGylated antibody.[147] Another application is an UAA-bearing antibody conjugate built by incorporating two *p*-acetylphenylalanines in Fab region, cytotoxic payloads were further introduced *via* a stable oxime linkage to generate the conjugate with a DAR of 2.[148] As a combination of THIOMAB and UAA techniques, a novel antibody Fab platform was engineered with nonnatural cysteines and inserted *p*-acetylphenylalanines. This Fab platform further incorporated two different payloads sequentially and orthogonally, resulting in the dual-modality Fab conjugate with a DAR of 1 for each payload. It proved that the Fab conjugate was fully capable of internalisation into the target cells. Therefore, the novel dual-conjugated Fab with functional diversity is able to overcome drug resistance and has enhanced therapeutic efficacy.[149]
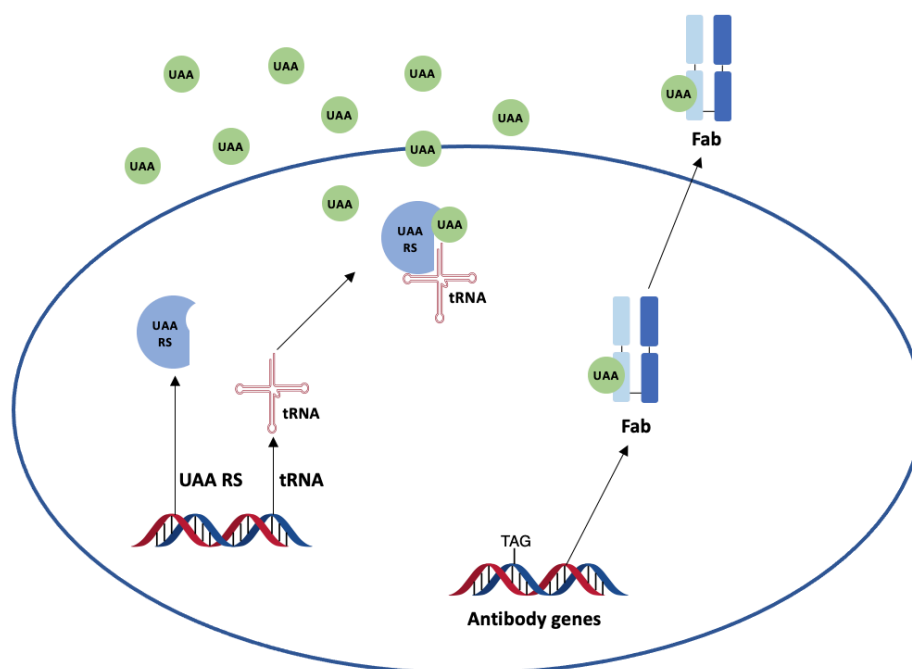
Figure 12 – Biological process for inserting UAAs into antibody fragments.[145,146]

1.3.2.3 Enzyme-directed modification

To introduce unnatural and bio-orthogonal groups to antibody *via* enzymes is known as enzyme-directed modification. Transglutaminases (TGs) catalyse acyl-transfer reactions between the carboxamide group of a glutamine and the primary amine of a lysine, to form catabolically stable isopeptide bonds.[150] An antibody bearing aldehyde tags was generated by inserting formylglycine-generating enzyme (FGE) recognition sequence and then loading FGE to the antibody. FGE catalyses the conversion of the thiol on cysteine to an aldehyde group. The engineered antibody was further site-specifically conjugated with a hydrazino-*iso*-Pictet-Spengler (HIPS) linker and payload.[151] Selective sortase-enzyme mediated conjugation of maytansine and MMAE payloads to the antibody was performed *via* a sortase A-mediated transpeptidation reaction.[152] Other enzymes such as glycosyl transferase[153] and endoglycosidase[154] were also utilised to generate selective antibody conjugation.

In conclusion, antibody modification usually involves native antibody modification and antibody engineering. Native antibody modification is simple and financially feasible but not always selective, whilst antibody engineering is highly specific but more complex and expensive.

1.4 Next generation maleimides (NGMs)

This project focuses on next generation maleimide (NGM) reagents. Tedaldi *et al.* first reported bromomaleimides as NGMs for selective and reversible cysteine modification.[155] NGMs have been developed to offer new opportunities for cysteine conjugation and disulfide bridging, here are the key examples.

1.4.1 NGMs in cysteine conjugation

The application of NGM cysteine conjugation has mostly been demonstrated on proteins containing single accessible cysteine residue, such as growth factor receptor-bound protein 2 (Grb2) and human serum albumin (HSA). Both monobromomaleimides (MBMs) and dibromomaleimides (DBMs) can enable three attachments where two more functionalities can be reversibly or irreversibly introduced to those proteins. For example, MBMs and DBMs were bioconjugated to the SH2 domain of Grb2 and then one equivalent of glutathione was added to obtain three attachments (**Figure 14a-14b**). Excess TCEP or thiols could be applied to regenerate native Grb2, which proved the reversibility of MBM and DBM conjugation. It was also found that if the attached maleimide was hydrolysed, excess thiols cannot cleave the maleamic acid, enabling irreversible cysteine conjugation (**Figure 14c**). Based on the hydrolysis study, *N*-alkylated mono- or bisthio-maleimides were quite stable to hydrolysis, even at pH 8.0 and physiological temperature, yielding thiol-cleavable conjugates. In contrast, *N*-arylated mono- or bisthio-maleimides hydrolysed rapidly at pH 8.0, yielding non-thiol-cleavable conjugates.[107] Another example of NGMs targeting single cysteine is a class of aryloxymaleimides designed with attenuated reactivity, they reacted with Grb2 SH2 at a reduced rate compared to MBMs (**Figure 14d**).[156] Therefore, the reactivity of NGMs can be tuned by varying leaving groups on the maleimide ring, which helped to expand the scope of NGMs.
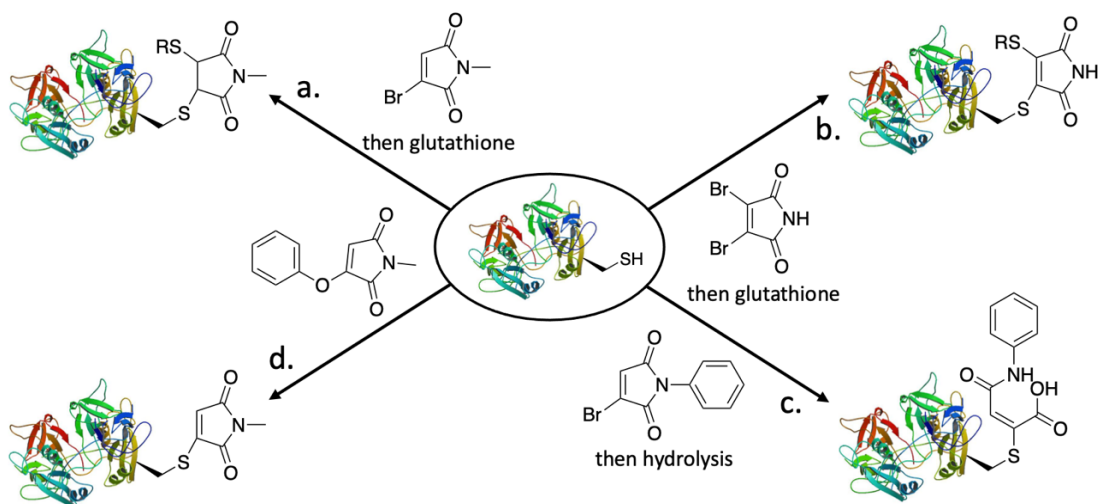
Figure 13 – a. Reversible MBM, [106] b. reversible DBM, [106] c. irreversible MBM modifications on Grb2 SH2 domain, [107] d. aryloxymaleimide conjugation to Grb2 SH2 cysteine.[156]

MBMs and DBMs also have a broad application on HSA that has a single accessible cysteine residue and a long half-life of around 19 days. This makes HSA a suitable candidate in extending the half-life of drugs.[87] A robust HSA conjugate was developed by applying a MBM-C_2 linker with the drug paclitaxel attached on HSA, where the maleimide core underwent a post-conjugation hydrolysis.[157] Moreover, the dual-reactive HSA conjugate could be generated *via* the bioconjugation of a *N*-functionalised DBM-biotin to HSA, where a functionalised amine was further introduced to replace the other bromine on the maleimide ring (**Scheme 2**).[158]
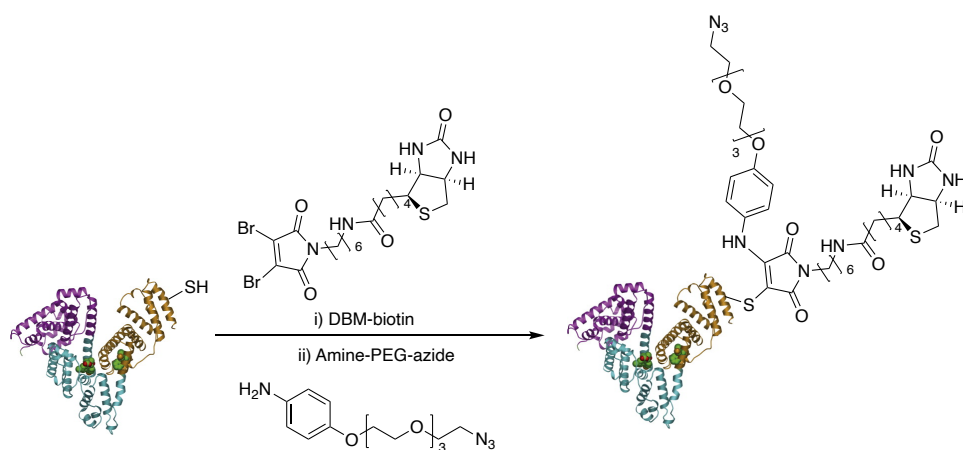
Scheme 2 – Preparation of a dual-reactive HSA conjugate.[158]

By reacting with cysteine residues, NGMs are able to 'turn on' fluorophores that can be utilised for reporting on intracellular delivery. These NGMs are also known as novel fluorescence turn-on reagents. The fluorophore attached to a maleimide would be activated once the maleimide core became a succinimide by adding excess thiols (**Figure 15**).[159] Both MBMs and monothiomaleimides (MTMs) were found to serve as highly effective quenchers of a covalently attached dansyl fluorophore. Once the maleimide core was deactivated or cleaved, the fluorophores would emit radiation.

a.
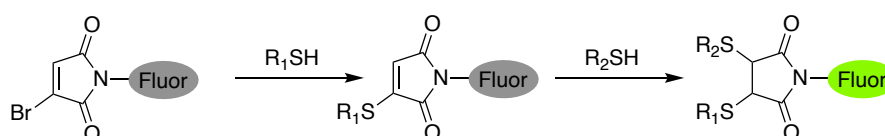
b.
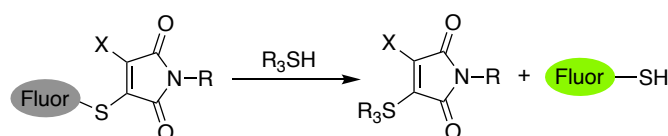
Figure 14 – Fluorescence turn-on *via* a. maleimide deactivation, b. maleimide cleavage.[159]

1.4.2 NGMs in disulfide bridging

The application of NGMs in disulfide bridging has been developed as an extremely promising reagent class with applications including delivering highly homogeneous antibody conjugates and constructing bispecifics. To improve the serum-stability of antibody conjugates, it was proposed that DBMs *N*-functionalised with electron-withdrawing groups, can undergo accelerated post-conjugation hydrolysis. When DBM conjugated to a phenyl ring or a C_2 linker, it took less than 1 h at pH 8.5 to lock DBMs on the antibody as stable maleamic acids (**Figure 16a**).[160] The homogeneity of the generated conjugates was also improved by the accelerated hydrolysis design, which was confirmed by mass spectrometry analysis. Based on the conclusion of hydrolysis study, a DBM-C_2-BCN reagent underwent disulfide bridging and rapid post-conjugation hydrolysis on IgG1. The strained alkyne in the BCN moiety further incorporated the proteolysis-targeting chimeras (PROTAC) *via* a strain promoted alkyne-azide cycloaddition (SPAAC) to generate the antibody-PROTAC conjugate with a DAR of 4 (**Figure**

16b).[161] PROTACs are increasingly popular as anti-cancer therapies, and this method has provided a way of combining benefits of PROTACs on an antibody-based platform.

a.
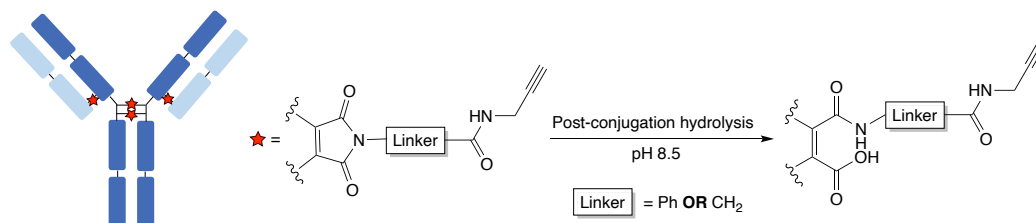
b.
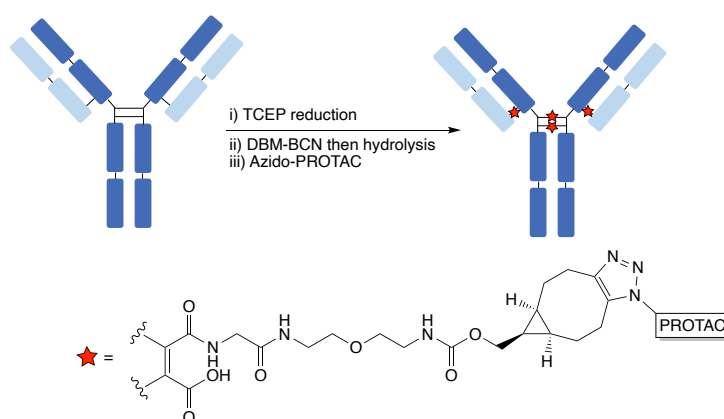
Figure 15 – a. DBMs hydrolysis on antibody at pH 8.5,[160] b. preparation of the antibody-PROTAC conjugate.[161]

Even though DBMs can be locked on the antibody *via* post-conjugation hydrolysis, they can also serve as cleavable linkers during the action of ADCs. A class of acid-labile DBMs have been explored that they can be cleaved at increasingly acidic conditions after hydrolysis. The DBM linker loaded with doxorubicin (DOX) was conjugated to Fab and then hydrolysed at pH 7.4. The hydrolysed conjugate was further incubated at pH 4.5 to release the payload (**Scheme 3**).[162]
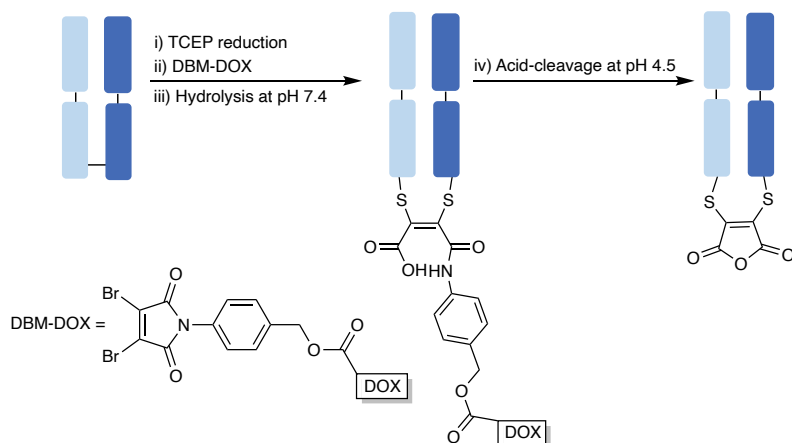
Scheme 3 – The attachment and release of DOX on Fab.[162]

Other than DBMs, a class of dithiomaleimides (DTMs) when the thiophenol serving as a good leaving group, have also been explored as disulfide bridging reagent. This dithiophenolmaleimide was also found to enable *in situ* bridging disulfide bonds with reducing reagents. Schumacher *et al.* reported that dithiophenolmaleimides, designed with reduced reactivity to TCEP, can enable *in situ* disulfide bridging on somatostatin.[163] The DTMs were further applied as *in situ* bridging reagents in antibody conjugation, offering opportunities to yield ADCs with increased homogeneity (**Scheme 4**).[164] The *in situ* protocol would enable rapid sequestration of free cysteine residues, to reduce the problems caused in sequential protocol such as protein unfolding, aggregation, and disulfide scrambling.
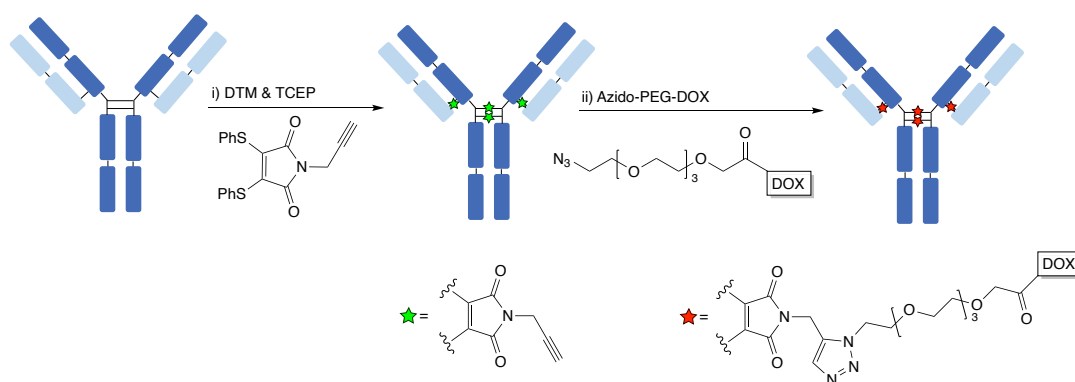
Scheme 4 – *In situ* bioconjugation of DTMs to antibody.[164]

NGMs have also been explored as a linker to join two or three antibody fragments together. For example, a bis-DBM linker was explored to join the anti-CEA scFv fragment and the

trastuzumab Fab fragment together to form a bispecific conjugate (**Figure 17a**). Carcinoembryonic antigen (CEA) is a cell surface glycoprotein overexpressed in a wide range of cancers. The bis-DBM linker was composed of two *N*-functionalised DBMs and a long PEG spacer in the middle. By sequentially conjugating to anti-CEA scFv and the trastuzumab Fab, the bis-DBM linker finally generated a homogeneous bispecific, which can bind to two different antigens.[165] Another NGM reagent tri-diiodomaleimide (DIM) was developed to join three antibody scFv fragments *via* disulfide bridging, generating a tri-scFv conjugate (**Figure 17b**). The trimerization of scFv exhibited a significant increase of half-life compared to the unmodified monomer. Long half-life also brought various *in vivo* applications for the trimer.[166]

a.
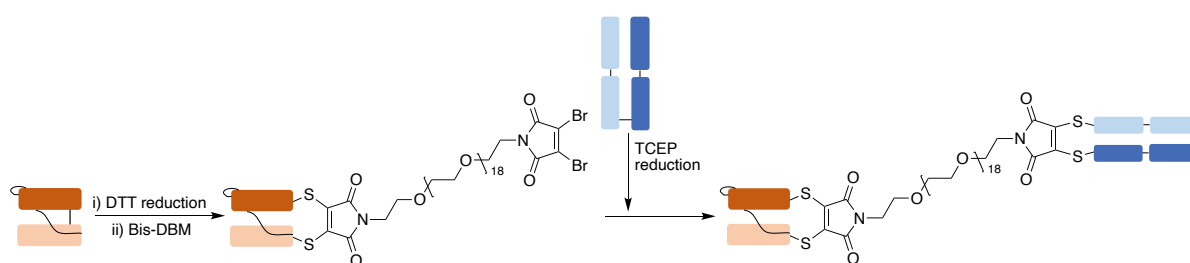
b.
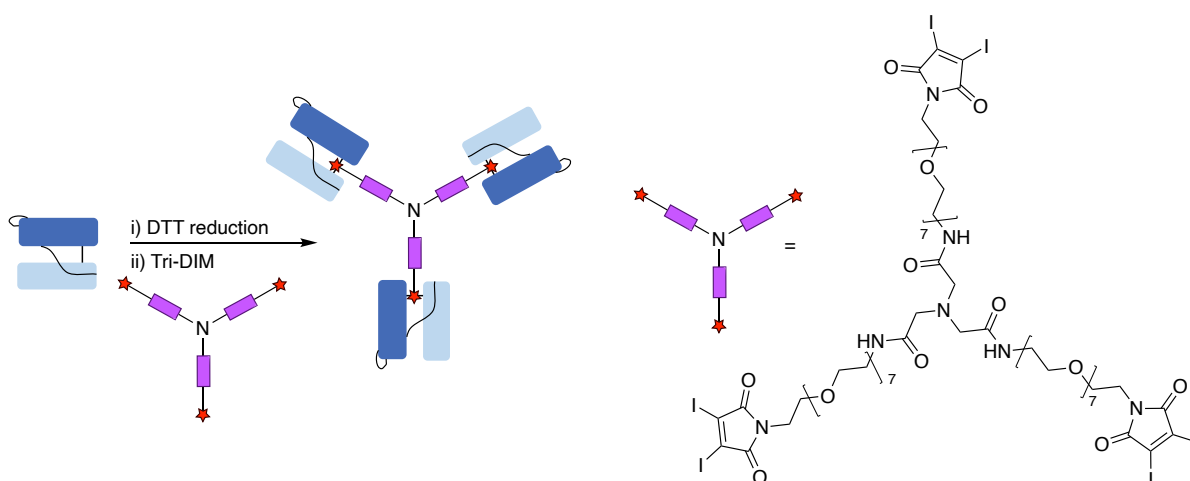
Figure 16 – Preparation of a. anti-CEA/anti-HER2 scFv-Fab bispecific conjugate,[165] b. tri-scFv conjugate.[166]

Another strategy to reconnect disulfide bonds using NGMs is to modify cysteines separately with MBMs, and then join the adjacent MBMs *via* a photochemical reaction (**Figure 18a**).

Thiomaleimides, which could be prepared by the addition of thiols to bromomaleimides, underwent [2 + 2] photocycloadditions between the two C=C bonds on the maleimide core to reconnect the crosslink between the two cysteine residues. This photo-triggered methodology paved a new way for photochemical manipulation of biomolecules.[167] The MBM was further replaced with a bis-MBM and performed an intramolecular [2 + 2] photocycloaddition reaction on the Fab conjugate (**Figure 18b**).[168]

a.

R = PEG **OR** Biotin
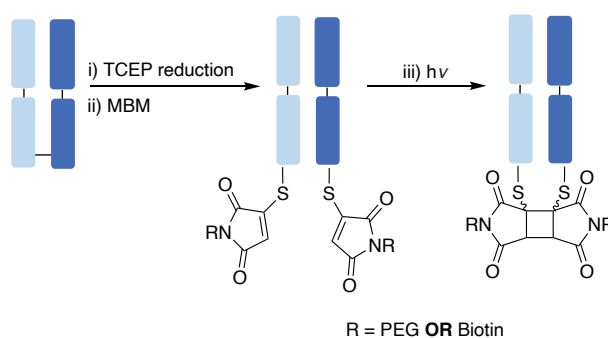
b.
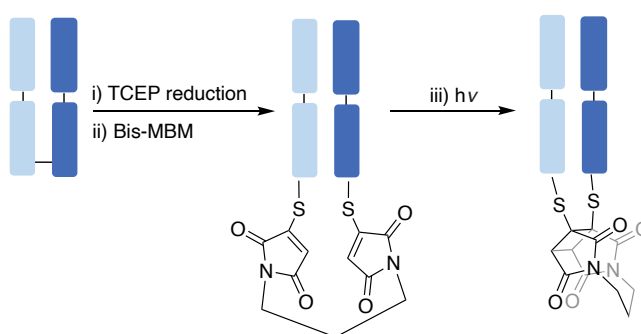
Figure 17 – Fab disulfide bridging with a. MBM,[167] b. bis-MBM[168] *via* photoactivation.

In summary, NGMs modify cysteines and bridge disulfide bonds in a highly specific and rapid manner where ADCs with high homogeneity can be prepared. NGMs designed with tuned reactivity can also deliver *in situ* antibody bioconjugation, which can resolve the problem encountered in sequential bioconjugation. The construction of bispecifics or antibody fragment trimers can be achieved by conjugating a bis-NGM or tri-NGM to antibody fragments.

1.5 Click and bioorthogonal chemistry

Click chemistry is a class of simple, quick, selective and atom-economic reactions that are commonly used to join two molecular moieties under mild conditions, and require minimal purification due to inoffensive by-products.[169] Examples of click chemistry include 1,3-dipolar cycloaddition, Michael addition and Diels-Alder reaction.[170] Bioorthogonal chemistry describes highly specific and fast reactions that the two involved reactants are mutually reactive but do not cross-react with biological moieties or interfere biological reactions.[76] Bioorthogonal chemistry and click chemistry therefore overlap significantly, reflecting the similar underlying chemical principles. Therefore, click reactions enabling mild bioorthogonal conjugation with high yields and selectivity makes them ideal candidates for the functionalisation of proteins.

1.5.1 CuAAC

Being small and stable, the azide can be involved in smooth ligations with various reactive handles under mild conditions, which make them popular for biorthogonal click reactions.[171] Azides undergo Huisgen cycloadditions with terminal alkynes where copper is required to ensure this reaction happen at a suitable rate.[170,172,173] This copper-catalysed reaction, also known as copper-catalysed azide-alkyne cycloaddition (CuAAC), takes place in aqueous solutions to yield chemically robust triazoles (**Scheme 5**).[174] Consequently, CuAAC has been universally applied in organic synthesis, drug discovery, polymer preparation and bioconjugation.
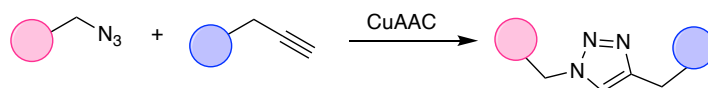
Scheme 5 – Azide-alkyne ligation using copper as the catalyst (CuAAC).

The CuAAC yields covalent C-N bonds between an azide and an alkyne to form a 5-membered ring in a one-pot reaction. During the CuAAC reaction, Cu(I) species work as catalysts to facilitate the reaction. Various copper reagents, also known as pre-catalysts, can be utilised to form Cu(I) compounds during the reaction. The pre-catalyst can be a Cu(II) salt with a

reducing reagent, a Cu(I) compound with a base or amine ligand with a reducing reagent, or a Cu(0) compound with a surface of the required Cu(I) species. The function of the reducing reagents is to protect Cu(I) from being oxidised to Cu(II), which loses activity.[175] It was demonstrated that if ligands, for example tris-hydroxypropyltriazolylmethylamine (THPTA), were added to CuAAC reaction, the reactive oxygen species can be rapidly reduced without decreasing the reaction rate significantly.[176]

1.5.2 SPAAC

CuAAC is not ideal for *in vivo* studies where the contained copper salts are toxic to living tissues, due to their coordination to biomolecules. The generation of catalytic Cu(I), always yielded from mixing Cu(II) and sodium ascorbate *in vitro*, is hard to form *in vivo*.[177] Alternatively, a copper-free cycloaddition, termed strain promoted alkyne-azide cycloaddition (SPAAC) was developed.[178,179] SPAAC is a strain-promoted reaction where cycloalkynes and alkynophiles, for example azides, exclusively and efficiently react with each other to generate stable adducts (**Scheme 6**). SPAAC is driven by the highly favourable enthalpic release of the ring strain in cycloalkynes.[180] In this way, SPAAC is capable to take place efficiently without catalysts under mild conditions, which results in promising *in vivo* applications. Nowadays, SPAAC has been widely applied to tag proteins containing azides in live cells[181,182] and in living organisms.[183,184,185]
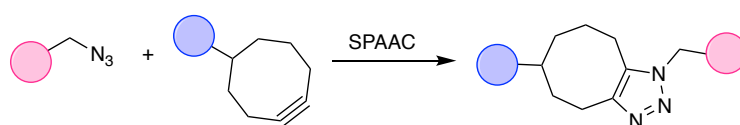
Scheme 6 – Azide-strained alkyne ligation (SPAAC).

Further application combining CuAAC and SPAAC is a dual-click tool protocol to incorporate two different moieties orthogonally. The dual-click tool involved a strained alkyne and a linear alkyne that can participate in SPAAC and CuAAC reactions sequentially under orthogonal conditions.[186]

1.5.3 IEDDA

Another efficient bioorthogonal cycloaddition is termed as inverse electron-demand Diels-Alder (IEDDA). The first record of IEDDA was demonstrated by Carboni *et al.* that a reaction

between a phenylstyrene and a fluorinated tetrazine occurred rapidly at room temperature.[187] In addition, strained alkenes, especially trans-cyclooctenes (TCO), were proved to react rapidly with electron-deficient tetrazines under mild aqueous conditions, due to their large ring strain.[188,189] TCO-tetrazine ligation is proved to be the fastest bioorthogonal click reaction on record (**Scheme 7**), [190] hence this reaction has extensive applications in live animal imaging.[191,192,193] For example, a stable and reactive antibody-tetrazine conjugate was developed to generate real-time fluorescence cell imaging using TCO probes.[194] TCO-tetrazine ligation could also provide small molecule target identification with high protein enrichment yields, ensuring the identification of unknown and low expressed target proteins.[195,196]
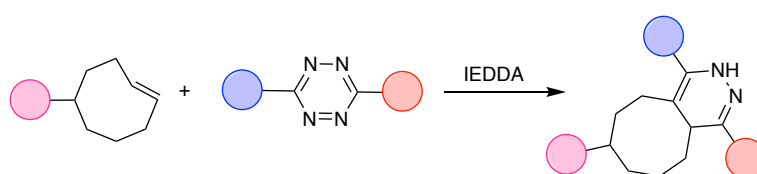
Scheme 7 – TCO-tetrazine ligation (IEDDA).

1.6 Selenium in antibody conjugation

Selenium was discovered by Berzelius in 1817. Berzelius and Gahn, two Swedish chemists, isolated 3 g of a precipitate when roasting 200 kg of sulfur from pyrite. The precipitate was identified wrongly as tellurium at the beginning. But after extensive analysis by Berzelius, this precipitate appeared to be a new element, which was named as selenium (Greek: *Selene*, moon) as it resembled tellurium (Latin: *Tellus*, earth).[197]

Selenium is toxic to most organisms but also essential to some bacteria and of fundamental importance to human health. Selenium is a key moiety of some major metabolic pathways, such as thyroid hormone metabolism, antioxidant defence systems, and immune function.[198] Pinsent first reported that selenium was essential for *E. coli* to form an active formic dehydrogenase.[199] Further work found that the addition of methionine, vitamin E or a Factor 3 containing selenium, to diet can help prevent liver necrosis in rats.[200,201] Later, it was identified that the selenocysteine residue played a significant role in biological activities of selenoproteins.[202] It was then reported that the key catalytic site in glutathione peroxidase was the selenocysteine moiety found in reduced form of selenols at the catalytic site.[203] The

amino acid sequence of glutathione peroxidase was fully determined, hence the active site selenocysteine was confirmed at position 45.[204] It was also proved that the necessity of selenocysteine as a catalytic site by replacing it with a cysteine, which caused a significant decrease on the reaction rate.[205]

1.6.1 Uniqueness of selenium

Selenium is a nonmetal element with atomic number 34, located in the fourth period of period table in the chalcogen group, along with oxygen, sulfur and tellurium. In the chalcogen group, selenium is in the middle of sulfur and tellurium and is found to have more similar characteristics to that of sulfur than tellurium. Selenium and sulfur are so similar in structures that their analogous compounds can easily co-crystallise. Thus, the physiochemical properties of selenium are introduced in comparison to sulfur (**Table 3**).

Table 3 – Physiochemical Properties of Sulfur and Selenium.

Element	Sulfur (S)	Selenium (Se)
Atomic Number	16	34
Atomic Weight	32.065	78.96
Electronic Configuration	[Ne] $3s^2\ 3p^4$	[Ar] $3d^{10}\ 4s^2\ 4p^4$
Electronic Shell Structure	2, 8, 6	2, 8, 18, 6
Oxidation State	-2, 2, 4, 6	-2, 2, 4, 6
Atomic Radius[206]	88 pm	103 pm
Molecular Volume[207]	15.53 cm^3	16.42cm^3
Bond length (dichalcogen)[207]	205 pm	232 pm
Bond length (carbon-chalcogen)[208]	180 pm	196 pm
Pauling Electronegativity[209,210]	2.58	2.55
pKa of -XH[211]	8.3	5.2

As showed in this table, sulfur and selenium have a lot in common, such as oxidation states and electronegativity. Selenium, being a heavier element, is more polarisable and softer than sulfur, which usually leads to more rapid electrophilic and nucleophilic substitutions. The large atomic radius and molecular volume of selenium demonstrate that the electrons in selenium are loosely bound, hence selenium is a better electron donor than sulfur. The large bond length of diselenide (Se-Se) and carbon-selenide (C-Se) corresponds to weak bonds, where fast bond-breaking reactions often occur. Compared to sulfur, selenium is also a better electron acceptor because the sigma orbital of Se-X bond is lower in energy than that of S-X bond.[212] Hence, selenium is both a good electron donor and a good electron acceptor. The significant difference of pKa value between selenols (pKa 5.2) and thiols (pKa 8.3) also demonstrates that selenolates are less basic than thiolates. However, due to higher polarisability of selenium, selenolate ions are more nucleophilic than thiolates. At physiological pH, difference in nucleophilicity between selenium and sulfur is more significant, as selenols are completely converted to selenolates, whereas thiols are only partially ionised.[212] Furthermore, due to size difference, selenolates are usually better leaving groups than thiolates. Overall, selenolates have better nucleophilicity and better leaving group ability at physiological pH compared to thiolates. This was proved by dynamic experimental data that the selenolate-diselenide exchange reaction was measured to be 10^7 times as fast as that of the thiolate-disulfide exchange reaction at pH 7.0.[213]

Other than high nucleophilicity of selenolates, selenols were also demonstrated to have catalytic ability in aqueous thiol-disulfide exchange, of which the reaction rate was dramatically enhanced with the benzeneselenol.[214] Diselenide or selenocyanate, as selenol precursors, can also be conveniently converted to selenols with strongly reducing thiols and further catalyse the thiol-disulfide exchange.[215] For example, selenocystamine, a commercially available diselenide, has been applied as a catalyst precursor for disulfide reduction where selenocystamine can be further reduced to selenols *in situ*.[216] Selenols are not only useful in chemistry reactions as a class of catalysts, it is also applicable as reducing agents in biology, because most peptides and proteins containing disulfide bonds.

1.6.2 Selenium in chemical biology

The catalytic ability of selenium in biological application was demonstrated when it was discovered to work as a catalyst in protecting cells from oxidative stress like UV and ionising

radiation.[217,218] The mechanism of this phenomenon was related to the idea that selenium could catalyse cysteine-disulfide transformations in some redox-regulated proteins.[219,220,221] Once selenols showed great catalytic ability in thiol-disulfide exchange in proteins, more research work has been performed to use selenols in the reduction of peptide or protein disulfides.

Extremely rapid reduction was observed in peptides and IgG Fab fragments using reducing agents and catalytic amount of selenols (eq. ratio 6:1). For example, Fab-dithiothreitol (DTT) reduction takes 90 min to complete, whilst Fab-DTT-selenocystamine reduction only needs 5 min.[222] A novel antibody-labelling approach involving the selenol-catalysed reduction on native disulfides and thiol-labelling with biotin-poly(ethylene oxide)-maleimide (biotin-PEO-maleimide) on released thiols was published (**Scheme 8**).[223] In this antibody labelling, selenocystamine was applied as a catalyst precursor, DTT or TCEP were applied as reductants. Since alkylselenols were applied as catalysts in antibody reduction, benzeneselenols also displayed great potential here. Due to the delocalisation effect of phenyl ring, the benzeneselenolate ion is more stable compared to the alkylselenolates. Benzeneselenols are also better leaving groups than alkylselenols. For example, benzeneselenols were once applied together with dithiophenolmaleimides to deliver *in situ* disulfide bridging on peptide somatostatin. The thiophenol, released from dithiophenolmaleimide during bioconjugation, worked as the reducing agent with the selenol to co-reduce the peptide.[224] The *in situ* disulfide bridging was further carried out on IgG1 antibody using benzeneselenols and dithiophenolmaleimides to give an average DAR of 4.[225] As benzeneselenols are air sensitive, diphenyl diselenides could be applied as a precursor which would be *in situ* reduced with TCEP.[226] However, even if the benzeneselenol has displayed great potential in chemical biology, it is also very toxic, volatile and intensely malodorous, which remains as a concern.
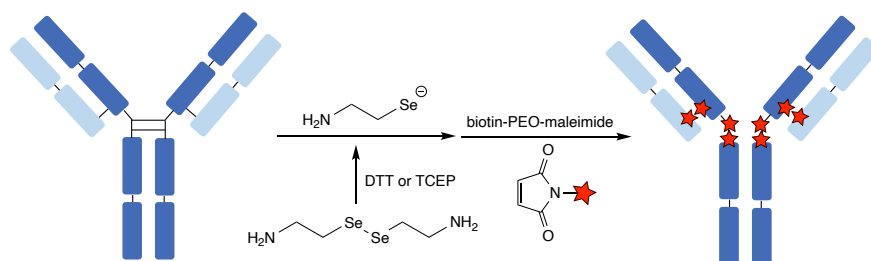
Scheme 8 – Selenol-catalysed reduction and thio-labelling on disulfide bonds.[223]

Chapter 2: Aims

The goal of this research project is to expand the scope of next generation maleimides (NGMs) and develop optimised methods for antibody bioconjugation to yield antibody conjugates with improved homogeneity.

The first aim of this project is to develop trifunctional NGM reagents for antibody conjugation. The design of trifunctional NGMs is based on a dibromomaleimide (DBM) platform and a lysine derived core, bearing two clickable handles for the incorporation of functionalities (**Figure 19**). DBMs deliver rapid antibody conjugation as well as fast self-hydrolysis to result in serum-stable conjugates under mild conditions. It has been reported that DBMs with electron withdrawing C_2 linkers hydrolyse more rapidly post conjugation. A lysine core is selected because it inserts an electron-withdrawing group to enable fast hydrolysis. Lysine molecule also has three functional groups suitable for modification. By coupling an amine group to dibromomaleic acid, the DBM core is then formed. The remaining amine and carboxylic acid on the lysine could be separately modified into two clickable handles. The clickable handles include alkynes, strained alkynes, azides and tetrazines that could undergo further bioorthogonal click reactions to incorporate functionalities.
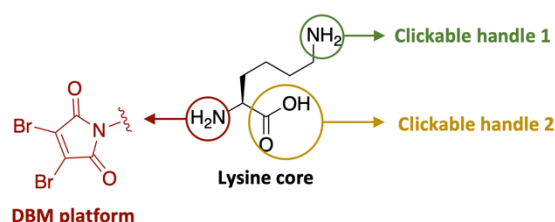

Figure 18 – Design of trifunctional DBMs.

Therefore, the designed trifunctional DBMs would undergo disulfide bridging, hydrolysis and click reactions to construct dual-modality antibody conjugates (**Figure 20**). Such dual-modality antibody conjugates could offer new opportunities in targeted cancer therapy due to the diverse potential as therapeutics, for example, with two different drugs attached, which have orthogonal modes of action to overcome drug resistance, or as 'theranostics' with a drug and an imaging agent attached.
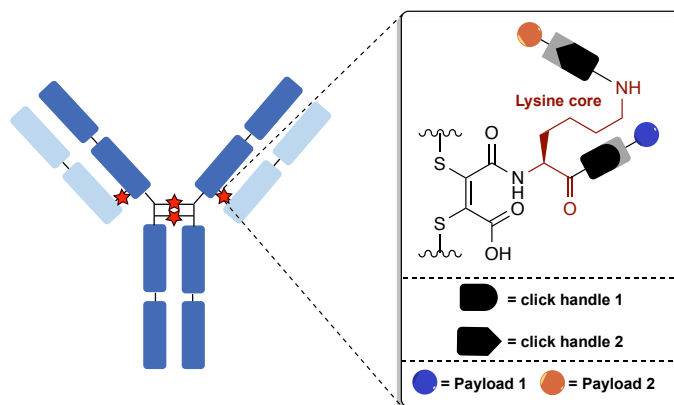
Figure 19 – The dual-modality antibody conjugate.

The second aim of this project is to attempt to optimise NGM-based antibody bioconjugation by avoiding disulfide scrambling in hinge region, to generate more homogeneous conjugates. The *in situ* technique is hypothesised to allow one-pot simultaneous reduction and bridging of disulfide bonds on antibodies, offering the greatest homogeneity in antibody conjugates. The *in situ* technique requires that no cross-reaction occurs between typical reducing agents (usually TCEP) and bridging reagents (such as NGMs). It will require a fine-tuning of the reactivity of these reagents to achieve this strategy in a robust manner. DBM *in situ* bioconjugation was not viable as DBMs demonstrating cross-reaction with TCEP. Previous attempts have shown that dithiomaleimides (DTMs) with attenuated TCEP-reactivity can be promising.[163] However, they were still not able to fully prevent disulfide scrambling or give fully bridged antibody conjugates with a reliable DAR of 4. Therefore, DTMs will be the focus of this work to attempt to optimise *in situ* bioconjugation, by generating correctly bridged full-antibody conjugates (**Figure 21**).
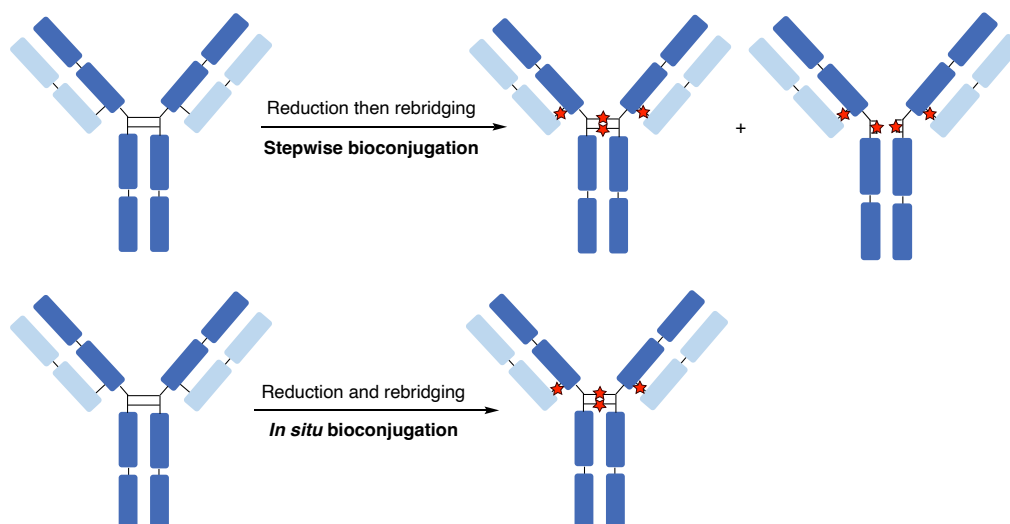
Figure 20 – a. Typical stepwise bioconjugation, b. attempted *in situ* bioconjugation.

The third aim is to develop novel reducing reagents that can also participate in *in situ* bioconjugation by enabling rapid antibody reduction, whilst delivering no cross-reaction with bridging reagents (such as NGMs). Alkylselenols (can be prepared from selenocystamine)[222] are known to offer rapid reduction on antibody fragment. However, selenocystamine might cross-react with bridging reagents (such as NGMs) *via* the amine moiety or *Se*-to-*N* transfer during *in situ* bioconjugation. Compared to alkylselenols, arylselenols (such as benzeneselenol) are better leaving groups due to the electron delocalisation effect of the phenyl ring, hence they are potentially ideal reducing reagents for *in situ* bioconjugation. However, benzeneselenols are volatile, giving an extremely pungent smell and have limited aqueous solubility, which probably limits their further applications in chemical biology. To overcome these issues, novel benzeneselenols with polar substituents (i.e. -COOH, -NH$_2$) will be designed and developed (**Figure 22**).
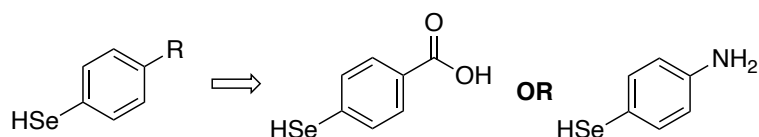

**Figure 21** – Examples of novel target benzeneselenols.

Chapter 3: Results and Discussion

3.1 Trifunctional DBMs for dual-modality antibody conjugates

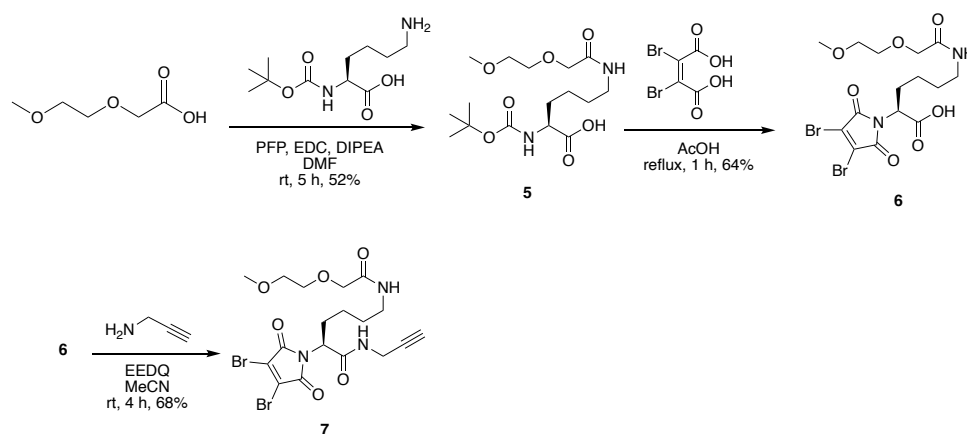### 3.1.1 Synthesis of Trifunctional DBMs

The lysine core could be conveniently exploited for the pursuit of dual-modality DBM reagents due to its trifunctionality. The *N*-terminus could be functionalised with the DBM, whilst the side-chain amine and the C-terminus could undergo amide coupling separately to introduce clickable handles (**Figure 19**, **Chapter 2**). Linear alkynes, strained alkynes and azides were considered initially as potential clickable handles, as they could undergo copper-catalysed azide-alkyne cycloaddition (CuAAC) and strain promoted azide-alkyne cycloaddition (SPAAC) reactions.[186] Tetrazines are also able to introduce functionalities *via* inverse electron-demand Diels-Alder cycloaddition (IEDDA), which could be selected as another example.[177]

The dual-alkyne trifunctional DBMs **3** and **4** were designed by connecting the amine of lysine core to a linear alkyne and the carboxylic acid to a linear or strained alkyne. The compound **1** was synthesised by coupling 4-pentynoic acid to the side-chain amine of Boc-Lysine, loading a linear alkyne to the platform. DBM-alkyne-acid **2** was then accessed by a one-pot Boc-deprotection and condensation with dibromomaleic acid. Finally, the carboxylic acid of DBM **2** was coupled to a propargylamine, to give bis-alkyne **3** which can incorporate two identical functionalities. DBM **2** was then reacted with BCN-amine to yield orthogonally clickable reagent **4** which can sequentially incorporate two different functionalities by altering the conditions of click reactions (**Scheme 9**). Due to the incorporation of a PEG group, the reagent **4** is a polar compound and needs careful purification when EEDQ is applied as the coupling reagent.
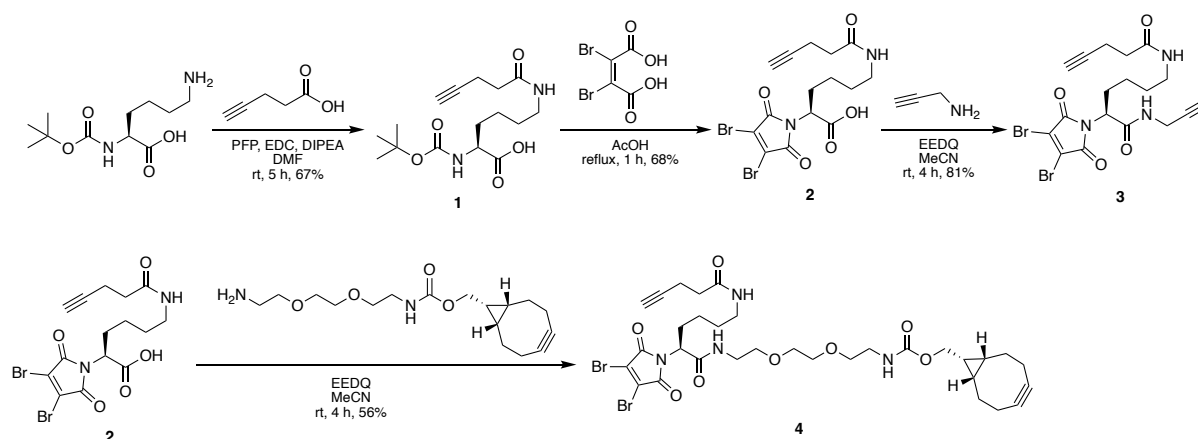
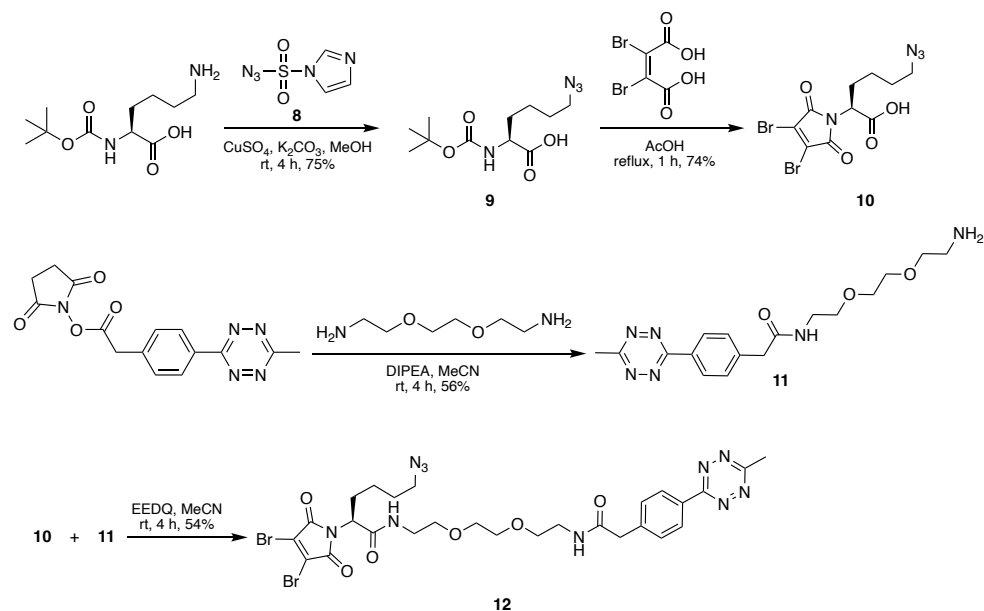**Scheme 9** – Synthesis of trifunctional DBM **3** and **4**.

Similarly, another trifunctional DBM **7** was synthesised by applying Boc-lysine and 2-(2-methoxyethoxy)acetic acid as starting materials. Similarly, compound **5** was formed by loading a PEG chain to side-chain amine of Boc-lysine and then functionalised with dibromomaleic acid to give DBM **6**. The carboxylic acid of DBM **6** was then coupled to a propargylamine, resulting in the trifunctional DBM **7** with a linear alkyne and a PEG chain (**Scheme 10**). This represents a model design for the attachment of PEGs to antibody conjugates, which has been reported to aid hydrophilicity and therapeutic indexes in antibody drug conjugates (ADCs)[227], or for half-life extension by PEGylation.[228,229]

Scheme 10 – Synthesis of trifunctional DBM **7**.

Furthermore, the compound **9** was prepared by converting the side-chain amine of Boc-Lysine to an azide using the freshly prepared imidazole-1-sulfonyl azide **8**.[230] Upon reaction with

dibromomaleic acid, the DBM-azide-acid **10** was yielded, which further reacted with previously prepared PEG-methyltetrazine **11** to generate trifunctional DBM-azide-tetrazine **12**. The reagent **11** was prepared by coupling methyl-tetrazine NHS ester to a PEG-diamine (**Scheme 11**). The prepared trifunctional DBMs **3**, **4**, **7** and **12** were then explored for disulfide bridging bioconjugation to trastuzumab Fab fragments and trastuzumab native antibodies.


Scheme 11 – Synthesis of trifunctional DBM **12**.

3.1.2 Bioconjugation of DBMs to trastuzumab Fab fragment

The monoclonal antibody trastuzumab is an FDA-approved therapeutic for the treatment of HER2+ breast cancer.[16] The trastuzumab Fab fragment was selected as a model for initial antibody functionalisation and obtained by in-house enzymatic digestion of trastuzumab (full protocol in **Chapter 5.3.4**). A sequential bioconjugation protocol, in which the reduction of the disulfide bond was followed by the addition of bridging reagents without intermediate purification, was applied. To attach model payloads and to aid analysis by UV-Vis spectrometry, photostable and water-soluble fluorophores Azide-Fluor 488 (AF488) with a maximum absorbance at 501 nm, Sulfo-Cy5.5-azide (Cy5.5-azide) with a maximum absorbance at 673 nm and 5-carboxyfluorescein-PEG$_3$-BCN (BCN-Fluor) with a maximum absorbance at 494 nm were chosen. A TCO-biotin was also selected as a further model
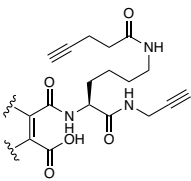
payload, notably biotin-containing conjugates have been reported to be favourably assimilated by tumour cells *via* over-expressed biotin-selective transporters.[231,232]
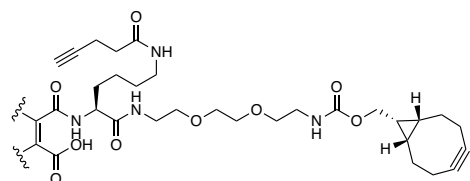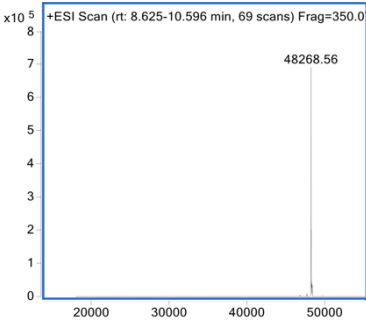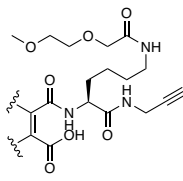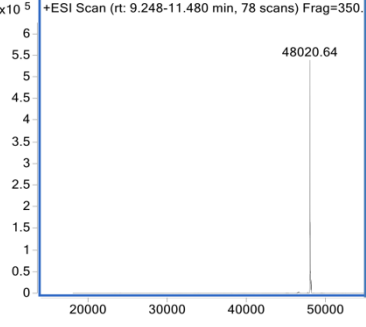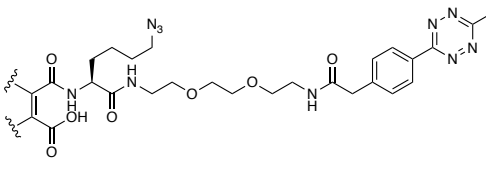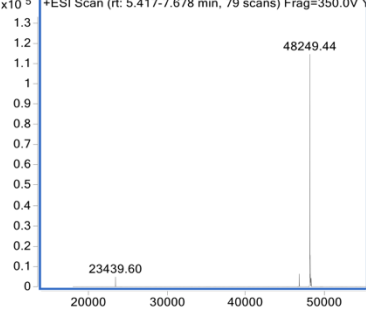
Trastuzumab Fab was reduced with TCEP, and then bridged with DBMs **3**, **4**, **7** and **12**. The resultant Fab conjugates were further hydrolysed to obtain enhanced serum stability (**Scheme 12**). The prepared Fab conjugates were analysed by LC-MS and confirmed to have one moiety loaded (**Table 4**). Fab bridging resulted in clean conjugates on LC-MS, where conjugate **16** showed a very small amount of unconjugated light chains and light chain dimers. The LC-MS of conjugate **16** in the sequential click reactions also showed a small peak corresponding to unreacted light chains. SDS-PAGE of all the bridged conjugates (even conjugate **16**) displayed <10% unmodified heavy and light chains according to densitometry measurement (**Figure 23**).
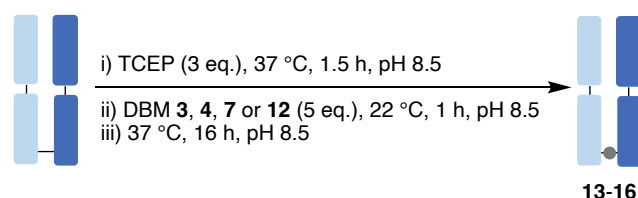
Scheme 12 – Preparation of Fab conjugates **13**-**16**: i) 3 eq. of TCEP, 37 °C, 1.5 h, pH 8.5, ii) 5 eq. of DBMs, 22 °C, 1 h, pH 8.5, iii) 37 °C, 16 h, pH 8.5.

Table 4 – LC-MS of Fab conjugates **13**-**16**.

● =	LC-MS	Mass Expected	Mass Observed
13		47999	48001

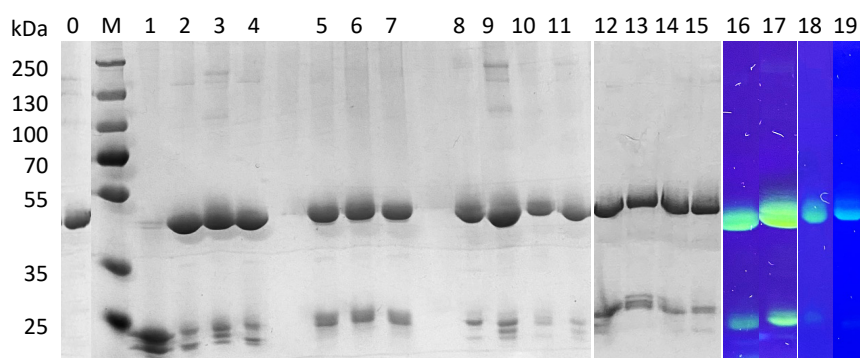|			
14		48268	48269
15		48035	48021
16		48250	48249

Figure 22 – SDS-PAGE of Fab conjugates (spaces left between lanes cut from different gels): M. Protein ladder, 0. Native Fab, 1. Reduced Fab, 2. Fab conjugate **13**, 3. Fab conjugate **14**, 4. Fab conjugate **15**, 5. Fab conjugate **13** (DTT), 6. Fab conjugate **14** (DTT), 7. Fab conjugate **15** (DTT), 8. Fab conjugate **17**, 9. Fab conjugate **19**, 10. Fab conjugate **18**, 11. Fab conjugate **20**, 12. Fab conjugate **16**, 13. Fab conjugate **16** (DTT), 14. Fab conjugate **21**, 15. Fab

conjugate **22**, 16. Fab conjugate **17** (UV), 17. Fab conjugate **20** (UV), 18. Fab conjugate **18** (UV), 19. Fab conjugate **22** (UV).

The resulting Fab-DBM conjugates **13** and **15** were further functionalised with AF488 *via* CuAAC to give Fab-DBM-AF488 conjugates **17** and **18** (**Scheme 13**). CuAAC protocols were adopted from Maruani *et al.*[233] and further optimised by adjusting the reaction temperature and the equivalents of ligand THPTA, pre-catalyst $CuSO_4$ and reductant sodium ascorbate.[234] The prepared Fab conjugates were analysed by LC-MS and confirmed to have one target moiety loaded (**Table 5**). SDS-PAGE under UV-Vis analysis (**Figure 23**) also confirmed the successful attachments of fluorophores.
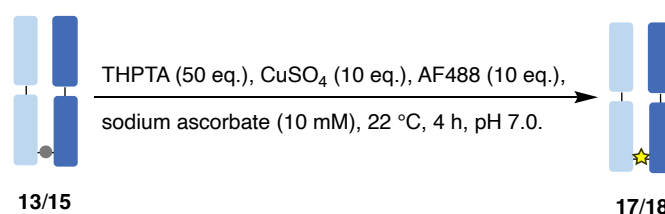
Scheme 13 – CuAAC on conjugates **13** or **15**: 50 eq. of THPTA, 10 eq. of $CuSO_4$, 10 eq. of AF488, 10 mM sodium ascorbate, 22 °C, 4 h, pH 7.0.

Table 5 – LC-MS of Fab conjugates **17**-**18**.

⭐ =	LC-MS	Mass Expected	Mass Observed
17		49146	49147

18		48608	48595
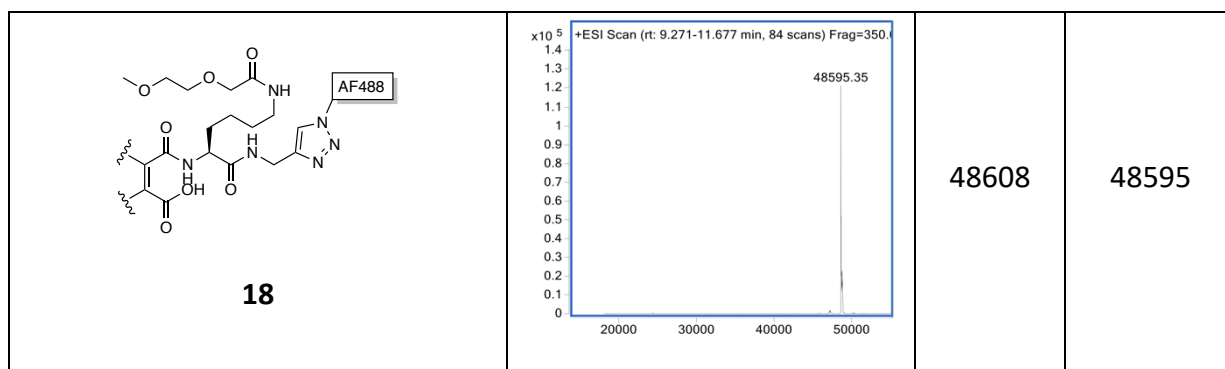
In addition, to further determine the fluorophore-to-antibody ratio (FAR) based on extinction coefficients of fluorophores and antibodies,[235] UV-Vis spectroscopy (900-200 nm) was performed on Fab-DBM-AF488 conjugate **17** and **18**. However, two absorption bumps were observed near the wavelength of maximum AF488 absorbance (501 nm) on the spectrum of conjugate **17** (**Figure 24a**) whilst the spectrum of conjugate **18** only showed one absorption bump (**Figure 24b**). The possible reason could be that the absorption of some attached fluorophores on conjugate **17** blue-shifted. Compared to conjugate **18**, conjugate **17** has two attached AF488 per disulfide bond. The two attached fluorophores are theoretically supposed to absorb at the same wavelength, however, they can potentially aggregate with each other, showing shifted absorption wavelength compared to original monomers.[236] It did not prove possible to calculate the FAR of conjugate **17** accurately, based on the shifted absorption of fluorophores. Hence, the UV-Vis spectra were displayed instead to demonstrate the attachments of fluorophores. Similar outcomes were also observed in the following trastuzumab-fluorophore conjugates, so their UV-Vis spectra were again just used to provide evidence for the attachments of fluorophores (see **Chapter 5**).
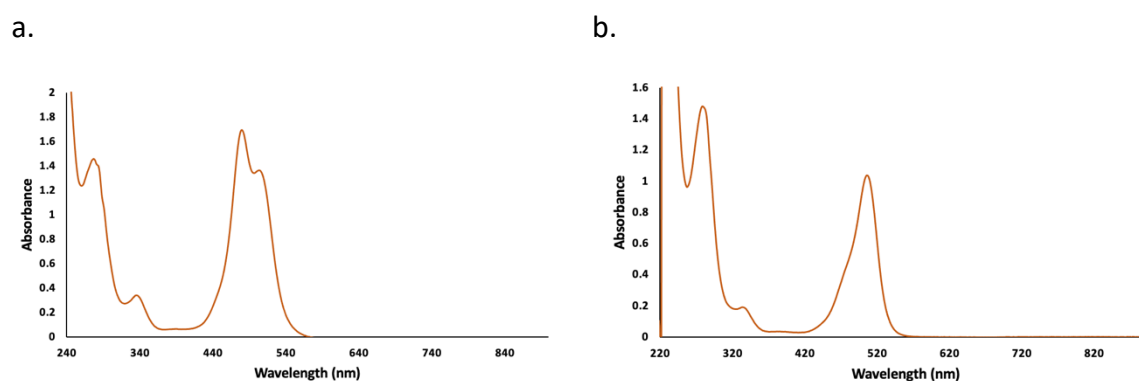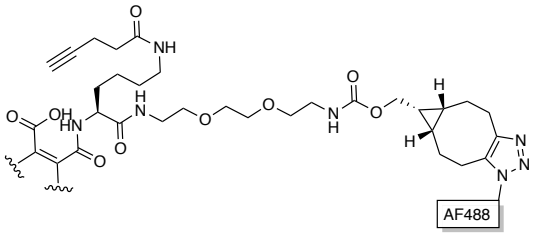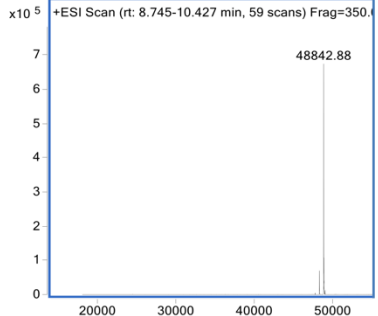
a.

b.

Figure 23 – UV-Vis spectra of a. Fab conjugates **17**, b. Fab conjugate **18**.

The Fab-DBM conjugate **14** was then functionalised with AF488 *via* SPAAC to generate Fab-DBM-AF488 conjugate **19**. The Fab-DBM-AF488 conjugate **19** further incorporated Cy5.5-azide to yield a dual-modality conjugate **20** (**Scheme 14**). The prepared Fab conjugates were analysed by LC-MS and confirmed to have the target moiety loaded (**Table 6**). The conjugate **19** showed a small amount of unmodified conjugate as the attached strained alkyne was oxidised over the course of the post-conjugation hydrolysis. SDS-PAGE under UV lamp (**Figure 23**) and UV-Vis spectroscopy confirmed the successful attachments of fluorophores (**Figure S11**-**S12**, **Chapter 5**).
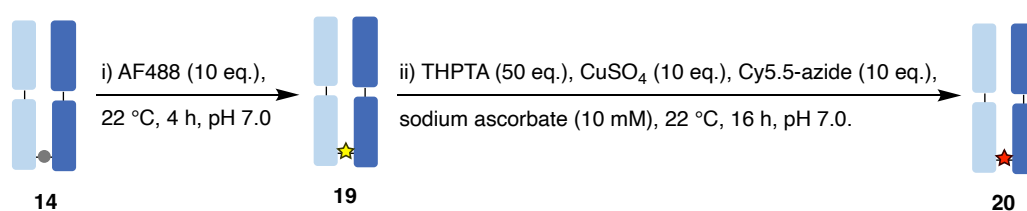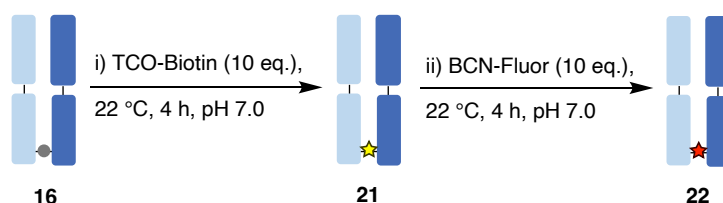

Scheme 14 – Preparation of dual-modality conjugate **20**: i) 10 eq. of AF488, 22 °C, 4 h, pH 7.0, ii) 50 eq. of THPTA, 10 eq. of CuSO$_4$, 10 eq. of Cy5.5-azide, 10 mM sodium ascorbate, 22 °C, 16 h, pH 7.0.

Table 6 – LC-MS of Fab conjugates **19**-**20**.

⭐ or ⭐ =	LC-MS	Mass Expected	Mass Observed
19		48842	48843

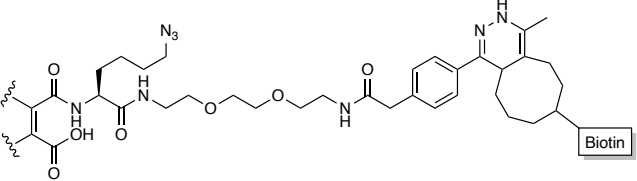|		Mass Expected	Mass Observed
20		49826	49830
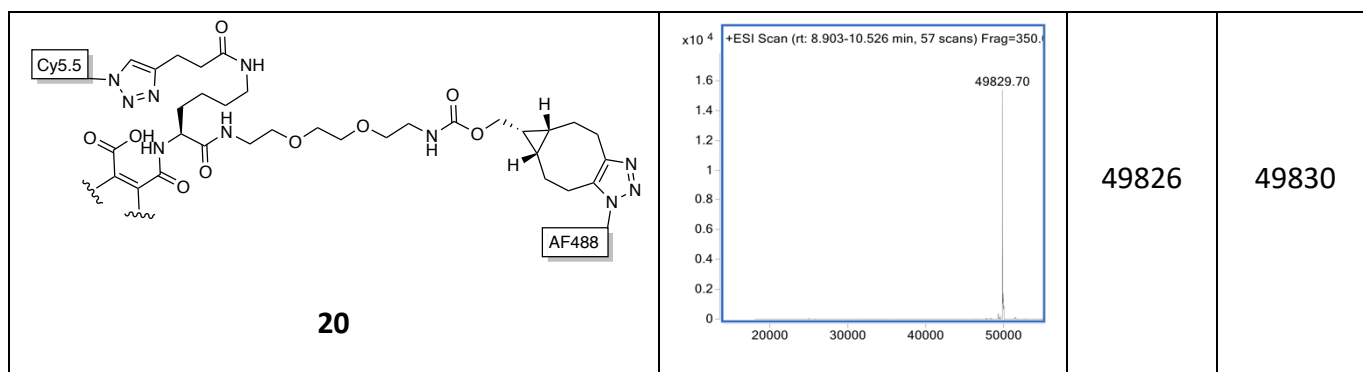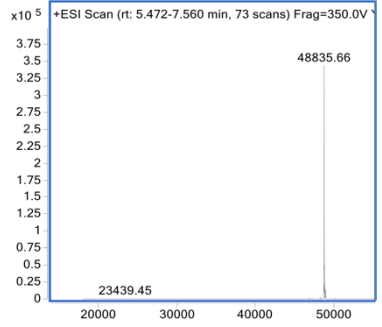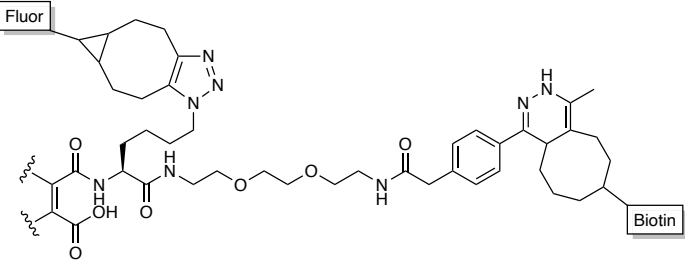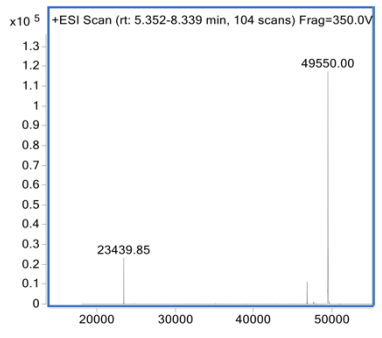
The tetrazine handle of Fab-DBM conjugate **16** allowed the attachment of a trans-cyclooctene (TCO)-Biotin to yield Fab-DBM-Biotin conjugate **21** *via* IEDDA.[177] The Fab-DBM-Biotin conjugate **20** further incorporated BCN-fluor to yield dual-modality conjugate **22** (**Scheme 15**). The conjugate **22** showed unmodified light chains and light chain dimers, which were <10% by densitometry analysis. The prepared Fab conjugates were analysed by LC-MS and confirmed to have one target moiety loaded (**Table 7**). The successful attachments of fluorophores were also monitored by SDS-PAGE under UV lamp (**Figure 23**) and UV-Vis spectroscopy (**Figure S14**, **Chapter 5**).

Scheme 15 – Preparation of dual-modality conjugate **22**: i) 10 eq. of TCO-Biotin, 22 °C, 4 h, pH 7.0, ii) 10 eq. of BCN-Fluor, 22 °C, 4 h, pH 7.0.

Table 7 – LC-MS of Fab conjugates **21**-**22**.

⭐ or ⭐ =	LC-MS	Mass Expected	Mass Observed

Structure	LC-MS	Calc.	Found
21		48836	48836
22		49563	49550

Dual functionalisation was successfully achieved on trastuzumab Fab, which demonstrated the trifunctionality of the prepared DBMs, and this protocol could be further applied on the trastuzumab full antibody. Of all these click strategies, copper-free click reactions are more efficient and resulted in the cleanest LC-MS as leftover copper ions distorted the LC-MS.

To test the antigen binding activity of bridged Fab conjugates, enzyme-linked immunosorbent assay (ELISA) was performed on both native Fab and Fab-DBM conjugate **14**. A 96-well polystyrene plate was coated first with HER2 antigen at 4 °C for 16 h. Following that, native Fab and Fab conjugate **14** were applied to it. Upon completing the incubation time with a secondary antibody linked to the enzyme horseradish peroxidase (HRP), o-phenylenediamine HCl was added to quench the reaction. This was converted to 2,3-diaminophenazine by HRP, which shows strong absorbance at 490 nm, allowing for spectrophotometric quantification of the antigen-binding activity of native Fab and the Fab conjugate **14**. The Fab conjugate **14** showed comparable antigen binding activity to the native Fab (**Figure 25**). Previous reports exploring bridging of IgG1 interchain disulfide residues showed little to no impact on antigen binding, which is in line with results in this study.[237]
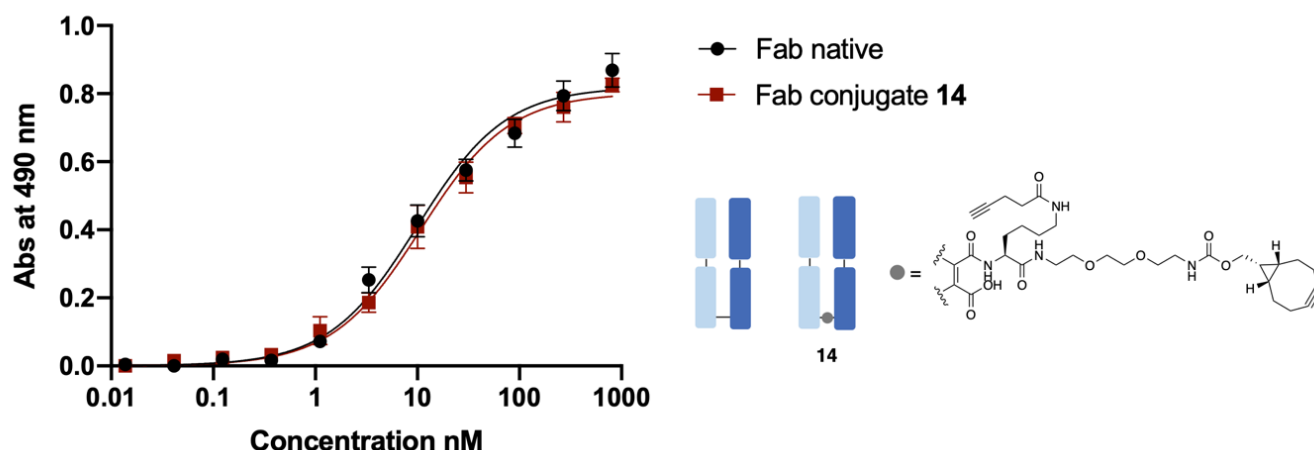
Figure 24 – Binding activity to HER2 of trastuzumab native Fab and Fab conjugate **14** over concentration ranges from 0.0137-810 nM, absorbance was measured at 490 nm.
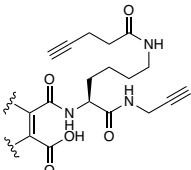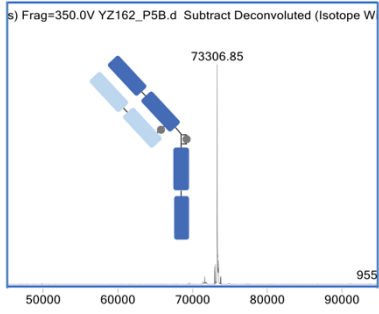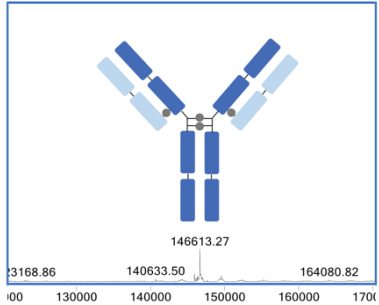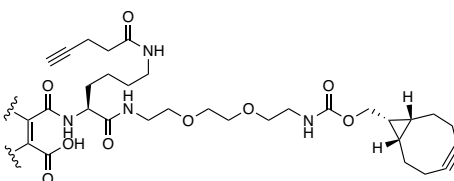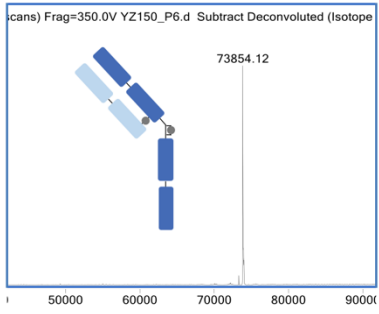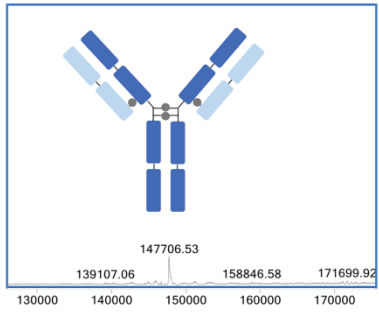
3.1.2 Bioconjugation of DBMs to trastuzumab native antibody
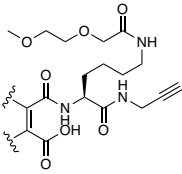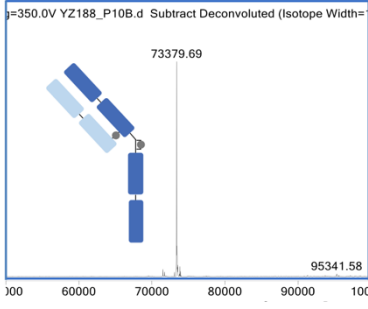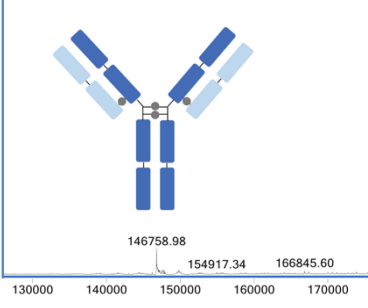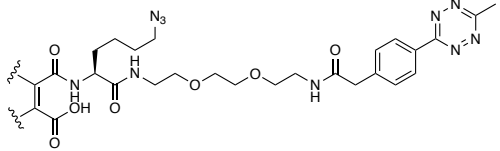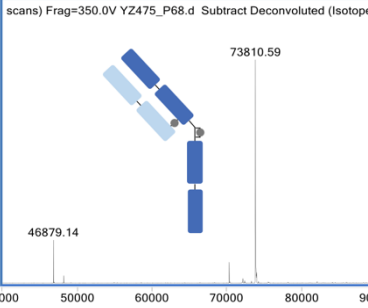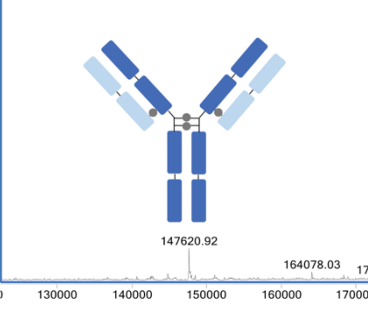
Similarly, trastuzumab was bridged with trifunctional DBMs **3**, **4**, **7** and **12**, generating Ab-DBM conjugates **23**, **24**, **25** and **26** (**Scheme 16**). The prepared Ab conjugates were analysed by LC-MS and confirmed that four disulfide bonds were fully bridged (**Table 8**). LC-MS of conjugate **26** showed a small amount of unmodified light chains left after bridging, whilst LC-MS of other conjugates all showed clean conjugation, with the expected mixture of full antibody with 4+4 attachments and the half-antibody with 2+2 attachments (full LC-MS spectra of trastuzumab antibody displayed in **Chapter 5**). The half-antibody conjugates are observed due to well-known hinge disulfide scrambling, and only detectable due to harsh denaturing conditions of LC-MS.[238] Due to densitometry analysis of SDS-PAGE, the ratio of full-antibody and half-antibody conjugates was 7:3, and bridged conjugates demonstrated <10% unmodified heavy and light chains (**Figure 26**).
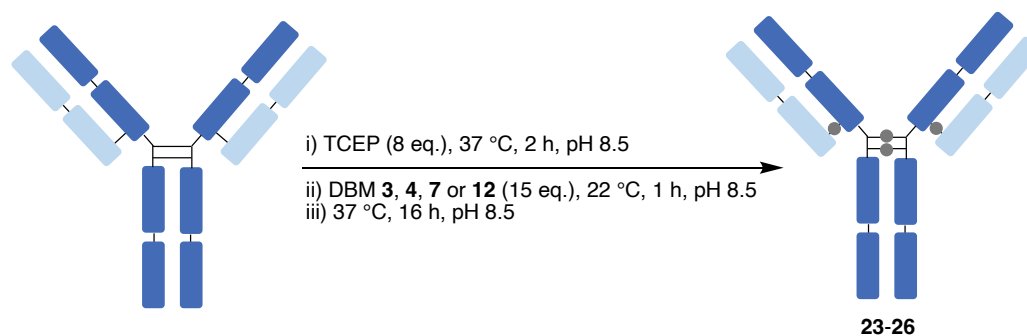
Scheme 16 – Preparation of Ab conjugates **23**-**26**: i) 8 eq. of TCEP, 37 °C, 2 h, pH 8.5, ii) 15 eq. of DBMs, 22 °C, 1 h, pH 8.5, iii) 37 °C, 16 h, pH 8.5.

Table 8 – LC-MS of Ab conjugates **23**-**26**.

● =	LC-MS	Mass Expected	Mass Observed
23		73316	73307
		146631	146613
24		73855	73854
		147707	147707

25		73388	73380
		146775	146759
26		73819	73811
		147635	147621
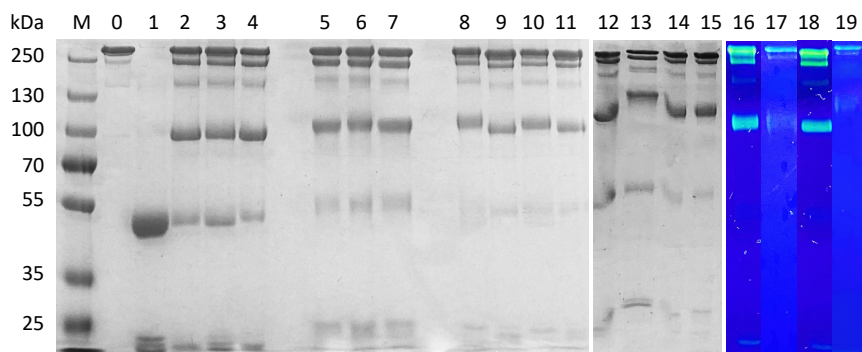
Figure 25 – SDS-PAGE of Ab conjugates (spaces left between lanes cut from different gels): M. Protein ladder, 0. Native Ab, 1. Reduced Ab, 2. Ab conjugate **23**, 3. Ab conjugate **24**, 4. Ab conjugate **25**, 5. Ab conjugate **23** (DTT), 6. Ab conjugate **24** (DTT), 7. Ab conjugate **25** (DTT), 8. Ab conjugate **27**, 9. Ab conjugate **29**, 10. Ab conjugate **28**, 11. Ab conjugate **30**, 12. Ab conjugate **26**, 13. Ab conjugate **26** (DTT), 14. Ab conjugate **31**, 15. Ab conjugate **32**, 16. Ab conjugate **27** (UV), 17. Ab conjugate **30** (UV), 18. Ab conjugate **28** (UV), 19. Ab conjugate **32** (UV).
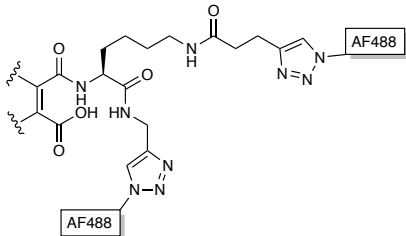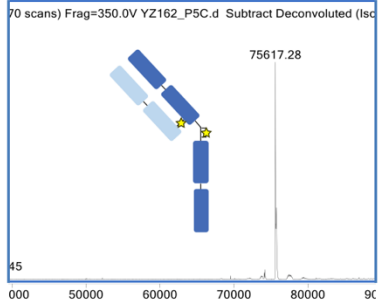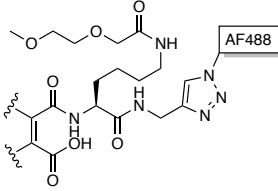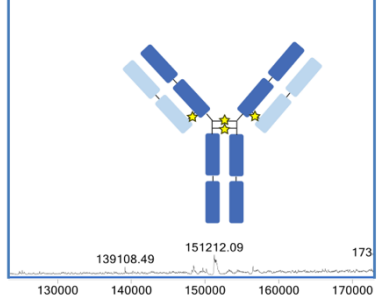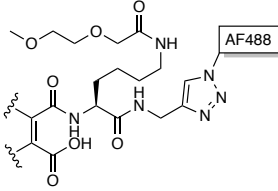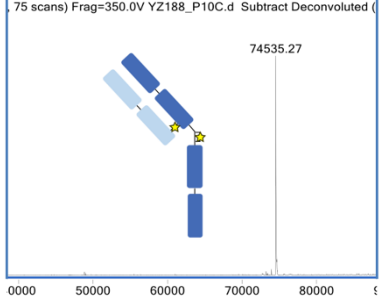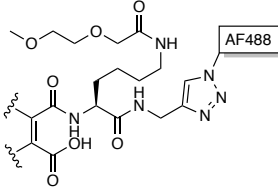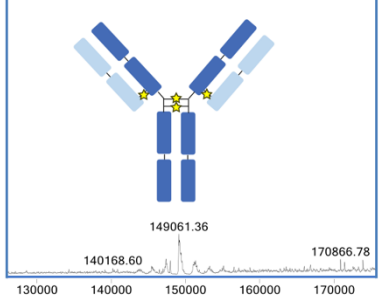
The resulting Ab-DBM conjugates **23** and **25** were further functionalised with AF488 *via* CuAAC, yielding Ab-DBM-AF488 conjugates **27** and **28** (**Scheme 17**). The prepared Ab conjugates were analysed by LC-MS and confirmed to have four moieties loaded (**Table 9**). The attachments of fluorophores were also confirmed by SDS-PAGE under UV lamp (**Figure 26**) and UV-Vis spectroscopy (**Figure S21**-**S22**, **Chapter 5**).
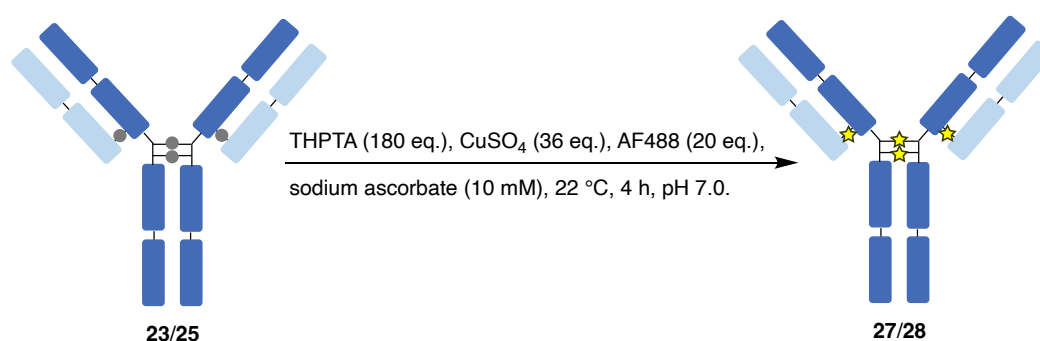
Scheme 17 – CuAAC on conjugates **23** or **25**: 180 eq. of THPTA, 36 eq. of CuSO$_4$, 20 eq. of AF488, 10 mM sodium ascorbate, 22 °C, 4 h, pH 7.0.

Table 9 – LC-MS of Ab conjugates **27**-**28**.

☆ =	LC-MS	Mass Expected	Mass Observed

Structure	Spectrum		
27		75613	75617
		151225	151212
28		74537	74535
		149072	149061

The Ab-DBM conjugate **24** was then functionalised with AF488 *via* SPAAC to generate Ab-DBM-AF488 conjugate **29**. The Ab-DBM-AF488 conjugate **29** further incorporated another AF488 to yield antibody conjugate **30** as the introduction of a different fluorophore Cy5.5-azide was unsuccessful due to potential steric hinderance (**Scheme 18**). The prepared Ab conjugates were analysed by LC-MS and confirmed that each disulfide bond has two AF488 moieties attached (**Table 10**). LC-MS of conjugate **29** showed minor incomplete modification, due to the oxidation of the attached strained alkyne. The attachments of fluorophores were

also monitored by SDS-PAGE under UV lamp (**Figure 26**) and UV-Vis spectroscopy (**Figure S23**-**S24**, **Chapter 5**).
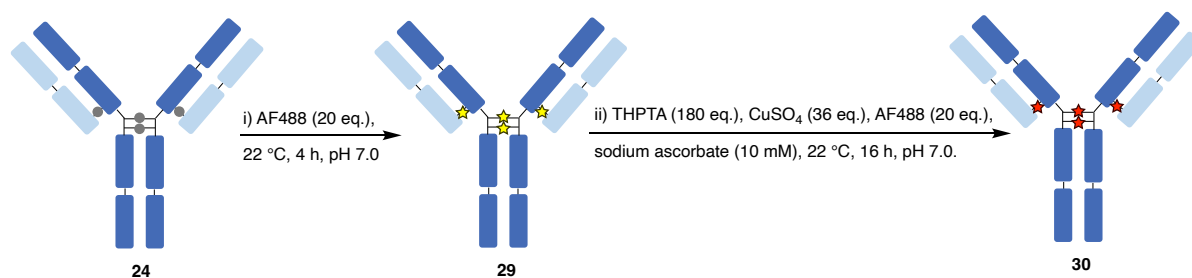
Scheme 18 – Preparation of antibody conjugate **30**: i) 20 eq. of AF488, 22 °C, 4 h, pH 7.0, ii) 180 eq. of THPTA, 36 eq. of CuSO$_4$, 20 eq. of AF488, 10 mM sodium ascorbate, 22 °C, 16 h, pH 7.0.

Table 10 – LC-MS of Ab conjugates **29**-**30**.

⭐ or ⭐ =	LC-MS	Mass Expected	Mass Observed
29		75003	74995
		150004	149988

| | | 76152 | 76149 |
| | | 152301 | 152288 |
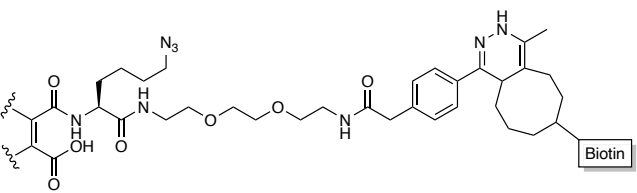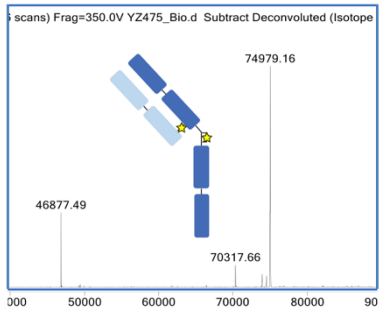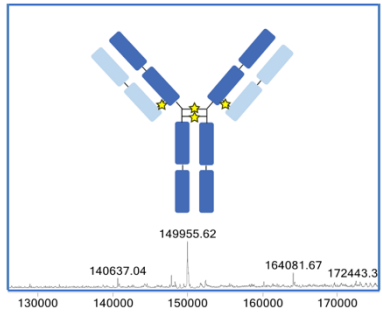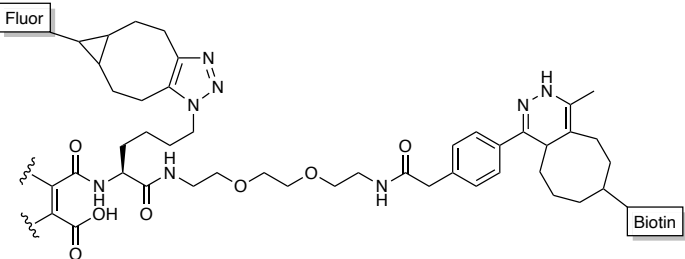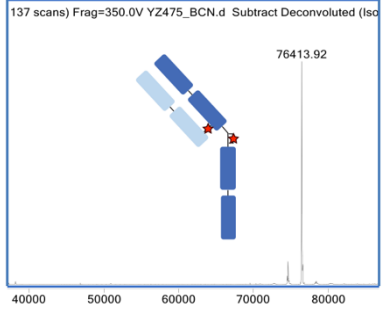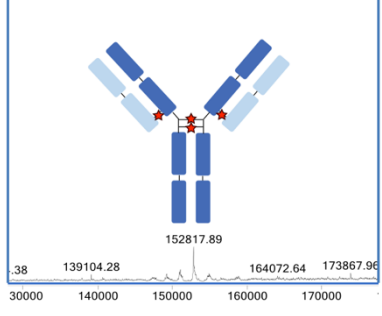
TCO-Biotin was introduced to the tetrazine handle of Ab-DBM conjugate **26** to yield Ab-DBM-Biotin conjugate **31**. The Ab-DBM-Biotin conjugate **31** further incorporated BCN-fluor to yield dual-modality conjugate **32** (**Scheme 19**). The prepared Ab conjugates were analysed by LC-MS and confirmed that each disulfide bond had two functionalities attached (**Table 11**). LC-MS of conjugate **31** and conjugate **32** showed unidentified species possibly due to the decomposition of the TCO reagent, and they were insignificant compared to the main species. SDS-PAGE under UV lamp (**Figure 26**) and UV-Vis spectroscopy confirmed the successful attachments of fluorophores (**Figure S26**, **Chapter 5**).
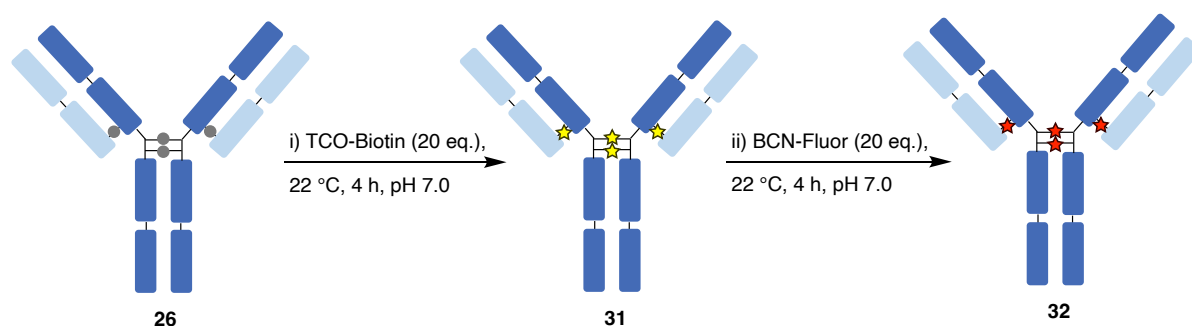
Scheme 19 – Preparation of dual-modality conjugate **32**: i) 20 eq. of TCO-Biotin, 22 °C, 4 h, pH 7.0, ii) 20 eq. of BCN-Fluor, 22 °C, 4 h, pH 7.0.

Table 11 – LC-MS of Ab conjugates **31**-**32**.

⭐ or 🔴 =	LC-MS	Mass Expected	Mass Observed
31		74992	74979
		149980	149956
32		76445	76414
		152885	152818

Although the dual-functionalisation of DBM-alkyne-BCN **4** on trastuzumab antibody encountered issues in the CuAAC step, it did exhibit effective performance on trastuzumab Fab to demonstrate the trifunctionality. The DBM-azide-tetrazine **12** successfully introduced

52

a biotin and a fluorescein to both trastuzumab Fab and full antibody *via* IEDDA and SPAAC reactions. Hence, CuAAC reactions showed limited efficiency compared to IEDDA and SPAAC reactions under similar biologic conditions. Among these click reaction, only CuAAC requires catalyst, which could possibly affect the reaction efficiency.

In summary, a new DBM-derived scaffold built around a lysine core, has been developed to deliver robustly stable dual-modality antibody conjugates with four loadings *via* well-tolerated 'click' chemistry. The trifunctional DBMs, composed of two clickable handles, were bioconjugated to trastuzumab Fab and full antibody. The resultant conjugates further underwent bioorthogonal click reactions to incorporate functional payloads. It is envisaged that such dual-modality antibody conjugates could provide enhanced therapeutic windows for cancer treatments.

3.2 Antibody-DFO conjugates

Desferrioxamine B (DFO), a metal chelator, was discovered in the late 1950s as a natural tris-hydroxamate siderophore and a growth-promoting agent secreted by *Streptomyces pilosus,* a soil bacterium firstly isolated in Rome, to acquire ferric ions from the environment.[239] The exquisite affinity of DFO for Fe(III) identified its potential for removing excess iron from patients with transfusion-dependent hemoglobin disorders.[240] DFO also showed binding affinity to Zr(IV), which is a radioactive isotope that can be harnessed for application in the development of positron emission tomography (PET).[241] PET is a functional imaging technique that provides sensitive, quantitative, and non-invasive images of various molecular processes and targets.[242] Therefore, DFO conjugates can be traced *in vivo* with PET (**Figure 27a**).[243] As part of an ongoing project into dibromomaleimide (DBM)-DFO for antibody labelling and imaging between our group and Dr Michelle Ma's group at King's College London,[243] we were interested to prepare and optimise antibody-DFO conjugates. The DFO reagents DBM-DFO and azide-DFO were kindly prepared by Dr Matthew Farleigh (**Figure 27b**).

a.
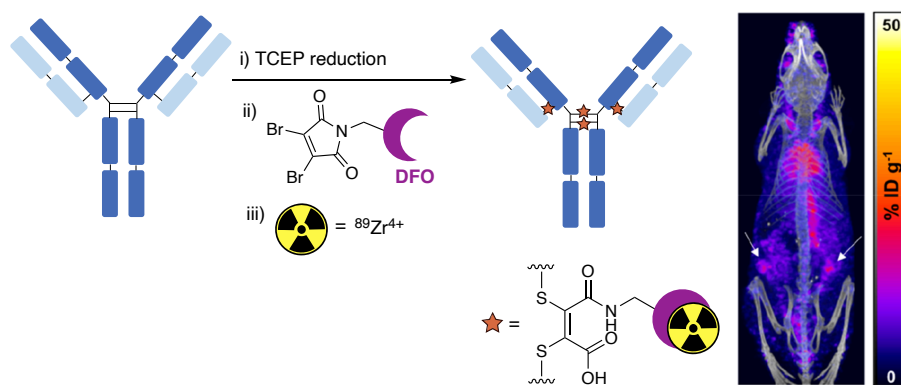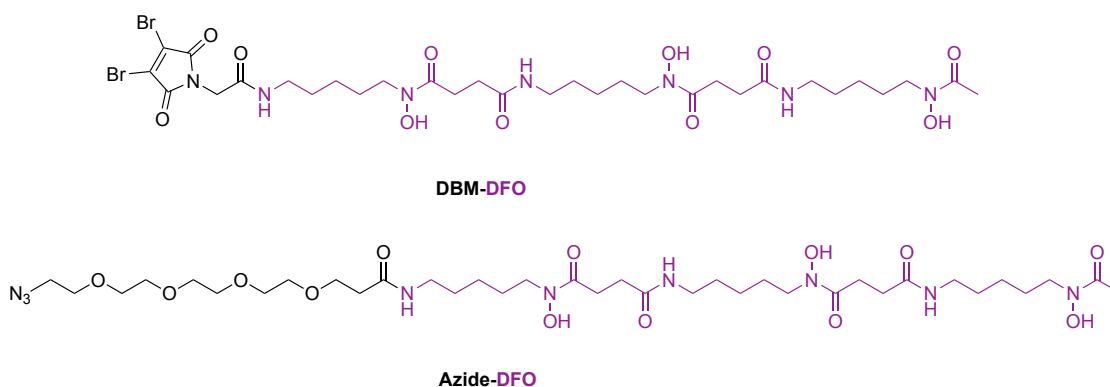
Figure 26 – a. Tracing DFO *in vivo* using PET,[243] b. structure of DBM-DFO and azide-DFO (DFO moiety in purple).

3.2.1 Bioconjugation of DBM-DFO to trastuzumab native antibody

To generate DFO antibody conjugates, DBM-DFO was applied by Dr Matthew Farleigh on the full antibody using the pH 8.5 protocol which has been optimised for DBMs.[244] Due to incomplete conjugation, the pH 8.5 protocol delivered a heterogeneous mixture of antibody-DFO conjugates containing two to four DFO moieties per antibody and unmodified species (**Figure 28a**).[243] It is possible that the DBM-DFO reagents are too bulky which would result in slow disulfide bridging due to steric hinderance. As *N*-C$_2$ linker DBMs, DBM-DFO reagents can also deliver fast hydrolysis at pH 8.5, leading to maleamic acids with no thiol reactivity.[235] Hence, both slower bridging and competing hydrolysis could possibly cause incomplete antibody conjugation. To resolve this issue, the rate of DBM hydrolysis could be reduced by lowering the pH. To generate more homogeneous antibody-DFO conjugates, the antibody bioconjugation at lower pH has been attempted in this project where pH 6.0 protocol showed

promising results by respectively adding 10 eq., 20 eq., 30 eq. and 40 eq. of DBM-DFO to the full antibody, generating the same Ab-DFO conjugate **33** (**Figure 28b**). The resultant Ab-DFO conjugates were analysed by SDS-PAGE (**Figure 28c**) and LC-MS (**Figure 28d**). The 10 eq. attempt showed ~30% of unmodified heavy and light chains whilst 20-40 eq. attempts showed ~15% unmodified heavy and light chains from densitometry analysis. After post-conjugation hydrolysis, all the Ab-DBM-DFO conjugates gave ~15% of unreacted heavy and light chains in SDS-PAGE. According to the LC-MS of 40 eq. attempt (10-30 eq. attempts in **Figure S27**-**S29**, **Chapter 5**), it results in a major product with 2 additions on HL and 4 additions on HHLL, and a minor product with 1 addition on HL and 2 additions on HHLL. However, the masses seen on LC-MS did not correspond to the expected mass of the bridged conjugate, which is also observed in Dr Matthew Farleigh's results. The extra mass could be caused by the chelator DFO moiety coordinating to free metals from buffers, or being an artifact created during the LC-MS analysis. Another reason could be the DBM-DFO reagent was contaminated with metals during storage and transport prior to bioconjugation.

a.
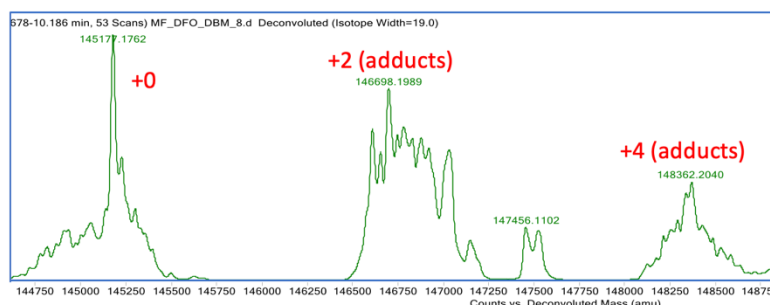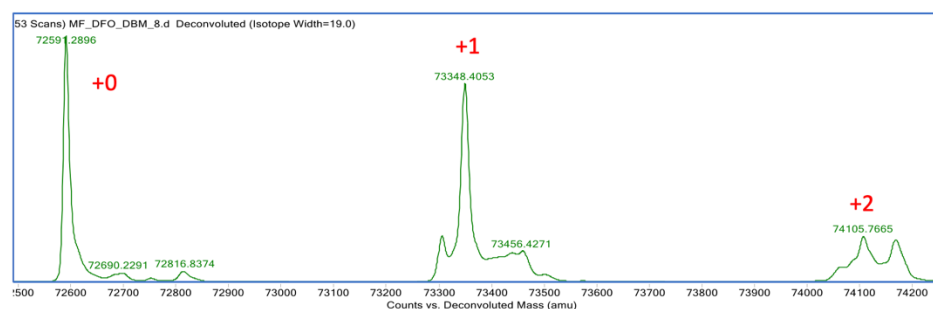
b.   c.
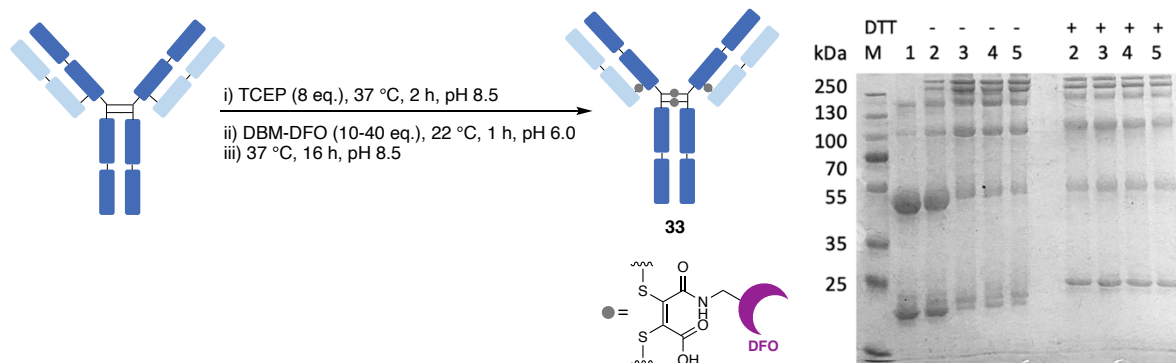
d.
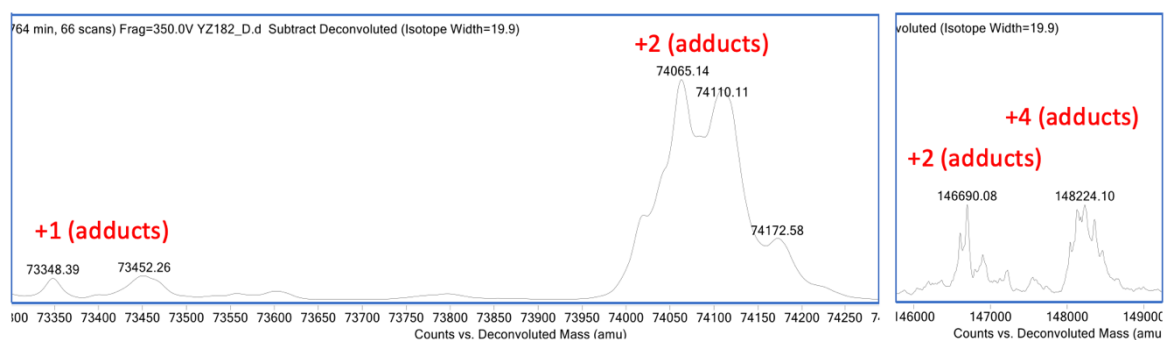
Figure 27 – a. Dr Matthew Farleigh's LC-MS of Ab-DBM-DFO conjugate: HL expected 74021 Da, observed 72591 Da (native HL), 73348 Da (+1 moiety), 74106 Da (+2 moieties), HHLL expected 148039 Da, observed 145177 Da (native HHLL), 146698 Da (+2 moieties with adducts), 148362 Da (+4 moieties with adducts), b. Preparation of Ab-DBM-DFO conjugate **33** using DBM-DFO: i) 8 eq. of TCEP, 37 °C, 2 h, pH 8.5, ii) 10-40 eq. of DBMs, 22 °C, 1 h, pH 6.0, iii) 37 °C, 16 h, pH 8.5; c. SDS-PAGE of Ab-DBM-DFO conjugate **33** (10-40 eq.): M. Protein ladder, 1. Reduced Ab, 2. 10eq. DBM-DFO, 3. 20eq. DBM-DFO, 4. 30eq. DBM-DFO, 5. 40eq. DBM-DFO; d. LC-MS of Ab-DBM-DFO conjugate **33** (40 eq.): HL expected 74021 Da, observed 73348 Da (+1 moiety with adducts), 74065 Da (+2 moieties with adducts), HHLL expected 148039 Da, observed 146690 Da (+2 moieties with adducts), 148224 Da (+4 moieties with adducts).

3.2.2 Incorporation of azide-DFO to trastuzumab native antibody

Since the antibody conjugation of DBM-DFO was unable to deliver clean conjugates, azide-DFO was applied to generate DFO conjugates alternatively, where a linker between the azide moiety and the antibody is necessary. The DBM and dibromopyridazinedione (diBrPD)

platforms with clickable alkyne handles, for example DBM-BCN and diBrPD-BCN (**Figure 29**), have been chosen as linkers to demonstrate useful comparison between bridging reagents in constructing antibody-DFO conjugates. DBM-BCN[161] was synthesised by Dr Nafsika Forte (UCL Chemistry) and diBrPD-BCN[128] was synthesised by Ioanna Thanasi (UCL Chemistry).
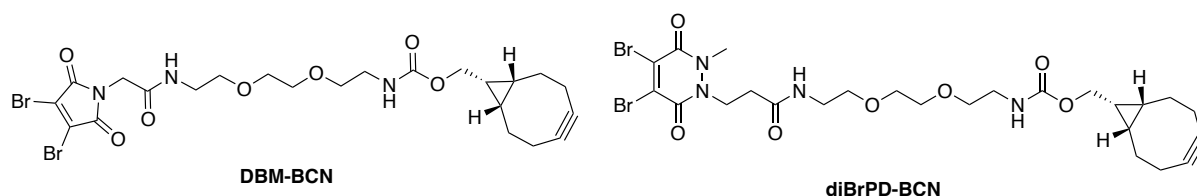
Figure 28 – Structures of DBM-BCN and diBrPD-BCN.

To optimise the condition of azide-DFO click reaction, trastuzumab Fab fragment was selected as the initial bioconjugation model. DBM-BCN was applied on reduced Fab to give a Fab-DBM conjugate **34**, which was further clicked with azide-DFO to construct the Fab-DBM-DFO conjugate **35**. However, the click reaction was incomplete at 22 °C after 4 h. The click protocol was further optimised using same equivalents of azide-DFO at 37 °C where reactions gave clean Fab-DBM-DFO conjugate **35** and confirmed by LC-MS (**Figure 30a**). Compared to the LC-MS of DFO conjugates from DBM-DFO, the azide-DFO resulted in a clean conjugate without any adducts. This also illustrated that DFO conjugates will not coordinate to metals in the LC-MS instrument under the same analytical conditions. Therefore, the initially observed increased masses in the previous DFO conjugates could be potentially caused by prior contamination in DBM-DFO. The Fab attempt was further translated on the trastuzumab antibody where the reduced antibody was bridged with DBM-BCN to give clean Ab-DBM conjugate **36** (**Figure S31**, **Chapter 5**) and then clicked with azide-DFO to yield the Ab-DBM-DFO conjugate **37** (**Figure 30b**). The resulting conjugate was confirmed by SDS-PAGE (**Figure 30c**) and LC-MS (**Figure 30d**). Whilst there is a noisy baseline, the peaks of Ab-DBM-DFO conjugate **37** are still identifiable (full spectra in **Figure S32**, **Chapter 5**).

a.
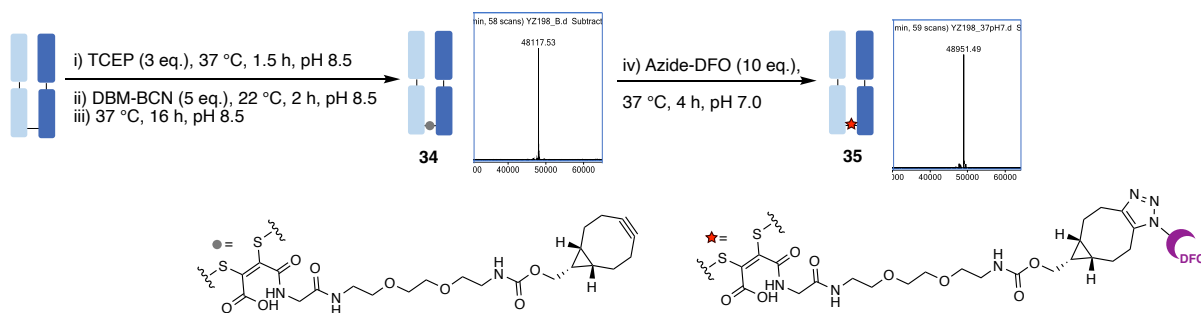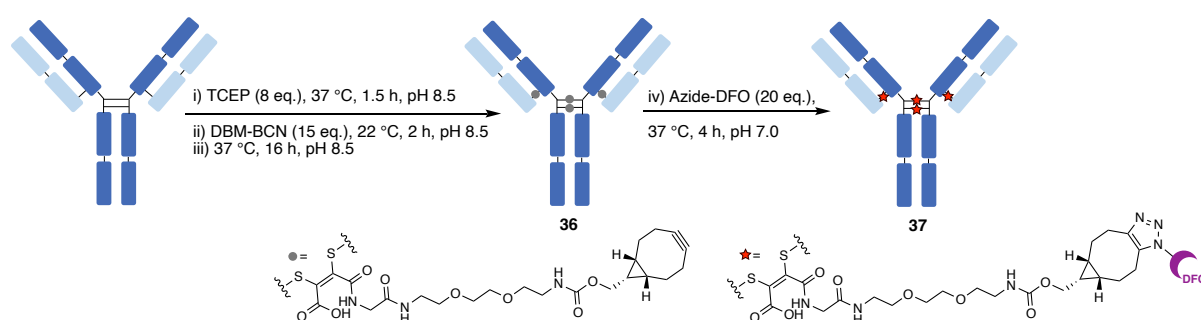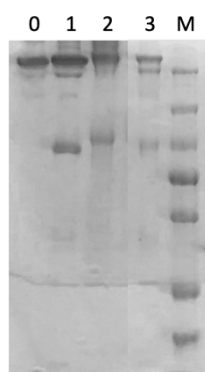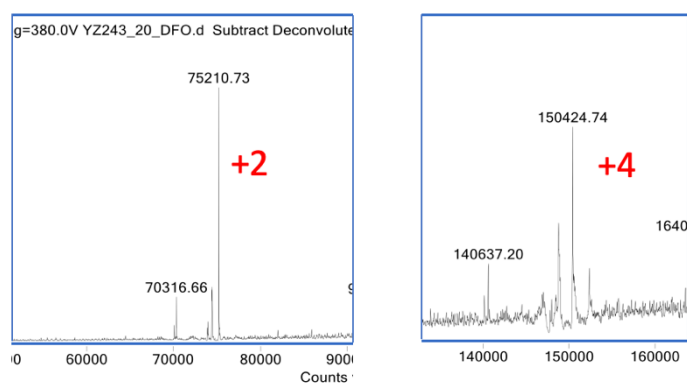
Figure 29 – a. Preparation of Fab conjugates **34** and **35**: i) 3 eq. of TCEP, 37 °C, 1.5 h, pH 8.5, ii) 5 eq. of DBM-BCN, 22 °C, 1 h, pH 8.5, iii) 37 °C, 16 h, pH 8.5, iv) 20 eq. of azide-DFO, 37 °C, 4 h, pH 7.0; LC-MS of Fab-DBM conjugate **34**: HL expected 48116 Da, observed 48118 Da; LC-MS of Fab-DBM-DFO conjugate **35**: HL expected 48948 Da, observed 48951 Da; b. Preparation of Ab conjugates **36** and **37**: i) 8 eq. of TCEP, 37 °C, 2 h, pH 8.5, ii) 15 eq. of DBM-BCN, 22 °C, 1 h, pH 8.5, iii) 37 °C, 16 h, pH 8.5, iv) 20 eq. of azide-DFO, 37 °C, 4 h, pH 7.0; c. SDS-PAGE of Ab-DFO conjugates: M. Protein ladder, 0. Native Ab, 1. Ab-diBrPD conjugate **38** 4 °C, 2. Ab-diBrPD-DFO conjugate **39** 37 °C, 3. Ab-DBM-DFO conjugate **37**; d. LC-MS of Ab-DBM-DFO conjugate **37**: HL expected 75215 Da, observed 70317 Da (LC*3),

74440 Da (+2 moieties lost 771 Da), 75211 Da (+2 moieties), HHLL expected 150429 Da, observed 140637 Da (LC*6), 148798 Da (+4 moieties lost 1627 Da), 150425 Da (+4 moieties).

Similarly, diBrPD-BCN was applied on full antibody using the optimised *in situ* protocol for PD conjugation.[128] The Ab-diBrPD conjugate **38** was then clicked with azide-DFO to yield the Ab-diBrPD-DFO conjugate **39** (**Figure 31a**). SDS-PAGE (**Figure 30c**) and LC-MS (**Figure 31b**) confirmed the resulting DFO conjugate. Compared to Ab-DBM-BCN-DFO conjugate, the Ab-diBrPD-BCN-DFO conjugate was more homogeneous due to the *in situ* antibody conjugation, which was confirmed by the cleaner SDS-PAGE and LC-MS.

a.
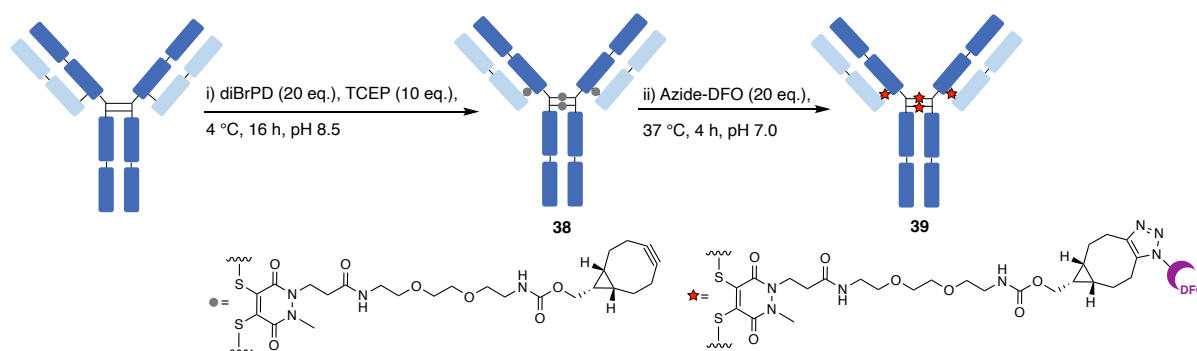
b.
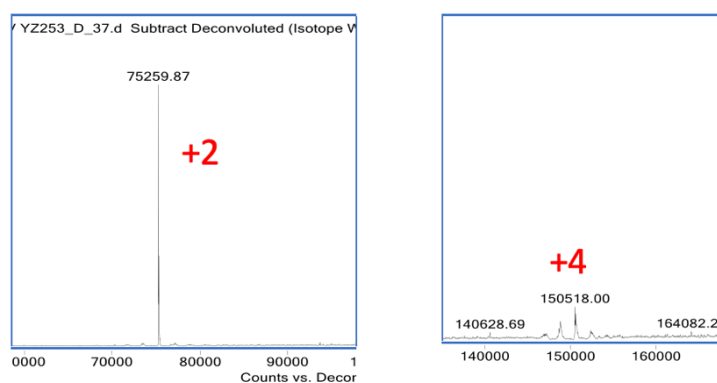
Figure 30 – a. Preparation of Ab conjugates **38** and **39**: i) 20 eq. of diBrPD-BCN, 10 eq. of TCEP, 4 °C, 16 h, pH 8.5, ii) 20 eq. of azide-DFO, 37 °C, 4 h, pH 7.0; b. LC-MS of Ab-diBrPD-DFO conjugate **39**: HL expected 75265 Da, observed 75260 Da, HHLL expected 150529 Da, observed 150518 Da.

In conclusion, the DBM-DFO reagent is a good example of novel DBM reagents, whereas its antibody conjugation gave inefficient results in the initial trials. The bioconjugation of the DBM-DFO reagent was further optimised in this project to yield antibody-DFO conjugates with improved homogeneity. However, the DFO conjugates prepared from DBM-DFO reagents were always observed with adducts in LC-MS analysis, implying DBM-DFO reagents were possibly contaminated. Alternatively, DFO conjugates were prepared from azide-DFO reagents where a DBM and a diBrPD linker were selected to connect the azide moiety and the antibody. Compared to the DBM sequential bioconjugation, the *in situ* bioconjugation of diBrPDs delivered more homogeneous antibody conjugates. The DFO conjugates prepared from azide-DFO attempts are preferable since the DBM-DFO conjugation is still not as efficient as the conjugation of DBM or diBrPD linkers. The resultant DFO conjugates will be radiolabelled and characterised under PET *in vivo* in the future in Dr Michelle Ma's lab at King's College London.

3.3 Dithiomaleimides for *in situ* antibody conjugation

3.3.1 Synthesis of dithiomaleimides

In conventional DBM-based bioconjugation, a problematic formation of half-antibody conjugates is due to the disulfide scrambling where disulfide bonds are incorrectly bridged in antibody hinge region. The half-antibody conjugates also lower the homogeneity of target antibody conjugates. *In situ* bioconjugation is investigated to facilitate immediate bridging upon the reduction of disulfides on trastuzumab in one pot. This approach requires that the reducing agent (usually TCEP) and the bridging reagent (such as NGMs) can be present simultaneously in the buffer without cross-reaction. Whilst dibromomaleimides (DBMs) can cross-react with TCEP, dithiomaleimides (DTMs) are less reactive and more resistant towards TCEP.[163] It was hypothesised that novel DTMs can be designed with tuned TCEP reactivity and allow a robust *in situ* bioconjugation strategy. DTMs incorporating a negative charge could potentially reduce TCEP reactivity due to negative-charge repulsion. In addition, DTMs with bulky groups could possibly reduce TCEP reactivity due to steric hindrance (**Scheme 20**).
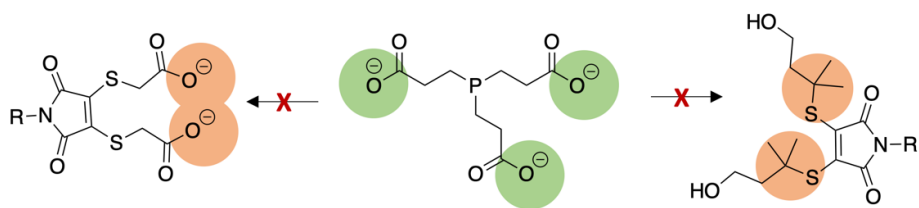
Scheme 20 – DTMs with reduced reactivity to TCEP.

Once conjugated, NGMs with *N*-electron-withdrawing groups would self-hydrolyse fast at high pH to lock themselves on the antibody, generating serum-stable conjugates.[235] To design efficient DTMs, both the disulfide bridging rate and the maleimide hydrolysis rate need to be considered where DTMs are preferably able to deliver fast conjugation and post-conjugation hydrolysis. It has been reported that *N*-C$_2$ linker-DBMs and *N*-phenyl-DBMs self-hydrolyse faster compared to *N*-C$_6$ linker-DBMs, hence the *N*-phenyl maleimide was involved in the DTM design.[235] The commercially available 3,4-dichloro-*N*-phenylmaleimide has been chosen as a starting material for the synthesis of *N*-phenyl-DTMs. To select the leaving group (-SR) on maleimide ring is the next step of the design as it determines disulfide bridging rate. During the bioconjugation, cysteine thiolates attack the double bond on maleimide ring to generate the antibody-maleimide conjugate. If the R group is an electron-withdrawing group (EWG), the carbon-carbon double bond on the maleimide ring would be less electron-rich, and thus more susceptible towards incoming thiolates (**Scheme 21**). Hence, DTMs substituted with EWGs could accelerate the bioconjugation. However, a potential drawback of DTM conjugation is that the released thiol RSH could reattack the double bond, which can potentially lead to some degree of reversibility.
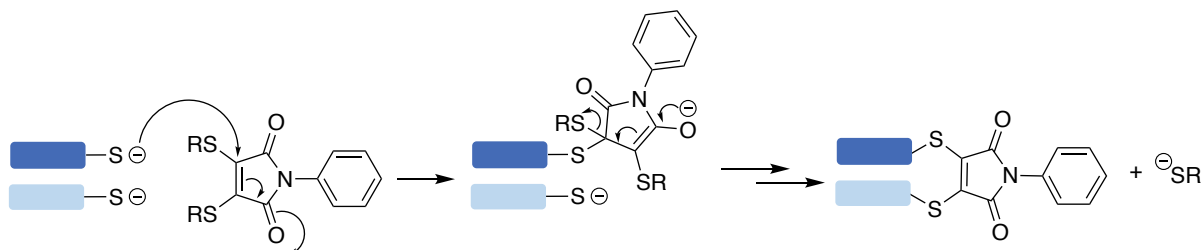
Scheme 21 – Bioconjugation of DTMs to the antibody.

Therefore, *N*-phenyl-DTMs were synthesised by loading various thiols onto 3,4-dichloro-*N*-phenylmaleimide upon presence of the base triethylamine (**Scheme 22**).[245] A range of target DTMs were identified with varying EWGs, the sterics and electronics adjacent to the thiol (**Table 12**).
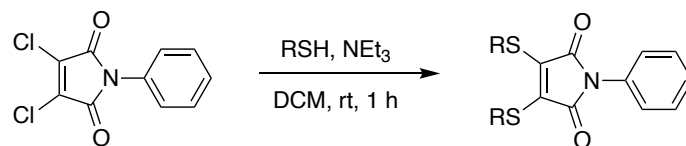
Scheme 22 – Synthesis of DTMs.

Table 12 – Synthesised DTMs.

Entry	Thiols (RSH)	DTMs	Compound (Yield)
1			**40** (35%)
2			**41** (33%)
3			**42** (49%)
4			**43** (49%)
5			**44** (20%)

6			**45** (68%)
7			**46** (43%)
8			**47** (36%)
9			**48** (85%)
10			**49** (75%)

3.3.2 Kinetics study of DTMs by UV-Vis spectroscopy

All DTMs listed in **Table 12** were tested for their hydrolysis rates in BBS buffer (pH 8.5) to mimic bioconjugation conditions, monitored by UV-Vis at room temperature. UV-Vis spectra of DTMs were obtained to identify the wavelength of maximum absorbance for further kinetics study. For example, the UV-Vis full scan (800-200 nm) of DTM **40** in BBS buffer (pH 8.5) was performed to identify the wavelength of maximum absorbance was 404 nm (**Figure 32a**). Afterwards, the UV-Vis absorbance of DTM **40** was monitored at 404 nm for 1 h in BBS buffer (pH 8.5) to obtain the kinetics data of hydrolysis (**Figure 32b**). Once DTM **40** fully

hydrolysed, another UV-Vis full scan of the hydrolysed thiomaleamic acid in BBS buffer (pH 8.5) was performed to show that the thiomaleamic acid did not absorb significantly at 404 nm (**Figure 32a**).[235]

a.   b.
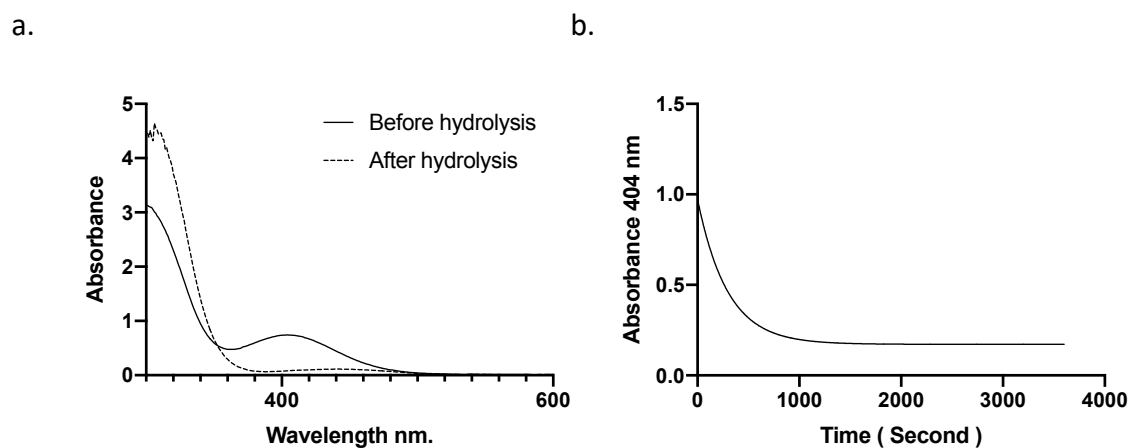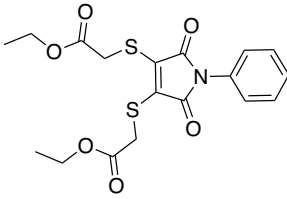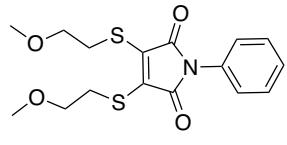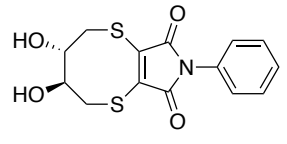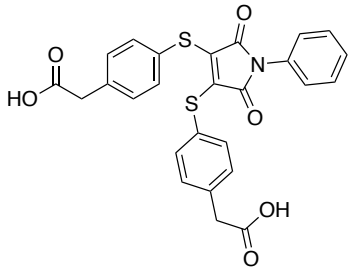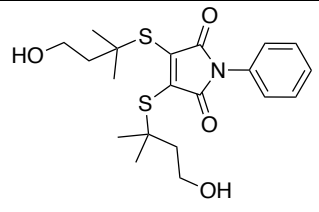
Figure 31 – a. UV-Vis spectra (800-200 nm) of DTM **40** in BBS buffer before and after hydrolysis (pH 8.5), b. 1 h hydrolysis of DTM **40** in BBS buffer (pH 8.5) monitored by UV-Vis at wavelength of 404 nm.

Kinetics study was performed on hydrolysis timepoints to obtain the ranking of hydrolysis rate was found to be: DTM **40** > DTM **41** > DTM **42** > DTM **47** > DTM **48** > DTM **46** > DTM **45** > DTM **43** > DTM **44** (**Table 13**, listed in the order of ranking). DTM **40** and **41** containing ester groups (strong EWGs) hydrolysed a lot faster than DTM **43** and **44** with carboxylate ions (weak EWGs). DTM **44** with four carboxylate groups showed the longest half-life. DTM **49** showed limited water solubility, due to highly hydrophobic aryl groups, and precipitated immediately, thus the hydrolysis study failed to give useful results. To conclude, DTMs with strong EWGs hydrolyse faster than that with weaker EWGs in BBS buffer (pH 8.5) at room temperature.

Table 13 – Kinetics study of DTM hydrolysis in BBS buffer (pH 8.5) at room temperature.

DTMs	Rate constant k (s^{-1})	Half-life t$_{1/2}$ (s)	Ranking
	0.003407	203.4	1

40			
 41	0.002348	295.2	2
 42	0.001012	685	3
 47	0.0008982	771.7	4
 48	0.0005863	1182	5
 46	0.0005169	1341	6

45	0.0004162	1665	7
43	0.0003929	1764	8
44	0.0001647	4209	9

3.3.3 TCEP reactivity test in NMR experiments

To further test if the developed DTMs would cross-react with TCEP, NMR experiments were performed by placing both DTMs and TCEP in NMR tubes at room temperature. To ensure NMR experiments happen in homogeneous solutions, the mixture of CD_3CN and BBS buffer (for organic compound solubility, volume ratio 2:3, final pH 8.5) was applied as solvent. DTMs and TCEP (eq. ratio 2:3) were dissolved in the described solvent mixture and further monitored in NMR at 0 h, 1 h, 2 h and 24 h. The same amount of DTMs and TCEP were separately dissolved in the solvent mixture and monitored as controls. Taking DTM **40** as an example, the TCEP and DTM **40** reaction in BBS:CD_3CN (pH 8.5) were monitored (**Figure 33**).
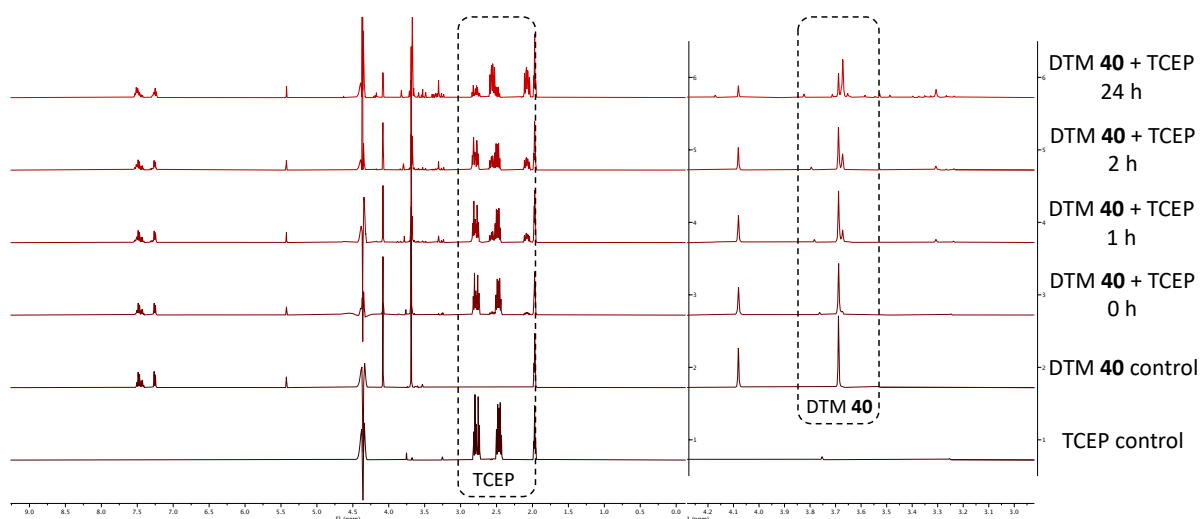
Figure 32 – Full (9.0-0.0 ppm) and zoomed-in (4.5-3.0 ppm) NMR spectra of TCEP and DTM **40** reaction, DTM **40** control and TCEP control.

According to the NMR, TCEP protons and methyl protons of DTM **40** have shifted in the timeframe of 24 h. The shift of TCEP protons implied the TCEP has reacted (likely oxidised) over the time. The shift of methyl protons could imply the cross-reaction between TCEP and DTM **40**. In addition, the TCEP control NMR did not show any shift of TCEP protons after 24 h (**Figure S38**, **Chapter 5**), whereas NMRs of some TCEP-DTM samples showed obvious shifts of TCEP protons (**Figure S39**-**S48**, **Chapter 5**). Both TCEP-DTM cross-reaction and TCEP oxidation could possibly lead to the shift of TCEP protons, so it might lack reliability. Therefore, conclusions have been deducted based on the shift of DTM protons. DTM **40**, **41**, **42**, **48** and **49** showed some cross-reaction with TCEP by 2 h (typical timeframe for bioconjugation), whilst there were no obvious reactions between the other DTMs and TCEP (**Figure S39**-**S48**, **Chapter 5**). DTM **40**, **41**, **42**, **48** and **49** have EWGs adjacent to the carbon-carbon double bond on maleimide ring, making it electron poor and more vulnerable to nucleophilic attack. DTM **43**, **44** and **45** have carboxylate ions that would likely protect the maleimide moiety from TCEP attacking by repelling the carboxylate ions. DTM **46** is less TCEP reactive, likely due to the steric hinderance near the carbon-carbon double bond. DTM **47** also showed limited TCEP reactivity possibly because the carbon-carbon double bond is more electron-rich compared to electron-poor DTMs. In summary, DTMs substituted with EWGs are still TCEP reactive whilst DTMs involving negative charges or bulky groups showed reduced TCEP reactivity.

3.3.4 Bioconjugation of DTMs to trastuzumab Fab fragment

Although each DTM displayed different TCEP reactivity in NMR experiments, all the prepared DTMs were still applied on trastuzumab Fab fragment and native antibody to obtain a clear idea of DTM reactivity in antibody bioconjugation. DTMs were applied in sequential Fab bioconjugation where Fab was reduced with TCEP first, and then bridged with DTMs (**Figure 34a**). Sequential bioconjugation was monitored by reducing SDS-PAGE (using the reducing dye containing 10 mM DTT) where all DTMs showed reasonable bridging ability showing ~12% unmodified heavy and light chains according to densitometry analysis (**Figure 34b**). Compared to DBM sequential bioconjugation (**Figure 23**), the DTM sequential bioconjugation resulted in more unconjugated heavy and light chains. It is likely due to the released thiols reattacking the formed conjugates, leading to some extent of reversibility.

a.

b.

Figure 33 – a. Fab-DTM sequential bioconjugation: i) 3 eq. of TCEP, 37 °C, 1.5 h, pH 8.5, ii) 10 eq. of DTMs, 37 °C, 1 h, pH 8.5, b. SDS-PAGE of Fab-DTM conjugates: M. Protein ladder, 0. Native Fab, 1. Reduced Fab, 2. Fab-DTM **40** conjugate (DTT), 3. Fab-DTM **42** conjugate (DTT), 4. Fab-DTM **45** conjugate (DTT), 5. Fab-DTM **48** conjugate (DTT), 6. Fab-DTM **43** conjugate (DTT), 7. Fab-DTM **41** conjugate (DTT), 8. Fab-DTM **44** conjugate (DTT), 9. Fab-DTM **46** conjugate (DTT), 10. Fab-DTM **47** conjugate (DTT), 11. Fab-DTM **49** conjugate (DTT).

The *in situ* bioconjugation was performed by adding TCEP and DTMs together, at the same time, to native Fab (**Figure 35a**) where results were monitored by reducing SDS-PAGE (**Figure 35b**). Fab *in situ* conjugation did not give efficient bridging, leaving ~30% unconjugated native species. The free thiols released from DTM bioconjugation likely established some

reversibility. Surprisingly, DTMs with different TCEP reactivity did not display huge difference in Fab disulfide bridging under this bioconjugation condition.

a.

b.

Figure 34 – a. Fab-DTM *in situ* bioconjugation: 10 eq. of DTMs, 3 eq. of TCEP, 37 °C, 2 h, pH 8.5, b. SDS-PAGE of Fab-DTM conjugates: M. Protein ladder, 0. Native Fab, 1. Fab-DTM **40** conjugate (DTT), 2. Fab-DTM **42** conjugate (DTT), 3. Fab-DTM **45** conjugate (DTT), 4. Fab-DTM **48** conjugate (DTT), 5. Fab-DTM **43** conjugate (DTT), 6. Fab-DTM **41** conjugate (DTT), 7. Fab-DTM **44** conjugate (DTT), 8. Fab-DTM **46** conjugate (DTT), 9. Fab-DTM **47** conjugate (DTT), 10. Fab-DTM **49** conjugate (DTT).

3.3.5 Bioconjugation of DTMs to trastuzumab native antibody

The prepared DTMs underwent sequential bioconjugation to trastuzumab to demonstrate if the developed DTMs can bridge disulfides efficiently on trastuzumab antibody. The antibody was reduced with TCEP first, and then bridged with DTMs (**Figure 36a**). Sequential bridging results were monitored by reducing SDS-PAGE where all DTMs showed good bridging ability (**Figure 36b**). However, the sequential protocol resulted in a large amount of half antibody species. Compared to DBM sequential bioconjugation (**Figure 26**), DTM sequential bioconjugation also resulted in more varieties of antibody species, which is probably caused by the released free thiols.

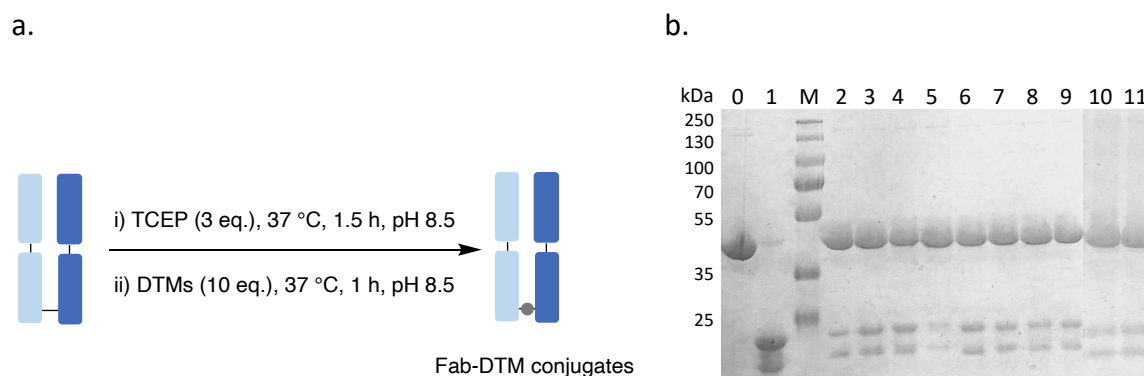a.   b.
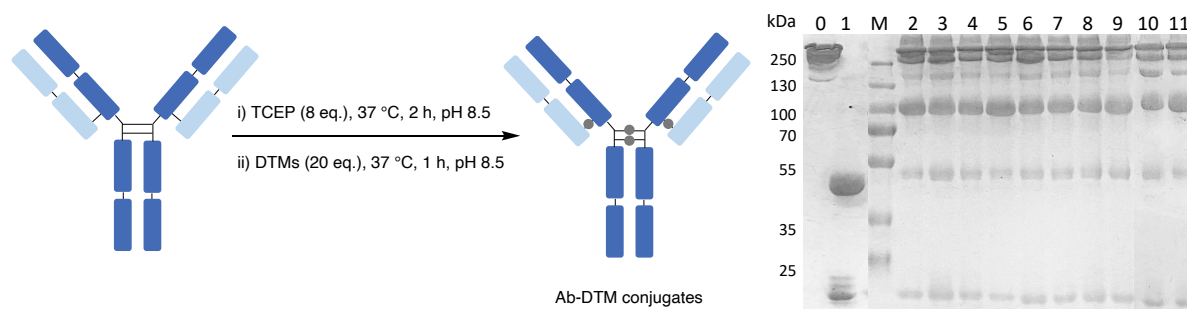
Figure 35 – a. Ab-DTM sequential bioconjugation: i) 8 eq. of TCEP, 37 °C, 2 h, pH 8.5, ii) 20 eq. of DTMs, 37 °C, 1 h, pH 8.5, b. SDS-PAGE of Ab-DTM conjugates: M. Protein ladder, 0. Native Ab, 1. Reduced Ab, 2. Ab-DTM **40** conjugate (DTT), 3. Ab-DTM **42** conjugate (DTT), 4. Ab-DTM **45** conjugate (DTT), 5. Ab-DTM **48** conjugate (DTT), 6. Ab-DTM **43** conjugate (DTT), 7. Ab-DTM **41** conjugate (DTT), 8. Ab-DTM **44** conjugate (DTT), 9. Ab-DTM **46** conjugate (DTT), 10. Ab-DTM **47** conjugate (DTT), 11. Ab-DTM **49** conjugate (DTT).

In situ antibody bioconjugation at 37 °C generated a huge amount of unconjugated heavy and light chains. Instead, *in situ* bioconjugation was optimised using 4 °C protocol which is a well-developed *in situ* bioconjugation method for dibromopyridazinediones (diBrPDs).[128] To the trastuzumab, TCEP and DTMs were added at the same time (**Figure 37a**) where results were monitored by reducing SDS-PAGE (**Figure 37b**). The amount of half antibody decreased as expected, suggesting that the *in situ* protocol worked in reducing hinge disulfide scrambling. Despite that, there were also some unwanted mis-bridged antibody species that could be a problem, potentially caused by the released thiols during the bioconjugation. DTM **40**, **42**, **48** and **49** failed to result in good amounts of bridged conjugates, which corresponded to their relatively high TCEP reactivity in NMR experiments. DTM **43** and **45** displayed <10% unmodified heavy and light chains, due to their limited TCEP reactivity in small molecule reactions. DTM **46** and **47** also showed promising results, yielding <10% unreacted heavy and light chains. In their NMR experiments, no TCEP reaction in maleimide moiety and no side-reaction TCEP oxidation were observed. Surprisingly, DTM **41** demonstrated TCEP reactivity in the NMR reactions, however, it gave the least unmodified heavy and light chains here. DTM **40** and **41** have similar structures, it lacks rationale that they displayed such difference *in situ* bridging ability. One possible reason could be that the ester group of DTM **41** hydrolysed in the stock solution over time, thus giving unconvincing results.
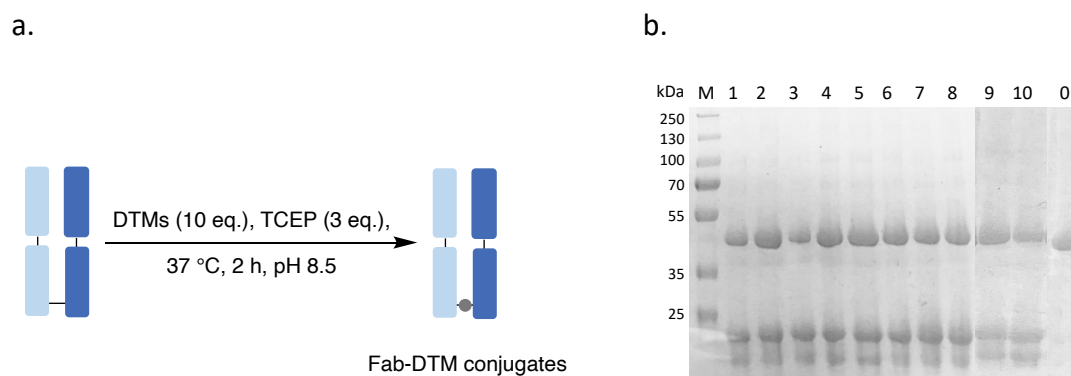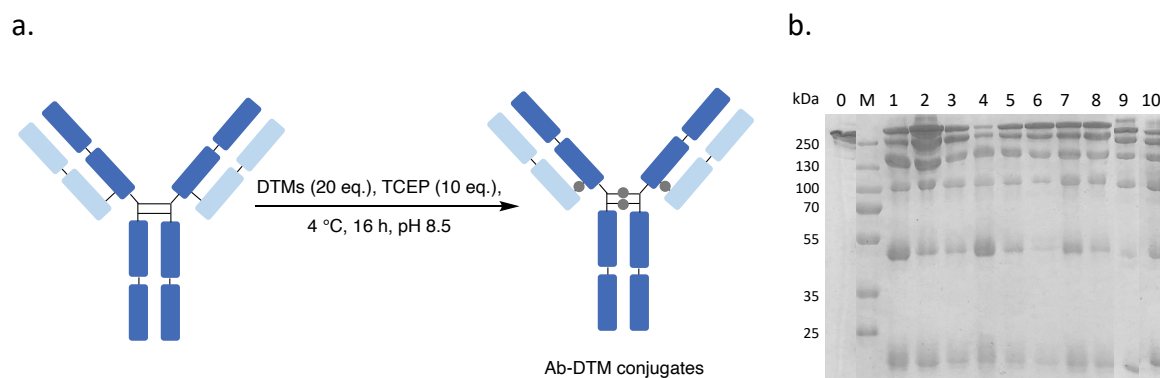
Figure 36 – a. Ab-DTM *in situ* bioconjugation: 20 eq. of DTMs, 10 eq. of TCEP, 4 °C, 16 h, pH 8.5, b. SDS-PAGE of Ab-DTM conjugates: M. Protein ladder, 0. Native Ab, 1. Ab-DTM **40** conjugate (DTT), 2. Ab-DTM **42** conjugate (DTT), 3. Ab-DTM **45** conjugate (DTT), 4. Ab-DTM **48** conjugate (DTT), 5. Ab-DTM **43** conjugate, 6. Ab-DTM **41** conjugate (DTT), 7. Ab-DTM **44** conjugate (DTT), 8. Ab-DTM **46** conjugate (DTT), 9. Ab-DTM **47** conjugate (DTT), 10. Ab-DTM **49** conjugate (DTT).

In conclusion, DTMs developed with negative charges or bulky groups in this study showed attenuated TCEP reactivity as expected. As for antibody conjugation, all the DTMs showed disulfide bridging ability, even it is not as good as the developed DBMs. DTMs with reduced TCEP reactivity did show better results in *in situ* antibody bioconjugation than those which showed relatively high TCEP reactivity. The *in situ* bioconjugation displayed a reduced formation of half-antibody conjugates, however, the mis-bridged antibody species were also observed, as the released thiols from DTM bridging can potentially reattack the maleimide bridge. Hence, the *in situ* antibody bioconjugation still needs more investigation and optimisation by exploring potential *in situ* reagents.

3.4 Benzeneselenols delivering rapid antibody reduction

To further investigate *in situ* antibody bioconjugation, an alternative strategy is to explore novel reducing reagents such as selenols. Selenols can resemble thiols in some characteristics, for example they both can deliver reversible disulfide reduction *via* selenol- or thiol-disulfide exchange. In addition, selenols are more nucleophilic than thiols and they can perform faster nucleophilic attack (**Chapter 1.6**). Selenols (pKa 5.2) also have lower pKas than thiols (pKa 8.3), hence at physiological pH, selenols are completely converted to selenolates, but thiols are

only partially ionised. Under this condition, the reactivity difference between selenolates and thiolates is more significant. One good example is that the addition of catalytic amount of alkylselenol together with DTT in trastuzumab Fab reduction (selenocystamine:DTT=1:6) can accelerate the reduction from 90 min to 5 min (rt, pH 7.0).[222] However, this Fab-DTT-selenocystamine reduction used 5 mM of DTT (140 eq. to Fab) which is not ideal for *in situ* antibody bioconjugation as post-reduction ultrafiltration might be necessary. In addition, selenocystamine might cross-react with the bridging reagent (such as NGMs) *via* the amine moiety during *in situ* bioconjugation.

Alternatively, benzeneselenols have also been reported to have superior reducing ability on antibody disulfides.[246,156] Benzeneselenols are better leaving groups and have lower pKa compared to alkylselenols, as a consequence of the electron delocalisation effect of the phenyl ring. However, due to the non-polar phenyl ring, benzeneselenols are volatile with pungent smell and have limited aqueous solubility. The poor water solubility of benzeneselenols currently limits further applications in chemical biology where the large excess of benzeneselenols is always required.[247,248] The reactivity of benzeneselenols can be tuned by modifying the substituents present on the phenyl ring (**Scheme 23**). This could include incorporating polar groups such as amines or carboxylic acids, which would also provide a reactive site for further functionalisation. In addition, benzeneselenols are highly sensitive to air oxidation where diselenide would form once in contact with air. To develop more stable and robust selenium reagents, diaryl diselenides will be synthesised instead, and then reduced with TCEP to form aryl selenols prior to antibody conjugation (**Scheme 23**).
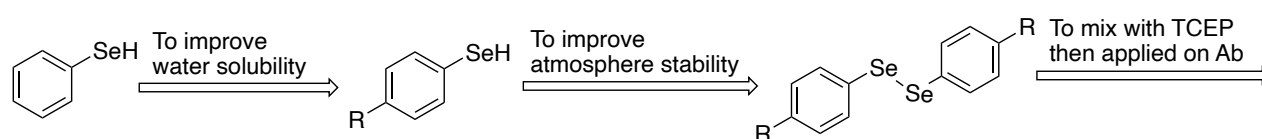
**Scheme 23** – Initial design of diaryl diselenides.

3.4.1 Synthesis of diaryl diselenides

The initial design of diaryl diselenides is to introduce polar groups to the phenyl ring that can improve the aqueous solubility as well as limit the volatility. A carboxylic acid group (-COOH) or an amine group (-NH$_2$) could be the ideal choice as they can also provide available reactive

sites for further functionalisation. A polyethylene glycol (PEG) chain and the sulfonic acid (-SO_3H) are also ideal to improve the aqueous solubility as polar moieties. To further expand the scope of diaryl diselenides, novel diselenides with tuned reactivity can be designed where both electron-rich and electron-poor substituents are involved. The hypothesis is that the arylselenol with electron-rich substituents is a better nucleophile in disulfide reduction, whilst it is more unstable to air oxidation. The arylselenol with electron-poor substituents is less reactive in nucleophilic attacking and more stable in atmosphere. For electron-poor diaryl diselenides, the electron-withdrawing groups (EWGs) on the phenyl ring could be carboxylic acids (-COOH), esters (-COOR), aldehydes (-CHO), ketones (-COR), halides (-X), nitro groups (-NO_2) or sulfonic acids (-SO_3H). Alternative electron-poor diaryl diselenides could involve heteroatoms on the phenyl ring, for example the dipyridine diselenide. For electron-rich diaryl diselenides, the electron-donating groups (EDGs) on the phenyl ring could involve amines (-NH_2), amides (-NHCOR), alkoxy groups (-OR). The synthesis of diaryl diselenides will follow published protocols for known compound.

The iodine mediated synthesis of diaryl diselenides has been developed as a base-free and metal-free procedure using selenium dioxide, as selenium source, and commercially available aryl boronic acids (**Scheme 24**).[249] This methodology is applicable to a broad scope of aryl boronic acids containing electron-rich and electron-poor substituents. Diphenyl diselenide **50** was synthesised to test this synthetic strategy (**Table 14** entry 1). The electron-rich diaryl diselenide **51** with *para*-methoxyl groups was also successfully prepared using this method (**Table 14** entry 2). Another electron-rich diaryl diselenide **52** with *para*-bromine groups was synthesised and confirmed with NMR and MS by comparing to literature,[249] however, it was not possible to isolate the target compound as it coeluted with other unidentified by-products (**Table 14** entry 3). For electron-poor diselenides, bis(4-carboxylphenyl)diselenide **53** was attempted using the synthetic route, however, no product was obtained (**Table 14** entry 4). Similarly, another example of electron-poor diaryl diselenide **54** with *para*-nitro groups could not be synthesised using this protocol (**Table 14** entry 5). The proposed mechanism is that the iodine and selenium dioxide interacted to form selenium iodide, however the mechanism of forming selenium iodide was not elucidated in the literature. The phenyl ring of the phenylboronic acid was likely to attack selenium iodide to give phenylselenium iodide, which was detected by GCMS and ^{77}Se NMR.[249] The formation of phenylselenium iodide was also
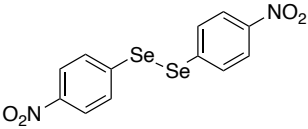
observed in previous *ipso*-substitution of phenylboronic acid.[250,251] Lastly, the intermediate phenylselenium iodide possibly attacked another phenylselenium iodide molecule. During the formation of phenylselenium iodide, electron-rich aryl compounds are more likely to attack the selenium iodide, which could possibly explain why the attempted synthesis of electron-poor diaryl diselenides failed.
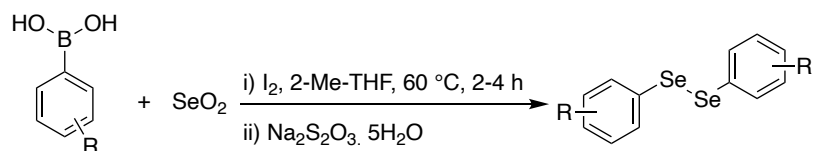
Scheme 24 – Iodine-mediated synthesis for diaryl diselenides.[249]

Table 14 – Attempted *para*-diaryl diselenides compounds.

Entry	R group	Structure of diaryl diselenides (yield)
1	-	**50** (56%)
2	-OCH₃	**51** (66%)
3	-Br	**52** (Not isolated)
4	-COOH	**53** (Not obtained)

5	-NO$_2$	O$_2$N—⟨⟩—Se—Se—⟨⟩—NO$_2$
		54 (Not obtained)

It was not possible to synthesise the bis(4-carboxylphenyl)diselenide **53** using the initially developed procedure. To develop diaryl diselenides with other polar substituents, bis(4-aminophenyl)diselenide **55** involving two amine groups was then synthesised following a known protocol. The triselenium dicyanide was prepared by reaction of selenium dioxide and malononitrile in dimethyl sulfoxide (DMSO) and then aniline to give the intermediate phenyl selenocyanate (**Scheme 25**).[252] It is known that the selenium-carbon bond is much stronger than selenium-selenium bond in the tri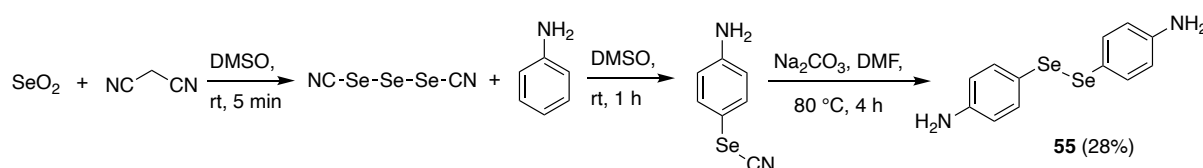selenium dicyanide.[253,254] Triselenium dicyanide is a common selenocyanating reagent for the synthesis of aromatic and metallo-organic selenocyanates.[255,256] The intermediate phenyl selenocyanate could possibly attack another phenyl selenocyanate molecule to give the target bis(4-aminophenyl)diselenide **55**.[257,258]

SeO$_2$ + NC—CN $\xrightarrow{\text{DMSO, rt, 5 min}}$ NC-Se-Se-Se-CN + aniline(NH$_2$) $\xrightarrow{\text{DMSO, rt, 1 h}}$ 4-NH$_2$-C$_6$H$_4$-Se-CN $\xrightarrow{\text{Na}_2\text{CO}_3,\ \text{DMF, 80 °C, 4 h}}$ H$_2$N—⟨⟩—Se—Se—⟨⟩—NH$_2$ **55** (28%)

Scheme 25 – Synthesis of bis(4-aminophenyl)diselenide **55**.[253,257]

The introduction of an amine functional group enables subsequent installation of a wide variety of other functional groups, through amide coupling. To improve the aqueous solubility of diselenides, a PEG chain (**Scheme 26a**) and a carboxylic acid group (**Scheme 26b**) were respectively coupled to bis(4-aminophenyl)diselenide **55** to give diselenide **56** and **57** respectively. The synthesis of disulfamic acid product **58** was also attempted, but only starting material bis(4-aminophenyl)diselenide **55** was isolated, probably as the target compound is labile under this condition thus reforming the starting material (**Scheme 26c**).

a.
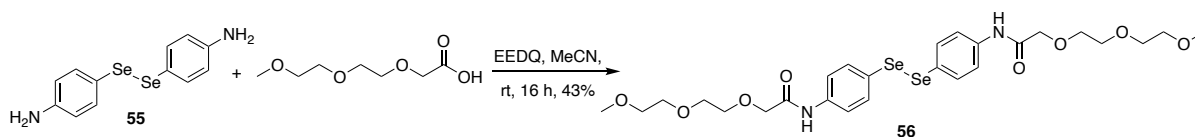
b.
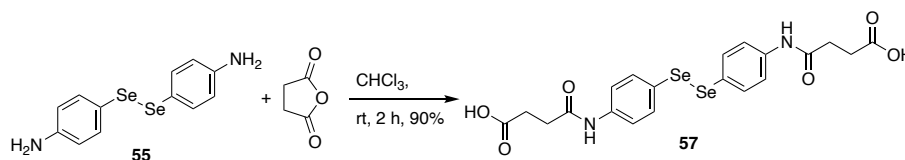
c.
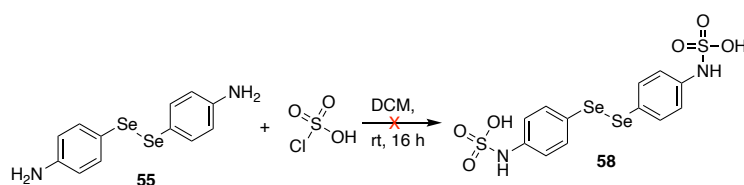
Scheme 26 – Synthesis of diselenide: a. diPEG **56**, b. diCOOH **57**, c. diSO₃H **58**.

To further expand the scope of the electron-poor diselenides, the bis(4-acetylphenyl)diselenide **59** was designed and obtained *via* a simple Friedel-Crafts reaction on diphenyl diselenide **50** (**Scheme 27a**). The diselenide **59** displayed limited aqueous solubility and was then functionalised with hydrazine *via* a Wolff-Kishner reaction to give diselenide **60** to improve the aqueous solubility (**Scheme 27b**).

a.
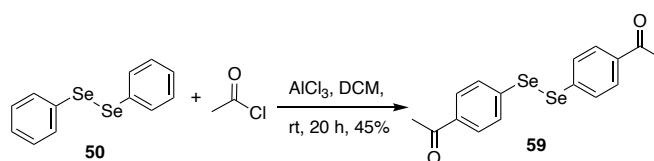
b.
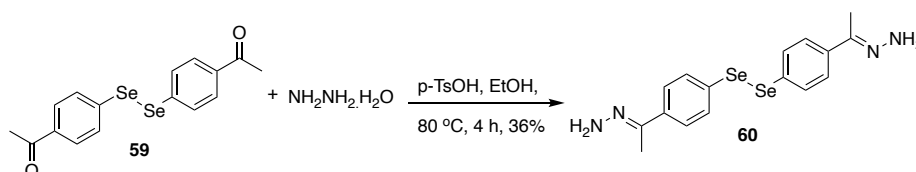
Scheme 27 – Synthesis of diselenides: a. diacetyl **59**, b. dihydrazone **60**.

As discussed above, a strong electron-withdrawing pyridine ring was introduced for the synthesis of a dipyridine diselenide. Selenium reacted with sodium hydroxide in the presence of hydrazine to give disodium diselenide, which further nucleophilic attacked 2 eq. of 2-bromopyridine to give the target dipyridine diselenide **61** (**Scheme 28**).[259,260]
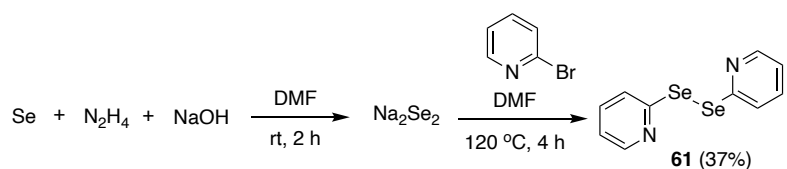
Scheme 28 – Synthesis of dipyridine diselenide **61**.[259,260]

The developed *para*-substituted diaryl diselenides were mixed with TCEP to test if the idea of reducing diselenides to selenols prior to antibody conjugation works. For example, the LC-MS experiments were run with bis(4-aminophenyl)diselenide **55** treated with 1 eq. of TCEP (**Figure 38a**) and bis(4-aminophenyl)diselenide **55** treated with 1 eq. of TCEP and 2 eq. of *N*-methylmaleimide (**Figure 38b**). The masses of the corresponding aminophenylselenol of bis(4-aminophenyl)diselenide **55** and the maleimide-capped selenol were observed.

a.
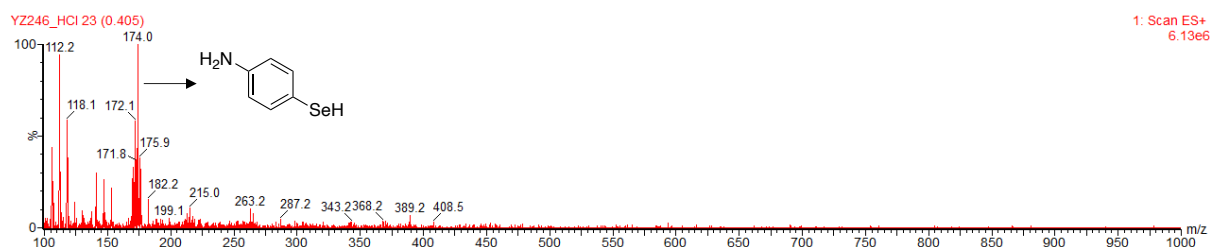
b.

Figure 37 – LC-MS of a. bis(4-aminophenyl)diselenide **55** treated with 1 eq. of TCEP: expected [M+H]$^+$ 174 Da, observed 174 Da, b. bis(4-aminophenyl)diselenide **55** treated with 1 eq. of TCEP and 2 eq. of N-methylmaleimide: expected [M+H]$^+$ 285 Da, observed 285 Da.

In the attempted experiments of diaryl diselenide reduction, it was observed that the resultant *para*-substituted aryl selenols are prone to fast reoxidation, as the significant yellow colour of diaryl diselenides reappeared immediately. Fast reoxida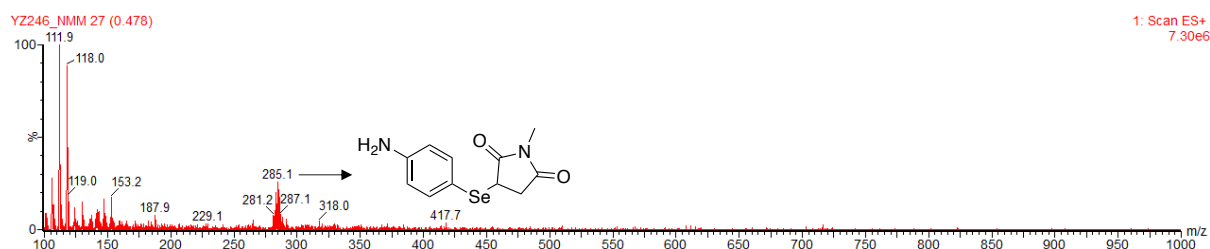tion of *para*-selenols might lead to insufficient antibody reduction, limiting their potential application. Therefore, *ortho*-substituted diselenides could be alternative diselenide reagents, as the corresponding *ortho*-selenols might be less air-sensitive due to increased steric hinderance near the selenol site. The *ortho*-substituted diselenides **62** and **63** (**Table 15**) were synthesised by reacting selenium with aryl iodides where copper oxide nanopowder works as a catalyst, according to the predicted mechanism in the literature (**Scheme 29**).[261,262] The reason to involve a methoxy group or an amine group is to easily compare with the corresponding *para*-substituted products **51** or **55** (**Table 15**).
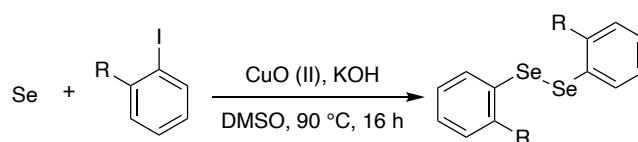
Scheme 29 – Synthesis of *ortho*-diaryl diselenides.[261,262]

Table 15 - Attempted *ortho*-substituted diaryl diselenides compounds.

Entry	R group	Structure of diaryl diselenides (yield)	To compare with *para*-substituted diaryl diselenides
1	-OCH$_3$	**62** (80%)	**51**
2	-NH$_2$	**63** (61%)	**55**

3.4.2 Antibody reduction using the prepared diaryl diselenides

The prepared diselenides were reduced with TCEP *in situ* to generate the corresponding benzeneselenols, which were then applied on trastuzumab Fab immediately to test their reducing ability. Each diselenide reacts with 1 eq. of TCEP to generate 2 eq. of selenols, which could further reduce 1 eq. of disulfide bonds (**Figure 39**). However, selenols are also prone to reoxidation by air to reform diselenides, which could reoxidise the free thiols released from disulfide bonds. Excess TCEP was used in the Fab reduction, to ensure enough selenols present in solution for complete and maintained reduction of the disulfide bond.
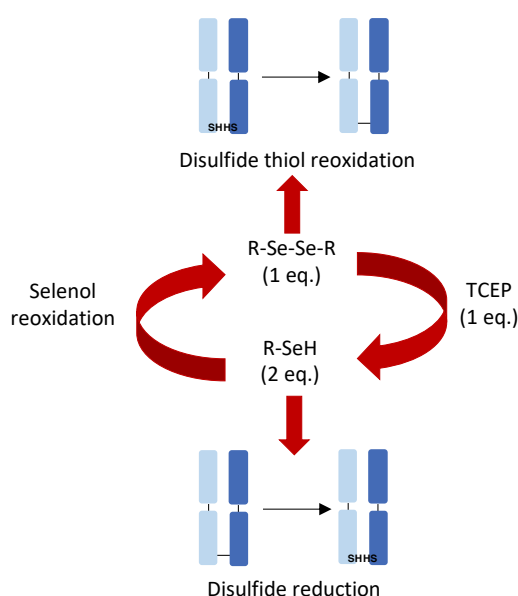
Figure 38 – Possible selenol-diselenide and thiol-disulfide exchange reactions.

Therefore, Fab reduction was performed where diselenides and TCEP (eq. ratio 1:2) were premixed and directly added to Fab *in situ* (**Scheme 30**). All the buffers and stock solutions were degassed with argon in advance to remove air, which may interfere with reduction by promoting oxidation of the selenol compounds. The Fab reduction results were illustrated on SDS-PAGE, with timepoints collected at 2 min, 5 min, 10 min and 30 min since the start of the reduction (**Table 16**). The diphenyl diselenide **50** was applied in Fab reduction as a control. The diselenide **51**, **62** and **63** did not demonstrate notable reducing ability by showing partial Fab reduction after 30 min, which is consistent with TCEP reduction. The bis(4-aminophenyl)diselenide **55** gave the most promising results, delivering full disulfide reduction

within 2 min, which is even faster than diphenyl diselenide **50**. The diselenide **56**, **57**, **59** and **60** all resulted in partial Fab reduction. The diselenide **61** showed poor reactivity in reducing Fab fragment, possibly due to the strong electron-withdrawing effect of pyridine. In addition, the bis(4-aminophenyl)diselenide **55**-Fab reduction displayed that the completely reduced Fab was reoxidised overtime. Once excess TCEP was fully consumed, the reformed diselenides can potentially reoxidise the reduced Fab (**Figure 39**).
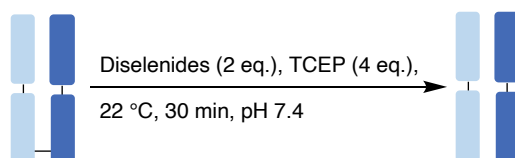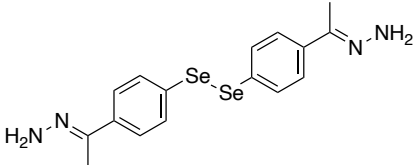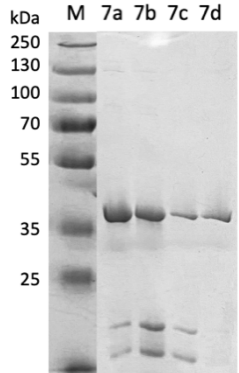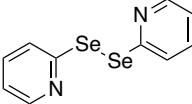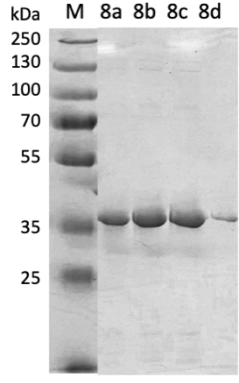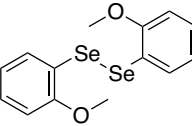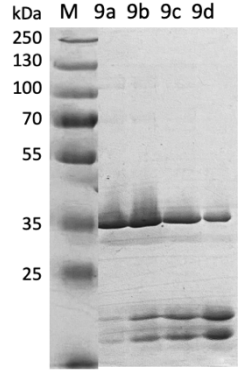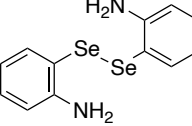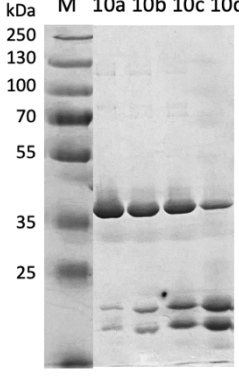
Scheme 30 – Fab reduction: 2 eq. of diselenides, 4 eq. of TCEP, 22 °C, 30 min, pH 7.4.

Table 16 – SDS-PAGE of Fab reduction using 2 eq. of diselenides, 4 eq. of TCEP, 22 °C, pH 7.4: a. 2min, b. 5min, c. 10 min, d. 30 min.

Entry	Diselenides	SDS-PAGE
1	**50**	
2	**51**	

3	 **55**	
4	 **56**	
5	 **57**	
6	 **59**	

7	**60**	
8	**61**	
9	**62**	
10	**63**	

In conclusion, bis(4-aminophenyl)diselenide **55**-TCEP attempt demonstrated the best ability for reducing disulfide bonds, achieving rapid reduction in as quickly as 2 minutes. The *para-*

amine group has improved reactivity due to its electron-donating ability, and enabled improved solubility due to its polarity, which enables it to behave as a highly useful and effective reducing agent. As initially set out, bis(4-aminophenyl)diselenide **55** is non-smelly and highly stable in contact with air, avoiding the pungent odour and air sensitivity of benzeneselenols. Hence, it is easier to store this reagent where inert atmosphere is not necessary. The corresponding aminobenzeneselenol demonstrated improved aqueous solubility in comparison to benzeneselenols, as it never precipitated in aqueous buffers even when used in excess.

Furthermore, this diselenide also showed catalytic ability because the diselenide is reusable in disulfide reduction - once reacted with the disulfide, selenols would reform diselenides which can further involve in the next round of disulfide reduction (**Figure 39**). To prove this hypothesis, the bis(4-aminophenyl)diselenide **55**-Fab reduction was then optimised to require only catalytic amount of bis(4-aminophenyl)diselenide **55** (0.5 eq.) with TCEP (2 eq.) that can deliver full Fab reduction within 2 min. As only a sub-stochiometric amount of diselenides was needed, it demonstrated that a catalytic process possibly occurred. Notably, if insufficient TCEP is present, the antibody reoxidises overtime, indicating again that the redox active diselenide can also play a role in reoxidising the cysteine residues (**Figure 39**). Further work involving bis(4-aminophenyl)diselenide **55** has been optimised to deliver full trastuzumab reduction within 4 min requiring 4 eq. of diselenide **55** and 30 eq. of TCEP.

Benzeneselenol has previously shown *in situ* reducing ability together with dithiophenolmaleimide **64**,[163] therefore, bis(4-aminophenyl)diselenide **55** and TCEP were also applied with dithiophenolmaleimide **64** on trastuzumab antibody, attempting *in situ* reduction and bridging (**Figure 40**). However, this *in situ* attempt did not generate the desired homogeneous antibody conjugate with a DAR of 4, instead giving mixtures of antibody conjugates with DAR of 3 and DAR of 4. This is possibly caused by reactive diselenides reoxidising antibody disulfide bonds too fast (can also be explained as the reaction circle in **Figure 39** happens too fast), whilst the disulfide bridging occurs relatively slow. Therefore, the diselenide-TCEP *in situ* bioconjugation requires further optimisation by developing more diaryl diselenides with tuned reactivity.

a.   b.
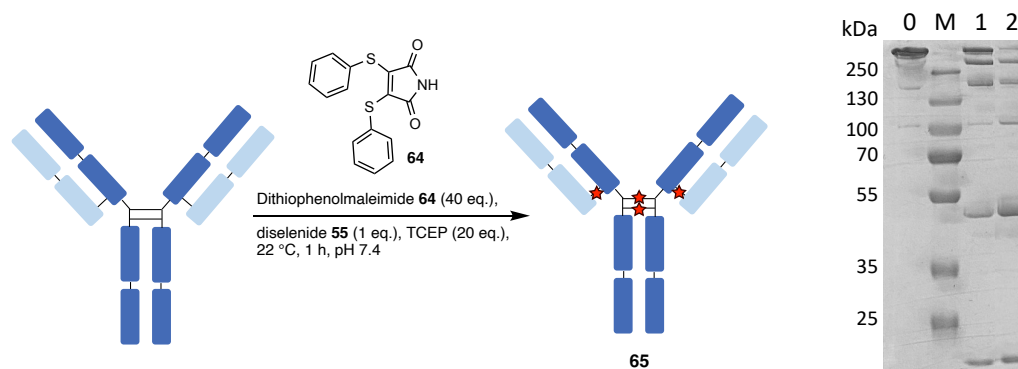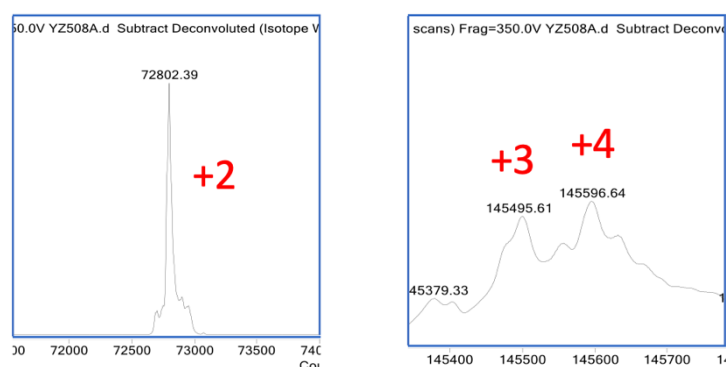
Figure 39 – Antibody *in situ* bioconjugation using dithiophenolmaleimide **64**, bis(4-aminophenyl)diselenide **55** and TCEP: a. 40 eq. of dithiophenolmaleimide **64**, 1 eq. of bis(4-aminophenyl)diselenide **55**, 20 eq. of TCEP, 22 °C, 1 h, pH 7.4, b. SDS-PAGE of *in situ* bioconjugation: M. Protein ladder, 0. Native Ab, 1. Ab conjugate **65**, 2. Ab conjugate **65** (DTT), c. LC-MS of antibody conjugate **65**: HL expected 72781 Da, observed 72802 Da (+2 moieties), HHLL expected 145559 Da, observed 145496 Da (+3 moieties) and 145597 Da (+4 moieties).

3.4.3 Rapid protocol to construct trastuzumab tri-conjugates

The novel diselenide was further tested on trastuzumab antibody to deliver rapid disulfide reduction that can further accelerate the construction of tri-conjugates in combination with the developed trifunctional DBMs. The first step involves the reduction of the trastuzumab antibody, which conventionally requires TCEP for 2 h at 37 °C. To accelerate this step, the bis(4-aminophenyl)diselenide **55** used in conjunction with TCEP could deliver complete antibody reduction in 4 min at toom temperature. Dual-modality full antibody conjugates

were accessed in 20 min total time, *via* a selenol catalysed reduction-bridging-IEDDA-SPAAC four-step sequence to afford the dual-modality antibody conjugate **66** (**Figure 41**). The diselenide protocol enabled rapid construction of the non-hydrolysed version of conjugate **66**, which then hydrolysed during MS sample preparation. The hydrolysed species enables serum stable products, so overnight hydrolysis is still required for this protocol to generate a very stable conjugate.

a.

b.

c.
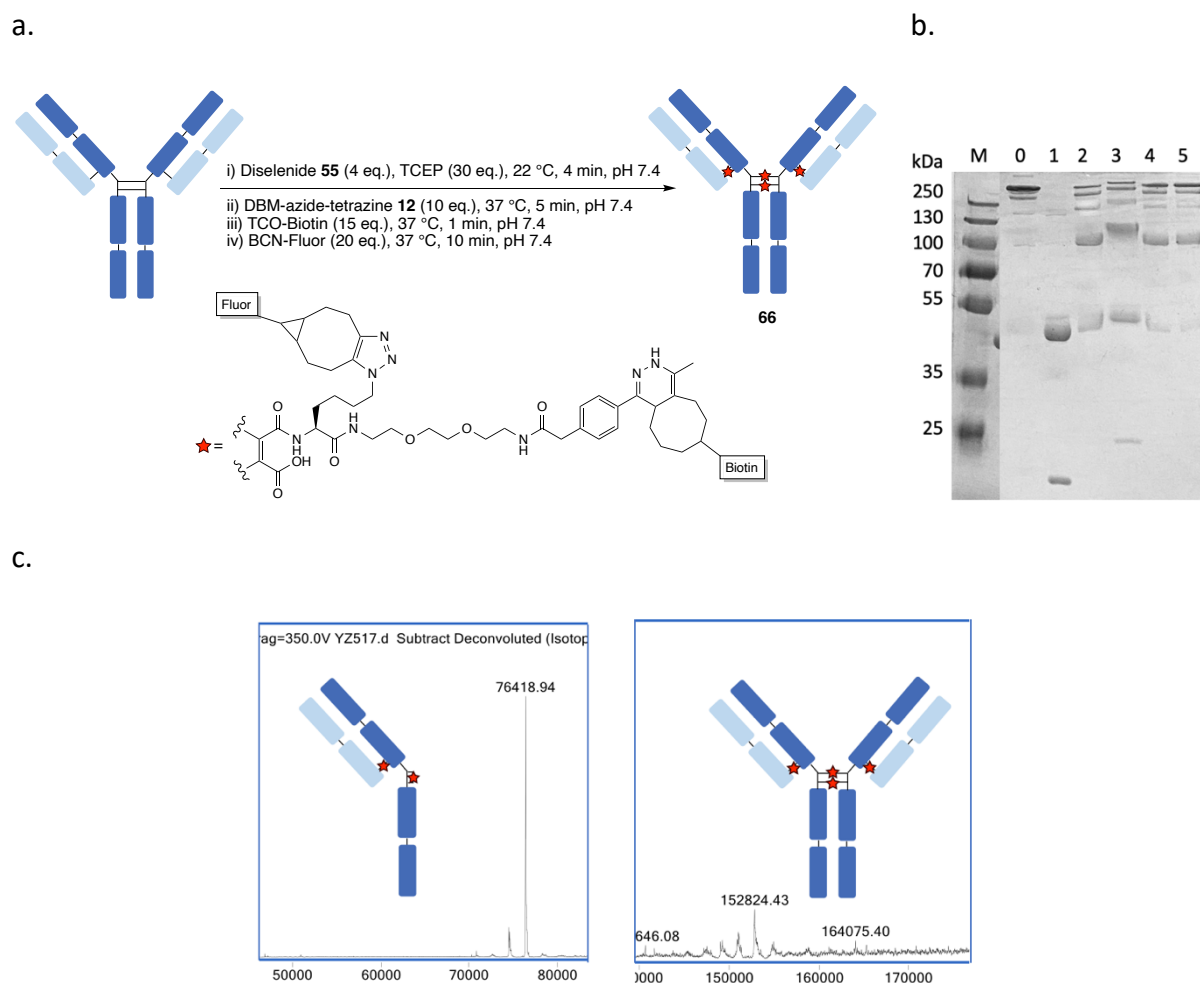
Figure 40 – a. Selenol catalysed reduction-bridging-IEDDA-SPAAC on IgG1: i) 4 eq. of aminodiselenide, 30 eq. of TCEP, 22 °C, 4 min, pH 7.4; ii) 10 eq. of DBM-azide-tetrazine **12**, 37 °C, 5 min, pH 7.4; iii) 15 eq. of TCO-Biotin, 37 °C, 1 min, pH 7.4; iv) 20 eq. of BCN-Fluor, 37 °C, 10 min, pH 7.4, b. SDS-PAGE of rapid selenol protocol: M. Protein ladder, 0. Native Ab, 1. Selenol-reduced Ab, 2. Ab-DBM-azide-tetrazine conjugate, 3. Hydrolysed Ab-DBM-biotin-fluor conjugate (DTT), 4. Ab-DBM-biotin-tetrazine conjugate, 5. Ab-DBM-biotin-fluor conjugate, c. LC-MS of Ab-DBM-biotin-fluor conjugate **66** generated in rapid selenol

protocol: HL expected 76441 Da, observed 76419 Da, 74510 Da (showed < 5% of unidentified species), HHLL expected 152879 Da, observed 152824 Da.

Based on the known literature, a variety of diaryl diselenides substituted with EDGs or EWGs have been designed and synthesised. These diaryl diselenides have been proved to immediately generate the corresponding aryl selenols in presence of TCEP, hence diselenides with a pre-treatment of TCEP can potentially enable disulfide reduction on antibodies. Among all the synthesised diselenides, bis(4-aminophenyl)diselenide **55** demonstrated the highest performance in Fab reduction attempts, as well as showed improved aqueous solubility. This diselenide **55** together with a DTM reagent also performed *in situ* antibody bioconjugation to deliver conjugates with DARs of 3-4. Another application of this diselenide **55** is to completely reduce trastuzumab within 4 min, helping to construct a tri-conjugate in an accelerated strategy.

3.5 DBM-PEG-disulfide

To yield antibody conjugates with controlled drug-to-antibody ratios (DARs), a novel class of DBMs with an incorporated disulfide bond were envisaged. The hypothesis was that the target DBM-disulfide reagent can undergo intermolecular reaction to bridge antibody disulfides *via* the DBM moiety, and then undergo 'pseudo-intramolecular' reaction where the disulfide moiety reoxidises the remaining cysteine residues (**Scheme 31**). To ensure the hypothesis works, the rate of DBM-thiol reaction should be faster than that of disulfide-mediated reoxidation. Once DBMs are conjugated, the rate of disulfides reoxidising thiols is accelerated as the intermolecular reaction is replaced by a 'pseudo-intramolecular' reaction. Intramolecular reactions are faster than intermolecular reactions because there is less entropic cost.
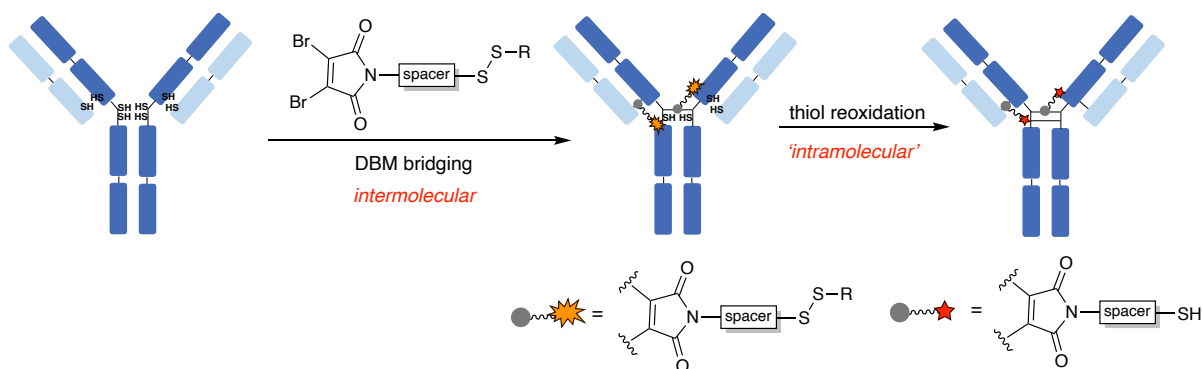
Scheme 31 – Proposed mechanism of the DBM-disulfide reagent on IgG1.
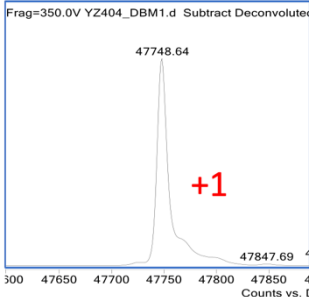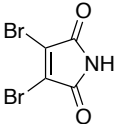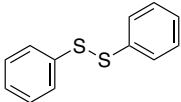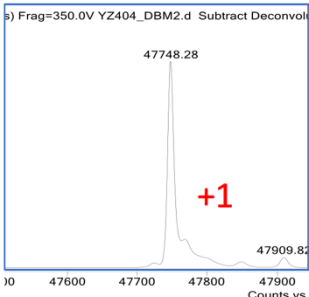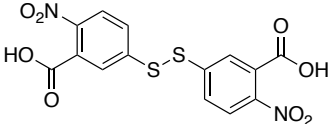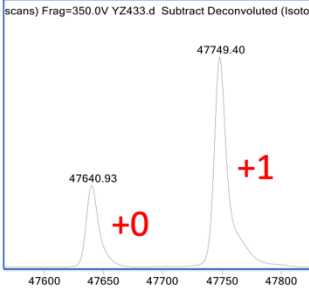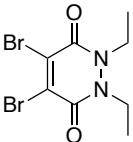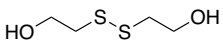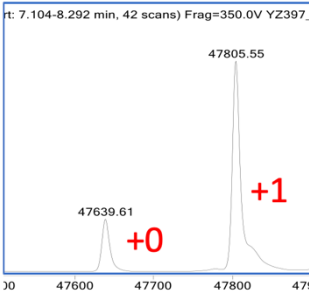
3.5.1 Design and synthesis of the DBM-disulfide reagent

Before the actual design of DBM-disulfide reagent, a competition experiment was conducted on Fab to understand of the reaction rate of disulfide-induced reoxidation of thiols (**Table 17**). In the competition reaction, DBMs, dibromopyridazinediones (diBrPDs), alkyl disulfides and aryl disulfides were used to obtain a reactivity rankin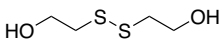g. The Fab was reduced with TCEP first. TCEP was removed before a premixed solution of DBM or diBrPD and disulfide (1:1) were added (**Scheme 32**). The resulting mixture was left at 22 °C for 1 h (DBMs) or 37 °C for 2 h (diBrPDs) to reach complete reaction. LC-MS analysis was further conducted to show the ratio of bridged Fab and native Fab. The ratio of the bridged Fab conjugate represents the rate of DBM- or diBrPD-thiol reaction, whilst the ratio of native Fab represents the rate of disulfide-mediated reoxidation. The results obtained indicate the bridging reagents react in the following order: DBM > Ellmans > aryl disulfide > diBrPD > alkyl disulfide. Superior DBM reactivity over disulfide reactivity indicates it is a suitable basis for the bridging-disulfide design.
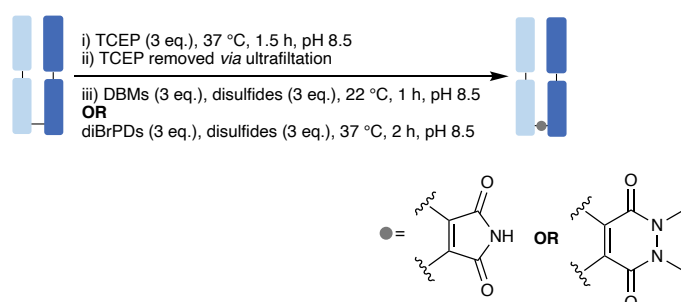
Scheme 32 – Fab competition reaction using DBMs or diBrPDs with disulfides.

Table 17 – Competition reaction on Fab using DBMs or diBrPDs and commercially available alkyl or aryl disulfides.

DBM or diBrPD	Disulfides	LC-MS (+0: native Fab, +1: bridged Fab)
	HO-S-S-OH	Frag=350.0V YZ404_DBM1.d Subtract Deconvoluted 47748.64 +1 47847.69 …00 47650 47700 47750 47800 47850 Counts vs. [
Br...O NH O (dibromomaleimide)	(diphenyl disulfide) S-S	s) Frag=350.0V YZ404_DBM2.d Subtract Deconvol 47748.28 +1 47909.82 …00 47600 47700 47800 47900 Counts vs.
	O₂N, HO₂C—S-S—CO₂H, NO₂ (DTNB)	scans) Frag=350.0V YZ433.d Subtract Deconvoluted (Isoto 47749.40 47640.93 +0 +1 47600 47650 47700 47750 47800
Br...O N(Et) N(Et) O Br	HO-S-S-OH	rt: 7.104-8.292 min, 42 scans) Frag=350.0V YZ397_ 47805.55 47639.61 +0 +1 …00 47600 47700 47800 47900

It is necessary to understand the distance between the Fab disulfide bonds and the hinge region disulfides on a full antibody, to ensure the DBM-disulfide reagent is long enough to achieve reoxidation. The maximum distance between any two interchain disulfides is ~20 Å, and any linker intended to connect multiple disulfides should be designed with this distance requirement in mind.[263] The distance between the two disulfides was also measured as ~19.6 Å by PyMOL (**Figure 42a**). Dannheim *et al.* developed a class of bis-divinylpyrimidine (DVP) linkers (~20 Å) that each linker molecule can bridge two disulfide bonds, resulting in an antibody conjugate with a DAR of 2.[263] Therefore, a DBM-PEG-disulfide reagent was designed, and distance between two reactive sites was measured as ~19.8 Å by PyMOL (**Figure 42b**).
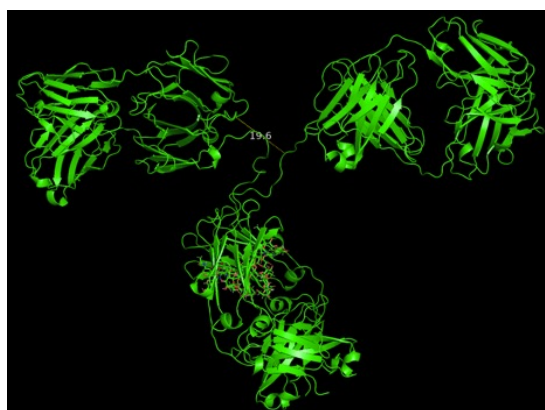
a.   b.

Figure 41 – PyMOL measurements of a. trastuzumab IgG1, b. designed DBM-PEG-disulfide reagent.

The proposed DBM-PEG-disulfide reagent **71** was synthesised (**Scheme 33**). The asymmetric aryl disulfide **67** with a *para*-carboxylic acid was prepared using dipyridyl disulfide. The asymmetric aryl disulfide **67** was further coupled to a PEG diamine **68** where one amine was

Boc-protected. The Boc-protected amine on the resulting asymmetric disulfide compound **69** was then deprotected with trifluoroacetic acid (TFA) and then coupled to a DBM-C$_2$-carboxylic acid **70**, which was prepared from dibromomaleic acid and glycine, to generate the final p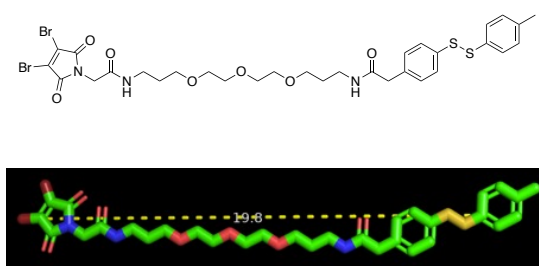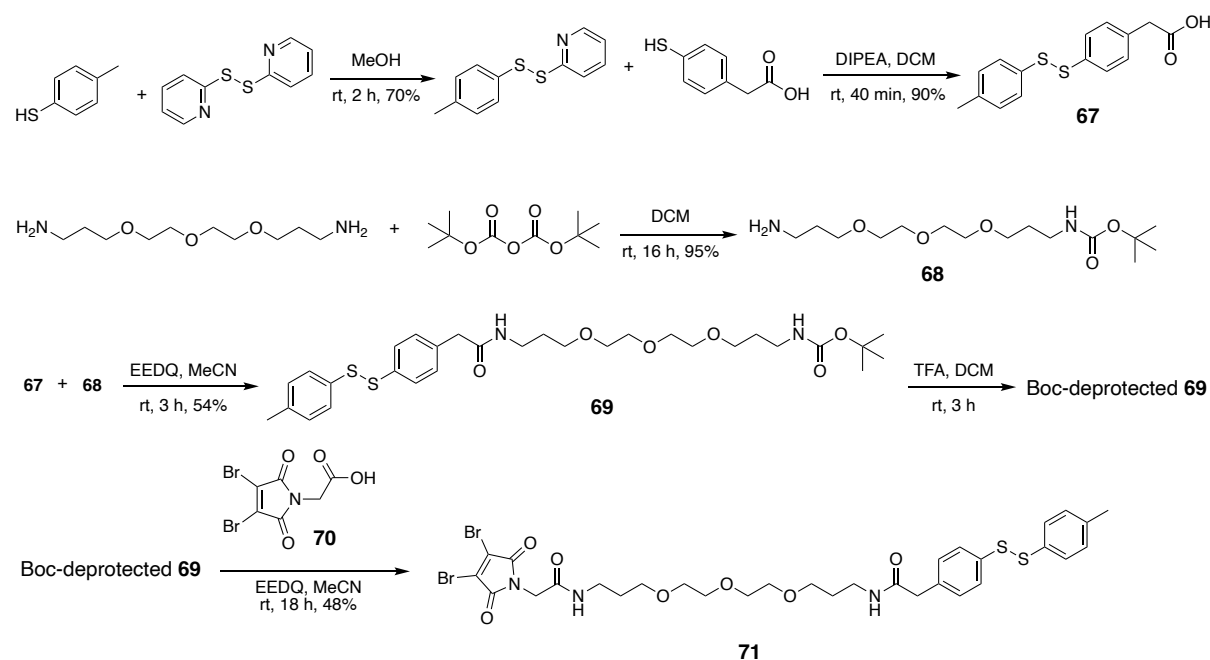roduct DBM-PEG-disulfide **71**. The DBM-PEG-disulfide **71** was then bioconjugated onto the full antibody to test the proposed hypothesis.

Scheme 33 – Synthesis of DBM-PEG-disulfide **71**.

3.5.2 Bioconjugation of DBM-disulfide to trastuzumab native antibody

Trastuzumab was reduced with TCEP, which was removed prior to the bioconjugation, before DBM-PEG-disulfide **71** was loaded on the reduced antibody (**Figure 43a**). The resulting antibody conjugate **72** was analysed by SDS-PAGE and LC-MS. According to the densitometry of SDS-PAGE, there were ~50% native disulfide bonds reformed after the bioconjugation which corresponded to our expectation (lane 3 in **Figure 43b**). If the hypothesis works, it would ideally lead to two DBM-bridged disulfide bonds and two native disulfide bonds where 1-2 moieties on HL and 2 moieties on HHLL would be observed. However, according to LC-MS, the DBM-PEG-disulfide linker gave 2 additions of moiety A on HL and mixtures of HHLL conjugates with 2 additions of moiety A, 1 addition of moiety A and 1 addition of moiety B, 2 additions of moiety A and 1 addition of moiety B, 4 additions of moiety A attached. (**Figure 43c**).

Figure 42 – Bioconjugation of DBM-PEG-disulfide **71** to antibody: a. i) 8 eq. of TCEP, 37 °C, 2 h, pH 8.5, ii) 10 eq. of DBM-PEG-disulfide **71**, 22 °C, 1 h, pH 8.5, b. SDS-PAGE: M. Protein ladder, 0. Native Ab, 1. Reduced Ab, 2. Ab-DBM-PEG-disulfide conjugate **72**, 3. Ab-DBM-PEG-disulfide conjugate **72** (DTT), c. LC-MS of antibody-DBM-PEG-disulfide conjugate **72**: HL expected 73113 Da (+ 1 moiety A), 73635 Da (+ 2 moiety A), observed 73633 Da (+ 2 moiety A), HHLL expected 146223 Da (+2 moiety A), observed 145179 Da (native Ab), 146222 Da (+2 moiety A), 146378 Da (+1 moiety A, +1 moiety B) and 146880 Da (+2 moiety A, +1 moiety B), 147265 Da (+4 moiety A).

In conclusion, a concept of bridging reagent-oxidant platform that can potentially deliver intermolecular disulfide bridging and then 'intramolecular' disulfide oxidation on

trastuzumab has been proposed to ideally generate antibody conjugates with controlled DARs. Based on this idea, a DBM-PEG-disulfide reagent **71** has been synthesised and conducted on antibody IgG1. This novel class of DBM-derived reagent however resulted in a mixture of antibody conjugates. There might be a competition of DBM bridging and disulfide reoxidation where both native antibody and fully bridged antibody conjugate with DAR of 4 as well as mixtures of intermediate conjugates have been observed. The concern in this methodology is that the oxidant moiety of reagent **71** reoxidises antibody thiols, generating free thiols which are likely to cyclise on its maleimide moiety or react with other DBMs. These side-reactions could result in the loss of bridging-available DBMs that would further lead to incomplete antibody conjugation.

Chapter 4: Conclusion and Future Work

Dibromomaleimides (DBMs), as a class of next generation maleimides (NGMs), can deliver rapid disulfide bridging and further result in robust IgG1 antibody conjugates with DARs of ~4 *via* post-conjugation hydrolysis. **Chapter 3.1** has expanded the scope of DBMs by developing trifunctional DBM reagents with two clickable handles derived from a lysine core. Upon antibody conjugation, trifunctional DBMs can undergo bioorthogonal click reactions to incorporate two different functionalities to further generate dual-modality antibody conjugates. However, CuAAC reactions have shown less efficiency than IEDDA and SPAAC reactions under similar antibody bioconjugation conditions, likely due to the requirement of catalyst. For further application, the dual-modality antibody conjugates can involve two different drugs or one drug and one imaging moiety which can provide more possibilities for the treatment of drug-resistant cancers or to trace the distribution of antibody drug conjugates (ADCs) *in vivo*.

Chapter 3.2 has shown another example of DBM-antibody conjugation where a metal chelator desferrioxamine B (DFO) is introduced to a DBM platform. As part of an ongoing project for antibody labelling and imaging between our group and Dr Michelle Ma's group at King's College London, we were interested to prepare and optimise antibody-DFO conjugates using DBM-DFO or azide-DFO reagents. The bioconjugation of DBM-DFO to antibody gave inefficient results in the initial trials of Dr Michelle Ma's group, which was further optimised in this project to yield antibody-DFO conjugates with improved homogeneity. However, it was observed that the DBM-DFO conjugation always led to adducts on the DFO conjugates, which implied the DBM-DFO might be contaminated. Instead, azide-DFO was applied to generate DFO conjugates where a DBM linker and a dibromopyridazinediones (diBrPD) linker were selected to connect the azide moiety and the antibody. In addition, compared to the DBM sequential bioconjugation, the *in situ* bioconjugation of diBrPDs delivered cleaner conjugates. The azide-DFO attempts demonstrated efficient antibody conjugation and the resultant DFO conjugates will be radiolabelled and characterised in Dr Michelle Ma's lab.

Chapter 3.3 has explored NGM-based *in situ* antibody bioconjugation to attempt to yield more homogeneous antibody conjugates. The half-antibody conjugates, formed in conventional bioconjugation due to disulfide scrambling in hinge region, have limited the

homogeneity of antibody conjugates. It was proved that the possibilities of forming half-antibody would be hugely reduced in *in situ* bioconjugation where reduction and bridging happen simultaneously.[163] To ensure bridging reagents are resistant to reducing reagent TCEP, dithiomaleimides (DTMs) have been developed with tuned reactivity compared to DBMs, which have demonstrated side-reactivity with TCEP. Some of the prepared DTMs in this project have shown limited TCEP reactivity and led to reduced formation of half-antibody conjugates. In addition, DTMs with reduced TCEP reactivity did show more promising results than that showed relatively high TCEP reactivity in *in situ* antibody bioconjugation. However, antibody-DTM conjugation also led to other mis-bridged antibody species as the released thiols from DTM bridging can potentially reattack the formed conjugates to cause deconjugation.

To further investigate *in situ* antibody bioconjugation, benzeneselenols have been attempted as alternative reducing reagents. Benzeneselenols can deliver rapid antibody reduction as well as have limited cross-reactions with bridging reagents (usually NGMs). However, benzeneselenols have pungent odour and poor aqueous solubility which made them less applicable in bioconjugation. Furthermore, benzeneselenols are highly sensitive to air oxidation and will form diselenides once in contact with air. To explore novel benzeneselenols with improved hydrophilicity and stability, several diaryl diselenides were synthesised and tested for antibody reduction in **Chapter 3.4**. Diaryl diselenides could be applied together with TCEP to generate the corresponding aryl selenols *in situ*. Among all the synthesised diselenides, bis(4-aminophenyl)diselenide exhibited the highest performance as a reducing reagent, due to its electron-donating amine group and the polarity of the amine group offering improved aqueous solubility. Bis(4-aminophenyl)diselenide has been employed with TCEP and dithiophenolmaleimide for *in situ* antibody bioconjugation, yielding antibody conjugates with DARs of 3-4. Other than the application in *in situ* bioconjugation, bis(4-aminophenyl)diselenide has also been applied to deliver complete antibody reduction in 4 min. Upon this rapid antibody reduction, the stepwise bioconjugation could be hugely accelerated where a 20-minute protocol to construct dual-modality antibody conjugates has been developed as a proof of concept.

Chapter 3.5 described an idea of generating antibody conjugates with controlled DAR of 2 by developing a disulfide bridging reagent-oxidant platform, for example a DBM-disulfide

reagent. The theory of this reagent is to undergo intermolecular DBM bridging first, and once the DBM is conjugated, the 'pseudo-intramolecular' disulfide reoxidation will occur to give antibody conjugates with ideally two DBM moieties inserted and two disulfide bonds reoxidised. However, the DBM-disulfide reagent delivered mixtures of antibody conjugate products, as there is a competition of DBM and disulfide reacting with reduced antibody. In addition, the leftover free thiol from the disulfide moiety could potentially lead to side-reactions. Therefore, more oxidants are currently under exploration to further develop the bridging reagent-oxidant platform to generate antibody conjugates with more controlled DARs.

Overall, by extending the scope of DBMs and exploring antibody conjugation using DBM related reagents, this project provided more opportunities for the design and construction of antibody conjugates with improved homogeneity.

Future work of this project could investigate more *ortho*-substituted diaryl diselenides that potentially have attenuated reactivity in comparison to para-substituted ones. The corresponding *ortho*-substituted aryl selenols with reduced reactivity could be promising for *in situ* antibody bioconjugation by delivering relatively slow reaction circle of disulfide reduction-reoxidation. Hence, the disulfide bridging on the antibody could be complete before disulfide reoxidation finishes. In addition, more interesting oxidants, for example sulfonyl chlorides,[264] diazenecaboxamides,[265] and *N*-chlorosuccinimide,[266] could be involved for future design of the bridging reagent-oxidant platform. The thiol reactivity of oxidants needs to be tested by performing competition reaction with bridging reagents (such as DBMs). Ideal oxidants would enable slower oxidant-thiol reaction than DBM-thiol reaction to make sure disulfide bridging occur first. The novel bridging reagent-oxidant scaffold can be promising to deliver antibody conjugates with controlled DARs.

Chapter 5: Experimental

5.1. Synthesis General Remarks

All chemical reagents and solvents were purchased from Merck, Thermo Fisher Scientific, VWR, Fluorochem, and used as per manufacturer instructions. All chemical reactions were carried out at atmospheric pressure, under argon. Room temperature is defined as between 15-25 °C. The term *in vacuo* refers to solvent removal using Büchi rotary evaporation between 15-60 °C, at approximately 10 mm Hg. All chemical reactions were monitored by thin-layer chromatography (TLC) using TLC plates pre-coated with silica gel 60 F_{254} on aluminium (Merck KGaA). Detection of synthesised compounds was done by UV (254 nm and 365 nm) or chemical stains ($KMnO_4$, ninhydrin and bromocresol green). Flash column chromatography was carried out using a Biotage Isolera with GraceResolv™ silica flash cartridges. ^1H and ^{13}C NMR spectra were recorded at ambient temperature on Bruker Advance AMX600 or AMX700 instruments, operating at 600 MHz of 700 MHz for ^1H and at 150 MHz or 175 MHz for ^{13}C in the stated solvents. Chemical shifts (δ) are reported in parts per million (ppm) and coupling constants (J) in Hertz (Hz). The multiplicity of each signal is indicated as s-singlet, d-doublet, t- triplet, q-quartet, quin-quintet, m-multiplet (i.e. complex peak obtained due to overlap) or a combination of these. All assignments were made with the aid of DEPT, COSY, HSQC, HMBC or NOESY correlation experiments. Infra-red spectra were recorded on a Bruker ALPHA FT-IR spectrometer operating in ATR mode, with frequencies given in reciprocal centimeters (cm^{-1}). Melting points were taken on a Gallenkamp apparatus and are uncorrected. High and low resolution mass spectra were recorded on a VG70 SE mass spectrometer, operating in modes ESI, EI, or CI (+ or -) depending on the sample, at the Department of Chemistry, University College London.

5.2. Syntheses

***N*2-(*Tert*-butoxycarbonyl)-*N*6-(pent-4-ynoyl)-L-lysine (1)**[267]
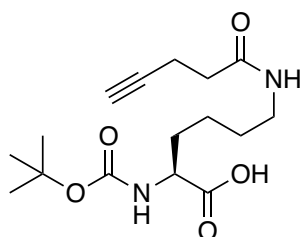
To a stirred solution of 4-pentynoic acid (196 mg, 2.00 mmol) and pentafluorophenol (260 µL, 2.40 mmol) in DMF (10 mL), 1-ethyl-3-(3-dimethylaminopropyl)carbodiimide (EDC) was added (479 mg, 2.50 mmol). The reaction mixture was stirred under argon at room temperature for 1 h. To the reaction mixture, Boc-lysine (443 mg, 1.80 mmol) and N,N-diisopropylethylamine (DIPEA) (940 µL, 5.4 mmol) were added. The reaction mixture was stirred under argon at room temperature for further 4 h. The solvent was co-evaporated *in vacuo* with toluene and then chloroform to give the crude product. Purification by flash chromatography on silica gel (methanol:DCM with 1% acetic acid, gradient elution from 0% to 5%) gave the product **1** as a pale-yellow oil (395 mg, 1.21 mmol, 67%).

^{1}H NMR (700 MHz, CDCl$_3$) δ = 6.12 (s, 1H, CO*NH*CH$_2$), 5.27 (d, *J* = 8.0 Hz, CO*NH*CH), 4.28 (q, *J* = 7.9 Hz, 1H, NH*CH*(CH$_2$)CO), 3.27 (q, *J* = 6.9 Hz, CH$_2$*CH$_2$*NH), 2.52 (t dt, *J* = 2.3, 7.2 Hz, 2H, C*CH$_2$*CH$_2$), 2.40 (t, *J* = 7.2 Hz, 2H, CH$_2$*CH$_2$*CO), 2.03 (t, *J* = 2.6 Hz, 1H, *HC*CCH$_2$), 1.87-1.83 (m, 1H, CH*CH$_2$*CH$_2$), 1.74-1.68 (m, 1H, H*CH$_2$*CH$_2$), 1.57-1.51 (m, 2H, CH$_2$*CH$_2$*CH$_2$NH), 1.44 (s, 11H, CH$_2$*CH$_2$*CH$_2$, COOC*(CH$_3$)$_3$*); ^{13}C NMR (175 MHz, CDCl$_3$) δ = 176.4 (C), 172.0 (C), 156.0 (C), 83.0 (C), 80.3 (C), 69.8 (CH), 53.3 (CH), 39.3 (CH$_2$), 35.5 (CH$_2$), 32.1 (CH$_2$), 28.9 (CH$_2$), 28.5 (CH$_3$), 22.5 (CH$_2$), 15.1 (CH$_2$); IR (oil) v_{max}/cm^{-1} 3237, 2938, 1728, 1636; LRMS (ESI) *m/z* (%) 325 ([M-H]$^-$, 100); HRMS (ESI) *m/z* calculated for [C$_{16}$H$_{25}$N$_2$O$_5$]$^-$ 325.1769, observed 325.1766.

**(*S*)-2-(3,4-dibromo-2,5-dioxo-2,5-dihydro-1*H*-pyrrol-1-yl)-6-(pent-4-ynamido)hexanoic acid (2)**
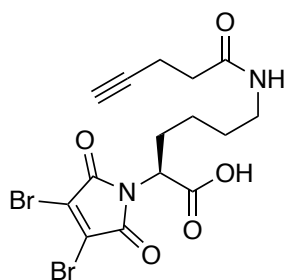
To a stirred solution of dibromomaleic acid (142 mg, 0.52 mmol) in acetic acid (10 mL), the compound **1** (104 mg, 0.32 mmol) was added. The resulting mixture was heated to reflux at 130 °C and stirred for 1 h. The solvent was co-evaporated with toluene and then chloroform *in vacuo* to give the crude product. Purification by flash chromatography on silica gel (ethyl

acetate:cyclohexane with 1% acetic acid, gradient elution from 0% to 100%) gave the product **2** as a yellow oil (101 mg, 0.22 mmol, 68%).

^{1}H NMR (700 MHz, CDCl$_3$) δ = 6.23 (s, 1H, CO*NH*CH$_2$), 4.70 (t, *J* = 7.8 Hz, 1H, N*CH*(CH$_2$)CO), 3.29-3.19 (m, 2H, CH$_2$*CH$_2$*NH), 2.48 (t, *J* = 7.3 Hz, 2H, C*CH$_2$*CH$_2$), 2.40 (t, *J* = 7.2 Hz, 2H, CH$_2$*CH$_2$*CO), 2.17 (q, *J* = 7.8 Hz, 2H, CH*CH$_2$*CH$_2$), 2.02 (t, *J* = 2.5 Hz, 1H, *HC*CCH$_2$), 1.58-1.49 (m, 2H, CH$_2$*CH$_2$*CH$_2$), 1.35-1.30 (m, 2H, CH$_2$*CH$_2$*CH$_2$); ^{13}C NMR (175 MHz, CDCl$_3$) δ = 172.8 (C), 171.6 (C), 163.7 (C), 129.8 (C), 82.8 (C), 70.1 (CH), 53.8 (CH), 39.5 (CH$_2$), 35.3 (CH$_2$), 28.5 (CH$_2$), 28.2 (CH$_2$), 23.6 (CH$_2$), 15.2 (CH$_2$); IR (oil) ν$_{max}$/cm^{-1} 3299, 2940, 1722, 1592; LRMS (ESI) *m/z* (%) 465 ([^{81,81}M-H]$^-$, 50), 463 ([^{81,79}M-H]$^-$, 100), 461 ([^{79,79}M-H]$^-$, 50); HRMS (ESI) *m/z* calculated for [C$_{15}$H$_{15}$^{81,79}Br$_2$N$_2$O$_5$]$^-$ 462.9333, observed 462.9332.

(*S*)-2-(3,4-dibromo-2,5-dioxo-2,5-dihydro-1*H*-pyrrol-1-yl)-6-(pent-4-ynamido)-*N*-(prop-2-yn-1-yl)hexanamide (3)
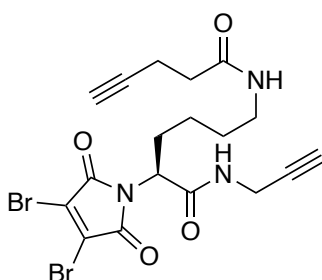
To a stirred solution of the compound **2** (32 mg, 0.07 mmol) in acetonitrile (5 mL), *N*-ethoxycarbonyl-2-ethoxy-1,2-dihydroquinoline (EEDQ) (35 mg, 0.14 mmol) was added. The resulting reaction mixture was stirred under argon at room temperature for 1 h. Propargylamine (5.4 µL, 0.08 mmol) was then added. The reaction mixture was stirred under argon at room temperature for 3 h. The solvent was removed *in vacuo* to afford the crude product. Purification by flash chromatography on silica gel (ethyl acetate:cyclohexane, gradient elution from 0% to 100%) gave the product **3** as a yellow oil (28 mg, 0.06 mmol, 81%).

^{1}H NMR (700 MHz, CDCl$_3$) δ = 6.82 (t, *J* = 5.0 Hz, 1H, CO*NH*CH$_2$), 5.85 (t, *J* = 5.0 Hz, 1H, CO*NH*CH$_2$), 4.66 (dd, *J* = 5.0, 10.7 Hz, 1H, N*CH*CO), 4.04, (td, *J* = 2.5, 5.3 Hz, 2H, CH$_2$*CH$_2$*NH), 3.40-3.35 (m, 1H, NH*CH$_2$*CCH), 3.22-3.17 (m, 1H, NH*CH$_2$*CCH), 2.56-2.47 (m, 2H, C*CH$_2$*CH$_2$), 2.38 (t, *J* = 6.8 Hz, 2H, CH*CH$_2$*CH$_2$), 2.29-2.25 (m, 1H, CH*CH$_2$*CH$_2$), 2.24 (t, *J* = 2.6 Hz, 1H, *HC*CCH$_2$NH), 2.17-2.12 (m, 1H, CH*CH$_2$*CH$_2$), 2.03 (t, *J* = 2.6 Hz, 1H, *HC*CCH$_2$CH$_2$), 1.58-1.50 (m, 2H, CH$_2$*CH$_2$*CH$_2$NH), 1.38-

1.29 (m, 2H, CH$_2$*CH$_2$*CH$_2$); ^{13}C NMR (175 MHz, CDCl$_3$) δ = 171.6 (C), 167.9 (C), 164.1 (C), 129.9 (C), 83.1 (C), 79.1 (C), 72.0 (CH), 69.7 (CH), 56.0 (CH), 38.5 (CH$_2$), 35.5 (CH$_2$), 29.8 (CH$_2$), 28.6 (CH$_2$), 28.0 (CH$_2$), 23.4 (CH$_2$), 15.1 (CH$_2$); IR (oil) ν$_{max}$/cm^{-1} 3280, 2927, 1722, 1638; LRMS (ESI) *m/z* (%) 504 ([^{81,81}M+H]$^+$, 50), 502 ([^{81,79}M+H]$^+$, 100), 500 ([^{79,79}M+H]$^+$, 50); HRMS (ESI) *m/z* calculated for [C$_{18}$H$_{19}$^{81,79}Br$_2$N$_3$O$_4$H]$^+$ 501.9801, observed 501.9798.

Bicyclo[6.1.0]non-4-yn-9-ylmethyl ((*S*)-11-(3,4-dibromo-2,5-dioxo-2,5-dihydro-1*H*-pyrrol-1-yl)-10,17-dioxo-3,6-dioxa-9,16-diazahenicos-20-yn-1-yl)carbamate (4)
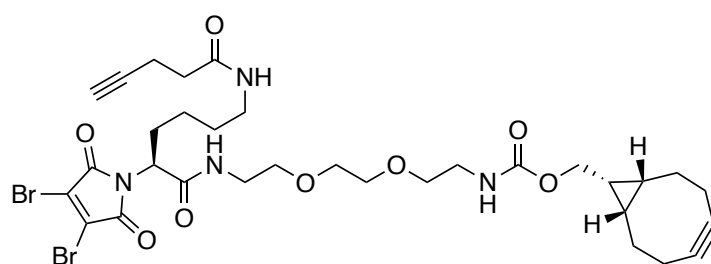
To a stirred solution of the compound **2** (100 mg, 0.22 mmol) in acetonitrile (5 mL), EEDQ (80 mg, 0.32 mmol) was added. The resulting reaction mixture was stirred under argon at room temperature for 1 h. BCN-amine (54 mg, 0.17 mmol) was then added. The reaction mixture was stirred under argon at room temperature for 3 h. The solvent was removed *in vacuo* to afford the crude product. Purification by flash chromatography on silica gel (first in ethyl acetate:cyclohexane, gradient elution from 0% to 100%; second in methanol:DCM, gradient elution from 0% to 5%) gave the product **4** as a yellow oil (72 mg, 0.09 mmol, 56%).

^{1}H NMR (600 MHz, CDCl$_3$) δ = 6.79 (s, 1H, CO*NH*CH$_2$), 5.89 (s, 1H, CO*NH*CH$_2$), 4.65 (td, *J* = 4.8, 10.8 Hz, 1H, N*CH*(CH$_2$)CO), 4.11, (d, *J* = 8.2 Hz, 2H, O*CH$_2$*CH), 3.60-3.52 (m, 8H, CH$_2$*CH$_2$*O), 3.48-3.40 (m, 2H, CH$_2$*CH$_2$*NH), 3.38-3.36 (m, 2H, CH$_2$*CH$_2$*NH), 3.33-3.29 (m, 1H, CH$_2$*CH$_2$*NH), 3.23-3.17 (m, 1H, CH$_2$*CH$_2$*NH), 2.50 (t, *J* = 6.6 Hz, 2H, C*CH$_2$*CH$_2$), 2.37 (t, *J* = 6.6 Hz, 2H, CH$_2$*CH$_2$*CO), 2.30-2.19 (m, 8H, C*CH$_2$*CH$_2$, CH$_2$*CH$_2$*CH), 2.09 (s, 2H, CH*CH$_2$*CH$_2$), 2.01 (s, 1H, *HC*CCH$_2$), 1.57-1.50 (m, 2H, CH$_2$*CH$_2$*CH$_2$), 1.36-1.27 (m, 3H, CH$_2$*CH$_2$*CH$_2$, CH$_2$*CH*CH), 0.93 (t, *J* = 8.8 Hz, 2H, CH*CH*CH$_2$); ^{13}C NMR (150 MHz, CDCl$_3$) δ = 171.4 (C), 168.1 (C), 164.1 (C), 157.0 (C), 129.9 (C), 99.0 (C), 83.2 (C), 70.4 (CH$_2$), 70.3 (CH$_2$), 70.2 (CH$_2$), 69.6 (CH$_2$), 69.5 (CH), 63.0 (CH$_2$), 60.6 (CH), 56.0 (CH), 40.9 (CH$_2$), 39.9 (CH$_2$), 38.7 (CH$_2$), 35.5 (CH$_2$), 29.2 (CH$_2$), 28.7 (CH$_2$), 28.1 (CH$_2$), 23.5 (CH$_2$), 21.6 (CH$_2$), 20.2 (CH), 17.9 (CH), 15.1 (CH$_2$); IR (oil) ν$_{max}$/cm^{-1} 3296, 2918, 1725, 1651;

LRMS (ESI) *m/z* (%) 773 ([^{81,81}M+H]$^+$, 50), 771 ([^{81,79}M+H]$^+$, 100), 769 ([^{79,79}M+H]$^+$, 50); HRMS (ESI) *m/z* calculated for [C$_{32}$H$_{42}$^{79,79}Br$_2$N$_4$O$_8$H]$^+$ 769.1442, observed 769.1492.

N2-(*tert*-butoxycarbonyl)-*N*6-(2-(2-methoxyethoxy)acetyl)-L-lysine (5)
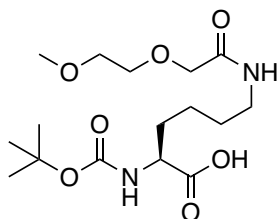
To a stirred solution of methoxyethoxy acetic acid (150 μL, 1.32 mmol) in DMF (10 mL), pentafluorophenol (170 μL, 1.65 mmol) and EDC (316 mg, 1.65 mmol) were added. The resulting mixture was stirred under argon at room temperature for 1 h. Boc-Lysine (256 mg, 1.01 mmol) and DIPEA (1.14 mL, 3.30 mmol) were added separately. The reaction mixture was stirred under argon at room temperature for 4 h to give a transparent solution. The solvent was co-evaporated with toluene and then chloroform *in vacuo* to give the crude product. Purification by flash chromatography on silica gel (methanol:DCM with 1% acetic acid, gradient elution from 0% to 5%) gave the product **5** as a pale-yellow oil (189 mg, 0.52 mmol, 52%).

^{1}H NMR (700 MHz, CDCl$_3$) δ = 7.13 (t, *J* = 5.8 Hz, 1H, CO*NH*CH$_2$), 5.28 (s, 1H, CO*NH*CH), 4.27 (dd, *J* = 6.3, 6.9 Hz, 1H, NH*CH*COOH), 3.98 (s, 2H, CO*CH$_2$*O), 3.65-3.64 (m, 2H, CH$_2$*CH$_2$*O), 3.57-3.56 (m, 2H, O*CH$_2$*CH$_2$), 3.40 (s, 3H, CH$_2$O*CH$_3$*), 3.32-3.23 (m, 2H, CH$_2$*CH$_2$*NH), 1.85-1.80 (m, 1H, CH*CH$_2$*CH$_2$), 1.74-1.69 (m, 1H, CH*CH$_2$*CH$_2$), 1.60-1.50 (m, 2H, CH$_2$*CH$_2$*CH$_2$NH), 1.42 (s, 11H, COO*C(CH$_3$)$_3$*, CH$_2$*CH$_2$*CH$_2$); ^{13}C NMR (175 MHz, CDCl$_3$) δ = 175.0 (C), 170.6 (C), 155.7 (C), 80.0 (C), 71.6 (CH$_2$), 70.8 (CH$_2$), 70.3 (CH$_2$), 59.0 (CH$_3$), 53.2 (CH), 38.5 (CH$_2$), 31.8 (CH$_2$), 28.5 (CH$_2$), 28.5 (OC(CH$_3$)$_3$), 22.2 (CH$_2$); IR (oil) v$_{max}$/cm^{-1} 2922, 1726, 1644; LRMS (ESI) *m/z* (%) 363 ([M+H]$^+$, 100); HRMS (ESI) *m/z* calculated for [C$_{16}$H$_{30}$N$_2$O$_7$H]$^+$ 363.2126, observed 363.2110.

(*S*)-2-(3,4-dibromo-2,5-dioxo-2,5-dihydro-1*H*-pyrrol-1-yl)-6-(2-(2-methoxyethoxy)acetamido)hexanoic acid (6)
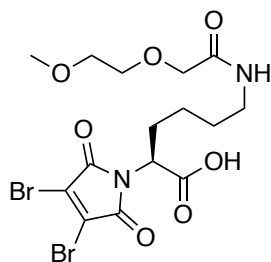
To a stirred solution of dibromomaleic acid (184 mg, 0.67 mmol) in acetic acid (10 mL), the compound **5** (157 mg, 0.43 mmol) was added. The resulting reaction mixture was heated to reflux at 130 °C and stirred for 1 h. The solvent was co-evaporated with toluene and then chloroform *in vacuo* to give the crude product. Purification by flash chromatography on silica gel (methanol:DCM with 1% acetic acid, gradient elution from 0% to 5%) gave the product **6** as a yellow oil (138 mg, 0.28 mmol, 64%).

^{1}H NMR (700 MHz, CDCl$_3$) δ = 7.18 (t, *J* = 5.8 Hz, 1H, CON*H*CH$_2$), 4.73 (dd, *J* = 5.8, 9.4 Hz, 1H, NC*H*COOH), 4.00 (s, 2H, OC*H$_2$*CO), 3.67-3.66 (m, 2H, OC*H$_2$*CH$_2$), 3.60-3.58 (m, 2H, CH$_2$C*H$_2$*O), 3.42 (s, 3H, OC*H$_3$*), 3.35-3.27 (m, 2H, CH$_2$C*H$_2$*NH), 2.28-2.23 (m, 1H, CHC*H$_2$*CH$_2$), 2.13-2.08 (m, 1H, CHC*H$_2$*CH$_2$), 1.60-1.56 (m, 2H, CH$_2$C*H$_2$*CH), 1.46-1.39 (m, 2H, CH$_2$C*H$_2$*CH$_2$); ^{13}C NMR (175 MHz, CDCl$_3$) δ = 170.9 (C), 170.8 (C), 163.6 (C), 129.8 (C), 71.7 (CH$_2$), 70.8 (CH$_2$), 70.3 (CH$_2$), 59.1 (CH$_3$), 53.6 (CH), 38.2 (CH$_2$), 28.1 (CH$_2$), 28.1 (CH$_2$), 23.5 (CH$_2$); IR (oil) v$_{max}$/cm^{-1} 2926, 1725, 1632; LRMS (ESI) *m/z* (%) 503 ([^{81,81}M+H]$^+$, 50), 501 ([^{81,79}M+H]$^+$, 100), 499 ([^{79,79}M+H]$^+$, 50); HRMS (ESI) *m/z* calculated for [C$_{15}$H$_{20}$^{79,79}Br$_2$N$_2$O$_7$H]$^+$ 498.9710, observed 498.9717.

(S)-2-(3,4-dibromo-2,5-dioxo-2,5-dihydro-1H-pyrrol-1-yl)-6-(2-(2-methoxyethoxy)acetamido)-N-(prop-2-yn-1-yl)hexanamide (7)
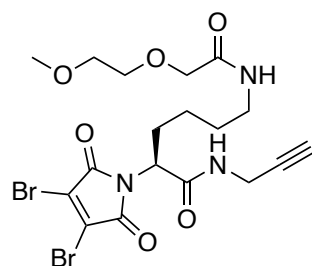
To a stirred solution of compound **6** (100 mg, 0.20 mmol) in acetonitrile (5 mL), EEDQ (78 mg, 0.32 mmol) was added. The resulting reaction mixture was stirred under argon at room temperature for 1 h. Propargylamine (20 µL, 0.31 mmol) was then added. The reaction

mixture was stirred under argon at room temperature for 3 h. The solvent was removed *in vacuo* to afford the crude product. Purification by flash chromatography on silica gel (ethyl acetate:cyclohexane, gradient elution from 0% to 100%) gave the product **7** as a yellow oil (73 mg, 0.14 mmol, 68%).

^{1}H NMR (700 MHz, CDCl$_3$) δ = 7.08 (t, *J* = 5.8 Hz, 1H, CO*NH*CH$_2$), 6.76 (t, *J* = 5.3 Hz, 1H, CO*NH*CH$_2$), 4.66 (dd, *J* = 5.0, 10.7 Hz, 1H, N*CH*CO), 4.03 (dd, *J* = 2.5, 5.3 Hz, 2H, NH*CH$_2$*CCH), 3.97 (s, 2H, O*CH$_2$*CO), 3.66-3.65 (m, 2H, O*CH$_2$*CH$_2$), 3.55-3.54 (m, 2H, CH$_2$*CH$_2$*O), 3.39 (s, 3H, *CH$_3$*O), 3.38-3.33 (m, 1H, CH$_2$*CH$_2$*NH), 3.24-3.19 (m, 1H, CH$_2$*CH$_2$*NH), 2.30-2.25 (m, 1H, CH*CH$_2$*CH$_2$), 2.23 (t, *J* = 2.5 Hz, 1H, *HC*C), 2.15-2.10 (m, 1H, CH*CH$_2$*CH$_2$), 1.59-1.52 (m, 2H, CH$_2$*CH$_2$*CH$_2$), 1.38-1.29 (m, 2H, CH$_2$*CH$_2$*CH$_2$); ^{13}C NMR (175 MHz, CDCl$_3$) δ = 170.4 (C), 167.8 (C), 164.0 (C), 129.9 (C), 79.2 (C), 72.0 (CH), 71.6 (CH$_2$), 71.2 (CH$_2$), 70.4 (CH$_2$), 59.2 (CH$_3$), 56.0 (CH), 38.0 (CH$_2$), 29.7 (CH$_2$), 28.6 (CH$_2$), 28.1 (CH$_2$), 23.6 (CH$_2$); IR (oil) v_{max}/cm^{-1} 3304, 1722, 1632; LRMS (ESI) *m/z* (%) 540 ([^{81,81}M+H]$^+$, 50), 538 ([^{81,79}M+H]$^+$, 100), 536 ([^{79,79}M+H]$^+$, 50); HRMS (ESI) *m/z* calculated for [C$_{18}$H$_{23}$^{81,79}Br$_2$N$_3$O$_6$H]$^+$ 538.0013, observed 537.9943.

1*H*-imidazole-1-sulfonyl azide (8)[230]
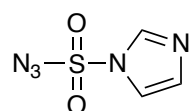
Sulfuryl chloride (400 µL, 5.00 mmol) was added dropwise to an ice-cooled suspension of sodium azide (320 mg, 5.00 mmol) in acetonitrile (5 mL). The resulting mixture was stirred under argon at room temperature for 16 h. Imidazole (680 mg, 10.00 mmol) was added to the ice-cooled mixture and the resulting slurry stirred under argon at room temperature for 4 h. The solvent was removed *in vacuo* to afford the crude product. Purification by flash chromatography on silica gel (ethyl acetate:cyclohexane, gradient elution from 0% to 100%) gave the product **8** as a colourless liquid (620 mg, 3.58 mmol, 72%).

^{1}H NMR (700 MHz, CDCl$_3$) δ = 8.02 (s, 1H, Ar-H), 7.38 (t, *J* = 1.5 Hz, 1H, Ar-H), 7.23 (d, *J* = 1.0 Hz, 1H, Ar-H); ^{13}C NMR (175 MHz, CDCl$_3$) δ = 136.8 (CH), 132.1 (CH), 117.8 (CH); IR (oil) v_{max}/cm^{-1} 3130, 2143, 1416; LRMS (ESI) *m/z* (%) 174 ([M+H]$^+$, 100); HRMS (ESI) *m/z* calculated for [C$_3$H$_3$N$_5$O$_2$SH]$^+$ 174.0080, observed 174.0079.

N2-(*tert*-butoxycarbonyl)-*N*6-diazo-L-lysine (9)[268]
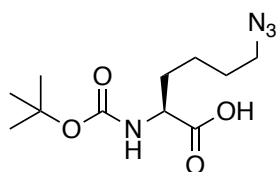
Compound **8** (416 mg, 2.4 mmol) was added to Boc-Lysine (493 mg, 2.0 mmol), K_2CO_3 (140 mg, 1.0 mmol) and $CuSO_4.5H_2O$ (5 mg, 20 µmol) in methanol (10 mL). The resulting mixture was stirred under argon at room temperature for 4 h. The solvent was removed *in vacuo* to afford the crude product. Purification by flash chromatography on silica gel (methanol:DCM with 1% acetic acid, gradient elution from 0% to 10%) gave the product **9** as a pale-yellow oil (410 mg, 1.51 mmol, 75%).

^{1}H NMR (600 MHz, CDCl$_3$) δ = 4.31 (q, *J* = 7.6 Hz, 1H, NH*CH*COOH), 3.28 (t, *J* = 6.8 Hz, 2H, CH$_2$*CH$_2$*N$_3$), 1.91-1.83 (m, 1H, CH*CH$_2$*CH$_2$), 1.72-1.66 (m, 1H, CH*CH$_2$*CH$_2$), 1.64-1.56 (m, 2H, CH$_2$*CH$_2$*CH$_2$), 1.51-1.45 (m, 2H, CH$_2$*CH$_2$*CH$_2$), 1.43 (s, 9H, OC*(CH$_3$)$_3$*); ^{13}C NMR (150 MHz, CDCl$_3$) δ = 177.1 (C), 155.8 (C), 80.6 (C), 53.3 (CH), 51.3 (CH$_2$), 32.0 (CH$_2$), 28.5 (CH$_2$), 28.4 (CH$_3$), 22.7 (CH$_2$); IR (oil) v$_{max}$/cm^{-1} 2936, 2096, 1710, 1456; LRMS (ESI) *m/z* (%) 271 ([M+H]$^+$, 100); HRMS (ESI) *m/z* calculated for [C$_{11}$H$_{20}$N$_4$O$_4$H]$^+$ 273.1557, observed 273.1553.

(*S*)-6-azido-2-(3,4-dibromo-2,5-dioxo-2,5-dihydro-1*H*-pyrrol-1-yl)hexanoic acid (10)
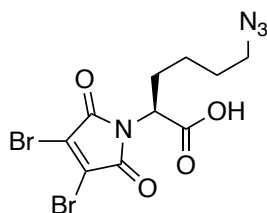
To a stirred solution of dibromomaleic acid (604 mg, 2.20 mmol) in acetic acid (10 mL), the compound **9** (400 mg, 1.47 mmol) was added. The resulting mixture was heated to reflux at 130 °C and stirred for 1 h. The solvent was co-evaporated with toluene and then chloroform *in vacuo* to give the crude product. Purification by flash chromatography on silica gel (ethyl acetate:cyclohexane with 1% acetic acid, gradient elution from 0% to 100%) gave the product **10** as a yellow oil (444 mg, 1.09 mmol, 74%).

^{1}H NMR (600 MHz, CDCl$_3$) δ = 4.76 (dd, J = 5.0, 10.8 Hz, 1H, NC*H*CO), 3.27 (td, J = 2.6, 6.7 Hz, 2H, CH$_2$C*H$_2$*NH), 2.28-2.21 (m, 1H, CHC*H$_2$*CH$_2$), 2.18-2.14 (m, 1H, CHC*H$_2$*CH$_2$), 1.63-1.55 (m, 2H, CH$_2$C*H$_2$*CH$_2$), 1.43-1.33 (m, 2H, CH$_2$C*H$_2$*CH$_2$); ^{13}C NMR (150 MHz, CDCl$_3$) δ = 174.2 (C), 163.5 (C), 129.9 (C), 53.5 (CH), 51.1 (CH$_2$), 28.2 (CH$_2$), 28.1 (CH$_2$), 23.7 (CH$_2$); IR (oil) v$_{max}$/cm^{-1} 2927, 2097, 1715; LRMS (ESI) *m/z* (%) 411 ([^{81,81}M+H]$^+$, 50), 409 ([^{81,79}M+H]$^+$, 100), 407 ([^{79,79}M+H]$^+$, 50); HRMS (ESI) *m/z* calculated for [C$_{10}$H$_{10}$^{81,79}Br$_2$N$_4$O$_4$H]$^+$ 408.8976, observed 408.8976.

N-(2-(2-(2-aminoethoxy)ethoxy)ethyl)-2-(4-(6-methyl-1,2,4,5-tetrazin-3-yl)phenyl)acetamide (11)
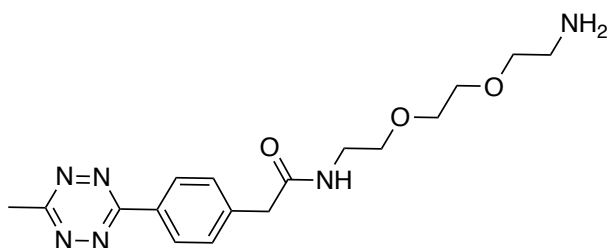
To a stirred solution of the 2,2′-(ethylenedioxy)bis(ethylamine) (17 μL, 0.12 mmol) and methyltetrazine-NHS ester (30 mg, 0.09 mmol) in acetonitrile (3 mL), DIPEA (24 μL, 0.14 mmol) was added. The resulting reaction mixture was stirred under argon at room temperature for 4 h. The solvent was removed *in vacuo* to afford the crude product. Purification by flash chromatography on silica gel (methanol:DCM, gradient elution from 0% to 100%) gave the product **11** as a pink oil (18 mg, 0.05 mmol, 56%).

^{1}H NMR (600 MHz, CDCl$_3$) δ = 8.54 (d, J = 8.2 Hz, 2H, Ar-H), 7.53 (d, J = 8.2 Hz, 2H, Ar-H), 3.67 (s, 2H, CC*H$_2$*CO), 3.60-3.55 (m, 8H, CH$_2$C*H$_2$*O), 3.46 (q, J = 5.0 Hz, 2H, CH$_2$C*H$_2$*NH$_2$), 3.09 (s, 3H, *CH$_3$*CNN), 2.95 (t, J = 5.1 Hz, 2H, NHC*H$_2$*CH$_2$); ^{13}C NMR (150 MHz, CDCl$_3$) δ = 170.5 (C), 167.4(C), 164.0 (C), 140.4 (C), 130.7 (C), 130.3 (CH), 128.4 (CH), 71.3 (CH$_2$), 70.4 (CH$_2$), 70.2 (CH$_2$), 70.0 (CH$_2$), 43.6 (CH$_2$), 41.0 (CH$_2$), 39.7 (CH$_2$), 21.3 (CH$_3$); IR (oil) v$_{max}$/cm^{-1} 3280, 2923, 2150, 1650, 1609, 1421, 1405; LRMS (ESI) *m/z* (%) 361 ([M+H]$^+$, 100); HRMS (ESI) *m/z* calculated for [C$_{17}$H$_{24}$N$_6$O$_3$H]$^+$ 361.1983, observed 361.1981.

(S)-6-azido-2-(3,4-dibromo-2,5-dioxo-2,5-dihydro-1H-pyrrol-1-yl)-N-(2-(2-(2-(4-(6-methyl-1,2,4,5-tetrazin-3-yl)phenyl)acetamido)ethoxy)ethoxy)ethyl)hexanamide (12)
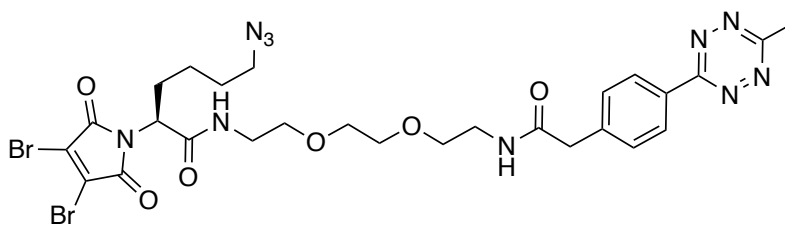
To a stirred solution of the compound **10** (26 mg, 0.06 mmol) in acetonitrile (3 mL), EEDQ (24 mg, 0.10 mmol) was added. The resulting reaction mixture was stirred under argon at room temperature for 1 h. The compound **11** (21 mg, 0.06 mmol) was then added. The reaction mixture was stirred under argon at room temperature for 3 h. The solvent was removed *in vacuo* to afford the crude product. Purification by flash chromatography on silica gel (first in ethyl acetate:cyclohexane, gradient elution from 0% to 100%; second in methanol:DCM, gradient elution from 0% to 10%) gave the product **12** as a pink oil (24 mg, 0.03 mmol, 54%).

^{1}H NMR (600 MHz, CDCl$_3$) δ = 8.57 (d, *J* = 8.0 Hz, 2H, Ar-H), 7.53 (d, *J* = 8.0 Hz, 2H, Ar-H), 6.65 (s, 1H, CO*NH*CH$_2$), 6.03 (s, 1H, CO*NH*CH$_2$), 4.66 (dd, *J* = 5.2, 11.0 Hz, 1H, N*CH*CO), 3.67 (s, 2H, CO*CH$_2$*C), 3.57-3.52 (m, 6H, CH$_2$*CH$_2$*O), 3.49-3.47 (m, 2H, CH$_2$*CH$_2$*O), 3.46-3.43 (m, 2H, CH$_2$*CH$_2$*NH), 3.42-3.32 (m, 2H, CH$_2$*CH$_2$*NH), 3.30-3.24 (m, 2H, CH$_2$*CH$_2$*N$_3$), 3.10 (s, 3H, *CH$_3$*CNN), 2.27-2.20 (m, 1H, CH*CH$_2$*CH$_2$), 2.11-2.05 (m, 1H, CH*CH$_2$*CH$_2$), 1.66-1.60 (m, 2H, CH$_2$*CH$_2$*CH$_2$), 1.37-1.32 (m, 2H, CH$_2$*CH$_2$*CH$_2$); ^{13}C NMR (150 MHz, CDCl$_3$) δ = 170.5 (C), 168.0(C), 167.5 (C), 164.0 (C), 164.0 (C), 140.0 (C), 130.9 (C), 130.5 (CH), 129.9 (C), 128.5(CH), 70.5 (CH$_2$), 70.2 (CH$_2$), 69.8 (CH$_2$), 69.6 (CH$_2$), 55.9 (CH), 51.1 (CH$_2$), 43.8 (CH$_2$), 39.9 (CH$_2$), 39.6 (CH$_2$), 28.3 (CH$_2$), 28.2 (CH$_2$), 23.8 (CH$_2$), 21.3 (CH$_3$); IR (oil) v_{max}/cm^{-1} 3292, 2925, 2149, 2908, 1729, 1670, 1460, 1422, 1405; LRMS (ESI) *m/z* (%) 755 ([^{81,81}M+H]$^+$, 50), 753 ([^{81,79}M+H]$^+$, 100), 751 ([^{79,79}M+H]$^+$, 50); HRMS (ESI) *m/z* calculated for [C$_{27}$H$_{32}$^{81,79}Br$_2$N$_{10}$O$_6$H]$^+$ 753.0925, observed 753.0908.

**Dimethyl 2,2'-((2,5-dioxo-1-phenyl-2,5-dihydro-1*H*-pyrrole-3,4-diyl)bis(sulfanediyl))diacetate (40)**
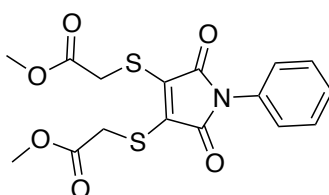
To a stirred solution of 2,3-dichloro-*N*-phenylmaleimide (145 mg, 0.60 mmol) and triethylamine (120 μL, 1.34 mmol) in DCM (10 mL), methyl thioglycolate (170 μL, 1.22 mmol) was added. The resulting reaction mixture was stirred under argon at room temperature for 1 h. The solvent was removed *in vacuo* to afford the crude product. Purification by flash chromatography on silica gel (ethyl acetate:cyclohexane, gradient elution from 0% to 50%) gave the product **40** as a yellow oil (80 mg, 0.21 mmol, 35%).

^{1}H NMR (700 MHz, CDCl$_3$): δ = 7.45 (t, *J* = 7.9 Hz, 2H, Ar-H), 7.36 (t, *J* = 7.5 Hz, 1H, Ar-H), 7.31 (d, *J* = 8.0 Hz, 2H, Ar-H), 4.13 (s, 4H, CO*CH$_2$*S), 3.77 (s, 6H, O*CH$_3$*); ^{13}C NMR (175 MHz, CDCl$_3$): δ = 169.0 (C), 165.0 (C), 134.9 (C), 131.3 (C), 129.3 (CH), 128.3 (CH), 126.3 (CH), 53.1 (CH$_3$), 33.2 (CH$_2$); IR (oil) ν$_{max}$/cm^{-1} 2952, 1735, 1706, 1501; LRMS (ESI) *m/z* (%) 382 ([M+H]$^+$, 100); HRMS (ESI) *m/z* calculated for [C$_{16}$H$_{16}$NO$_6$S$_2$H]$^+$ 382.0419, observed 382.0421.

Diethyl 2,2'-((2,5-dioxo-1-phenyl-2,5-dihydro-1*H*-pyrrole-3,4-diyl)bis(sulfanediyl))diacetate (41)
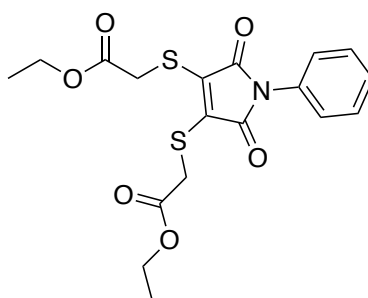
To a stirred solution of 2,3-dichloro-*N*-phenylmaleimide (145 mg, 0.60 mmol) and triethylamine (169 μL, 1.20 mmol) in DCM (10 mL), ethyl thioglycolate (145 μL, 1.33 mmol) was added. The resulting reaction mixture was stirred under argon at room temperature for 1 h. The solvent was removed *in vacuo* to afford the crude product. Purification by flash chromatography on silica gel (ethyl acetate:cyclohexane, gradient elution from 0% to 40%) gave the product **41** as a yellow oil (80 mg, 0.20 mmol, 33%).

^{1}H NMR (600 MHz, CHCl$_3$): δ = 7.45 (t, *J* = 7.8 Hz, 2H, Ar-H), 7.36 (t, *J* = 7.4 Hz, 1H, Ar-H), 7.31 (d, *J* = 7.7 Hz, 2H, Ar-H), 4.21 (q, *J* = 7.1 Hz, 4H, CH$_3$*CH$_2$*O), 4.12 (s, 4H, CO*CH$_2$*S), 1.28 (t, *J* = 7.2 Hz, 6H, *CH$_3$*CH$_2$); ^{13}C NMR (150 MHz, CHCl$_3$): δ = 168.5 (C), 165.1 (C), 135.0 (C), 131.3 (C), 129.3 (CH), 128.2 (CH), 126.3 (CH), 62.2 (CH$_2$), 33.4 (CH$_2$), 14.3 (CH$_3$); IR (oil) ν$_{max}$/cm^{-1} 2982,2927,

1709, 1502; LRMS (ESI) *m/z* (%) 410 ([M+H]$^+$, 100); HRMS (ESI) *m/z* calculated for [C$_{18}$H$_{19}$NO$_6$S$_2$H]$^+$ 410.0732, observed 410.0723.

## 3,4-bis((2-methoxyethyl)thio)-1-phenyl-1*H*-pyrrole-2,5-dione (42)
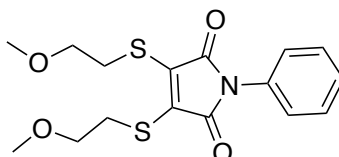
To a stirred solution of 2,3-dichloro-*N*-phenylmaleimide (121 mg, 0.50 mmol) and triethylamine (139 μL, 1.00 mmol) in DCM (10 mL), 2-methoxyethanethiol (99 μL, 1.00 mmol) was added. The resulting reaction mixture was stirred under argon at room temperature for 1 h. The solvent was removed *in vacuo* to afford the crude product. Purification by flash chromatography on silica gel (ethyl acetate:cyclohexane, gradient elution from 0% to 50%) gave the product **42** as a yellow oil (87 mg, 0.25 mmol, 49%).

^{1}H NMR (700 MHz, CDCl$_3$): δ = 7.45 (t, *J* = 7.8 Hz, 2H, Ar-H), 7.35 (t, *J* = 7.6 Hz, 1H, Ar-H), 7.32 (d, *J* = 7.8 Hz, 2H, Ar-H), 3.67 (t, *J* = 6.0 Hz, 4H, OC*H$_2$*CH$_2$), 3.54 (t, *J* = 6.0 Hz, 4H, CH$_2$C*H$_2$*S), 3.37 (s, 6H, OC*H$_3$*); ^{13}C NMR (175 MHz, CDCl$_3$): δ = 165.4 (C), 135.8 (C), 131.6 (C), 129.2 (CH), 128.1 (CH), 126.3 (CH), 72.0 (CH$_2$), 59.0 (CH$_3$), 31.6 (CH$_2$); IR (oil) v$_{max}$/cm^{-1} 2923, 2822, 1705, 1500; LRMS (ESI) *m/z* (%) 354 ([M+H]$^+$, 100); HRMS (ESI) *m/z* calculated for [C$_{16}$H$_{19}$NO$_4$S$_2$H]$^+$ 354.0834, observed 354.0828.

2,2'-((2,5-dioxo-1-phenyl-2,5-dihydro-1*H*-pyrrole-3,4-diyl)bis(sulfanediyl))diacetic acid (43)
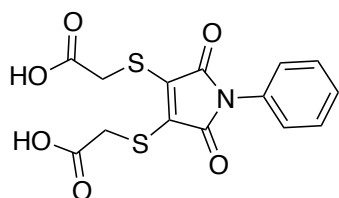
To a stirred solution of 2,3-dichloro-*N*-phenylmaleimide (145 mg, 0.60 mmol) and triethylamine (169 μL, 1.20 mmol) in DCM (10 mL), thioglycolic acid (92 μL, 1.32 mmol) was added. The resulting reaction mixture was stirred under argon at room temperature for 1 h. The solvent was removed *in vacuo* to afford the crude product. Purification by flash

chromatography on silica gel (methanol:DCM with 1% acetic acid, gradient elution from 0% to 10%) gave the product **43** as a yellow oil (103 mg, 0.29 mmol, 49%).

^{1}H NMR (600 MHz, CDCl$_3$): δ = 7.45 (t, *J* = 7.6 Hz, 2H, Ar-H), 7.36 (t, *J* = 7.2 Hz, 1H, Ar-H), 7.31 (d, *J* = 7.6 Hz, 2H, Ar-H), 4.18 (s, 4H, CO*CH$_2$*S); ^{13}C NMR (150 MHz, CDCl$_3$): δ = 174.7 (C), 165.2 (C), 135.5 (C), 131.1 (C), 129.3 (CH), 128.4 (CH), 126.3 (CH), 32.7 (CH$_2$); IR (oil) v$_{max}$/cm^{-1} 3018, 2925, 1704, 1501; LRMS (ESI) *m/z* (%) 354 ([M+H]$^+$, 100); HRMS (ESI) *m/z* calculated for [C$_{14}$H$_{11}$NO$_6$S$_2$H]$^+$ 354.0106, observed 354.0099.

2,2'-((2,5-dioxo-1-phenyl-2,5-dihydro-1*H*-pyrrole-3,4-diyl)bis(sulfanediyl))disuccinic acid (44)
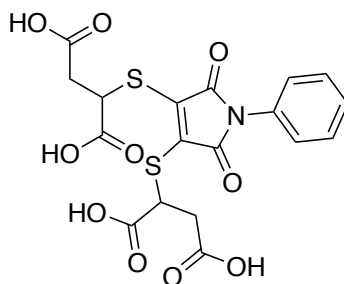
To a stirred solution of 2,3-dichloro-*N*-phenylmaleimide (145 mg, 0.60 mmol) and triethylamine (186 μL, 1.32 mmol) in acetonitrile (10 mL), mercaptosuccinic acid (180 mg, 1.20 mmol) was added. The resulting reaction mixture was stirred under argon at room temperature for 1 h. The solvent was removed *in vacuo* to afford the crude product. Purification by flash chromatography on silica gel (methanol:DCM with 1% acetic acid, gradient elution from 0% to 20%) gave the product **44** as a yellow oil (56 mg, 0.12 mmol, 20%).

^{1}H NMR (600 MHz, MeOD): δ = 7.47 (t, *J* = 7.8 Hz, 2H, Ar-H), 7.39 (t, *J* = 7.5 Hz, 1H, Ar-H), 7.36 (d, *J* = 8.2 Hz, 2H, Ar-H), 5.10-5.07 (m, 2H, CO*CH*S), 3.04-3.00 (m, 2H, CO*CH$_2$*CH), 2.96-2.91 (m, 2H, CO*CH$_2$*CH); ^{13}C NMR (150 MHz, MeOD): δ = 173.7 (C), 173.2 (C), 166.5 (C), 138.7 (C), 133.1 (C), 130.0 (CH), 129.2 (CH), 127.8 (CH), 44.1 (CH), 37.7 (CH$_2$); IR (oil) v$_{max}$/cm^{-1} 2920, 2557, 1700, 1500; LRMS (ESI) *m/z* (%) 470 ([M+H]$^+$, 100); HRMS (ESI) *m/z* calculated for [C$_{18}$H$_{15}$NO$_{10}$S$_2$H]$^+$ 470.0216, observed 470.0208.

(2R,2'R)-3,3'-((2,5-dioxo-1-phenyl-2,5-dihydro-1H-pyrrole-3,4-diyl)bis(sulfanediyl))bis(2-((tert-butoxycarbonyl)amino)propanoic acid) (45)
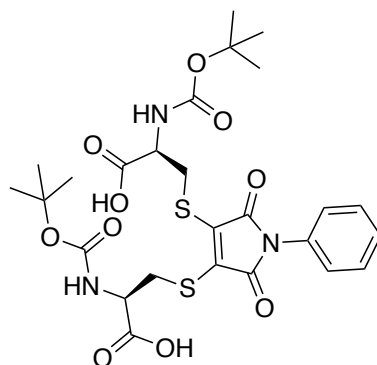

To a stirred solution of 2,3-dichloro-*N*-phenylmaleimide (194 mg, 0.80 mmol) and triethylamine (334 μL, 2.40 mmol) in DCM (10 mL), Boc-L-cysteine (354 mg, 1.60 mmol) was added. The resulting reaction mixture was stirred under argon at room temperature for 1 h. The solvent was removed *in vacuo* to afford the crude product. Purification by flash chromatography on silica gel (methanol:DCM with 1% acetic acid, gradient elution from 0% to 5%) gave the product **45** as a yellow solid (331 mg, 0.54 mmol, 68%).

m.p. 89-93 °C; ^{1}H NMR (700 MHz, CDCl$_3$): δ = 7.42-7.38 (m, 2H, Ar-H), 7.34-7.29 (m, 3H, Ar-H), 4.63 (s, 2H, NH*CH*CO), 4.02-3.12 (m, 4H, CH*CH$_2$*S), 1.39 (s, 18H, OC(*CH$_3$*)$_3$); ^{13}C NMR (175 MHz, CDCl$_3$): δ = 171.8 (C), 164.7 (C), 156.8 (C), 137.1 (C), 131.3 (C), 129.1 (CH),126.7 (CH), 126.3 (CH), 82.8 (C), 54.6 (CH), 34.8 (CH$_2$), 28.2 (CH$_3$); IR (solid) ν$_{max}$/cm^{-1} 2976, 2928, 1707, 1501; LRMS (ESI) *m/z* (%) 612 ([M+H]$^+$, 100); HRMS (ESI) *m/z* calculated for [C$_{26}$H$_{33}$N$_3$O$_{10}$S$_2$H]$^+$ 612.1635, observed 612.1654.

3,4-bis((4-hydroxy-2-methylbutan-2-yl)thio)-1-phenyl-1H-pyrrole-2,5-dione (46)
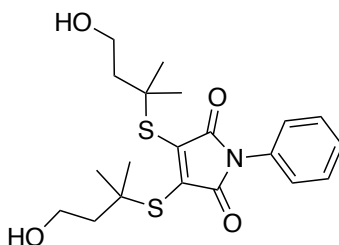
To a stirred solution of 2,3-dichloro-*N*-phenylmaleimide (194 mg, 0.80 mmol) and triethylamine (247 μL, 1.76 mmol) in DCM (10 mL), 3-mercapto-3-methylbutan-1-ol (196 μL,

1.60 mmol) was then added. The resulting reaction mixture was stirred under argon at room temperature for 1 h. The solvent was removed *in vacuo* to afford the crude product. Purification by flash chromatography on silica gel (ethyl acetate:cyclohexane, gradient elution from 0% to 100%) gave the product **46** as an orange oil (140 mg, 0.34 mmol, 43%).

^{1}H NMR (700 MHz, CDCl$_3$): δ = 7.49-7.46 (m, 2H, Ar-H), 7.39-7.35 (m, 3H, Ar-H), 3.93 (t, *J* = 6.8 Hz, 4H, CH$_2$*CH$_2$*OH), 2.08 (t, *J* = 6.7 Hz, 4H, C*CH$_2$*CH$_2$), 1.53 (s, 12H, C(*CH$_3$*)$_2$); ^{13}C NMR (175 MHz, CDCl$_3$): δ = 166.1 (C), 144.9 (C), 131.7 (C), 129.3 (CH), 128.3 (CH), 126.3 (CH), 60.2 (CH$_2$), 54.4 (C), 45.8 (CH$_2$), 30.6 (CH$_3$); IR (oil) v$_{max}$/cm^{-1} 2961, 2923, 1712, 1501; LRMS (ESI) *m/z* (%) 410 ([M+H]$^+$, 100); HRMS (ESI) *m/z* calculated for [C$_{20}$H$_{27}$NO$_4$S$_2$H]$^+$ 410.1460, observed 410.1454.

(3*S*,4*S*)-3,4-dihydroxy-8-phenyl-2,3,4,5-tetrahydro-7*H*-[1,4]dithiocino[2,3-c]pyrrole-7,9(8*H*)-dione (47)
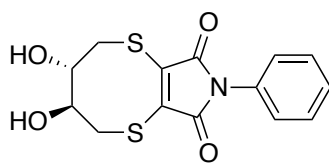
To a stirred solution of 2,3-dichloro-*N*-phenylmaleimide (145 mg, 0.60 mmol) and triethylamine (126 µL, 0.90 mmol) in chloroform (10 mL), DL-dithiothreitol (92 mg, 0.60 mmol) was added. The resulting reaction mixture was stirred under argon at room temperature for 1 h. The solvent was removed *in vacuo* to afford the crude product. Purification by flash chromatography on silica gel (ethyl acetate:cyclohexane, gradient elution from 0% to 100%) gave the product **47** as a yellow solid (70 mg, 0.22 mmol, 36%).

m.p. 85-95 °C; ^{1}H NMR (600 MHz, CDCl$_3$): δ = 7.45 (t, *J* = 7.5 Hz, 2H, Ar-H), 7.36 (t, *J* = 7.5 Hz, 1H, Ar-H), 7.33 (d, *J* = 7.5 Hz, 2H, Ar-H), 4.21 (m, 2H, CH*CH$_2$*S), 4.16 (m, 2H, CH$_2$*CH*OH), 3.11 (m, 2H, CH*CH$_2$*S); ^{13}C NMR (150 MHz, CDCl$_3$): δ = 166.5 (C), 138.0 (C), 131.4 (C), 129.3 (CH), 128.2 (CH), 125.9 (CH), 74.1 (CH), 34.7 (CH$_2$); IR (solid) v$_{max}$/cm^{-1} 3507, 3392, 1700, 1596, 1501; LRMS (ESI) *m/z* (%) 324 ([M+H]$^+$, 100); HRMS (ESI) *m/z* calculated for [C$_{14}$H$_{13}$NO$_4$S$_2$H]$^+$ 324.0364, observed 324.0356.

2,2'-(((2,5-dioxo-1-phenyl-2,5-dihydro-1H-pyrrole-3,4-diyl)bis(sulfanediyl))bis(4,1-phenylene))diacetic acid (48)
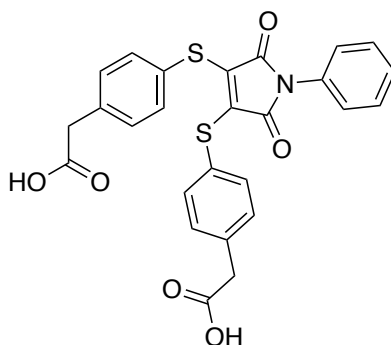
To a stirred solution of 2,3-dichloro-N-phenylmaleimide (145 mg, 0.60 mmol) and triethylamine (169 μL, 1.20 mmol) in DCM (10 mL), 4-mercaptophenylacetic acid (202 mg, 1.20 mmol) was added. The resulting reaction mixture was stirred under argon at room temperature for 1 h. The solvent was removed *in vacuo* to afford the crude product. Purification by flash chromatography on silica gel (methanol:DCM with 1% acetic acid, gradient elution from 0% to 10%) gave the product **48** as an orange solid (257 mg, 0.51 mmol, 85%).

m.p. 168-173 °C; ^{1}H NMR (600 MHz, MeOD): δ = 7.47-7.45 (m, 2H, Ar-H), 7.39-7.36 (m, 3H, Ar-H), 7.15 (d, J = 8.0 Hz, 4H, Ar-H), 7.00 (d, J = 8.0 Hz, 4H, Ar-H), 3.58 (s, 4H, COCH_2C); ^{13}C NMR (150 MHz, MeOD): δ = 175.0 (C), 167.8 (C), 136.2 (C), 135.4 (C), 133.1 (C), 131.9 (CH), 131.0 (C), 129.8 (CH), 128.9 (CH), 127.9 (CH), 127.5 (CH), 41.5 (CH_2); IR (solid) v_{max}/cm^{-1} 2921, 2554, 1696, 1491; LRMS (ESI) m/z (%) 506 ([M+H]$^+$, 100); HRMS (ESI) m/z calculated for [C$_{26}$H$_{19}$NO$_6$S$_2$H]$^+$ 506.0682, observed 506.0691.

1-phenyl-3,4-bis(phenylthio)-1H-pyrrole-2,5-dione (49)[269]
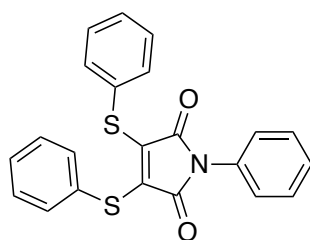
To a stirred solution of 2,3-dichloro-N-phenylmaleimide (193 mg, 0.80 mmol) and triethylamine (223 μL, 1.60 mmol) in DCM (10 mL), thiophenol (165 μL, 1.60 mmol) was added.

The resulting reaction mixture was stirred under argon at room temperature for 1 h. The solvent was removed *in vacuo* to afford the crude product. Purification by flash chromatography on silica gel (ethyl acetate:cyclohexane, gradient elution from 0% to 100%) gave the product **49** as a yellow solid (232 mg, 0.60 mmol, 75%).

m.p. 108-110 °C; ^{1}H NMR (600 MHz, CDCl$_3$): δ = 7.41 (m, 4H, Ar-H), 7.33-7.29 (m, 11H, Ar-H); ^{13}C NMR (150 MHz, CDCl$_3$): δ = 165.8 (C), 135.8 (C), 132.3 (C), 131.5 (C), 129.1 (CH), 129.1 (CH), 128.8 (CH), 128.7 (CH), 128.0 (CH), 126.0 (CH); IR (solid) v_{max}/cm^{-1} 3059, 1702, 1594, 1502; LRMS (ESI) *m/z* (%) 390 ([M+H]$^+$, 100); HRMS (ESI) *m/z* calculated for [C$_{22}$H$_{15}$NO$_2$S$_2$H]$^+$ 390.0572, observed 390.0578.

1,2-diphenyldiselane (50)[249]
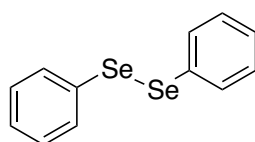
To a stirred solution of phenylboronic acid (61 mg, 0.50 mmol) in 2-methyltetrahydrofuran (2 mL), selenium dioxide (56 mg, 0.50 mmol) and iodine (127 mg, 0.50 mmol) were added. The resulting reaction mixture was heated up to 60 °C and stirred for 4 h. The solvent was removed *in vacuo* to afford the crude product. Purification by flash chromatography on silica gel (ethyl acetate:cyclohexane, gradient elution from 0% to 50%) gave the product **50** as a yellow solid (44 mg, 0.14 mmol, 56%).

m.p. 59-60 °C; ^{1}H NMR (600 MHz, CDCl$_3$): δ = 7.62-7.60 (dd, 4H, Ar-H), 7.27-7.26 (d, 6H, Ar-H); ^{13}C NMR (150 MHz, CDCl$_3$): δ = 131.6 (CH), 131.0 (C), 129.3 (CH), 127.9 (C); IR (solid) v_{max}/cm^{-1} 3040, 1585, 1475; LRMS (ESI) *m/z* (%) 309 (^{76,78}[M+H]$^+$, 15), 311 (^{76,80}[M+H]$^+$, 45), 313 (^{78,80}[M+H]$^+$, 90), 315 (^{80,80}[M+H]$^+$, 100), 317 (^{80,82}[M+H]$^+$, 30); HRMS (ESI) *m/z* calculated for [C$_{12}$H$_{10}$^{80,80}Se$_2$H]$^+$ 314.9186, observed 314.9114.

1,2-bis(4-methoxyphenyl)diselane (51)[249]
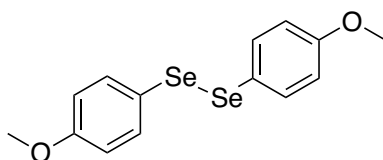
To a stirred solution of 4-methoxyphenylboronic acid (88 mg, 0.58 mmol) in 2-methyltetrahydrofuran (2 mL), selenium dioxide (64 mg, 0.58 mmol) and iodine (147 mg, 0.58 mmol) were added. The resulting reaction mixture was heated up to 60 °C and stirred for 4 h. The solvent was removed *in vacuo* to afford the crude product. Purification by flash chromatography on silica gel (ethyl acetate:cyclohexane, gradient elution from 0% to 50%) gave the product **51** as a yellow oil (71 mg, 0.19 mmol, 66%).

^{1}H NMR (600 MHz, CDCl$_3$): δ = 7.56 (d, *J* = 8.7 Hz, 4H, Ar-H), 6.69 (d, *J* = 8.7 Hz, 4H, Ar-H), 3.77 (s, 6H, O*CH$_3$*); ^{13}C NMR (150 MHz, CDCl$_3$): δ = 159.6 (C), 138.3 (CH), 116.5 (CH), 82.9 (C), 55.5 (CH$_3$); IR (oil) ν_{max}/cm^{-1} 3391, 1586, 1486; LRMS (ESI) *m/z* (%) 368 (^{76,78}[M+H]$^+$, 15), 370 (^{76,80}[M+H]$^+$, 45), 372 (^{78,80}[M+H]$^+$, 90), 374 (^{80,80}[M+H]$^+$, 100), 376 (^{80,82}[M+H]$^+$, 30); HRMS (ESI) *m/z* calculated for [C$_{14}$H$_{14}$O$_2$^{80,80}Se$_2$H]$^+$ 373.9319, observed 373.9324.

4,4'-diselanediyldianiline (55)[257,258]
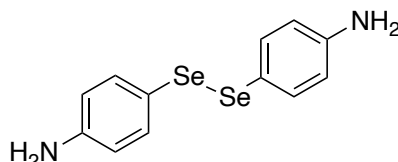
To a stirred solution of selenium dioxide (333mg, 3.00mmol) in DMSO (1 mL), malononitrile (99 mg, 1.50 mmol) was added and stirred for 5 min before aniline (228 µL, 2.50 mmol) was added. The resulting reaction mixture was stirred under argon at room temperature for 1 h. The reaction mixture was diluted in distilled water (5 mL) and filtered to give a crude intermediate as a black solid. The crude intermediate was further dissolved in a mixture of DMF (4 mL) and distilled water (4 mL), sodium carbonate (318mg, 3.00 mmol) was then added. The resulting mixture was heated up to 80 °C and stirred for 4 h. The solvent was co-evaporated with toluene and then chloroform *in vacuo* to give the crude product. Purification by flash chromatography on silica gel (ethyl acetate:cyclohexane, gradient elution from 0% to 80%) gave the product **55** as a yellow oil (122 mg, 0.35 mmol, 28%).

^{1}H NMR (600 MHz, CDCl$_3$): δ = 7.37 (d, *J* = 8.2 Hz, 4H, Ar-H), 6.57 (d, *J* = 8.2 Hz, 4H, Ar-H), 3.77 (s, 4H); ^{13}C NMR (150 MHz, CDCl$_3$): δ = 147.2 (C) 136.3 (CH), 119.5 (C), 115.7 (CH); IR (oil) v$_{max}$/cm^{-1} 3341, 2944, 1591, 1490; LRMS (ESI) *m/z* (%) 339 (^{76,78}[M+H]$^+$, 15), 341 (^{76,80}[M+H]$^+$, 45), 343 (^{78,80}[M+H]$^+$, 90), 345 (^{80,80}[M+H]$^+$, 100), 347 (^{80,82}[M+H]$^+$, 30); HRMS (ESI) *m/z* calculated for [C$_{12}$H$_{12}$N$_2$^{80,80}Se$_2$H]$^+$ 344.9404, observed 344.9394.

N,N'-(diselanediylbis(4,1-phenylene))bis(2-(2-(2-methoxyethoxy)ethoxy)acetamide) (56)
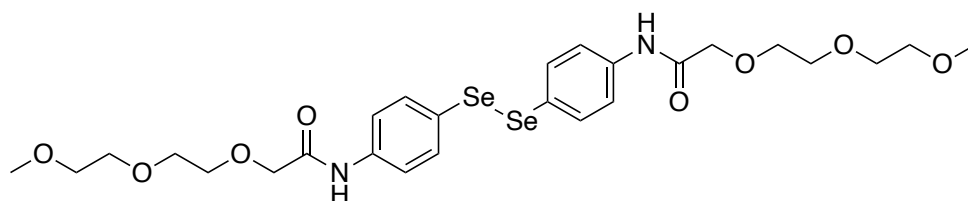
To a stirred solution of 2-[2-(2-Methoxyethoxy)ethoxy]acetic acid (108 µL, 0.70 mmol) in acetonitrile (4 mL), EEDQ (200 mg, 0.81 mmol) was added. The resulting reaction mixture was stirred under argon at room temperature for 1 h. To the reaction mixture, compound **55** (80 mg, 0.23 mmol) in acetonitrile (2 mL) was added dropwise. The resulting reaction mixture was stirred under argon at room temperature for 16 h. The solvent was removed *in vacuo* to afford the crude product. Purification by flash chromatography on silica gel (first in ethyl acetate:cyclohexane, gradient elution from 0% to 100%; second in methanol:DCM, gradient elution from 0% to 10%) gave the product **56** as a yellow oil (66 mg, 0.10 mmol, 43%).

^{1}H NMR (600 MHz, CDCl$_3$): δ = 7.56-7.52 (m, 8H, Ar-H), 4.10 (s, 4H, CO*CH$_2$*O), 3.77-3.75 (m, 4H, O*CH$_2$*CH$_2$), 3.72-3.70 (m, 8H, O*CH$_2$*CH$_2$), 3.58-3.56 (m, 4H, O*CH$_2$*CH$_2$), 3.34 (s, 6H, O*CH$_3$*); ^{13}C NMR (150 MHz, CDCl$_3$): δ = 168.5 (C), 137.8 (C), 133.7 (CH), 126.2 (C), 120.7 (CH), 71.9 (CH$_2$), 71.3 (CH$_2$), 70.9 (CH$_2$), 70.5 (CH$_2$), 70.3 (CH$_2$), 59.2 (CH$_3$); IR (oil) v$_{max}$/cm^{-1} 3330, 2926, 1681, 1586, 1525; LRMS (ESI) *m/z* (%) 659 (^{76,78}[M+H]$^+$, 15), 661 (^{76,80}[M+H]$^+$, 45), 663 (^{78,80}[M+H]$^+$, 90), 665 (^{80,80}[M+H]$^+$, 100), 667 (^{80,82}[M+H]$^+$, 30); HRMS (ESI) *m/z* calculated for [C$_{26}$H$_{36}$N$_2$O$_8$^{80,80}Se$_2$H]$^+$ 665.0875, observed 665.0862.

4,4'-((diselanediylbis(4,1-phenylene))bis(azanediyl))bis(4-oxobutanoic acid) (57)
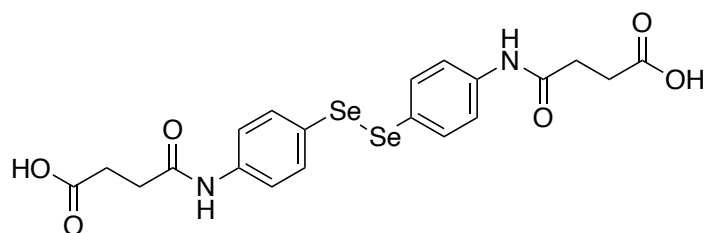
To a stirred solution of compound **55** (34 mg, 0.10 mmol) in chloroform (2 mL), succinic anhydride (25 mg, 0.25 mmol) was added. The resulting reaction mixture was stirred under argon at room temperature for 2 h. The solvent was removed *in vacuo* to afford the crude product. Purification by flash chromatography on silica gel (methanol:DCM with 1% acetic acid, gradient elution from 0% to 20%) gave the product **57** as a pale yellow solid (49 mg, 0.09 mmol, 90%).

m.p. 218-220 °C; ^{1}H NMR (600 MHz, MeOD): δ = 7.47-7.44 (m, 8H, Ar-H), 2.61 (t, *J* = 6.9 Hz, 4H, CO*CH₂*CH₂), 2.55 (t, *J* = 6.9 Hz, 4H, CO*CH₂*CH₂); ^{13}C NMR (150 MHz, MeOD): δ = 175.0 (C), 173.3 (C), 140.4 (C), 134.7 (CH), 126.4 (C), 121.5 (CH), 32.9 (CH₂), 30.2 (CH₂); IR (solid) v_{max}/cm[-1] 3349, 2945, 2834, 1664, 1585; LRMS (ESI) *m/z* (%) 539 ([76,78][M+H]+, 15), 541 ([76,80][M+H]+, 45), 543 ([78,80][M+H]+, 90), 545 ([80,80][M+H]+, 100), 547 ([80,82][M+H]+, 30); HRMS (ESI) *m/z* calculated for [$C_{20}H_{20}N_2O_6$[80,80]Se_2H]+ 544.9725, observed 544.9726.

1,1'-(diselanediylbis(4,1-phenylene))bis(ethan-1-one) (59)[270]
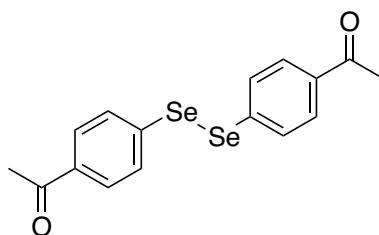
To a stirred solution of 1,2-diphenyldiselane (124 mg, 0.40 mmol) in DCM (5 mL), acetyl chloride (68 µL, 0.96 mmol) and aluminium trichloride (160 mg, 1.20 mmol) were added at 0 °C. The resulting reaction mixture was stirred under argon at room temperature for 16 h. The solvent was removed *in vacuo* to afford the crude product. Purification by flash chromatography on silica gel (ethyl acetate:cyclohexane, gradient elution from 0% to 100%) gave the product **59** as a yellow oil (72 mg, 0.18 mmol, 45%).

^{1}H NMR (600 MHz, CDCl$_3$): δ = 7.83 (d, J = 8.5 Hz, 4H, Ar-H), 7.68 (d, J = 8.5 Hz, 4H, Ar-H), 2.57 (s, 6H, COCH_3); ^{13}C NMR (150 MHz, CDCl$_3$): δ = 197.3 (C) 136.9 (C), 136.3 (C), 130.3 (CH), 129.2 (CH), 26.7 (CH$_3$); IR (oil) v$_{max}$/cm^{-1} 2928, 1658, 1501; LRMS (ESI) m/z (%) 393 (^{76,78}[M+H]$^+$, 15), 395 (^{76,80}[M+H]$^+$, 45), 397 (^{78,80}[M+H]$^+$, 90), 399 (^{80,80}[M+H]$^+$, 100), 401 (^{80,82}[M+H]$^+$, 30); HRMS (ESI) m/z calculated for [C$_{16}$H$_{14}$O$_2$^{80,80}Se$_2$H]$^+$ 398.9397, observed 398.9395.

1,2-bis(4-((*E*)-1-hydrazineylideneethyl)phenyl)diselane (60)
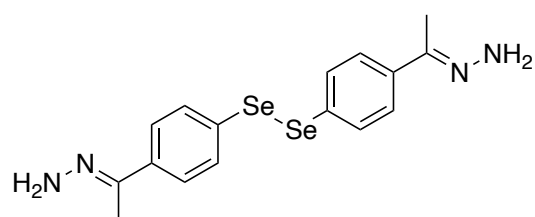
To a stirred solution of **59** (26 mg, 0.06 mmol) in ethanol (5 mL), hydrazine hydrate (20 μL, 0.40 mmol) and *p*-toluenesulfonic acid (0.5 mg, 2.60 μmol) were added. The resulting reaction mixture was heated to 80 °C and stirred for 4 h. The solvent was removed *in vacuo* to afford the crude product. Purification by flash chromatography on silica gel (ethyl acetate:cyclohexane, gradient elution from 0% to 100%) gave the product **60** as a yellow oil (9.0 mg, 0.02 mmol, 36%).

^{1}H NMR (600 MHz, CDCl$_3$): δ = 7.57 (d, J = 8.4 Hz, 4H, Ar-H), 7.54 (d, J = 8.4 Hz, 4H, Ar-H), 5.37 (s, 4H, CNNH_2), 2.10 (s, 6H, CNCH_3); ^{13}C NMR (150 MHz, CDCl$_3$): δ = 146.5 (C), 139.1 (C), 131.9 (CH), 130.9 (C), 126.3 (CH), 11.7 (CH$_3$); IR (oil) v$_{max}$/cm^{-1} 3388, 2926, 1662; LRMS (ESI) m/z (%) 421 (^{76,78}[M+H]$^+$, 15), 423 (^{76,80}[M+H]$^+$, 45), 425 (^{78,80}[M+H]$^+$, 90), 427 (^{80,80}[M+H]$^+$, 100), 429 (^{80,82}[M+H]$^+$, 30); HRMS (ESI) m/z calculated for [C$_{16}$H$_{18}$N$_4$^{80,80}Se$_2$H]$^+$ 426.9935, observed 426.9935.

1,2-di(pyridin-2-yl)diselane (61)[260]
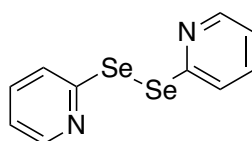
To a stirred solution of sodium hydroxide (64 mg, 1.60 mmol) and selenium (79 mg, 1.00 mmol) in DMF (4 mL), hydrazine hydrate (50 µL, 1.00 mmol) was added dropwise. The resulting mixture was stirred under argon at room temperature for 2 h. 2-Bromo pyridine (96 µL, 1.00 mmol) was added dropwise to the reaction mixture and refluxed at 120 °C for 4 h. The solvent was co-evaporated with toluene and then chloroform *in vacuo* to give the crude product. Purification by flash chromatography on silica gel (ethyl acetate:cyclohexane, gradient elution from 0% to 100%) gave the product **61** as an brown oil (59 mg, 0.19 mmol, 37%).

^{1}H NMR (600 MHz, CDCl$_3$): δ = 8.46 (d, *J* = 6.0 Hz, 2H, Ar-H), 7.80 (d, *J* = 8.0 Hz, 2H, Ar-H), 7.54 (dt, *J* = 7.8, 2.2 Hz, 2H, Ar-H), 7.08 (dt, *J* = 6.0, 2.4 Hz, 2H, Ar-H); ^{13}C NMR (150 MHz, CDCl$_3$): δ = 154.6 (C), 149.8 (CH), 137.7 (CH), 123.7 (CH), 121.4 (CH); IR (oil) v$_{max}$/cm^{-1} 3319, 2942, 2831, 1666; LRMS (ESI) *m/z* (%) 311 ([76,78][M+H]$^+$, 15), 313 ([76,80][M+H]$^+$, 45), 315 ([78,80][M+H]$^+$, 90), 317 ([80,80][M+H]$^+$, 100), 319 ([80,82][M+H]$^+$, 30); HRMS (ESI) *m/z* calculated for [C$_{10}$H$_8$N$_2$^{80,80}Se$_2$H]$^+$ 316.9091, observed 316.9088.

1,2-diphenyldiselane (62)[261]
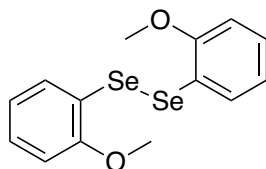
To a stirred solution of 2-iodoanisole (234 mg, 1.00 mmol) in DMSO (2 mL), selenium (158 mg, 2.00 mmol), copper oxide (8.0 mg, 0.1 mmol) and potassium hydroxide (112 mg, 2.00 mmol) was added. The resulting reaction mixture was heated to 90 °C and stirred for 16 h. The reaction mixture was then subjected to flash chromatography on silica gel (ethyl acetate:cyclohexane, gradient elution from 0% to 25%) gave the product **62** as a brown oil (149 mg, 0.40 mmol, 80%).

^{1}H NMR (600 MHz, CDCl$_3$): δ = 7.78 (dd, *J* = 7.7, 1.6 Hz, 2H, Ar-H), 7.31 (dt, *J* = 7.7, 1.6 Hz, 2H, Ar-H), 6.83 (dd, *J* = 8.2, 1.1 Hz, 2H, Ar-H), 6.71 (dt, *J* = 7.7, 1.3 Hz, 2H, Ar-H), 3.87 (s, 6H, O*CH$_3$*); ^{13}C NMR (150 MHz, CDCl$_3$): δ = 158.2 (C), 139.6 (CH), 129.7 (C), 122.7 (CH), 111.1 (CH), 86.1 (C), 56.4 (CH$_3$); IR (oil) v$_{max}$/cm^{-1} 3391, 2947, 1665, 1461; LRMS (ESI) *m/z* (%) 368 ([76,78][M+H]$^+$,

15), 370 (^{76,80}[M+H]$^+$, 45), 372 (^{78,80}[M+H]$^+$, 90), 374 (^{80,80}[M+H]$^+$, 100), 376 (^{80,82}[M+H]$^+$, 30); HRMS (ESI) *m/z* calculated for [C$_{14}$H$_{14}$O$_2$^{80,80}Se$_2$H]$^+$ 373.9319, observed 373.9319.

1,2-diphenyldiselane (63)[261]
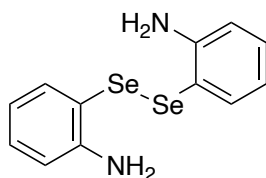
To a stirred solution of 2-iodoaniline (219 mg, 1.00 mmol) in DMSO (2 mL), selenium (158 mg, 2.00 mmol), copper oxide (8.0 mg, 0.1 mmol) and potassium hydroxide (112 mg, 2.00 mmol) was added. The resulting reaction mixture was heated to 90 °C and stirred for 16 h. The reaction mixture was then subjected to flash chromatography on silica gel (ethyl acetate:cyclohexane, gradient elution from 0% to 25%) gave the product **63** as a brown oil (105 mg, 0.31 mmol, 61%).

^{1}H NMR (600 MHz, CDCl$_3$): δ = 7.89 (d, *J* = 8.0 Hz, 2H, Ar-H), 7.80 (d, *J* = 8.0 Hz, 2H, Ar-H), 7.40 (t, *J* = 7.7 Hz, 2H, Ar-H), 7.22 (t, *J* = 7.7 Hz, 2H, Ar-H); ^{13}C NMR (150 MHz, CDCl$_3$): δ = 155.0 (C), 138.2 (C), 126.4 (CH), 124.4 (CH), 124.3 (CH), 123.0 (CH); IR (oil) v$_{max}$/cm^{-1} 3347, 2940, 1663, 1614, 1477, 1444; LRMS (ESI) *m/z* (%) 339 (^{76,78}[M+H]$^+$, 15), 341 (^{76,80}[M+H]$^+$, 45), 343 (^{78,80}[M+H]$^+$, 90), 345 (^{80,80}[M+H]$^+$, 100), 347 (^{80,82}[M+H]$^+$, 30); HRMS (ESI) *m/z* calculated for [C$_{12}$H$_{12}$N$_2$^{80,80}Se$_2$H]$^+$ 344.9404, observed 344.9408.

3,4-bis(phenylthio)-1*H*-pyrrole-2,5-dione (64)[163]
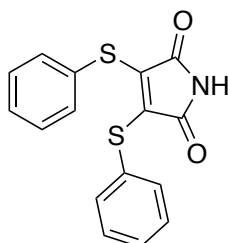
To a stirred solution of dibromomaleimide (153 mg, 0.60 mmol) in methanol (5 mL), thiophenol (130 μL, 1.26 mmol) and sodium hydrogen carbonate (252 mg, 3.00 mmol) were added. The resulting reaction mixture was stirred under argon at room temperature for 2 h.

The solvent was removed *in vacuo* to afford the crude product. Purification by flash chromatography on silica gel (ethyl acetate:cyclohexane, gradient elution from 0% to 100%) gave the product **64** as a yellow solid (170 mg, 0.54 mmol, 91%).

m.p. 102-104 °C; ^{1}H NMR (600 MHz, CDCl$_3$): δ = 7.30-7.28 (t, 2H, Ar-H), 7.26-7.25 (t, 4H, Ar-H), 7.20-7.18 (d, 4H, Ar-H); ^{13}C NMR (150 MHz, CDCl$_3$): δ = 166.2 (C), 136.7 (C), 132.0 (CH), 129.2 (CH), 128.9 (C), 128.6 (CH); IR (solid) v$_{max}$/cm^{-1} 3060, 1702, 1595, 1501; LRMS (ESI) *m/z* (%) 314 ([M+H]$^+$, 100); HRMS (ESI) *m/z* calculated for [C$_{16}$H$_{11}$NO$_2$S$_2$H]$^+$ 314.0310, observed 314.0309.

2-(*p*-tolyldisulfaneyl)pyridine[271]
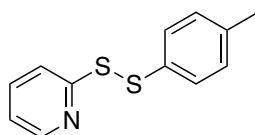
To a stirred solution of 2,2'-dipyridyldisulfide (1322 mg, 6.00 mmol) in dry methanol (5 mL) purged with argon, 4-methylbenzenethiol (497 mg, 4.00 mmol) was added dropwise. The resulting mixture was stirred under argon at room temperature for 2 h. The solvent was removed *in vacuo* to afford the crude product. Purification by flash chromatography on silica gel (ethyl acetate:cyclohexane, gradient elution from 0% to 50%) gave the product as a yellow oil (654 mg, 2.81 mmol, 70%).

^{1}H NMR (600 MHz, CDCl$_3$): δ = 8.46 (d, *J* = 4.4 Hz, 1H, Ar-H), 7.66 (td, *J* = 8.1, 0.9 Hz, 1H, Ar-H), 7.60 (dt, *J* = 7.8, 1.6 Hz, 1H, Ar-H), 7.41 (d, *J* = 8.2 Hz, 2H, Ar-H), 7.11 (d, *J* = 8.0 Hz, 2H, Ar-H), 7.07 (dt, *J* = 6.2, 0.9 Hz, 1H, Ar-H), 2.30 (s, 3H, C*CH$_3$*); ^{13}C NMR (150 MHz, CDCl$_3$): δ = 160.1 (C), 149.7 (CH), 137.8 (C), 137.4 (CH), 132.8 (C), 130.1 (CH), 128.2 (CH), 121.0 (CH), 119.7 (CH), 21.2 (CH$_3$); IR (oil) v$_{max}$/cm^{-1} 3046, 2921, 2348, 1573, 1445; LRMS (ESI) *m/z* (%) 234 ([M+H]$^+$, 100); HRMS (ESI) *m/z* calculated for [C$_{12}$H$_{11}$NS$_2$H]$^+$ 234.0411, observed 234.0403.

2-(4-(*p*-tolyldisulfaneyl)phenyl)acetic acid (67)
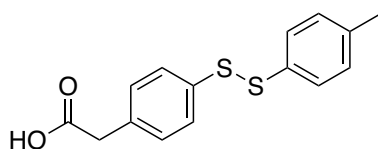
To a stirred solution of 2-(p-tolyldisulfaneyl)pyridine (800 mg, 3.43 mmol) in DCM (10 mL), 4-mercaptophenylacetic acid (492 mg, 2.92 mmol) and DIPEA (610 µL, 3.50 mmol) were added, and the resulting mixture was stirred under argon at room temperature for 30 min. The solvent was removed *in vacuo* to afford the crude product. Purification by flash chromatography on silica gel (ethyl acetate:cyclohexane with 1% acetic acid, gradient elution from 0% to 100%) gave the product **67** as a pale yellow solid (758 mg, 2.63 mmol, 90%).

m.p. 161-162 °C; ^{1}H NMR (700 MHz, MeOD): δ = 7.39 (d, *J* = 8.1 Hz, 2H, Ar-H), 7.32 (d, *J* = 8.2 Hz, 2H, Ar-H), 7.19 (d, *J* = 8.1 Hz, 2H, Ar-H), 7.07 (d, *J* = 8.1 Hz, 2H, Ar-H), 3.54 (s, 2H, COC*H$_2$*C), 2.26 (s, 3H, CC*H$_3$*); ^{13}C NMR (175 MHz, MeOD): δ = 175.1 (C), 138.9 (C), 136.8 (C), 135.4 (C), 134.7 (C), 131.2 (CH), 130.8 (CH), 129.6 (CH), 129.1 (CH), 41.2 (CH$_2$), 21.0 (CH$_3$); IR (solid) v_{max}/cm^{-1} 3016, 2910, 1721, 1691; LRMS (ESI) *m/z* (%) 289 ([M-H]$^-$, 100); HRMS (ESI) *m/z* calculated for [C$_{15}$H$_{13}$S$_2$O$_2$]$^-$ 289.0363, observed 289.0350.

tert-butyl (3-(2-(2-(3-aminopropoxy)ethoxy)ethoxy)propyl)carbamate (68)[272]
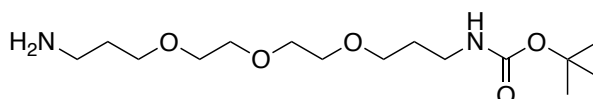
To a stirred solution of 4,7,10-Trioxa-1,13-tridecanediamine (548 µL, 2.5 mmol) in DCM (3 mL) at 0 °C, di-tert-butyl dicarbonate (110 mg, 0.50 mmol) in DCM (3 mL) was added dropwise. The resulting mixture was stirred under argon at room temperature for 16 h. The reaction mixture was washed with H$_2$O, the organic layer DCM was dried and removed *in vacuo* to give the product **68** as a colourless oil (152 mg, 0.48 mmol, 95%).

^{1}H NMR (600 MHz, CDCl$_3$): δ = 3.63-3.61 (m, 4H, OC*H$_2$*CH$_2$), 3.59-3.56 (m, 4H, OC*H$_2$*CH$_2$), 3.54-3.51 (m, 4H, OC*H$_2$*CH$_2$), 3.21 (q, *J* = 6.3 Hz, 2H, NHC*H$_2$*CH$_2$), 2.77 (t, *J* = 6.8 Hz, 2H, NH$_2$*CH$_2$*CH$_2$), 1.74 (quin, *J* = 6.1 Hz, 2H, CH$_2$*CH$_2$*CH$_2$), 1.71 (quin, *J* = 6.6 Hz, 2H, CH$_2$*CH$_2$*CH$_2$); ^{13}C NMR (150 MHz, CDCl$_3$): δ = 156.2 (C), 79.0 (C), 70.7 (CH$_2$), 70.7 (CH$_2$), 70.3 (CH$_2$), 70.3 (CH$_2$), 69.7 (CH$_2$), 69.6 (CH$_2$), 39.7 (CH$_2$), 39.6 (CH$_2$), 33.4 (CH$_2$), 29.7 (CH$_2$), 28.6 (CH$_3$); IR (oil) v_{max}/cm^{-1} 3356,

2927, 2867, 1692; LRMS (ESI) *m/z* (%) 321 ([M+H]$^+$, 100); HRMS (ESI) *m/z* calculated for [C$_{15}$H$_{32}$N$_2$O$_5$H]$^+$ 321.2384, observed 321.2383.

tert-butyl (2-oxo-1-(4-(p-tolyldisulfaneyl)phenyl)-7,10,13-trioxa-3-azahexadecan-16-yl)carbamate (69)
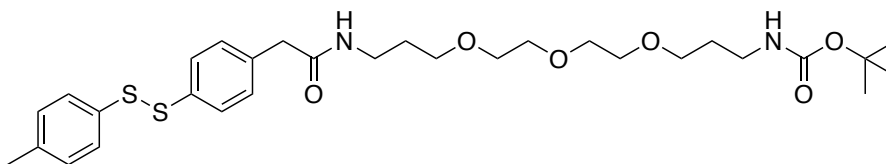
To a stirred solution of compound **66** (379 mg, 1.30 mmol) in acetonitrile (5 mL), EEDQ (968 mg, 1.96 mmol) was added. The resulting mixture was stirred under argon at room temperature for 1 h. To the reaction mixture, compound **67** (418 mg, 1.30 mmol) was added. The resulting mixture was stirred under argon at room temperature for 2 h. The solvent was removed *in vacuo* to afford the crude product. Purification by flash chromatography on silica gel (first in ethyl acetate:cyclohexane, gradient elution from 0% to 100%; second in methanol:DCM, gradient elution from 0% to 20%) gave the product **69** as a yellow oil (414 mg, 0.70 mmol, 54%).

^{1}H NMR (700 MHz, CDCl$_3$): δ = 7.44 (d, *J* = 8.1 Hz, 2H, Ar-H), 7.37 (d, *J* = 8.0 Hz, 2H, Ar-H), 7.20 (d, *J* = 8.1 Hz, 2H, Ar-H), 7.10 (d, *J* = 8.0 Hz, 2H, Ar-H), 3.59-3.57 (m, 2H, O*CH$_2$*CH$_2$), 3.56-3.52 (m, 4H, C*CH$_2$*CO, O*CH$_2$*CH$_2$), 3.51-3.47 (m, 8H, O*CH$_2$*CH$_2$), 3.31 (q, *J* = 6.6 Hz, 2H, NH*CH$_2$*CH$_2$), 3.19 (q, *J* = 5.8 Hz, 2H, NH*CH$_2$*CH$_2$), 2.31 (s, 3H, C*CH$_3$*), 1.77-1.69 (m, 4H, CH$_2$*CH$_2$*CH$_2$), 1.42 (s, 9H, C*(CH$_3$)$_3$*); ^{13}C NMR (175 MHz, CDCl$_3$): δ = 170.6 (C), 156.2 (C), 137.7 (C), 136.2 (C), 134.6 (C), 133.6 (C), 130.2 (CH), 130.0 (CH), 128.5 (CH), 128.3 (CH), 79.1 (C), 70.7 (CH$_2$), 70.6 (CH$_2$), 70.4 (CH$_2$), 70.3 (CH$_2$), 70.2(CH$_2$), 69.6 (CH$_2$), 43.4 (CH$_2$), 38.6 (CH$_2$), 38.3 (CH$_2$), 29.8 (CH$_2$), 28.9 (CH$_2$), 28.6 (CH$_3$), 21.2 (CH$_3$); IR (oil) v$_{max}$/cm^{-1} 3307, 2926, 2867, 1693, 1651; LRMS (ESI) *m/z* (%) 593 ([M+H]$^+$, 100); HRMS (ESI) *m/z* calculated for [C$_{30}$H$_{44}$N$_2$O$_6$S$_2$H]$^+$ 593.2714, observed 593.2704.

2-(3,4-dibromo-2,5-dioxo-2,5-dihydro-1H-pyrrol-1-yl)acetic acid (70)[161]
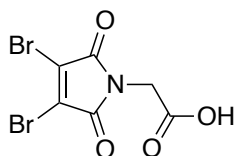
To a stirred solution of glycine (150 mg, 2.00 mmol) in acetic acid (1 mL), dibromomaleic acid (658 mg, 2.40 mmol) was added. The resulting mixture was heated to reflux at 130 °C and stirred for 1 h. The solvent was co-evaporated with toluene and then chloroform *in vacuo* to give the crude product. Purification by flash chromatography on silica gel (ethyl acetate:cyclohexane with 1% acetic acid, gradient elution from 0% to 100%) gave the product **70** as a white solid (532 mg, 1.71 mmol, 85%).

m.p. 205-206 °C; ^{1}H NMR (700 MHz, MeOD): δ = 4.31 (s, 2H, N*CH$_2$*CO); ^{13}C NMR (175 MHz, MeOD): δ = 170.5 (C), 164.7 (C), 130.5 (C), 40.8 (CH$_2$); IR (solid) v_{max}/cm^{-1} 2917, 1720; LRMS (ESI) *m/z* (%) 313 ([^{81,81}M-H]$^-$, 50), 311 ([^{81,79}M-H]$^-$, 100), 309 ([^{79,79}M-H]$^-$, 50); HRMS (ESI) *m/z* calculated for [C$_6$H$_2$^{81,79}Br$_2$NO$_4$]$^-$ 311.8336, observed 311.8335.

2-(3,4-dibromo-2,5-dioxo-2,5-dihydro-1*H*-pyrrol-1-yl)-*N*-(2-oxo-1-(4-(*p*-tolyldisulfaneyl)phenyl)-7,10,13-trioxa-3-azahexadecan-16-yl)acetamide (71)
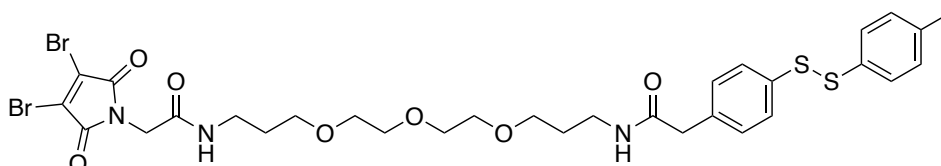
The starting material **69** (90 mg, 0.16 mmol) was treated with 25% trifluoroacetic acid (TFA) (2 mL) in DCM (6 mL) at room temperature for 2 h. The solvent was removed *in vacuo* to afford a yellow oil, which was diluted in ethyl acetate, washed with saturated Na$_2$CO$_3$ then brine. The organic layer was dried and removed *in vacuo* to give the deprotected product, which was diluted in acetonitrile (2 mL) and added dropwise to a stirred mixture of compound **70** (96 mg, 0.30 mmol) and EEDQ (90 mg, 0.36 mmol) in acetonitrile (4 mL). The resulting mixture was stirred under argon at room temperature for 16 h. The solvent was removed *in vacuo* to afford the crude product. Purification by flash chromatography on silica gel (first in ethyl acetate:cyclohexane, gradient elution from 0% to 100%; second in methanol:DCM, gradient elution from 0% to 20%) gave the product **71** as a yellow oil (60 mg, 0.08 mmol, 48%).

^{1}H NMR (700 MHz, CDCl$_3$): δ = 7.44 (d, *J* = 8.1 Hz, 2H, Ar-H), 7.37 (d, *J* = 8.1 Hz, 2H, Ar-H), 7.20 (d, *J* = 8.1 Hz, 2H, Ar-H), 7.10 (d, *J* = 8.1 Hz, 2H, Ar-H), 4.22 (s, 2H, NH*CH$_2$*CO), 3.60-3.59 (m, 2H, O*CH$_2$*CH$_2$), 3.57-3.54 (m, 6H, C*CH$_2$*CO, O*CH$_2$*CH$_2$), 3.50-3.47 (m, 6H, O*CH$_2$*CH$_2$), 3.35 (q, *J* = 5.3 Hz, 2H, NH*CH$_2$*CH$_2$), 3.30 (q, *J* = 6.1 Hz, 2H, NH*CH$_2$*CH$_2$), 2.31 (s, 3H, C*CH$_3$*), 1.77-1.73 (m, 2H, CH$_2$*CH$_2$*CH$_2$), 1.72-1.69 (m, 2H, CH$_2$*CH$_2$*CH$_2$); ^{13}C NMR (175 MHz, CDCl$_3$): δ = 170.8 (C), 165.3 (C), 163.9 (C), 137.8 (C), 136.3 (C), 134.4 (C), 133.6 (C), 130.2 (CH), 130.0 (CH), 129.9 (C), 128.5 (CH), 128.3 (CH), 70.4 (CH$_2$), 70.3 (CH$_2$), 70.0 (CH$_2$), 70.0 (CH$_2$), 69.7(CH$_2$), 69.7 (CH$_2$), 43.4 (CH$_2$), 41.8 (CH$_2$), 38.6 (CH$_2$), 38.0 (CH$_2$), 29.1 (CH$_2$), 28.4 (CH$_2$), 21.2 (CH$_3$); IR (oil) v$_{max}$/cm^{-1} 3292, 2921, 2868, 1726, 1647; LRMS (ESI) *m/z* (%) 790 ([^{81,81}M+H]$^+$, 50), 788 ([^{81,79}M+H]$^+$, 100), 786 ([^{79,79}M+H]$^+$, 50); HRMS (ESI) *m/z* calculated for [C$_{31}$H$_{37}$^{81,79}Br$_2$N$_3$O$_7$S$_2$H]$^+$ 788.0492, observed 788.0485.

((1*R*,8*S*,9*r*)-bicyclo[6.1.0]non-4-yn-9-yl)methyl   (2-(2-(2-(2-(3,4-dibromo-2,5-dioxo-2,5-dihydro-1*H*-pyrrol-1-yl)acetamido)ethoxy)ethoxy)ethyl)carbamate
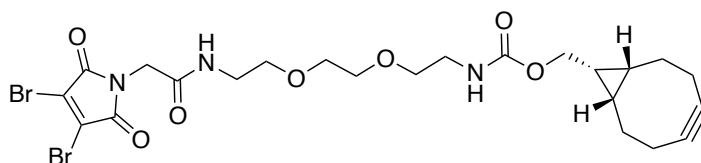
The compound was a kind gift from Dr Nafsika Forte. Full characterisation can be observed in Maneiro *et al.*, 2020.[161]

((1*R*,8*S*,9*r*)-bicyclo[6.1.0]non-4-yn-9-yl)methyl   (2-(2-(2-(3-(4,5-dibromo-2-methyl-3,6-dioxo-3,6-dihydropyridazin-1(2*H*)-yl)propanamido)ethoxy)ethoxy)ethyl)carbamate
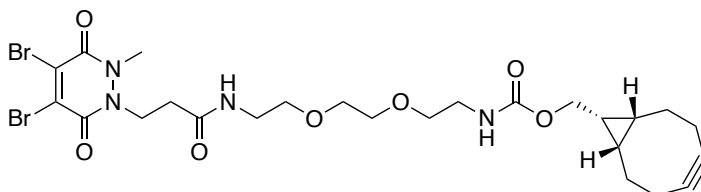
The compound was a kind gift from Ioanna Thanasi. Full characterisation can be observed in Bahou et al., 2021.[111]

4,5-dibromo-1,2-diethyl-1,2-dihydropyridazine-3,6-dione
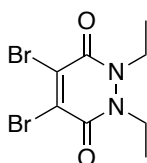
The compound was a kind gift from Ioanna Thanasi. Full characterisation can be observed in Bahou *et al.*, 2021.[111]

N1-(5-(2-(3,4-dibromo-2,5-dioxo-2,5-dihydro-1H-pyrrol-1-yl)acetamido)pentyl)-N1-hydroxy-N4-(5-(N-hydroxy-4-((5-(N-hydroxyacetamido)pentyl)amino)-4-oxobutanamido)pentyl)succinimide
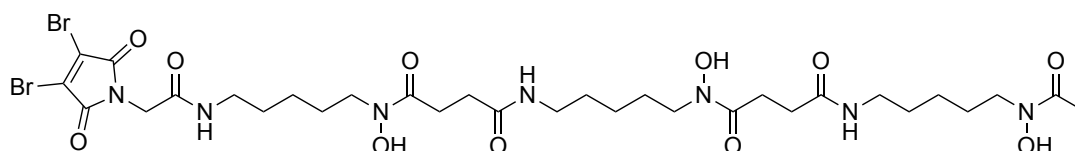
The compound was a kind gift from Dr Matthew Farleigh. Full characterisation can be observed in Farleigh *et al.*, 2021.[243]

N1-(1-azido-15-oxo-3,6,9,12-tetraoxa-16-azahenicosan-21-yl)-N1-hydroxy-N4-(5-(N-hydroxy-4-((5-(N-hydroxyacetamido)pentyl)amino)-4-oxobutanamido)pentyl)succinimide
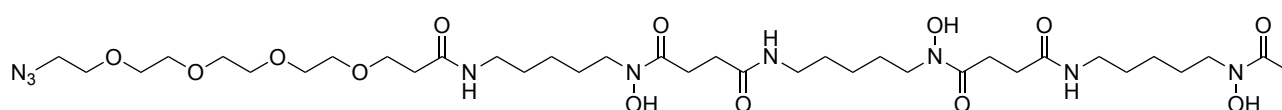
The compound was a kind gift from Dr Matthew Farleigh. Full characterisation can be observed in Farleigh M. (2021). Bifunctional chelators containing dibromomaleimides for the preparation of radioimmunoconjugates for PET imaging. King's College London.

5.3. Bioconjugation general remarks

5.3.1. Experiments on trastuzumab

All conjugation experiments were carried out in standard polypropylene Eppendorf safe-lock tubes (1.5 mL or 2.0 mL) at atmospheric pressure with mixing at the temperature stated. Reagents and solvents were purchased from Merck, Thermo Fisher Scientific, VWR, Lumiprobe and used as per manufacturer instructions. All buffer solutions were prepared with doubly deionised water and filter-sterilised (0.20 μm). All buffer solutions were degassed prior to use, where the term 'degassed' refers to the process of removing O_2 from a solution by bubbling argon through it. Borate-buffered saline (BBS) was 25 mM sodium borate, 25 mM NaCl and 0.5 mM ethylenediaminetetraacetic acid (EDTA) at pH 8.5 unless otherwise stated. Phosphate buffer (PB) was 100 mM sodium phosphates at pH 7.0. Ammonium acetate buffer was 50 mM ammonium acetate at pH 6.9. EDTA conjugation buffer was 40 mM sodium phosphates, 20mM NaCl and 6 mM EDTA at pH 7.0. The pH of buffers was adjusted using a Jenway 3510 pH meter. Ultrapure DMF was purchased from Sigma-Aldrich and stored under dry conditions. Ultrafiltration was carried out in Amicon® Ultra-4 Centrifugal Filter Units with a molecular weight cut-off (MWCO) of 10 kDa or in Vivaspin® 500 centrifugal concentrators (10 kDa MWCO). Centrifugation was carried out on an Eppendorf 5415R fixed angle rotor centrifuge operating at 14000 rcf at 20 °C or in an eppendorf 5810 swing-bucket rotor centrifuge operating at 3220 rcf at 20 °C. Trastuzumab (Ontruzant®) was purchased from UCLH in its clinical formulation (Samsung Bioepis, lyophilised). Trastuzumab Fab was prepared by a sequential enzymatic digest of the full antibody with pepsin and papain, following a literature procedure.[273] NanoDrop™ One^C Microvolume UV-Vis Spectrophotometer was applied to measurements of protein concentrations. Concentrations were determined by UV-Vis absorbance using molecular extinction coefficient of ε_{280} = 215380 $M^{-1}cm^{-1}$ for trastuzumab[274] and ε_{280} = 68590 $M^{-1}cm^{-1}$ for trastuzumab Fab.[275] Antibody conjugate concentration was determined using the same extinction coefficient as for native trastuzumab and trastuzumab Fab (maleamic acids were found to have negligible absorbance at 280 nm). A pre-packed, single-use column PD Minitrap™ G-25 was applied to remove excess fluorophore after click reactions.

5.3.2. Sodium dodecyl sulphate-polyacrylamide gel electrophoresis (SDS-PAGE)

Protein conjugation reactions were monitored by 12% glycine-SDS-PAGE with 6% stacking gel under non-reducing conditions. Gels were made in-house by preparing 12% separating and

6% stacking gel of components listed in **Table S1**. Gels were stored at 4 °C for up to a month. Samples were mixed 1:1 with SDS non-reducing loading buffer (composition for 6X SDS: 1 g SDS, 3 mL glycerol, 6 mL 0.5 M Tris buffer pH 6.8, 2 mg Coomassie Brilliant Blue R-250) or reducing loading buffer (composition for 4X SDS: 14 mg DTT, 0.8 g SDS, 4 mL glycerol, 2.5 mL 0.5 M Tris buffer pH 6.8 and 2 mg Coomassie Brilliant Blue R-250) and heated at 80 °C for 10 min before applied to the gel, each gel lane was loaded with 6 μL of 3 μg protein. For reference, Page Ruler Plus Pre-Stained Protein Ladder (Thermo Scientific) was used. Samples were run at a constant voltage of 200 V, 60 min in 1X running buffer (composition for 10X running buffer pH 8.3: 30 g Tris base, 144 g glycine, 10 g SDS and 1 L dH$_2$O). Gels were stained in 0.1% (w/v) Coomassie Blue Stain (composition for Coomassie Blue Stain: 100 g ammonium sulfate, 30 mL phosphoric acid, 200 mL ethanol, 0.5 g Coomassie Brilliant Blue R-250 and 670 mL dH$_2$O) and de-stained in dH$_2$O. Densitometry analysis of SDS-PAGE gels was conducted using the GelAnalyser V19.1 software.

Table S1 – Components of 12% SDS-PAGE gel. Listed volumes yield four gels.

Components	12% Separating	6% Stacking
dH$_2$O	7.95 mL	5.3 mL
Acrylamide	9.6 mL	2.0 mL
1.5 M Tris pH 8.8	6.0 mL	-
0.5 M Tris pH 6.8	-	2.5 mL
10% SDS	240 μL	100 μL
10% APS	240 μL	100 μL
TEMED	24 μL	10 μL

5.3.3. UV-Vis spectroscopy

UV-Vis spectroscopy using a Varian Cary 100 Bio UV-Visible spectrophotometer operating at 21 °C displayed absorbance spectra (200-900 nm) of antibody conjugates to show the attachment of fluorophores. Sample buffer was used as blank for baseline correction. Due to

the presence of multiple absorbing species, it was not possible to calculate fluorophore-to-antibody ratios (FAR) based on absorbance. Instead, FARs were calculated from LC-MS.

5.3.4. General procedure for the preparation of Trastuzumab (OntruzantTM) Fab fragment[276]

Trastuzumab (0.50 mL, 44.0 µM, 6.41 mg/mL) was buffer exchanged into sodium acetate (NaOAc) buffer (20 mM NaOAc, pH 3.1) *via* ultrafiltration (10 kDa MWCO), followed by determination of concentration. Immobilized pepsin (0.15 mL) was loaded onto a Pierce™ centrifuge column and washed with NaOAc buffer (20 mM NaOAc, pH 3.1) three times. Trastuzumab (0.50 mL) was then added to the pepsin and the mixture was incubated at 37 °C for 5 h, under constant agitation (1100 rpm). At the start at 4th hour of incubation, immobilized papain (0.65 mL) was loaded onto Pierce™ centrifuge column and activated with 10 mM DTT in digest buffer (50 mM phosphate, 150 mM NaCl, 1 mM EDTA, pH 6.8). This was incubated at 37 °C for 90 min under constant agitation (1100 rpm). The resin was then removed from the digest using a Pierce™ centrifuge column and washed with digest buffer (3 × 0.4 mL, 50 mM phosphate, 150 mM NaCl, 1 mM EDTA, pH 6.8). The digest was combined with the washes and the volume was concentrated and adjusted to 0.5 mL. The resin containing papain was washed with digest buffer (4 × 0.4 mL, 50 mM phosphate, 150 mM NaCl, 1 mM EDTA, pH 6.8) without DTT, using a Pierce™ centrifuge column. F(ab')$_2$ (0.5 mL) was added to the washed papain and the mixture incubated at 37 °C for 20 h under constant agitation (1,100 rpm). The resin was separated and washed with conjugation buffer (4 × 0.4 mL, 40 mM phosphate, 20 mM NaCl, 6 mM EDTA, pH 7.4). The digest was combined with the washes and the buffer was exchanged completely for conjugation buffer *via* ultrafiltration (10 kDa MWCO). The concentration was determined by UV-Vis absorbance and adjusted to 100 µM in BBS buffer (pH 8.5). Aliquots of Fab were stored at -20 °C for up to 6 months.

5.3.5. Enzyme-linked immunosorbent assay (ELISA)-Trastuzumab against HER2

A 96-well plate was coated for 16 h at 4 °C with HER2 (Sino Biological, 100 µL/well, 0.25 µg/mL solution in PBS), all wells except row D and H. After washing (3 × 0.1% Tween® 20 in PBS,

followed by 3 × PBS), wells were blocked for 1 h at room temperature with 5% Marvel milk powder (Premier foods) in PBS (200 µL/well). The wells were then washed (3 × 0.1% Tween® 20 in PBS, followed by 3 × PBS), and the following dilutions of Fab conjugate were applied: 810 nM, 270 nM, 90 nM, 30 nM, 10 nM, 3.33 nM, 1.11 nM, 0.37 nM, 0.123 nM, 0.0412 nM, 0.0137 nM, prepared in 1% Marvel solution in PBS (100 µL/well). The samples were added to rows A to C – 1-11 and E to G – 1-11. The assay was then incubated at room temperature for 1 h. After 1 h, the plate was washed (3 × 0.1% Tween® 20 in PBS, followed by 3 × PBS), and the detection antibody (anti-human IgG, Fab specific-horseradish peroxidase (HRP) antibody, Sigma Aldrich, 1:5000 in 1% Marvel solution in 0.1% Tween® 20 in PBS) was added to the whole plate (100 µL/well), and incubated for 1 h at room temperature. After that, the plate was washed (3 × 0.1% Tween® 20 in PBS, followed by 3 × PBS), and *o*-phenylenediamine hydrochloride (Sigma-Aldrich, 100 µL/well, 0.5 mg/mL in a phosphate-citrate buffer with sodium perborate) was added to the whole plate, left for 15-30 min in the dark (the colour development was monitored visually) at room temperature. Once a yellow-orange colour was observed, the reaction was stopped by addition of HCl to the whole plate (4 M, 50 µL/well).

Absorbance was immediately measured at 490 nm and was corrected by subtracting the average of negative controls (i.e., PBS had been added to some of the wells instead of HER2 or instead of the samples). Each sample was tested in triplicate and errors are shown as the standard deviation of the average. ELISA data was analysed with Graphpad Prism 8.0 (using equation Sigmoidal, 4PL, X is log(concentration)) and the values have been normalised.

5.4. LC-MS general remarks

Molecular masses of native and modified proteins were measured using an Agilent 6510 QTOF LC-MS system (Agilent, UK). Method A (25 min): Agilent 1200 HPLC system was equipped with an Agilent PLRP- S, 1000A, 8 µm, 150 mm x 2.1 mm column. 10 µL of a protein sample (at *ca.* 2-4 µM) was separated on the column using mobile phase A (water-0.1% formic acid) and B (acetonitrile-0.1% formic acid) with an eluting gradient (as shown in **Table S2**) at a flow rate of 300 µl/min. The oven temperature was maintained at 60 °C unless otherwise stated.

Table S2 – LC-MS mobile phase A/B gradient elution (Method A).

Time (min)	Solvent A (%)	Solvent B (%)
0.0	85	15
2.0	85	15
3.0	68	32
4.0	68	32
14.0	65	35
18.0	5	95
20.0	5	95
22.0	85	15
25.0	85	15

Method B (10 min): Agilent 1200 HPLC system was equipped with an Agilent PLRP- S, 1000A, 5 μm, 150 mm x 2.1 mm column. 10 μL of a protein sample (at *ca.* 2-4 μM) was separated on the column using mobile phase A (water-0.1% formic acid) and B (acetonitrile-0.1% formic acid) with an eluting gradient (as shown in **Table S3**) at a flow rate of 400 μL/min. The oven temperature was maintained at 60 °C unless otherwise stated.

Table S3 – LC-MS mobile phase A/B gradient elution (Method B).

Time (min)	Solvent A (%)	Solvent B (%)
0.0	85	15
2.0	85	15
2.1	68	32
3.0	68	32
8.0	52	48
8.1	5	95
9.0	5	95

9.1	85	15
10.0	85	15

Agilent 6510 QTOF mass spectrometer was operated in a positive polarity mode, coupled with an ESI ion source. The ion source parameters were set up with a VCap of 3500V, a gas temperature at 350 °C, a dry gas flow rate at 10 L/min and a nebulizer of 30 psig. MS Tof was acquired under conditions of a fragmentor at 350 V, a skimmer at 65 V and an acquisition rate at 0.5 spectra/s in a profile mode, within a scan range between 700 and 5000 m/z. The .d data was then analysed by deconvoluting a spectrum to a zero charge mass spectra using a maximum entropy deconvolution algorithm within the MassHunter software version B.07.00.

Trastuzumab samples (100 μL, 0.65 nmol, 6.5 μM) in ammonium acetate buffer (pH 6.9) were incubated with PNGase F, non-reducing format (1.0 μL, New England Biolabs) for 16 h at 37 °C. The sample was then diluted to 2 μM with ammonium acetate buffer (pH 6.9) and analysed by LC-MS.

The following acronyms are used to describe antibody fragments based on their constituent heavy and light chains: heavy-heavy-light (HHL), heavy-heavy (HH), heavy-light (HL, half antibody), heavy chain (HC) and light chain (LC). Expected mass was calculated according to MS data observed for IgG1 subunits and full antibody (LC: 23441 Da, HC: 49154 Da, HL: 72591 Da, HHLL: 145179 Da) and Fab fragment (LC: 23440 Da, HC: 24201 Da, HL: 47638 Da).

5.5. LC-MS results

LC-MS analysis of native trastuzumab Fab

a.
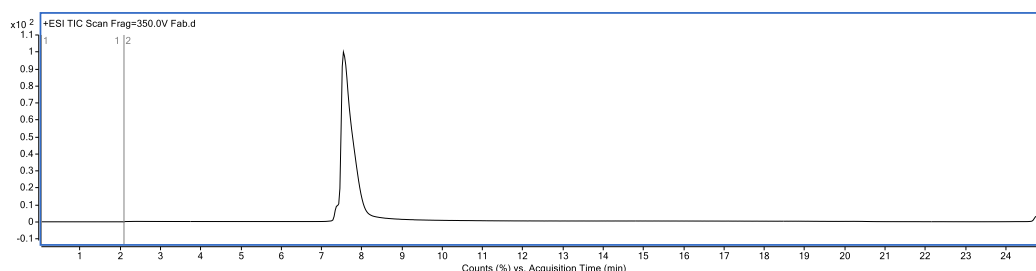
b.
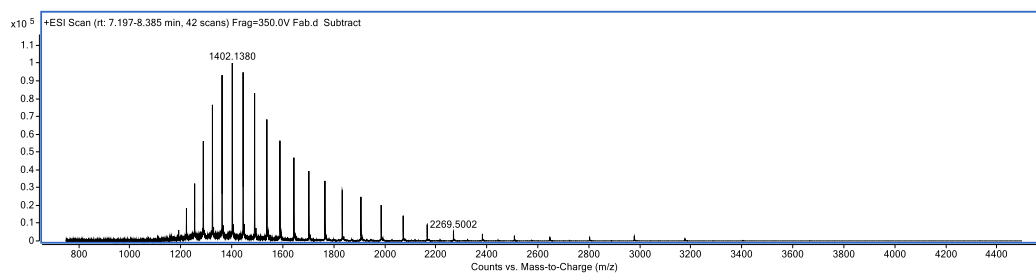
c.
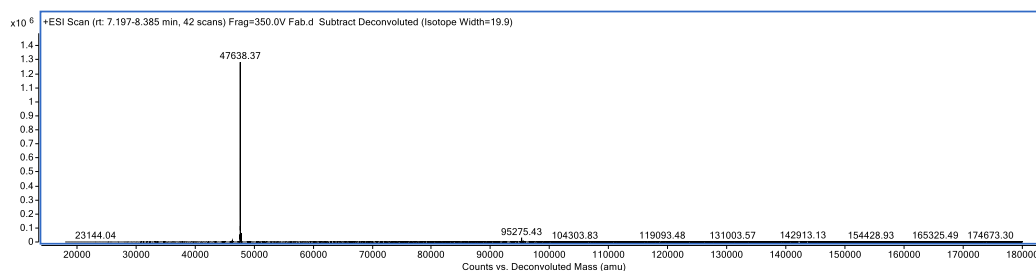
d.
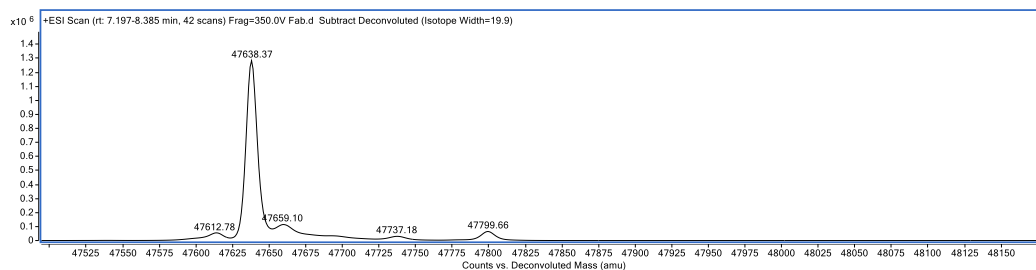
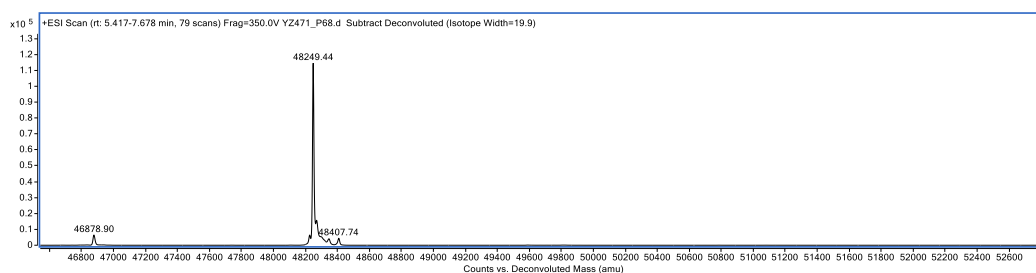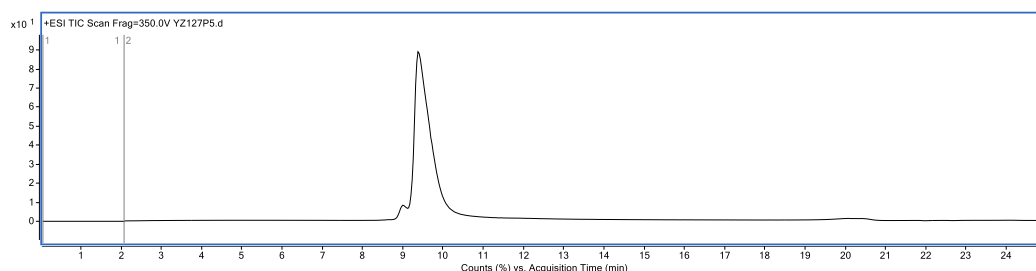**Figure S1** – LC-MS analysis of native trastuzumab Fab (Method A): a. TIC, b. non-deconvoluted ion-series, c. deconvoluted ion series mass spectrum: HL observed 47638 Da, d. zoomed in deconvoluted ion series mass spectrum.
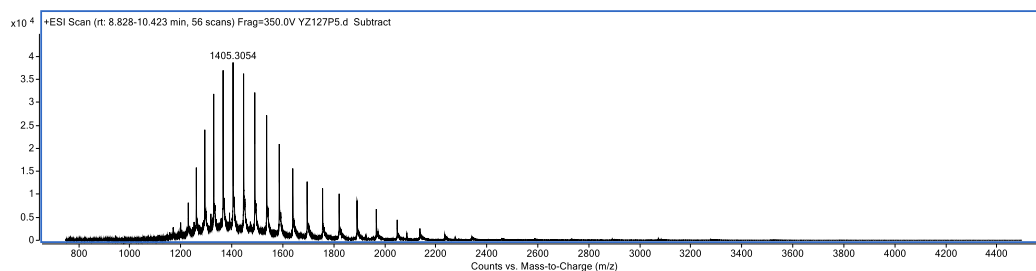
LC-MS analysis of reduced trastuzumab Fab

a.
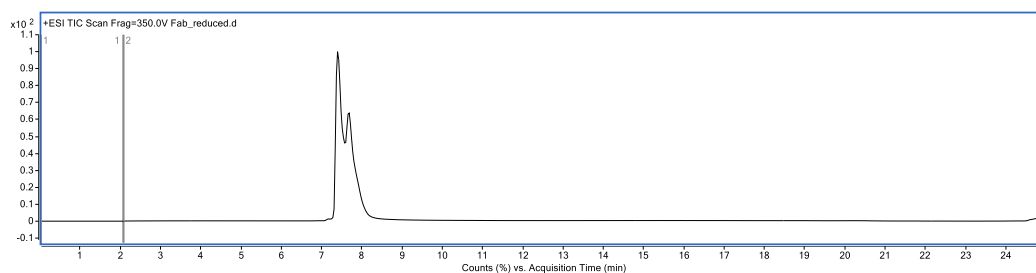
b.
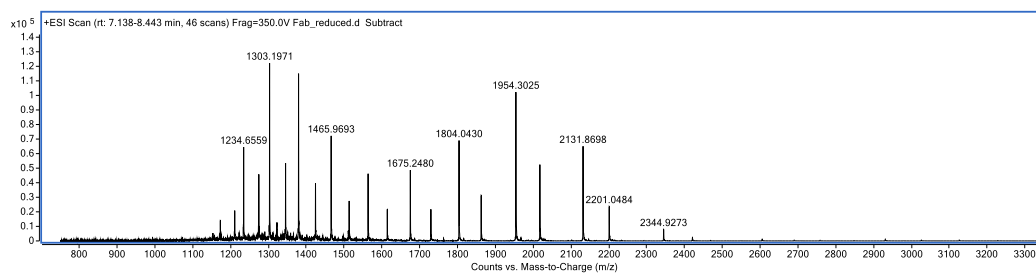
c.
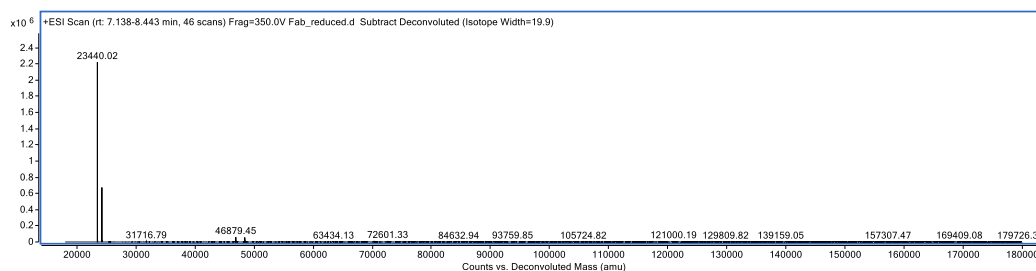
d.
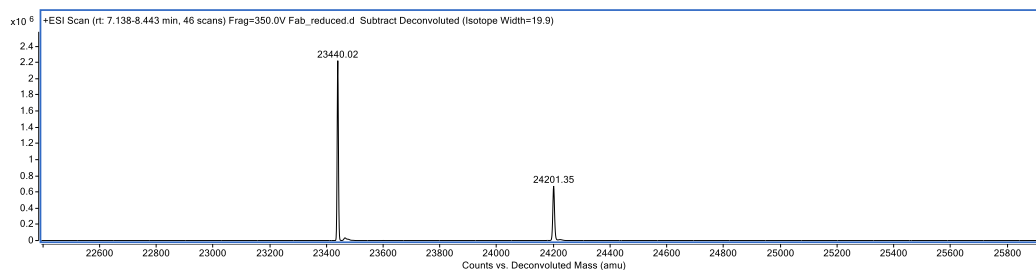
Figure S2 – LC-MS analysis of reduced trastuzumab Fab (Method A): a. TIC, b. non-deconvoluted ion-series, c. deconvoluted ion series mass spectrum: LC observed 23440 Da, HC observed 24201 Da, d. zoomed in deconvoluted ion series mass spectrum.

LC-MS analysis of native trastuzumab Ab

a.
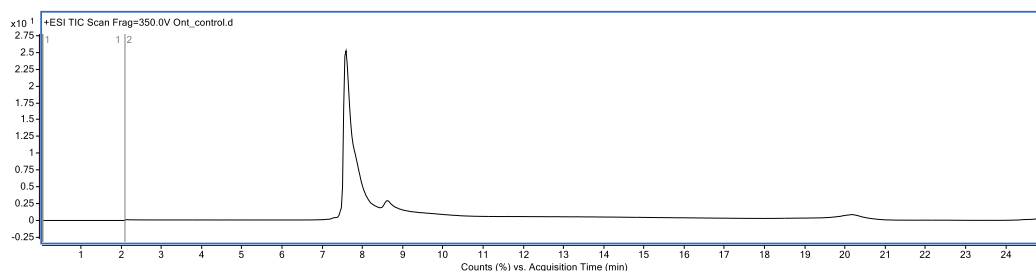
b.
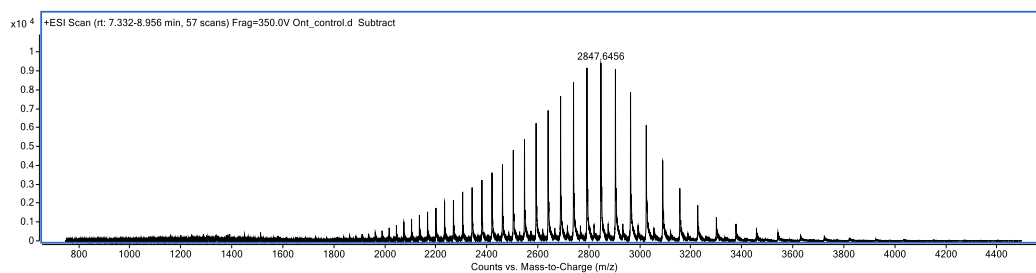
c.
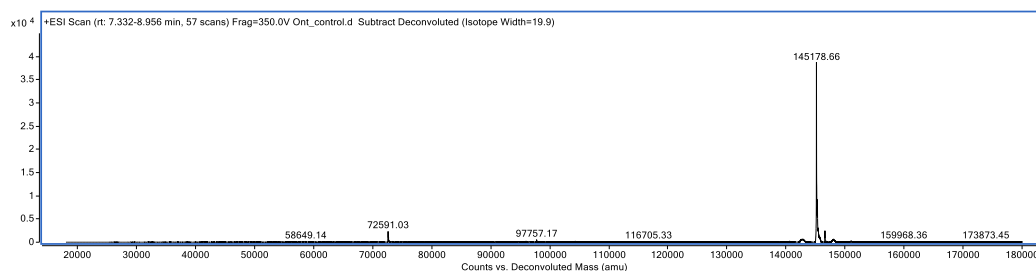
d.
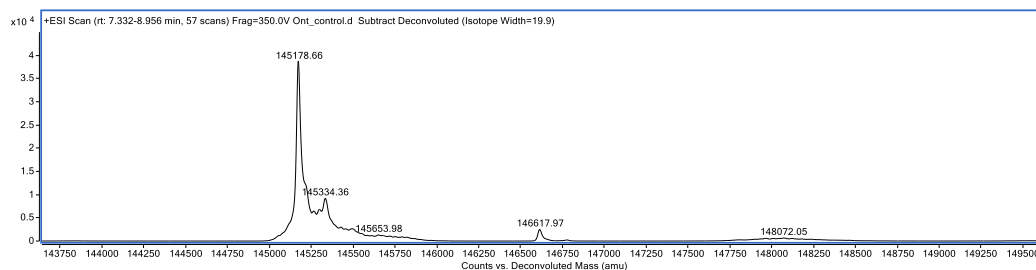
Figure S3 – LC-MS analysis of native trastuzumab (Method A): a. TIC, b. non-deconvoluted ion-series, c. deconvoluted ion series mass spectrum: HL observed 72591 Da, HHLL observed 145179 Da, d. zoomed in deconvoluted ion series mass spectrum.

LC-MS analysis of reduced trastuzumab Ab

a.
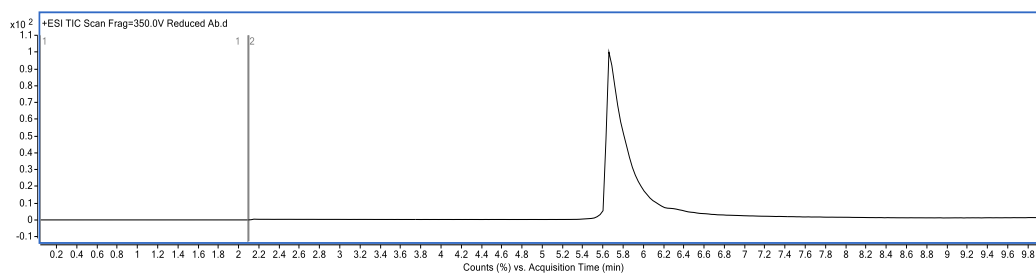
b.
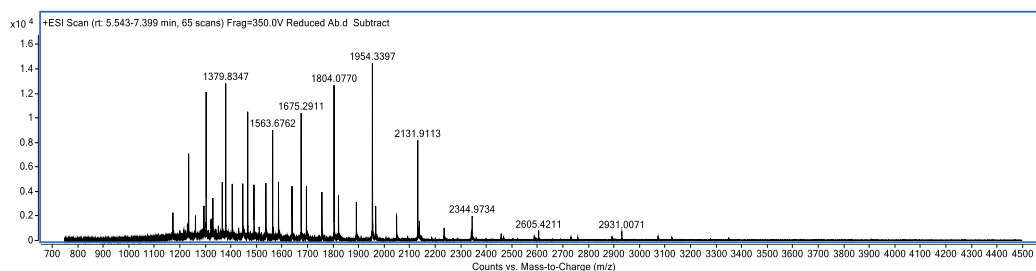
c.
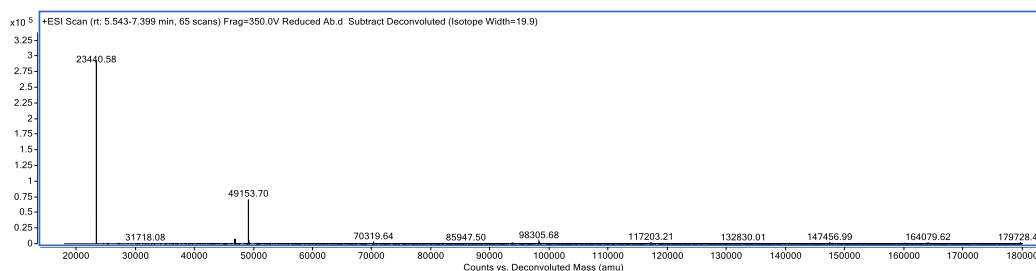
d.
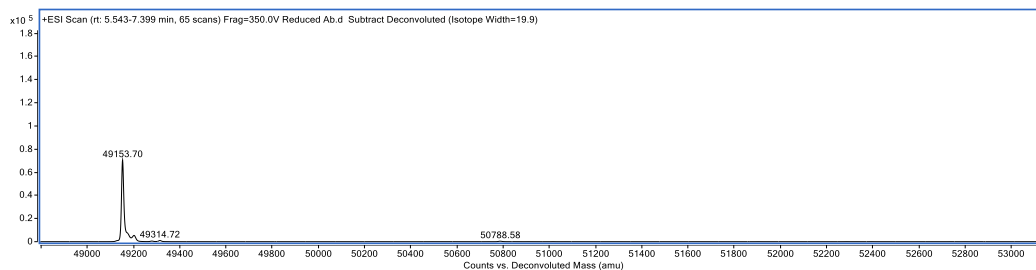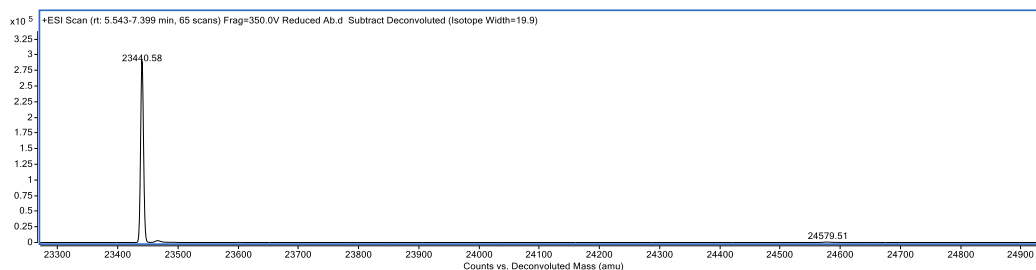
Figure S4 – LC-MS analysis of reduced trastuzumab (Method B): a. TIC, b. non-deconvoluted ion-series, c. deconvoluted ion series mass spectrum: LC observed 23441 Da, HC observed 49154 Da, d. zoomed in deconvoluted ion series mass spectrum.

LC-MS analysis of modified trastuzumab Fab

Preparation of trastuzumab Fab-DBM conjugate (13)

To trastuzumab Fab (100 µL, 0.012 µmol, 120 µM, 5.72 mg/mL) in BBS buffer (pH 8.5) was added TCEP.HCl (3.6 µL, 0.036 µmol, 10mM solution in dH$_2$O, 3 eq.). After 1.5 h at 37 °C, DBM **3** (6 µL, 0.060 µmol, 10 mM solution in anhydrous DMF, 5 eq.) was added and the resultant mixture was incubated for 1 h at 22 °C. The excess reagents were then removed *via* ultrafiltration (10 kDa MWCO) into BBS buffer (pH 8.5). The concentration was determined by UV-Vis absorbance and adjusted to 100 µM. The resultant solution was incubated for 16 h at 37 °C. The final trastuzumab Fab conjugates were desalted (7 kDa MWCO) and characterised by LC-MS.

a.
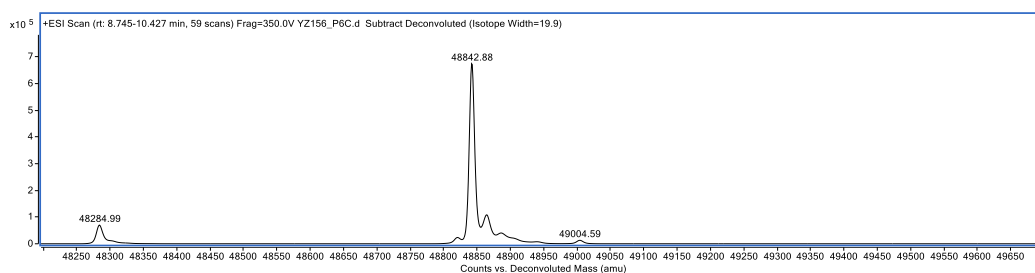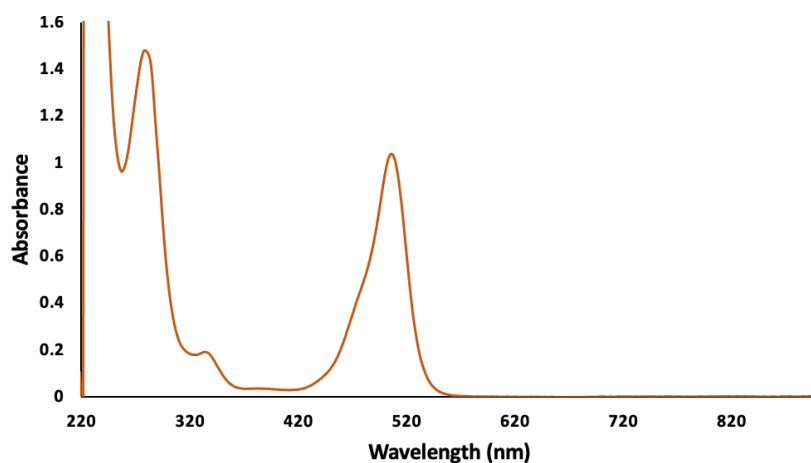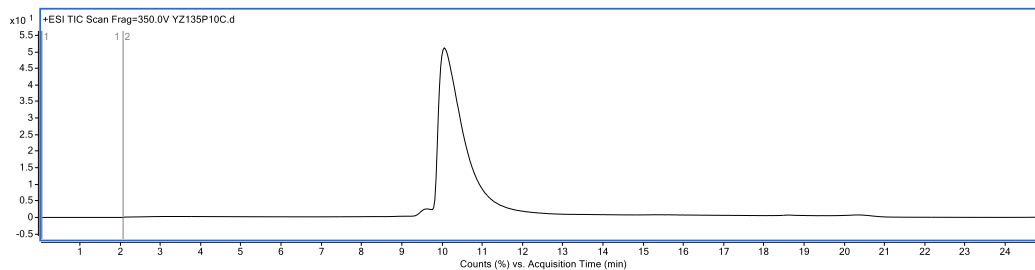

b.

c.

d.

Figure S5 – LC-MS analysis of trastuzumab Fab-DBM conjugate **13** (Method A): a. TIC, b. non-deconvoluted ion-series, c. deconvoluted ion series mass spectrum: HL expected 47999 Da, observed 48001 Da, d. zoomed in deconvoluted ion series mass spectrum.

Preparation of trastuzumab Fab-DBM conjugate (14)

To trastuzumab Fab (100 µL, 0.012 µmol, 120 µM, 5.72 mg/mL) in BBS buffer (pH 8.5) was added TCEP.HCl (3.6 µL, 0.036 µmol, 10mM solution in dH$_2$O, 3 eq.). After 1.5 h at 37 °C, DBM **4** (6 µL, 0.060 µmol, 10 mM solution in anhydrous DMF, 5 eq.) was added and the resultant mixture was incubated for 1 h at 22 °C. The excess reagents were then removed *via* ultrafiltration (10 kDa MWCO) into BBS buffer (pH 8.5). The concentration was determined by UV-Vis absorbance and adjusted to 100 µM. The resultant solution was incubated for 16 h at 37 °C. The final trastuzumab Fab conjugates were desalted (7 kDa MWCO) and characterised by LC-MS.

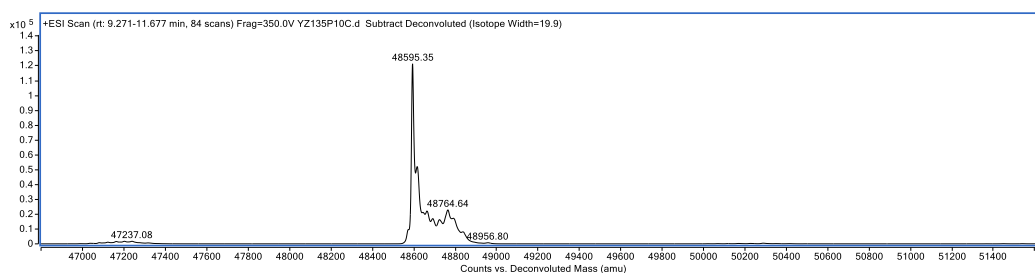a.

b.

c.

d.

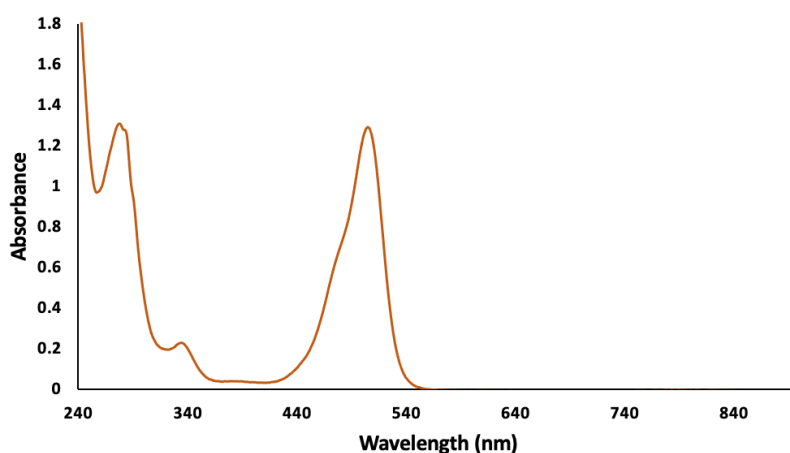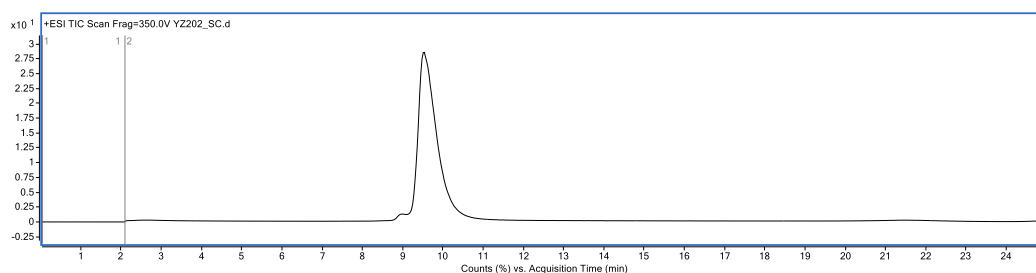**Figure S6** – LC-MS analysis of trastuzumab Fab-DBM conjugate **14** (Method A): a. TIC, b. non-deconvoluted ion-series, c. deconvoluted ion series mass spectrum: HL expected 48268 Da, observed 48269 Da, d. zoomed in deconvoluted ion series mass spectrum.

Preparation of trastuzumab Fab-DBM conjugate (15)

To trastuzumab Fab (100 µL, 0.012 µmol, 120 µM, 5.72 mg/mL) in BBS buffer (pH 8.5) was added TCEP.HCl (3.6 µL, 0.036 µmol, 10mM solution in dH$_2$O, 3 eq.). After 1.5 h at 37 °C, DBM **7** (6 µL, 0.060 µmol, 10 mM solution in anhydrous DMF, 5 eq.) was added and the resultant mixture was incubated for 1 h at 22 °C. The excess reagents were then removed *via* ultrafiltration (10 kDa MWCO) into BBS buffer (pH 8.5). The concentration was determined by UV-Vis absorbance and adjusted to 100 µM. The resultant solution was incubated for 16 h at 37 °C. The final trastuzumab Fab conjugates were desalted (7 kDa MWCO) and characterised by LC-MS.

a.

Figure S7 – LC-MS analysis of trastuzumab Fab-DBM conjugate **15** (Method A): a. TIC, b. non-deconvoluted ion-series, c. deconvoluted ion series mass spectrum: HL expected 48035 Da, observed 48021 Da, d. zoomed in deconvoluted ion series mass spectrum.

Preparation of trastuzumab Fab-DBM conjugate (16)

To trastuzumab Fab (100 µL, 0.012 µmol, 120 µM, 5.72 mg/mL) in BBS buffer (pH 8.5) was added TCEP.HCl (3.6 µL, 0.036 µmol, 10mM solution in dH$_2$O, 3 eq.). After 1.5 h at 37 °C, DBM **12** (6 µL, 0.060 µmol, 10 mM solution in anhydrous DMF, 5 eq.) was added and the resultant mixture was incubated for 1 h at 22 °C. The excess reagents were then removed *via* ultrafiltration (10 kDa MWCO) into BBS buffer (pH 8.5). The concentration was determined by UV-Vis absorbance and adjusted to 100 µM. The resultant solution was incubated for 16 h at 37 °C. The final trastuzumab Fab conjugates were desalted (7 kDa MWCO) and characterised by LC-MS.

a.

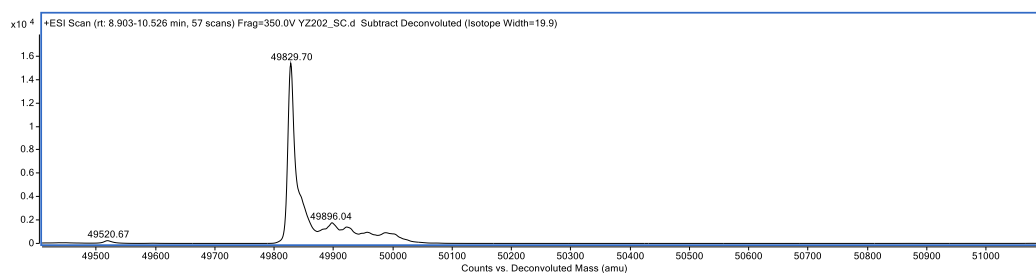b.

c.

d.

Figure S8 – LC-MS analysis of trastuzumab Fab-DBM conjugate **16** (Method B): a. TIC, b. non-deconvoluted ion-series, c. deconvoluted ion series mass spectrum: HL expected 48250 Da, observed 48249 Da, d. zoomed in deconvoluted ion series mass spectrum.

Preparation of trastuzumab Fab-DBM-AF488 conjugate (17)

To trastuzumab Fab-DBM conjugate **13** (100 µL, 0.010 µmol,100 µM, 4.77 mg/mL) in PB (pH 7.0) was added THPTA ligand (6.0 µL, 0.600 µmol, 100 mM solution in dH$_2$O, 60 eq.), followed by CuSO$_4$ (6.0 µL, 0.120 µmol, 20 mM solution in dH$_2$O, 12 eq.). To this mixture was added AF488 (10.0 µL, 0.100 µmol, 10 mM solution in anhydrous DMF, 10 eq.), followed by sodium ascorbate (13.6 µL, 1.360 µmol, 100 mM solution in dH$_2$O, final concentration 10 mM). The resultant mixture was incubated for 4 h at 22 °C. The excess reagent was then removed *via* PD column and ultrafiltration (10 kDa MWCO) into EDTA conjugation buffer (pH 7.0). The final trastuzumab Fab conjugates were desalted (7 kDa MWCO) and characterised by LC-MS. The sample was then analysed by UV-Vis spectroscopy.
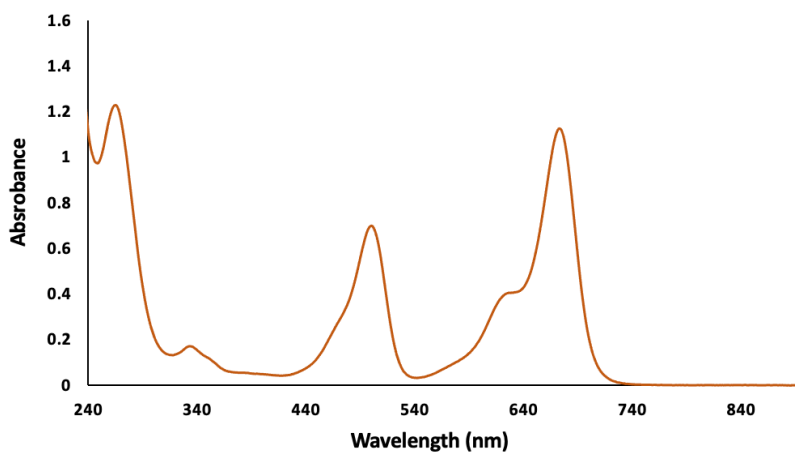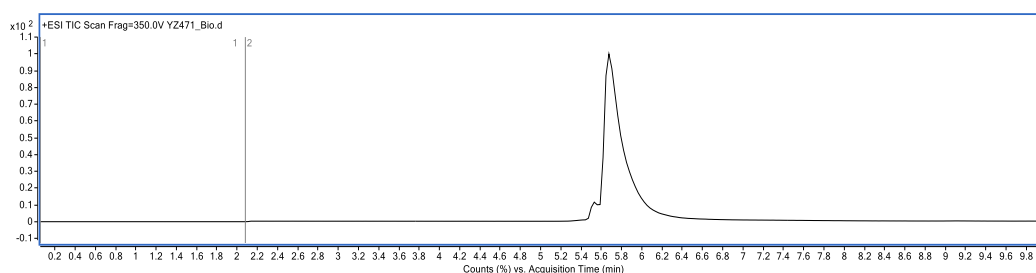
a.

b.

c.

d.

e.

Figure S9 – LC-MS and UV analysis of trastuzumab Fab-DBM-AF488 conjugate **17** (Method A): a. TIC, b. non-deconvoluted ion-series, c. deconvoluted ion series mass spectrum: HL expected 49148 Da, observed 49147 Da, d. zoomed in deconvoluted ion series mass spectrum, e. UV-Vis absorbance spectrum.
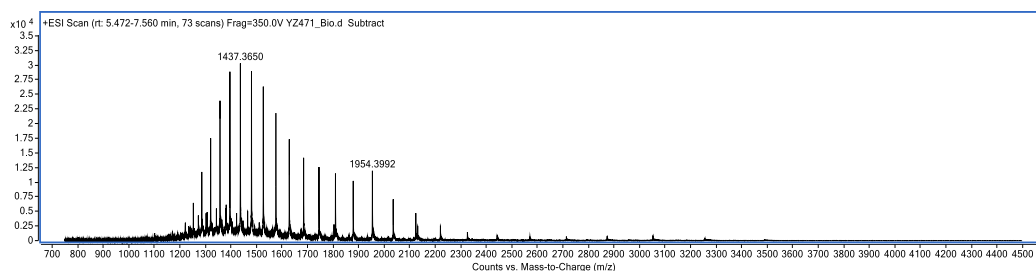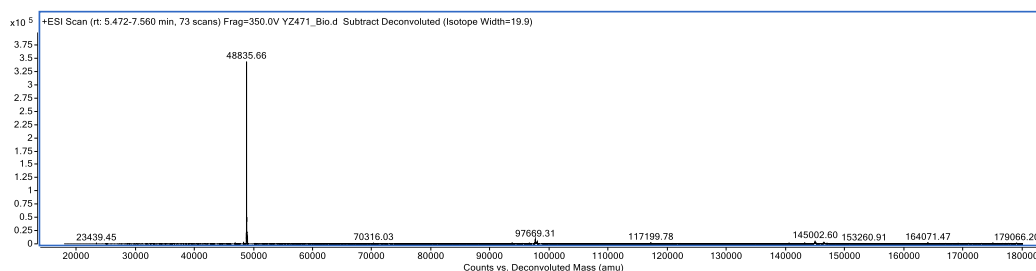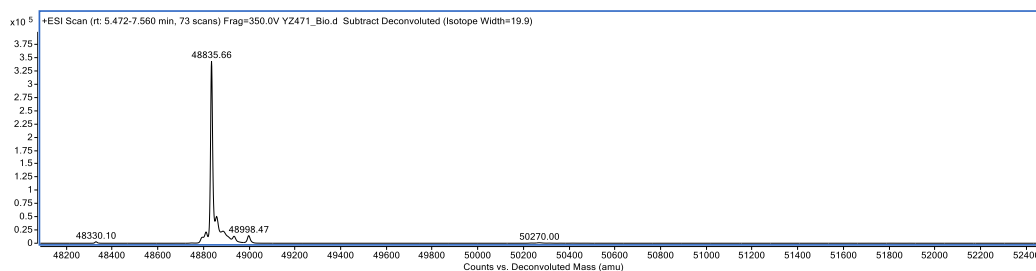
Preparation of trastuzumab Fab-DBM-AF488 conjugate (18)

To trastuzumab Fab-DBM conjugate **15** (100 μL, 0.005 μmol,100 μM, 4.77 mg/mL) in PB (pH 7.0) was added AF488 (10 μL, 0.100 μmol, 10 mM solution in anhydrous DMF, 10 eq.) and the resultant mixture was incubated for 4 h at 22 °C. The excess reagent was then removed *via* PD column and ultrafiltration (10 kDa MWCO) into EDTA conjugation buffer (pH 7.0). The final trastuzumab Fab conjugates were desalted (7 kDa MWCO) and characterised by LC-MS. The sample was then analysed by UV-Vis spectroscopy.
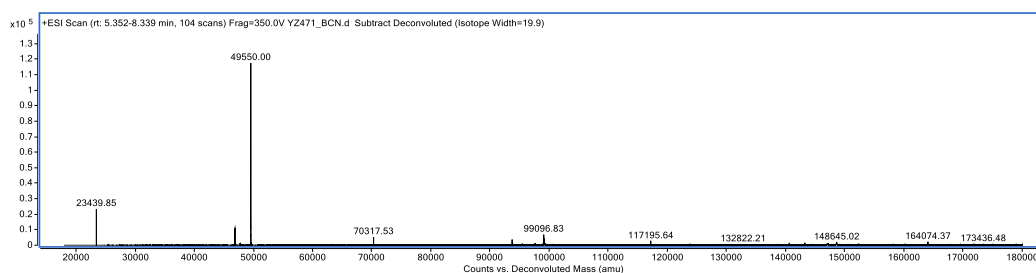
a.
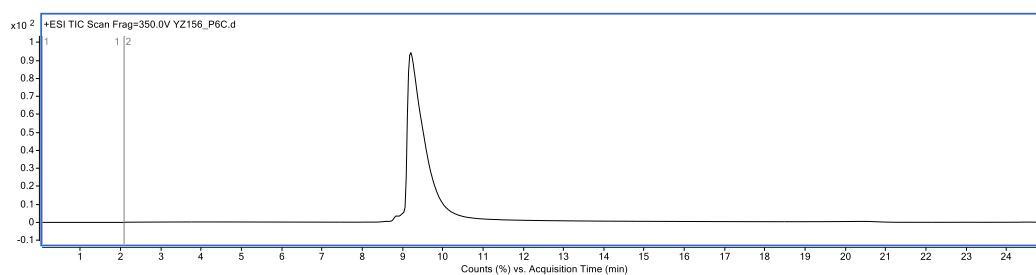
b.
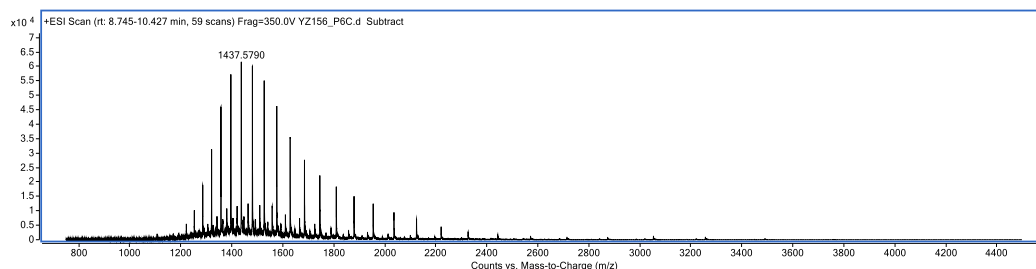
c.
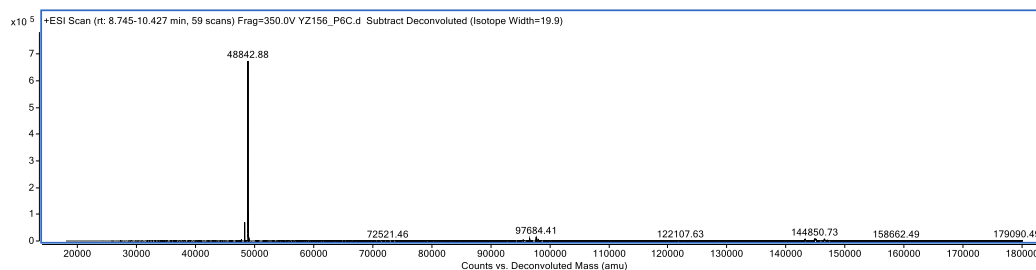
d.

e.

Figure S10 – LC-MS and UV analysis of trastuzumab Fab-DBM-AF488 conjugate **18** (Method A): a. TIC, b. non-deconvoluted ion-series, c. deconvoluted ion series mass spectrum: HL expected 48843 Da, observed 48843 Da, HL observed 48285 Da (possible oxidised strained alkyne), d. zoomed in deconvoluted ion series mass spectrum, e. UV-Vis absorbance spectrum.

Preparation of trastuzumab Fab-DBM-AF488 conjugate (19)

To trastuzumab Fab-DBM conjugate **14** (100 µL, 0.010 µmol,100 µM, 4.77 mg/mL) in PB (pH 7.0) was added THPTA ligand (6.0 µL, 0.600 µmol, 100 mM solution in dH$_2$O, 60 eq.), followed by CuSO$_4$ (6.0 µL, 0.120 µmol, 20 mM solution in dH$_2$O, 12 eq.). To this mixture was added AF488 (10.0 µL, 0.100 µmol, 10 mM solution in anhydrous DMF, 10 eq.), followed by sodium ascorbate (13.6 µL, 1.360 µmol, 100 mM solution in dH$_2$O, final concentration 10 mM). The resultant mixture was incubated for 4 h at 22 °C. The excess reagent was then removed *via* PD column and ultrafiltration (10 kDa MWCO) into EDTA conjugation buffer (pH 7.0). The final trastuzumab Fab conjugates were desalted (7 kDa MWCO) and characterised by LC-MS. The sample was then analysed by UV-Vis spectroscopy.
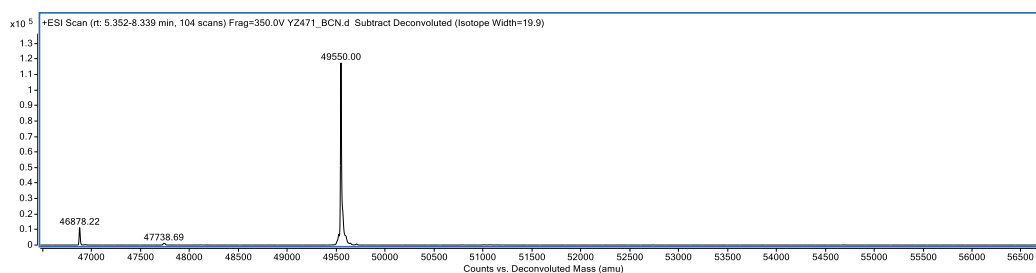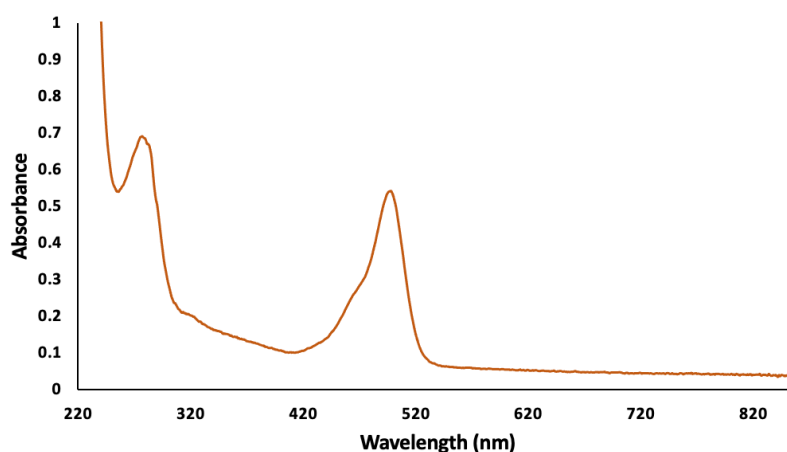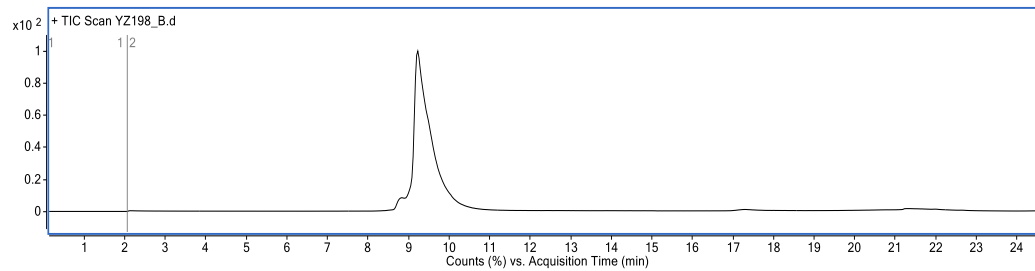
a.

b.

c.

d.

e.

Figure S11 – LC-MS and UV analysis of trastuzumab Fab-DBM-AF488 conjugate **19** (Method A): a. TIC, b. non-deconvoluted ion-series, c. deconvoluted ion series mass spectrum: HL expected 48609 Da, observed 48595 Da, d. zoomed in deconvoluted ion series mass spectrum, e. UV-Vis absorbance spectrum.

## Preparation of trastuzumab Fab-DBM-AF488-Cy5.5 conjugate (20)

To trastuzumab Fab-DBM-AF488 conjugate **19** (50 μL, 0.005 μmol,100 μM, 4.77 mg/mL) in PB (pH 7.0) was added THPTA ligand (3.0 μL, 0.300 μmol, 100 mM solution in dH$_2$O, 60 eq.), followed by CuSO$_4$ (3.0 μL, 0.060 μmol, 20 mM solution in dH$_2$O, 12 eq.). To this mixture was added Cy5.5-azide (5.0 μL, 0.050 μmol, 10 mM solution in anhydrous DMF, 10 eq.), followed by sodium ascorbate (6.8 μL, 0.680 μmol, 100 mM solution in dH$_2$O, final concentration 10 mM). The resultant mixture was incubated for 16 h at 22 °C. The excess reagent was then removed *via* PD column and ultrafiltration (10 kDa MWCO) into EDTA conjugation buffer (pH 7.0). The final trastuzumab Fab conjugates were desalted (7 kDa MWCO) and characterised by LC-MS. The sample was then analysed by UV-Vis spectroscopy.
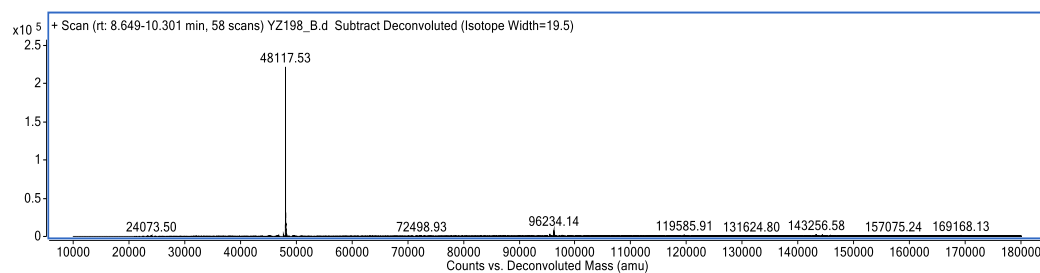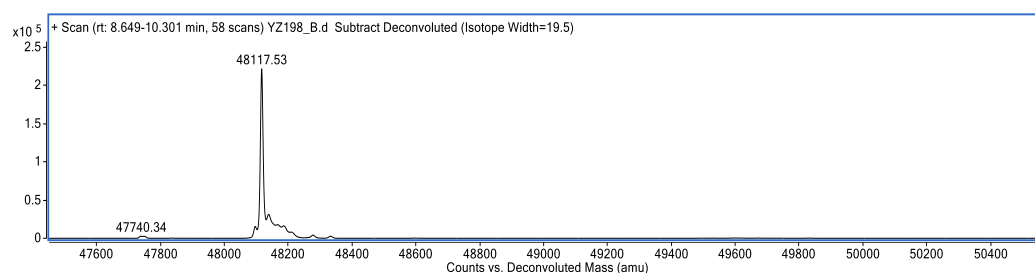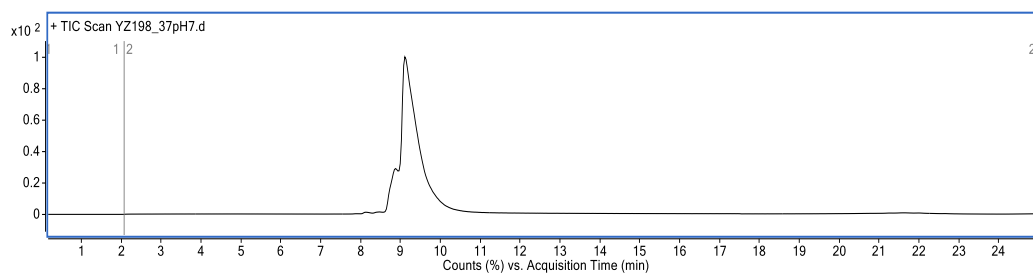
a.

b.
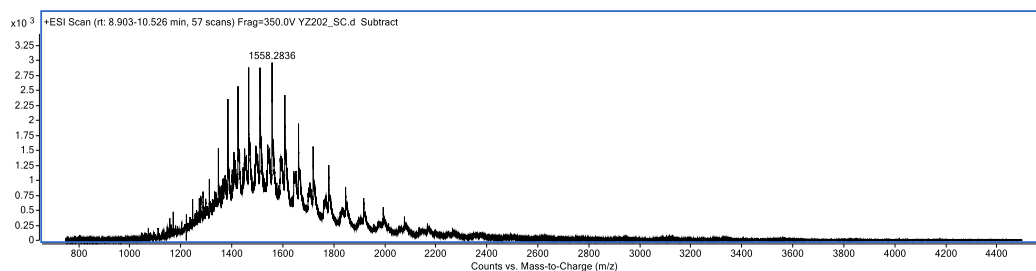
c.
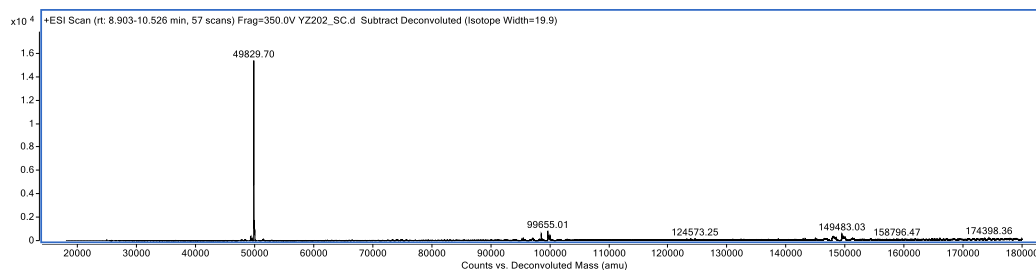
d.

e.

Figure S12 – LC-MS and UV analysis of trastuzumab Fab-DBM-AF488-Cy5.5 conjugate **20** (Method A): a. TIC, b. non-deconvoluted ion-series, c. deconvoluted ion series mass spectrum: HL expected 49827 Da, observed 49830 Da, d. zoomed in deconvoluted ion series mass spectrum, e. UV-Vis absorbance spectrum.

Preparation of trastuzumab Fab-DBM-Biotin conjugate (21)

To trastuzumab Fab-DBM conjugate **16** (100 µL, 0.010 µmol,100 µM, 4.77 mg/mL) in PB (pH 7.0) was added TCO-Biotin (5 µL, 0.100 µmol, 20 mM solution in anhydrous DMF, 10 eq.) and the resultant mixture was incubated for 4 h at 22 °C. The excess reagent was then removed *via* PD column and ultrafiltration (10 kDa MWCO) into EDTA conjugation buffer (pH 7.0). The final trastuzumab Fab conjugates were desalted (7 kDa MWCO) and characterised by LC-MS.
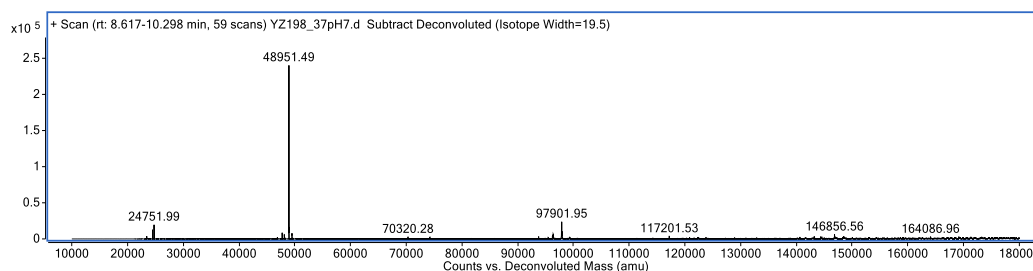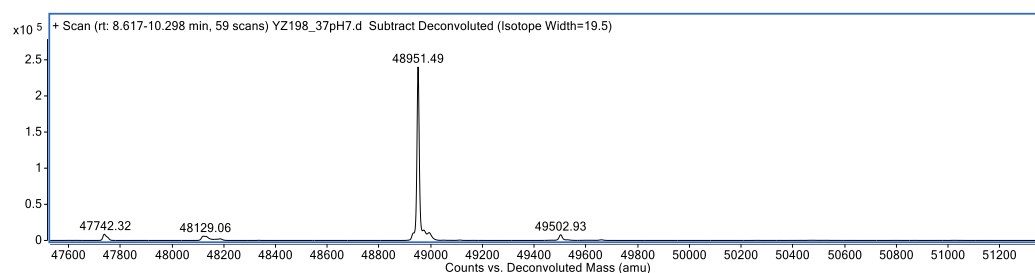
a.

b.

c.

d.

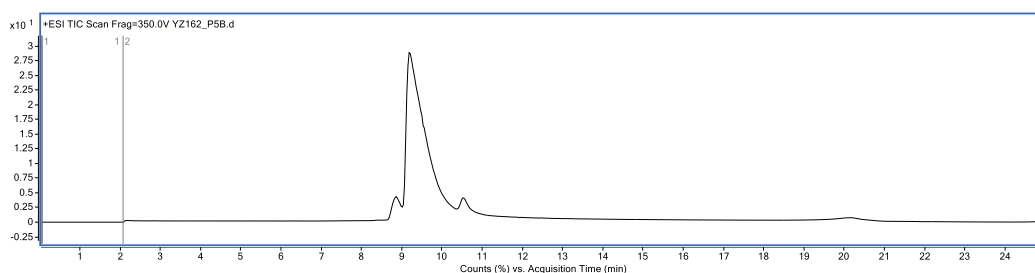**Figure S13** – LC-MS analysis of trastuzumab Fab-DBM-AF488 conjugate **21** (Method B): a. TIC, b. non-deconvoluted ion-series, c. deconvoluted ion series mass spectrum: HL expected 48837 Da, observed 48836 Da, d. zoomed in deconvoluted ion series mass spectrum.

Preparation of trastuzumab Fab-DBM-Biotin-Fluor conjugate (22)

To trastuzumab Fab-DBM-Biotin conjugate **21** (50 µL, 0.005 µmol,100 µM, 4.77 mg/mL) in PB (pH 7.0) was added BCN-Fluor (2.5 µL, 0.050 µmol, 20 mM solution in anhydrous DMF, 10 eq.). The resultant mixture was incubated for 4 h at 22 °C. The excess reagent was then removed *via* PD column and ultrafiltration (10 kDa MWCO) into EDTA conjugation buffer (pH 7.0). The final trastuzumab Fab conjugates were desalted (7 kDa MWCO) and characterised by LC-MS. The sample was then analysed by UV-Vis spectroscopy.

a.
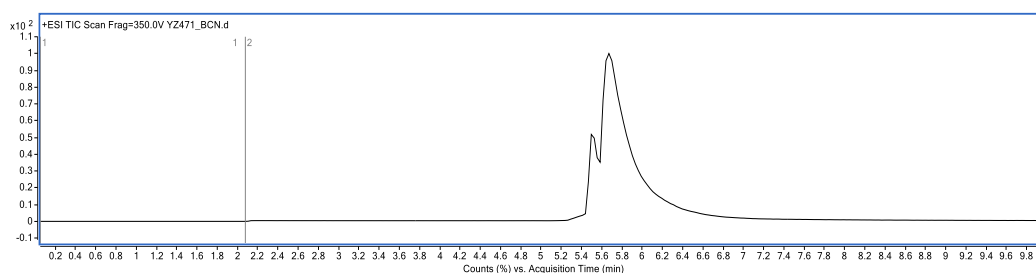
b.
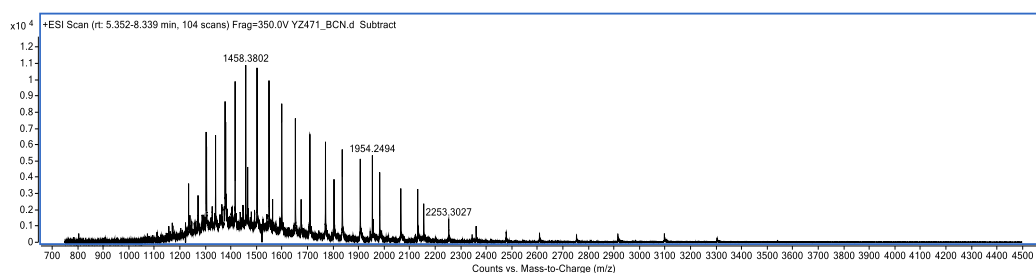
c.

d.

e.

Figure S14 – LC-MS and UV analysis of trastuzumab Fab-DBM-Biotin-Fluor conjugate **22** (Method B): a. TIC, b. non-deconvoluted ion-series, c. deconvoluted ion series mass spectrum: HL expected 49563 Da, observed 49550 Da, LC observed 23440 Da, 2*LC observed 46878 Da (SDS-PAGE showed <10% LC species), d. zoomed in deconvoluted ion series mass spectrum, e. UV-Vis absorbance spectrum.
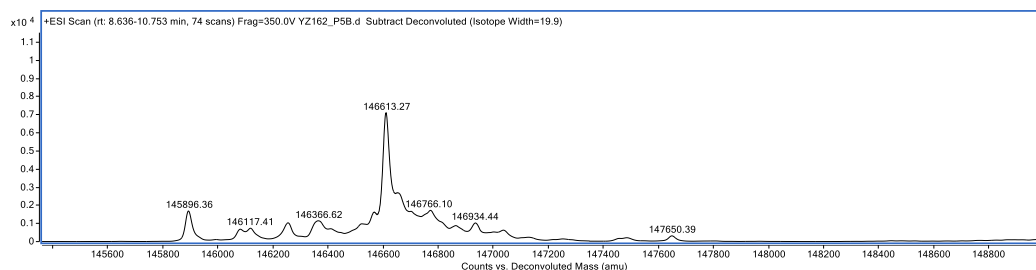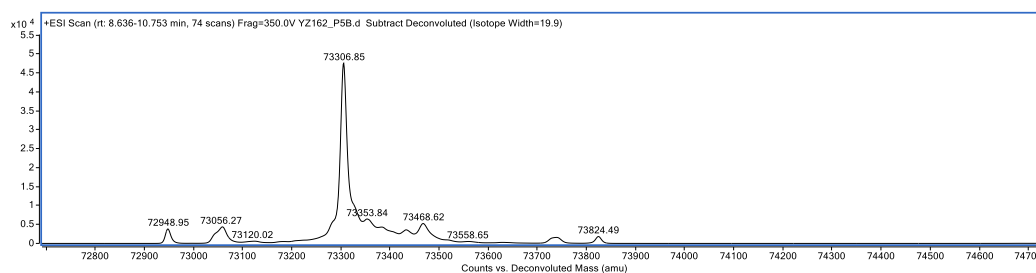
Preparation of trastuzumab Fab-DBM-BCN conjugate (34)

To trastuzumab Fab (50 µL, 0.006 µmol, 120 µM) in BBS buffer (pH 8.5) was added TCEP.HCl (1.8 µL, 0.018 µmol, 10mM solution in H_2O, 3 eq.). After 1.5 h at 37 °C, NGM-BCN (3.6 µL, 0.036 µmol, 10 mM solution in anhydrous DMF, 5 eq.) was added and the resultant mixture

was incubated for 1 h at 22 °C. The excess reagents were then removed *via* ultrafiltration (10 kDa MWCO) into BBS buffer (pH 8.5). The concentration was determined by UV-Vis absorbance and adjusted to 100 μM. The resultant solution was incubated for 16 h at 37 °C. The final trastuzumab Fab conjugates were desalted (7 kDa MWCO) and characterised by LC-MS.
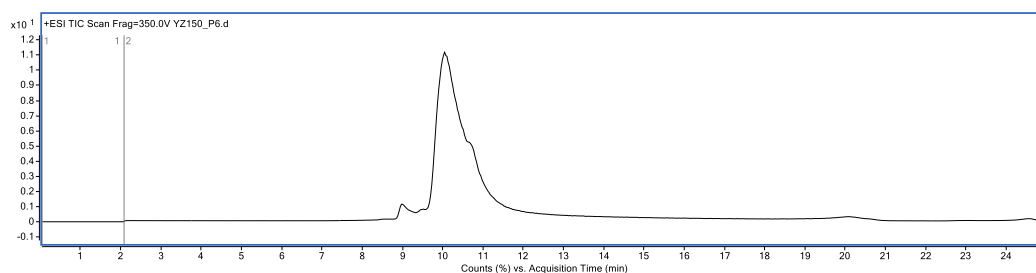
a.

b.
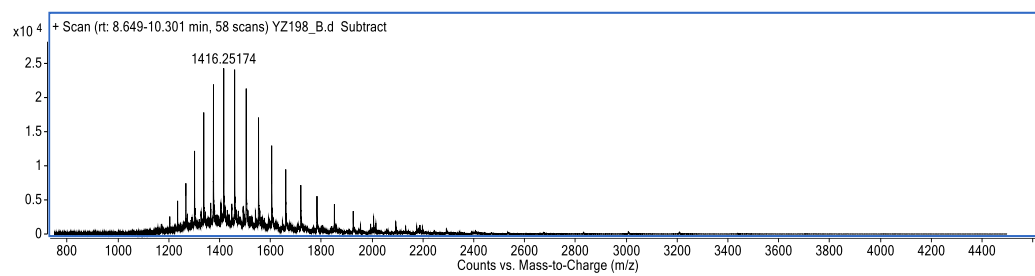
c.

d.

Figure S15 – LC-MS and UV analysis of trastuzumab Fab-DBM-BCN conjugate **34** (Method A): a. TIC, b. non-deconvoluted ion-series, c. deconvoluted ion series mass spectrum: HL expected 48114 Da, observed 48118 Da, d. zoomed in deconvoluted ion series mass spectrum, e. UV-Vis absorbance spectrum.

Preparation of trastuzumab Fab-DBM-BCN-DFO conjugate (35)

To Fab-DBM-BCN conjugate **34** (50 μL, 0.005 μmol,100 μM) in PB buffer (pH 7.0) was added DFO-azide (5 μL, 0.050 μmol, 10 mM solution in DMF, 10 eq.) and the resultant mixture was incubated for 16 h at 37 °C. The excess reagent was then removed *via* ultrafiltration (10 kDa MWCO) into EDTA conjugation buffer (pH 7.0). The final trastuzumab Fab conjugates were desalted (7 kDa MWCO) and characterised by LC-MS.

a.

b.
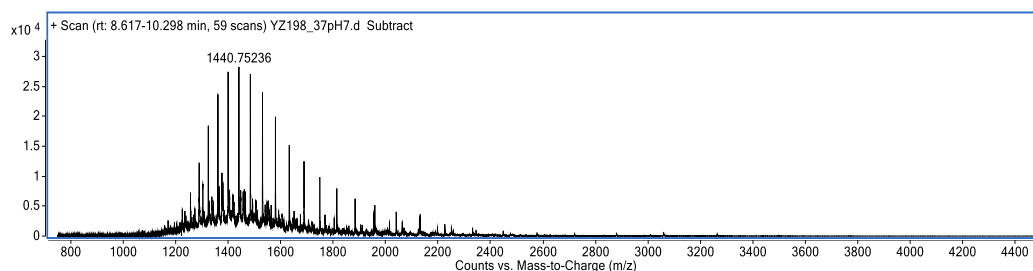
c.

d.

Figure S16 – LC-MS and UV analysis of trastuzumab Fab-DBM-BCN conjugate **35** (Method A):

a. TIC, b. non-deconvoluted ion-series, c. deconvoluted ion series mass spectrum: HL

expected 48948 Da, observed 48951 Da, d. zoomed in deconvoluted ion series mass

spectrum, e. UV-Vis absorbance spectrum.

LC-MS analysis of modified trastuzumab Ab

Preparation of trastuzumab Ab-DBM conjugate (23)

To trastuzumab Ab (100 µL, 0.002 µmol, 24 µM, 3.48 mg/mL) in BBS buffer (pH 8.5) was added TCEP.HCl (1.9 µL, 0.019 µmol, 10mM solution in dH$_2$O, 8 eq.). After 2 h at 37 °C, DBM **3** (3.6 µL, 0.036 µmol, 10 mM solution in anhydrous DMF, 15 eq.) was added and the resultant mixture was incubated for 1 h at 22 °C. The excess reagents were then removed *via* ultrafiltration (10 kDa MWCO) into BBS buffer (pH 8.5). The concentration was determined by UV-Vis absorbance and adjusted to 20.0 µM. The resultant solution was incubated for 16 h at 37 °C. The sample was then buffer exchanged into ammonium acetate (pH 6.9) *via* ultrafiltration (10 kDa MWCO). The final trastuzumab conjugates were deglycosylated and characterised by LC-MS.
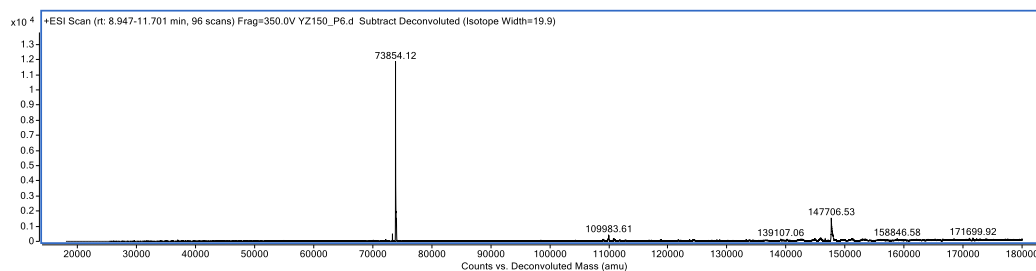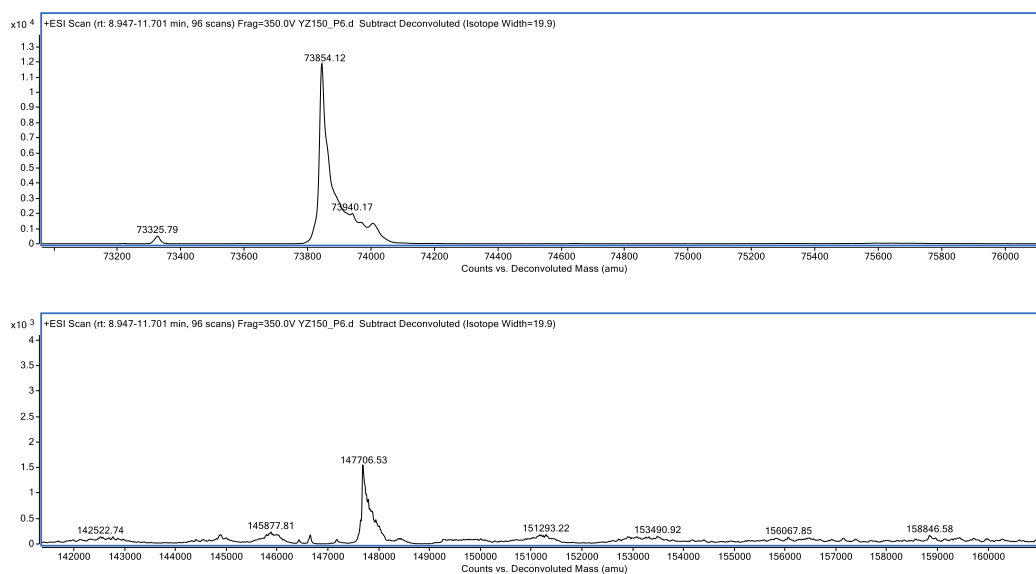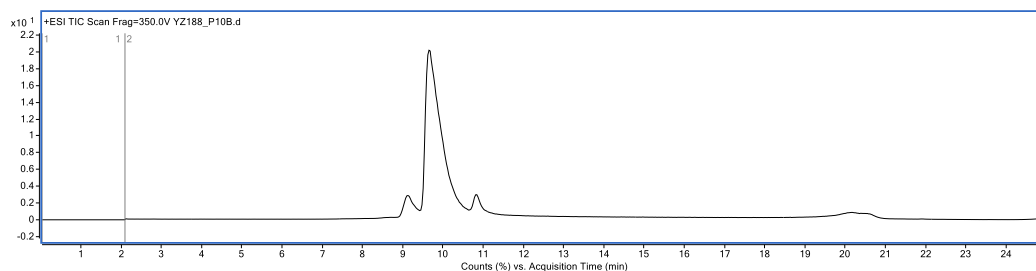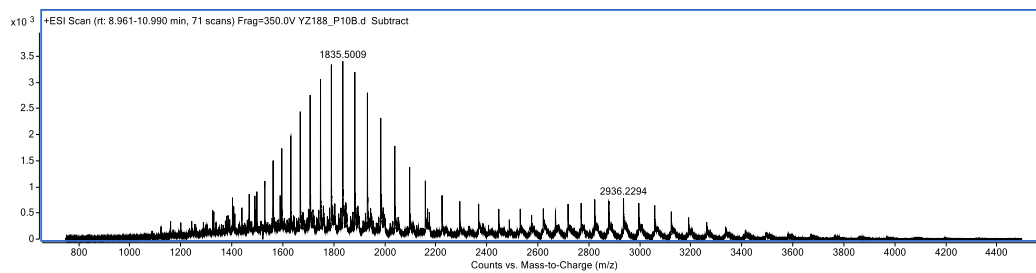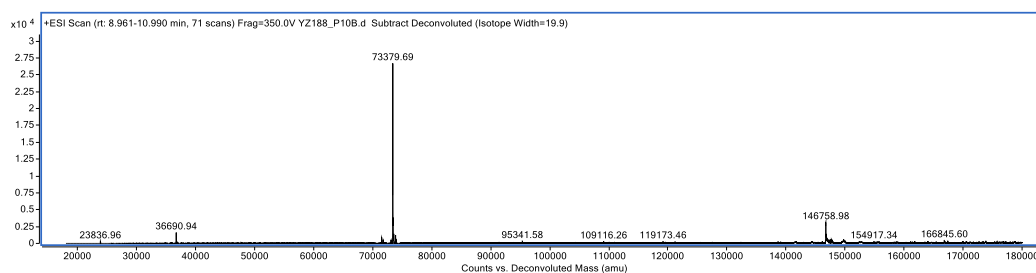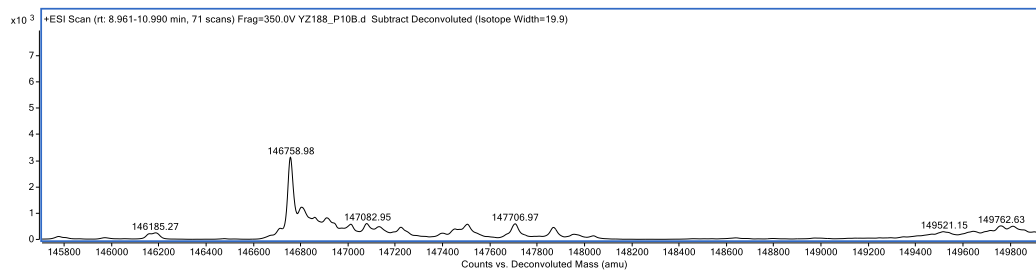
a.

b.

Figure S17 – LC-MS analysis of trastuzumab Ab-DBM conjugate **23** (Method A): a. TIC, b. non-deconvoluted ion-series, c. deconvoluted ion series mass spectrum: HL expected 73313 Da, observed 73307 Da, HHLL expected 146624 Da, observed 146613 Da, d. zoomed in deconvoluted ion series mass spectrum.

Preparation of trastuzumab Ab-DBM conjugate (24)

To trastuzumab Ab (100 µL, 0.002 µmol, 24 µM, 3.48 mg/mL) in BBS buffer (pH 8.5) was added TCEP.HCl (1.9 µL, 0.019 µmol, 10mM solution in dH$_2$O, 8 eq.). After 2 h at 37 °C, DBM **4** (3.6

153

µL, 0.036 µmol, 10 mM solution in anhydrous DMF, 15 eq.) was added and the resultant mixture was incubated for 1 h at 22 °C. The excess reagents were then removed *via* ultrafiltration (10 kDa MWCO) into BBS buffer (pH 8.5). The concentration was determined by UV-Vis absorbance and adjusted to 20.0 µM. The resultant solution was incubated for 16 h at 37 °C. The sample was then buffer exchanged into ammonium acetate (pH 6.9) *via* ultrafiltration (10 kDa MWCO). The final trastuzumab conjugates were deglycosylated and characterised by LC-MS.
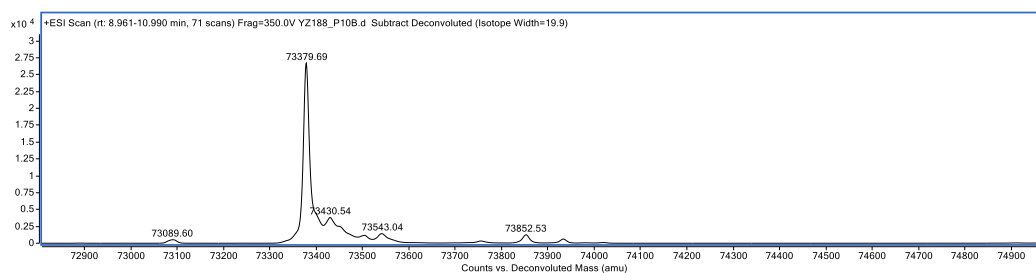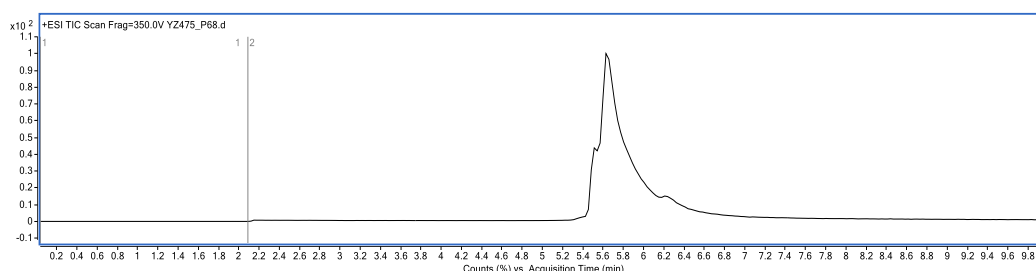
a.

b.

c.

d.

Figure S18 – LC-MS analysis of trastuzumab Ab-DBM conjugate **24** (Method A): a. TIC, b. non-deconvoluted ion-series, c. deconvoluted ion series mass spectrum: HL expected 73852 Da, observed 73854 Da, HHLL expected 147700 Da, observed 147707 Da, d. zoomed in deconvoluted ion series mass spectrum.

Preparation of trastuzumab Ab-DBM conjugate (25)

To trastuzumab Ab (100 µL, 0.002 µmol, 24 µM, 3.48 mg/mL) in BBS buffer (pH 8.5) was added TCEP.HCl (1.9 µL, 0.019 µmol, 10mM solution in dH$_2$O, 8 eq.). After 2 h at 37 °C, DBM **7** (3.6 µL, 0.036 µmol, 10 mM solution in anhydrous DMF, 15 eq.) was added and the resultant mixture was incubated for 1 h at 22 °C. The excess reagents were then removed *via* ultrafiltration (10 kDa MWCO) into BBS buffer (pH 8.5). The concentration was determined by UV-Vis absorbance and adjusted to 20.0 µM. The resultant solution was incubated for 16 h at 37 °C. The sample was then buffer exchanged into ammonium acetate (pH 6.9) *via* ultrafiltration (10 kDa MWCO). The final trastuzumab conjugates were deglycosylated and characterised by LC-MS.

a.

Figure S19 – LC-MS analysis of trastuzumab Ab-DBM conjugate **25** (Method A): a. TIC, b.

non-deconvoluted ion-series, c. deconvoluted ion series mass spectrum: HL expected 73385

Da, observed 73380 Da, HHLL expected 146768 Da, observed 146759 Da, d. zoomed in deconvoluted ion series mass spectrum.
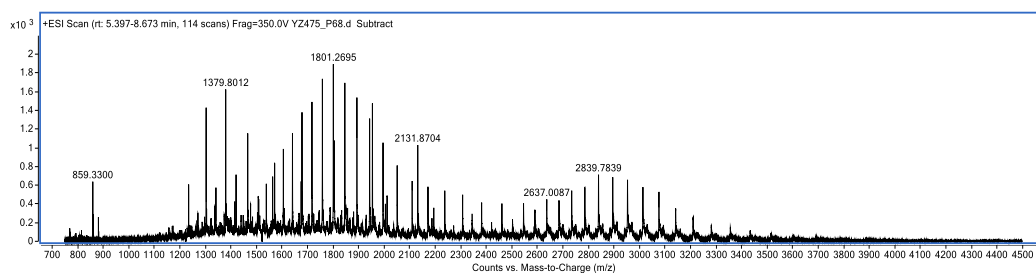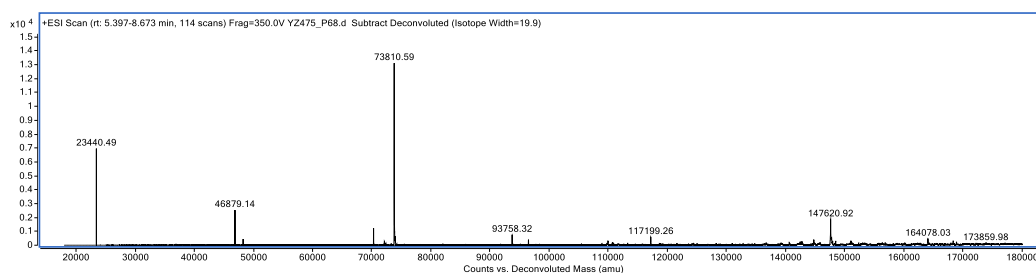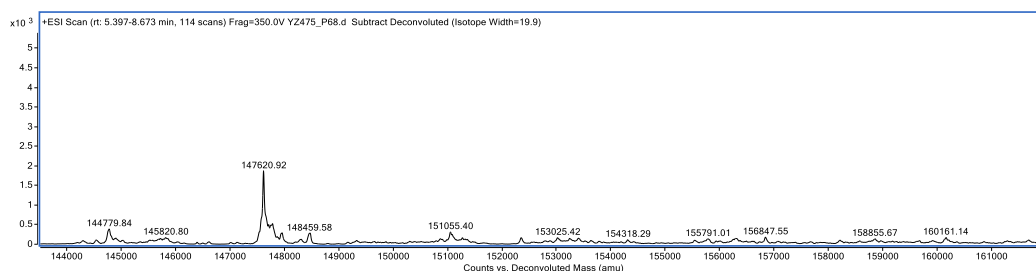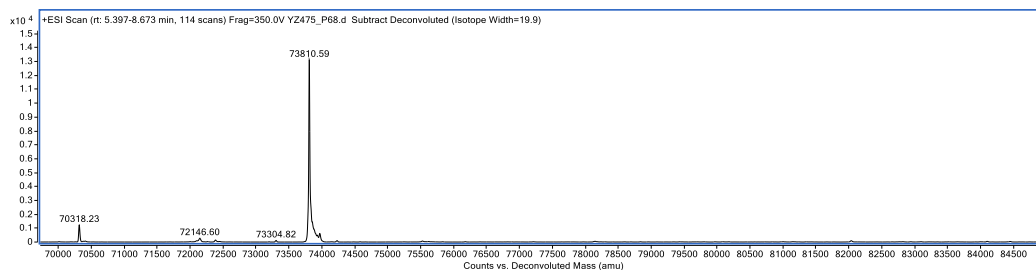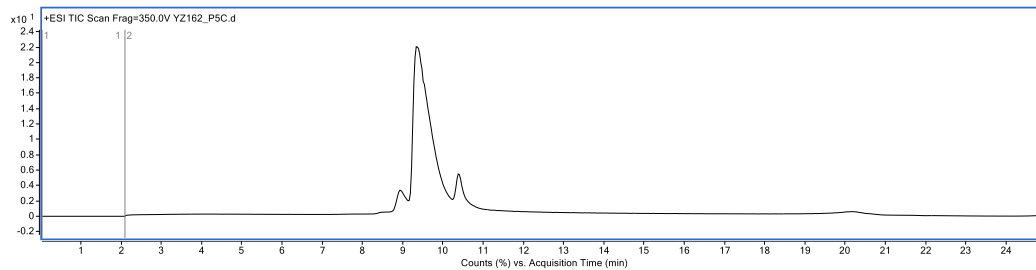
Preparation of trastuzumab Ab-DBM conjugate (26)

To trastuzumab Ab (100 µL, 0.002 µmol, 24 µM, 3.48 mg/mL) in BBS buffer (pH 8.5) was added TCEP.HCl (1.9 µL, 0.019 µmol, 10mM solution in dH$_2$O, 8 eq.). After 2 h at 37 °C, DBM **12** (3.6 µL, 0.036 µmol, 10 mM solution in anhydrous DMF, 15 eq.) was added and the resultant mixture was incubated for 1 h at 22 °C. The excess reagents were then removed *via* ultrafiltration (10 kDa MWCO) into BBS buffer (pH 8.5). The concentration was determined by UV-Vis absorbance and adjusted to 20.0 µM. The resultant solution was incubated for 16 h at 37 °C. The sample was then buffer exchanged into ammonium acetate (pH 6.9) *via* ultrafiltration (10 kDa MWCO). The final trastuzumab conjugates were deglycosylated and characterised by LC-MS.

a.

b.

c.

d.

Figure S20 – LC-MS analysis of trastuzumab Ab-DBM conjugate **26** (Method B): a. TIC, b. non-deconvoluted ion-series, c. deconvoluted ion series mass spectrum: HL expected 73816 Da, observed 73811 Da, HHLL expected 147628 Da, observed 147621 Da, LC observed 23440 Da, 2*LC observed 46879 Da, 3*LC observed 70318 Da (SDS-PAGE showed <10% LC species), d. zoomed in deconvoluted ion series mass spectrum.
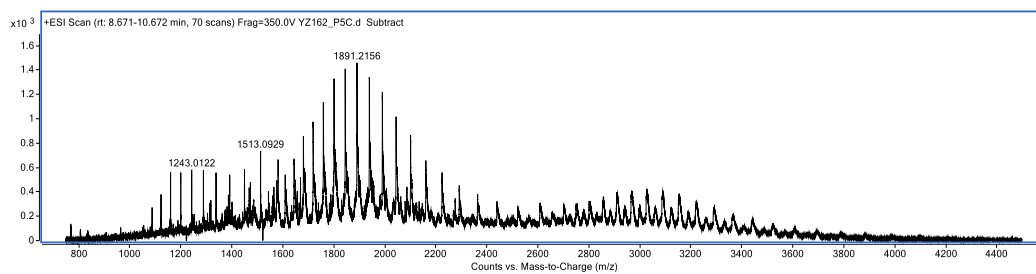
Preparation of trastuzumab Ab-DBM-AF488 conjugate (27)

To trastuzumab Ab-DBM conjugate **23** (100 µL, 0.002 µmol, 20 µM, 2.90 mg/mL) in PB (pH 7.0) was added THPTA ligand (3.6 µL, 0.360 µmol, 100 mM solution in dH$_2$O, 180 eq.), followed by CuSO$_4$ (3.6 µL, 0.072 µmol, 20 mM solution in dH$_2$O, 36 eq.). To this mixture was added AF488 (4.0 µL, 0.040 µmol, 10 mM solution in anhydrous DMF, 20 eq.), followed by sodium ascorbate (12.4 µL, 1.240 µmol, 100 mM solution in dH$_2$O, final concentration 10 mM). The resultant mixture was incubated for 4 h at 22 °C. The excess reagent was then removed *via* PD column and ultrafiltration (10 kDa MWCO) into EDTA conjugation buffer (pH 7.0). The

sample was then buffer exchanged into ammonium acetate (pH 6.9) *via* ultrafiltration (10 kDa MWCO). The final trastuzumab conjugates were deglycosylated and characterised by LC-MS. The sample was then analysed by UV-Vis spectroscopy.
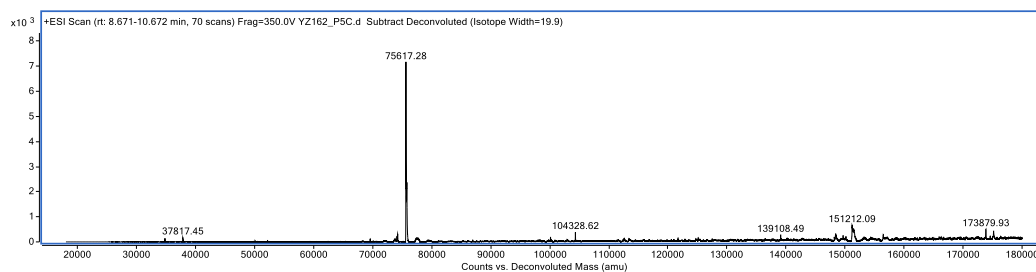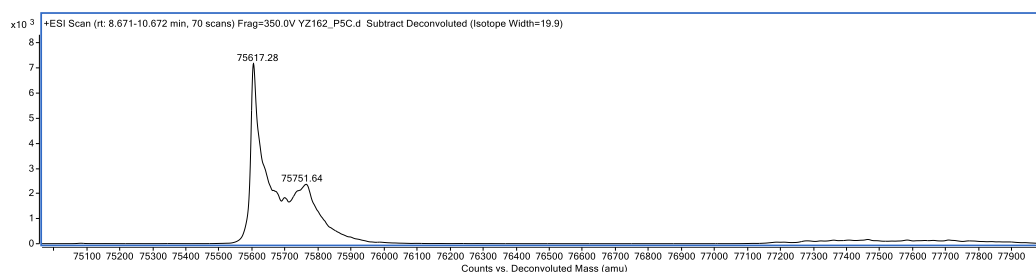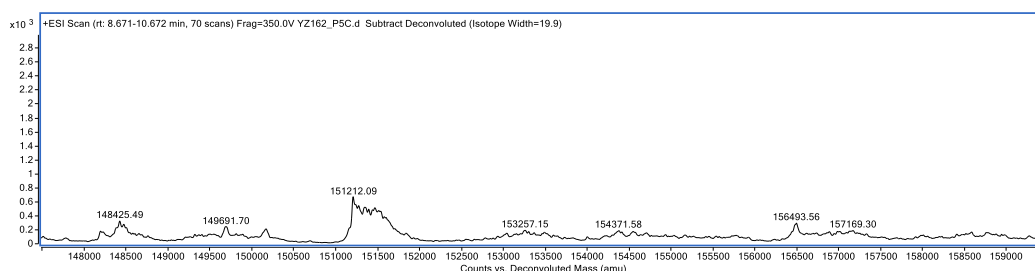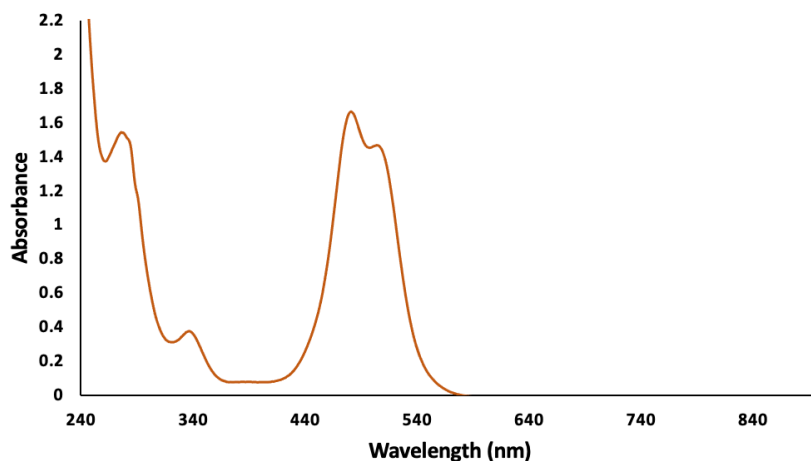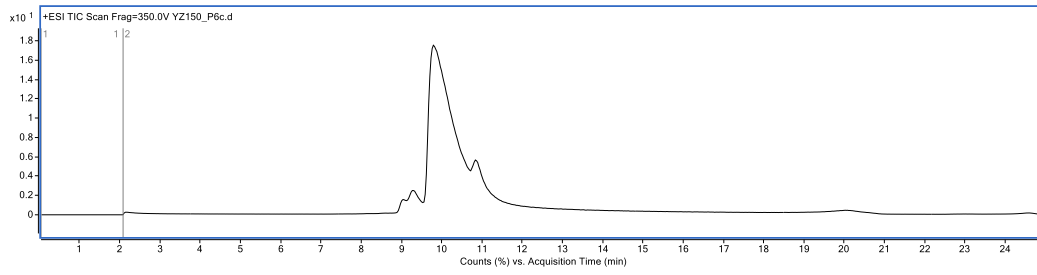
a.

b.

c.

d.

e.

Figure S21 – LC-MS and UV analysis of trastuzumab Ab-DBM-AF488 conjugate **27** (Method A): a. TIC, b. non-deconvoluted ion-series, c. deconvoluted ion series mass spectrum: HL expected 75610 Da, observed 75617 Da, HHLL expected 151217 Da, observed 151212 Da, d. zoomed in deconvoluted ion series mass spectrum, e. UV-Vis absorbance spectrum.
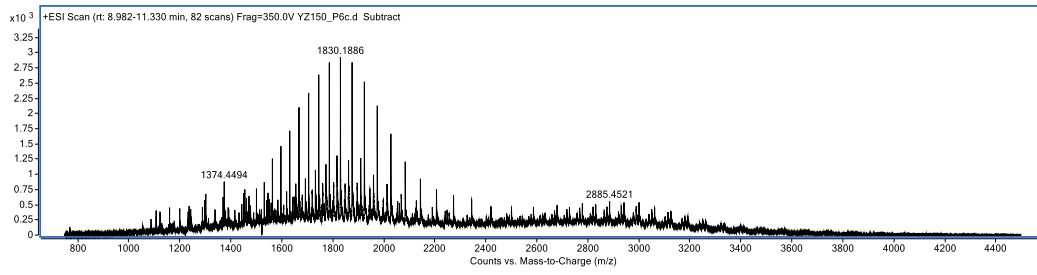
Preparation of trastuzumab Ab-DBM-AF488 conjugate (28)

To trastuzumab Ab-DBM conjugate **25** (100 µL, 0.002 µmol, 20 µM, 2.90 mg/mL) in PB (pH 7.0) was added AF488 (4.0 µL, 0.040 µmol, 10 mM solution in anhydrous DMF, 20 eq.). The resultant mixture was incubated for 4 h at 22 °C. The excess reagent was then removed *via* PD column and ultrafiltration (10 kDa MWCO) into EDTA conjugation buffer (pH 7.0). The sample was then buffer exchanged into ammonium acetate (pH 6.9) *via* ultrafiltration (10 kDa MWCO). The final trastuzumab conjugates were deglycosylated and characterised by LC-MS. The sample was then analysed by UV-Vis spectroscopy.
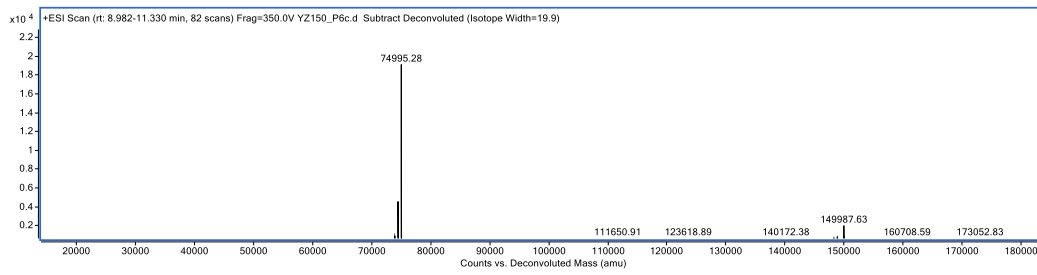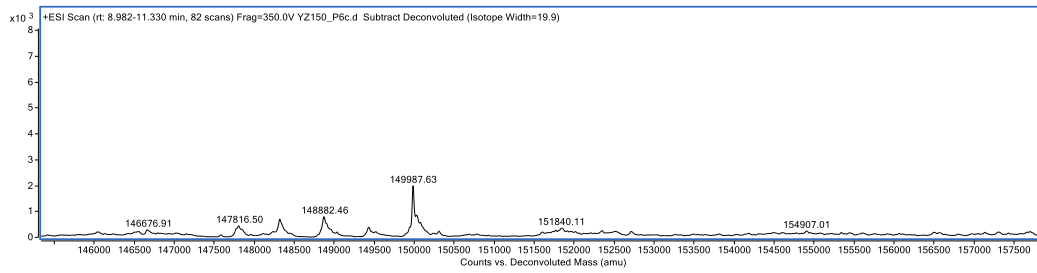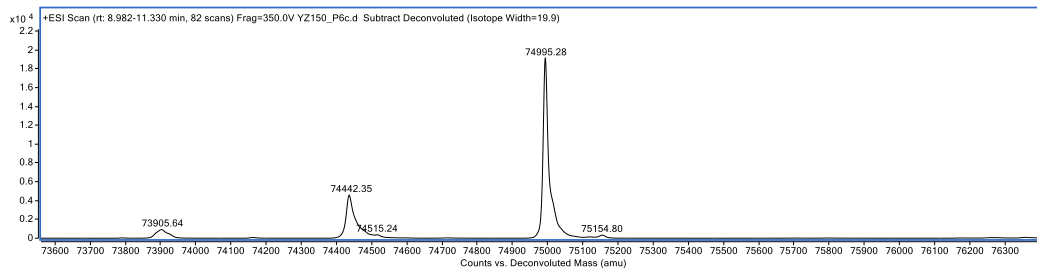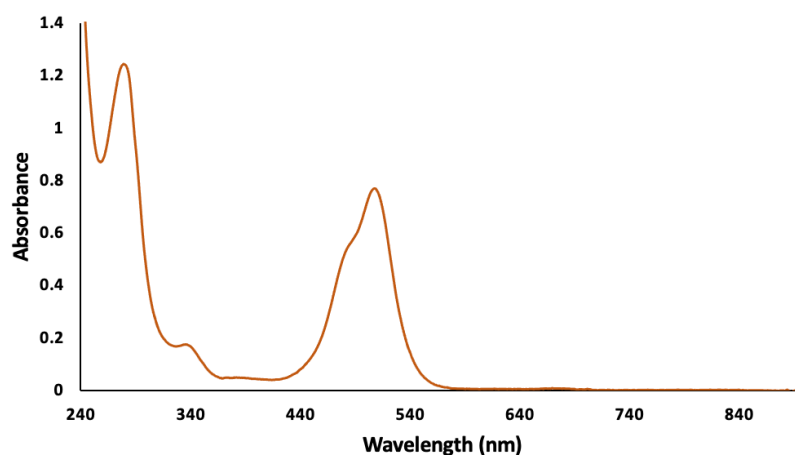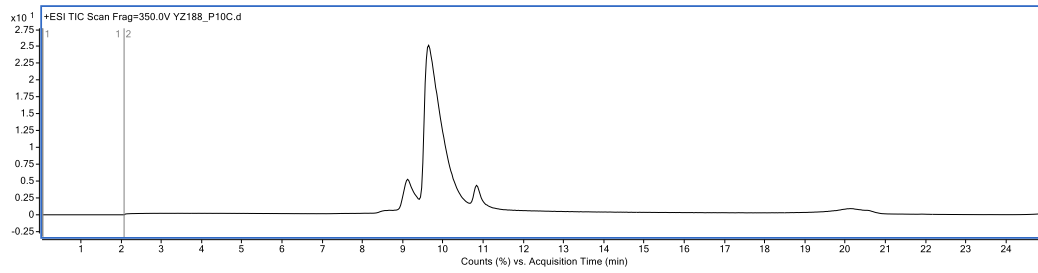
a.

b.

c.

d.

e.

Figure S22 – LC-MS and UV analysis of trastuzumab Ab-DBM-AF488 conjugate **28** (Method A): a. TIC, b. non-deconvoluted ion-series, c. deconvoluted ion series mass spectrum: HL expected 75000 Da, observed 74995 Da, HHLL expected 149997 Da, observed 149988 Da, HL observed 74442 Da, HHLL observed 148882 Da (possible oxidised strained alkyne), d. zoomed in deconvoluted ion series mass spectrum, e. UV-Vis absorbance spectrum.
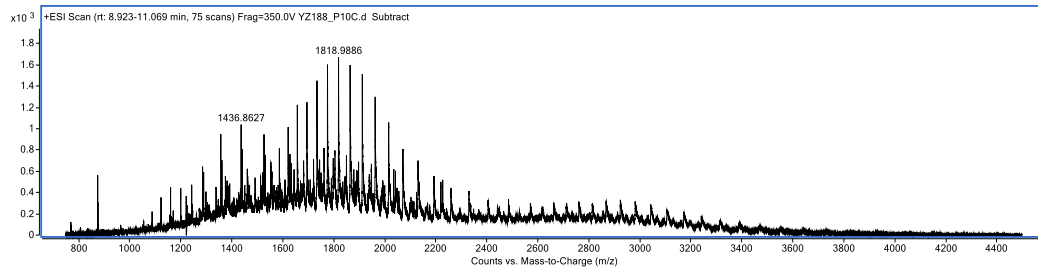
Preparation of trastuzumab Ab-DBM-AF488 conjugate (29)

To trastuzumab Ab-DBM conjugate **24** (100 µL, 0.002 µmol, 20 µM, 2.90 mg/mL) in PB (pH 7.0) was added THPTA ligand (3.6 µL, 0.360 µmol, 100 mM solution in dH$_2$O, 180 eq.), followed by CuSO$_4$ (3.6 µL, 0.072 µmol, 20 mM solution in dH$_2$O, 36 eq.). To this mixture was added AF488 (4.0 µL, 0.040 µmol, 10 mM solution in anhydrous DMF, 20 eq.), followed by sodium ascorbate (12.4 µL, 1.240 µmol, 100 mM solution in dH$_2$O, final concentration 10 mM). The resultant mixture was incubated for 4 h at 22 °C. The excess reagent was then removed *via* PD column and ultrafiltration (10 kDa MWCO) into EDTA conjugation buffer (pH 7.0). The sample was then buffer exchanged into ammonium acetate (pH 6.9) *via* ultrafiltration (10 kDa MWCO). The final trastuzumab conjugates were deglycosylated and characterised by LC-MS. The sample was then analysed by UV-Vis spectroscopy.
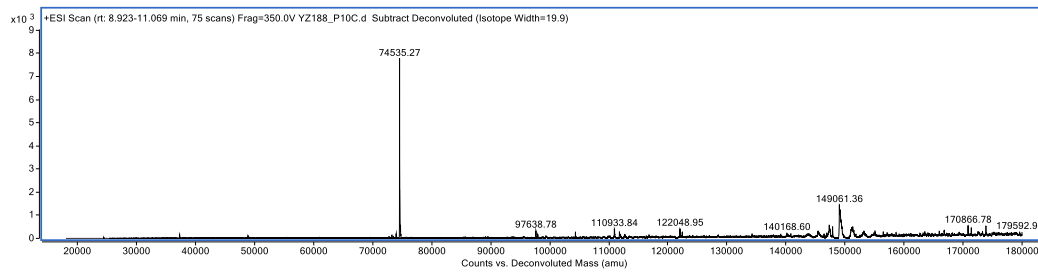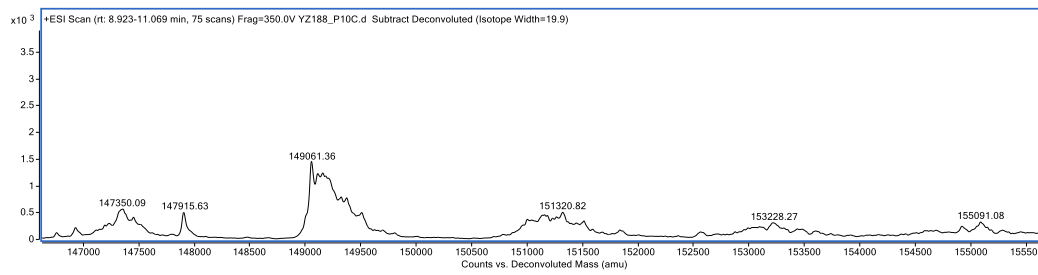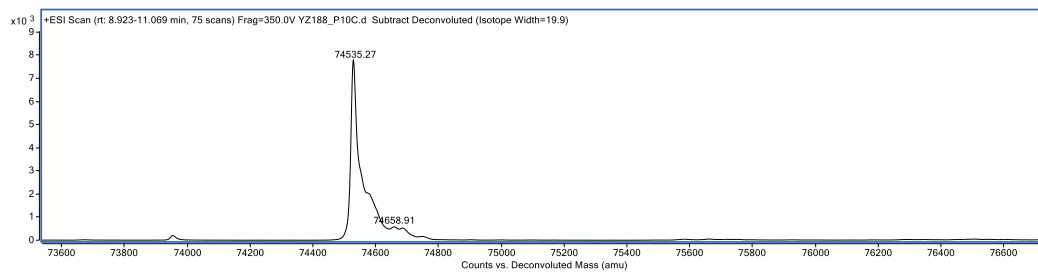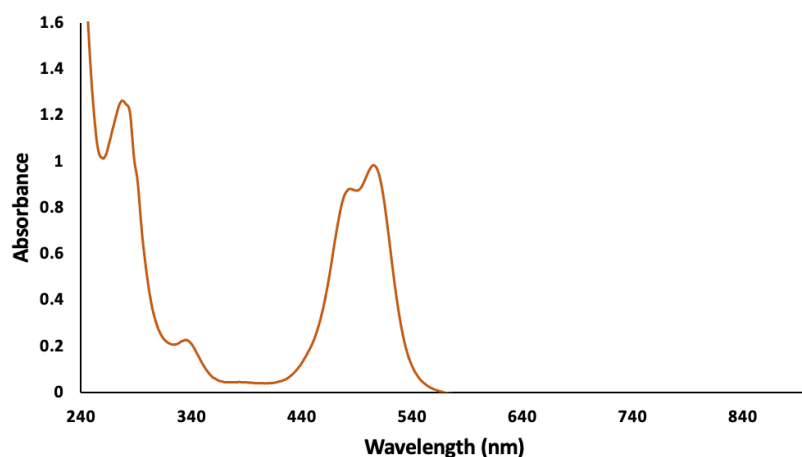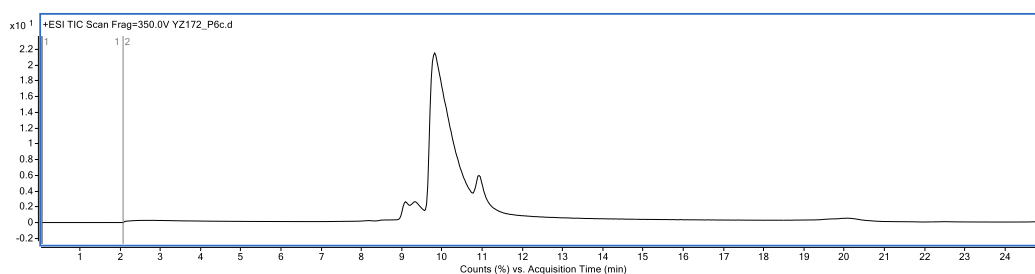
a.

b.

c.

d.

e.

Figure S23 – LC-MS and UV analysis of trastuzumab Ab-DBM-AF488 conjugate **29** (Method A): a. TIC, b. non-deconvoluted ion-series, c. deconvoluted ion series mass spectrum: HL expected 74534 Da, observed 74535 Da, HHLL expected 149065 Da, observed 149061 Da, d. zoomed in deconvoluted ion series mass spectrum, e. UV-Vis absorbance spectrum.
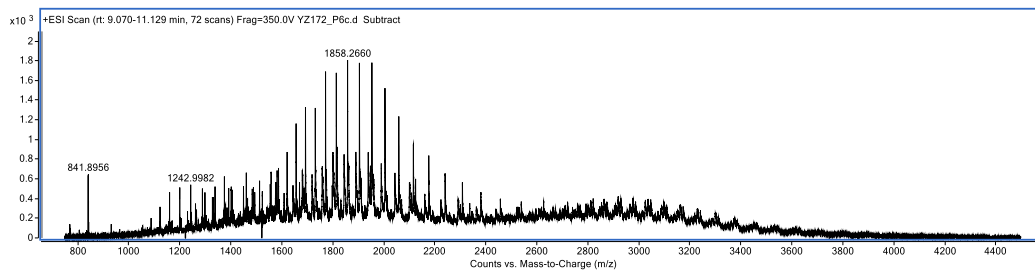
Preparation of trastuzumab Ab-DBM-AF488-AF488 conjugate (30)

To trastuzumab Ab-DBM-AF488 conjugate **29** (60 µL, 0.002 µmol, 20 µM, 2.90 mg/mL) in PB (pH 7.0) was added THPTA ligand (2.2 µL, 0.220 µmol, 100 mM solution in dH$_2$O, 180 eq.), followed by CuSO$_4$ (2.2 µL, 0.044 µmol, 20 mM solution in dH$_2$O, 36 eq.). To this mixture was added AF488 (2.4 µL, 0.024 µmol, 10 mM solution in anhydrous DMF, 20 eq.), followed by sodium ascorbate (7.4 µL, 0.740 µmol, 100 mM solution in dH$_2$O, final concentration 10 mM). The resultant mixture was incubated for 16 h at 22 °C. The excess reagent was then removed *via* PD column and ultrafiltration (10 kDa MWCO) into EDTA conjugation buffer (pH 7.0). The sample was then buffer exchanged into ammonium acetate (pH 6.9) *via* ultrafiltration (10 kDa MWCO). The final trastuzumab conjugates were deglycosylated and characterised by LC-MS. The sample was then analysed by UV-Vis spectroscopy.
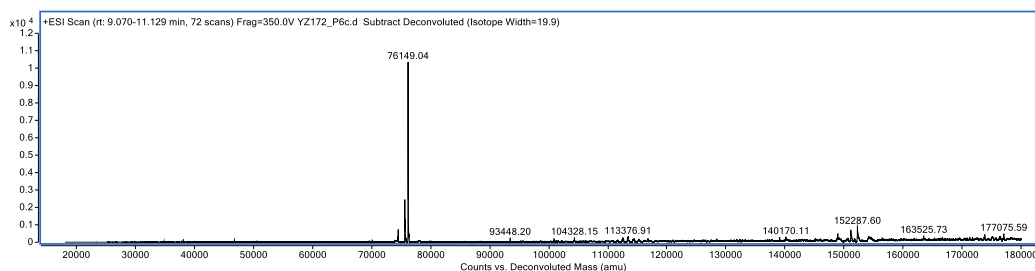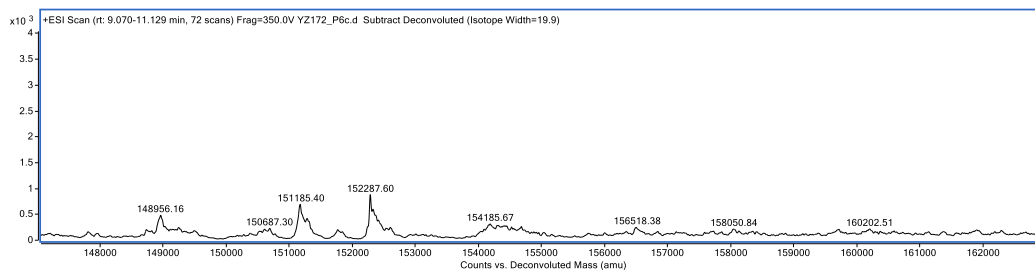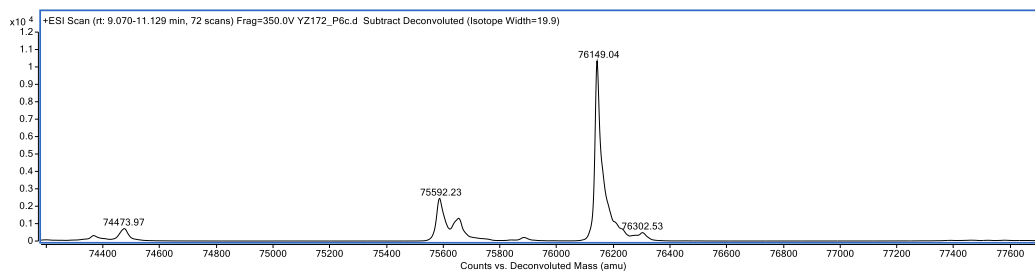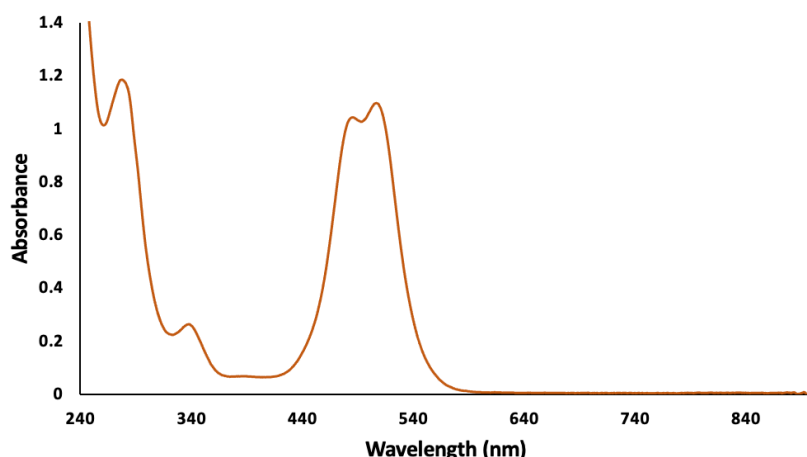
a.

b.

c.

d.

e.

Figure S24 – LC-MS and UV analysis of trastuzumab Ab-DBM-AF488-AF488 conjugate **30** (Method A): a. TIC, b. non-deconvoluted ion-series, c. deconvoluted ion series mass spectrum: HL expected 76149 Da, observed 76149 Da, HHLL expected 152294 Da, observed 152288 Da, HL observed 75592 Da, HHLL observed 151185 Da (incomplete modification with AF488 as inefficient CuAAC and increased steric hinderance), d. zoomed in deconvoluted ion series mass spectrum, e. UV-Vis absorbance spectrum.

Preparation of trastuzumab Ab-DBM-Biotin conjugate (31)

To trastuzumab Ab-DBM conjugate **26** (100 µL, 0.002 µmol, 20 µM, 2.90 mg/mL) in PB (pH 7.0) was added TCO-Biotin (2.0 µL, 0.040 µmol, 20 mM solution in anhydrous DMF, 20 eq.). The resultant mixture was incubated for 4 h at 22 °C. The excess reagent was then removed *via* PD column and ultrafiltration (10 kDa MWCO) into EDTA conjugation buffer (pH 7.0). The sample was then buffer exchanged into ammonium acetate (pH 6.9) *via* ultrafiltration (10 kDa MWCO). The final trastuzumab conjugates were deglycosylated and characterised by LC-MS.

a.

b.

c.

d.

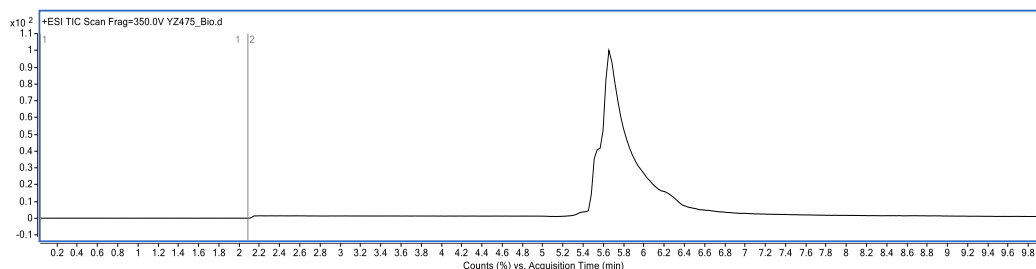**Figure S25** – LC-MS analysis of trastuzumab Ab-DBM-Biotin conjugate **31** (Method B): a. TIC, b. non-deconvoluted ion-series, c. deconvoluted ion series mass spectrum: HL expected 74988 Da, observed 74979 Da, HHLL expected 149973Da, observed 149956 Da, LC observed 23440 Da, 2*LC observed 46877 Da, 3*LC observed 70318 Da (SDS-PAGE showed <10% LC species), d. zoomed in deconvoluted ion series mass spectrum.
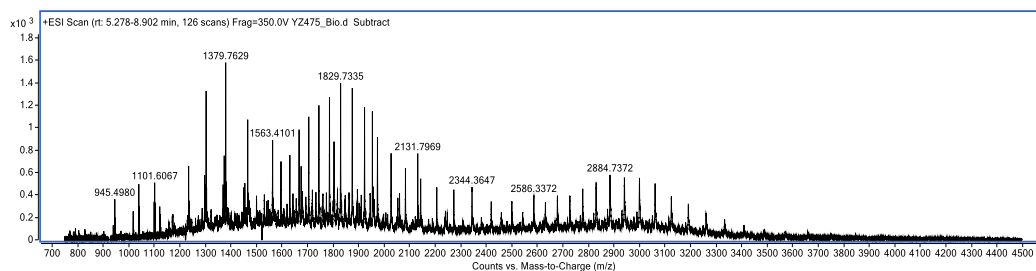
Preparation of trastuzumab Ab-DBM-Biotin-Fluor conjugate (32)

To trastuzumab Ab-DBM-Biotin conjugate **26** (60 μL, 0.002 μmol, 20 μM, 2.90 mg/mL) in PB (pH 7.0) was added BCN-Fluor (1.2 μL, 0.024 μmol, 20 mM solution in anhydrous DMF, 20 eq.). The resultant mixture was incubated for 16 h at 22 °C. The excess reagent was then removed *via* PD column and ultrafiltration (10 kDa MWCO) into EDTA conjugation buffer (pH 7.0). The sample was then buffer exchanged into ammonium acetate (pH 6.9) *via* ultrafiltration (10 kDa MWCO). The final trastuzumab conjugates were deglycosylated and characterised by LC-MS. The sample was then analysed by UV-Vis spectroscopy.
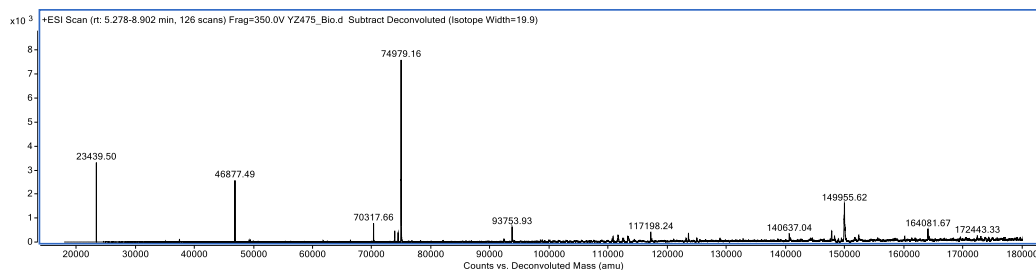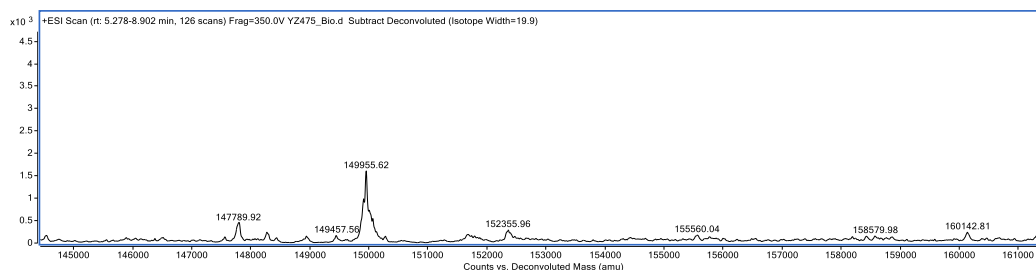
a.

b.

c.

d.

e.

Figure S26 – LC-MS and UV analysis of trastuzumab Ab-DBM-Biotin-Fluor conjugate **32** (Method B): a. TIC, b. non-deconvoluted ion-series, c. deconvoluted ion series mass spectrum: HL expected 76441 Da, observed 76414 Da, HHLL expected 152879 Da, observed 152818 Da, HL observed 74607 Da, HHLL observed 151043 Da (showed < 5% negligible amounts of unidentified species), d. zoomed in deconvoluted ion series mass spectrum, e. UV-Vis absorbance spectrum.

Preparation of trastuzumab Ab-DBM-DFO conjugate (33)

To trastuzumab (100 µL, 0.0023 µmol, 23 µM) in BBS buffer (pH 6.0) was added TCEP.HCl (1.84 µL, 0.0184 µmol, 10mM solution in H_2O, 8 eq.). After 2 h at 37 °C, DBM-DFO (2.30-9.20 µL, 0.023-0.092 µmol, 10 mM solution in anhydrous DMSO, 10-40 eq.) was added and the

resultant mixture was incubated for 1h at 22 °C. The excess reagents were then removed *via* ultrafiltration (10 kDa MWCO) into BBS buffer (pH 8.5). The concentration was determined by UV-Vis absorbance and adjusted to 20 μM. The resultant solution was incubated for 16 h at 37 °C. The sample was then buffer exchanged into ammonium acetate (pH 6.9) *via* ultrafiltration (10 kDa MWCO). The final trastuzumab conjugates were deglycosylated and characterised by LC-MS.
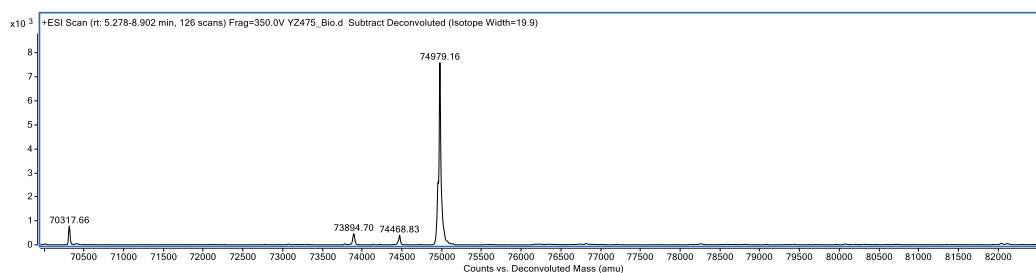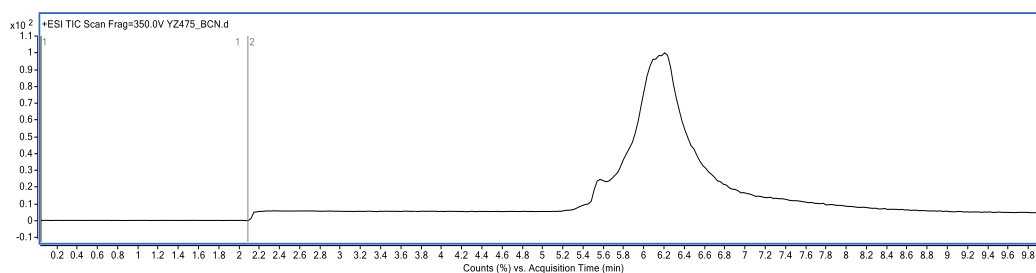
i)10 eq. of DBM-DFO

a.
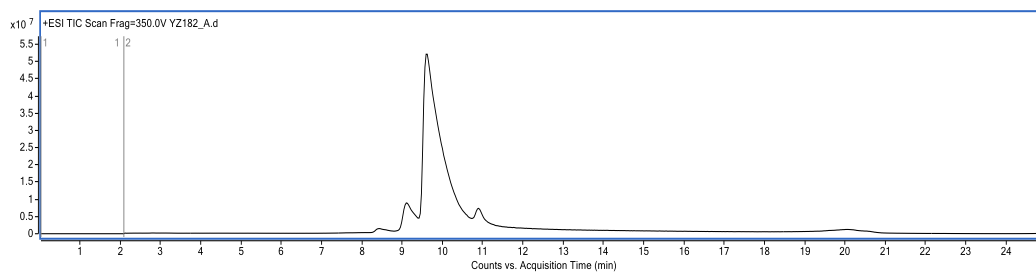
b.
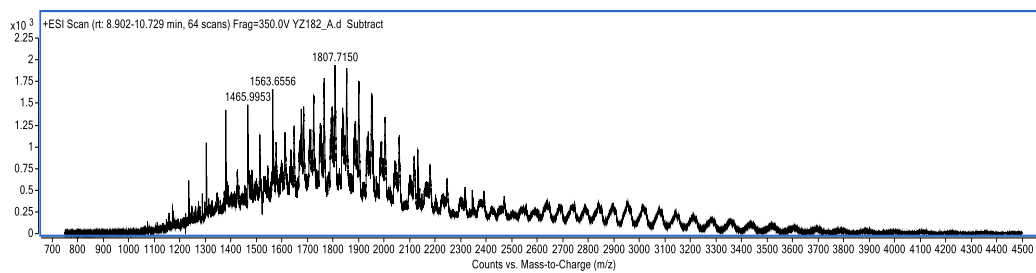
c.

d.

Figure S27 – LC-MS analysis of trastuzumab Ab-DBM-DFO conjugate **33** (Method A): a. TIC, b. non-deconvoluted ion-series, c. deconvoluted ion series mass spectrum: HL expected 74021 Da, observed 74066 Da and 74103 Da (adducts on DFO moiety), HHLL expected 148039 Da, observed 148194 Da (adducts on DFO moiety), d. zoomed in deconvoluted ion series mass spectrum.

ii) 20 eq. of DBM-DFO
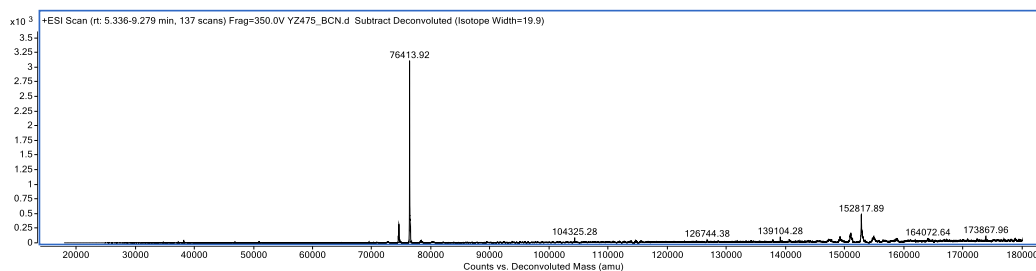
a.

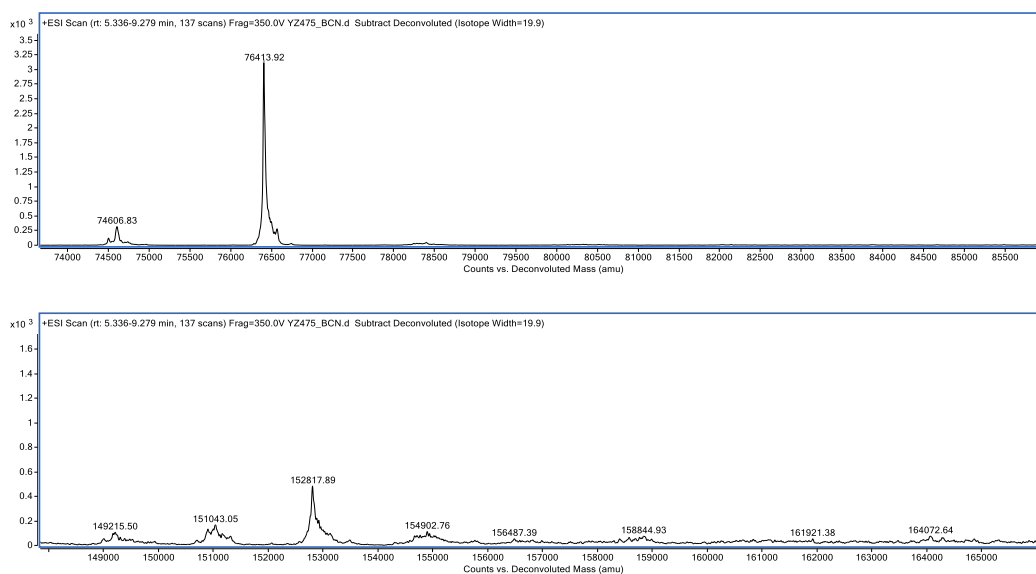b.

c.
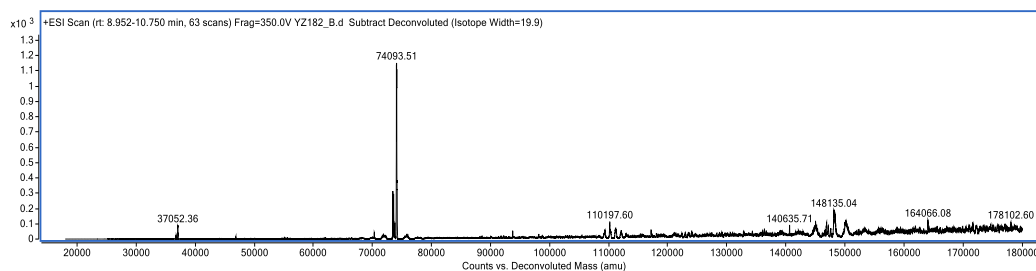
d.

Figure S28 – LC-MS analysis of trastuzumab Ab-DBM-DFO conjugate **33** (Method A): a. TIC, b. non-deconvoluted ion-series, c. deconvoluted ion series mass spectrum: HL expected 74021 Da, observed 74094 Da (adducts on DFO moiety), HHLL expected 148039 Da, observed 148135 Da (adducts on DFO moiety), d. zoomed in deconvoluted ion series mass spectrum.

iii)30 eq. of DBM-DFO

a.

b.

c.
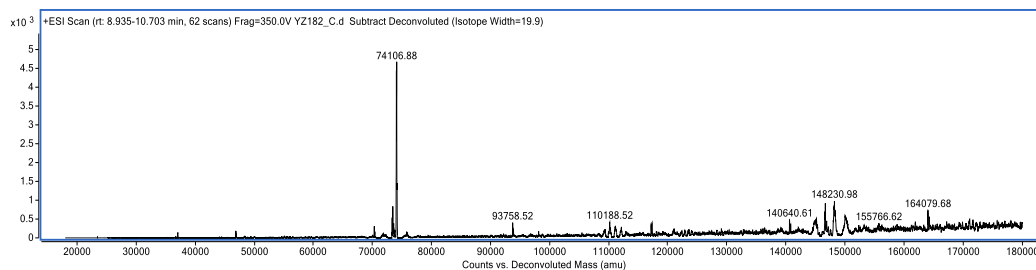
d.
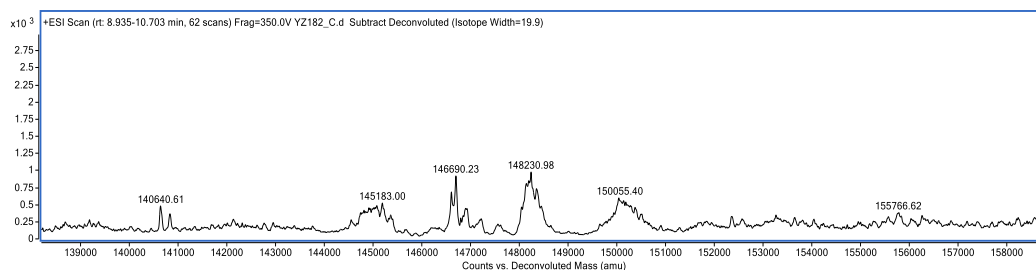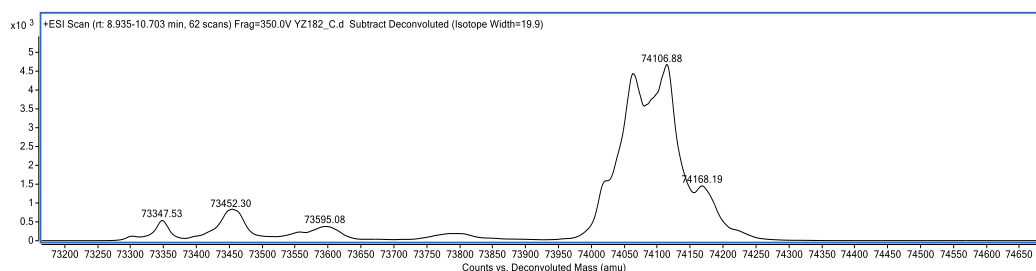
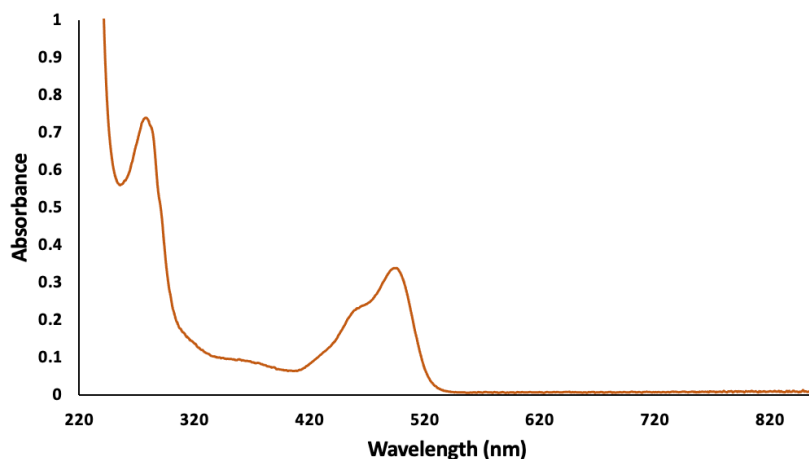**Figure S29** – LC-MS analysis of trastuzumab Ab-DBM-DFO conjugate **33** (Method A): a. TIC, b. non-deconvoluted ion-series, c. deconvoluted ion series mass spectrum: HL expected 74021 Da, observed 74107 Da (adducts on DFO moiety), HHLL expected 148039 Da, observed 148231 Da (adducts on DFO moiety), d. zoomed in deconvoluted ion series mass spectrum.

iv)40 eq. of DBM-DFO

a.
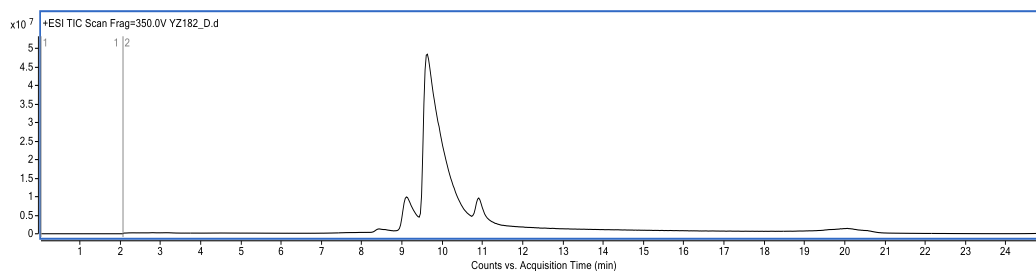
Figure S30 – LC-MS analysis of trastuzumab Ab-DBM-DFO conjugate **33** (Method A): a. TIC,

b. non-deconvoluted ion-series, c. deconvoluted ion series mass spectrum: HL expected

74021 Da, observed 74065 Da and 74110 Da (adducts on DFO moiety), HHLL expected 148039 Da, observed 148224 Da (adducts on DFO moiety), d. zoomed in deconvoluted ion series mass spectrum.

Preparation of trastuzumab Ab-DBM-BCN conjugate (36)

To trastuzumab (100 µL, 0.0023 µmol, 23 µM) in BBS buffer (pH 8.5) was added TCEP.HCl (1.84 µL, 0.0184 µmol, 10mM solution in H_2O, 8 eq.). After 2 h at 37 °C, NGM-BCN (3.45 µL, 0.0345 µmol, 10 mM solution in anhydrous DMF, 15 eq.) was added and the resultant mixture was incubated for 1h at 22 °C. The excess reagents were then removed *via* ultrafiltration (10 kDa MWCO) into BBS buffer (pH 8.5). The concentration was determined by UV-Vis absorbance and adjusted to 20 µM. The resultant solution was incubated for 16 h at 37 °C. The sample was then buffer exchanged into ammonium acetate (pH 6.9) *via* ultrafiltration (10 kDa MWCO). The final trastuzumab conjugates were deglycosylated and characterised by LC-MS.
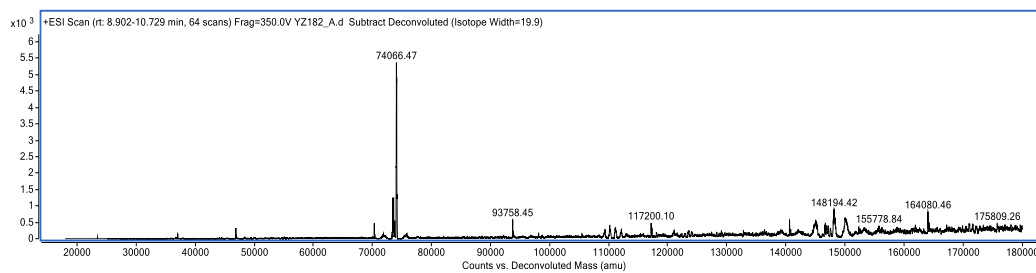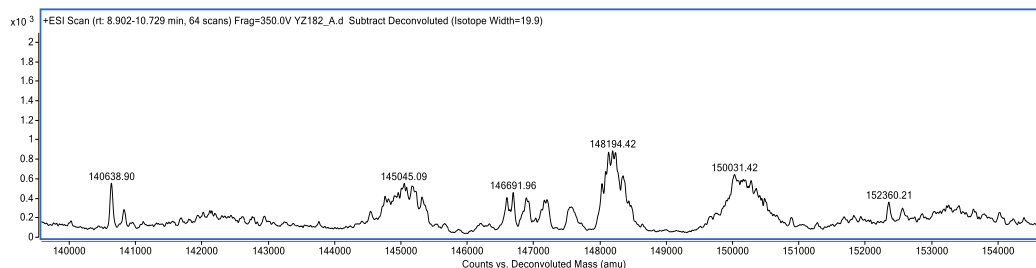
a.

b.
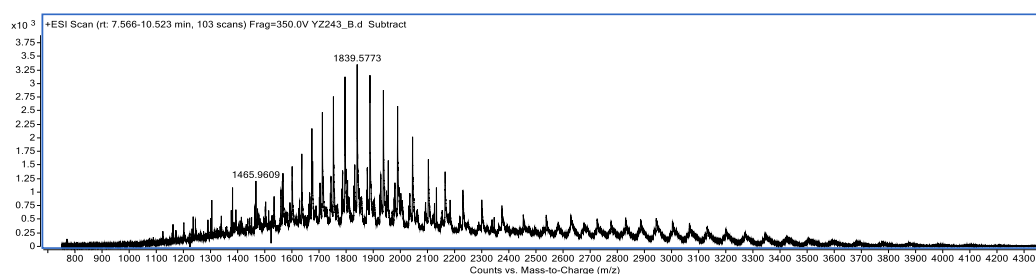
c.

d.

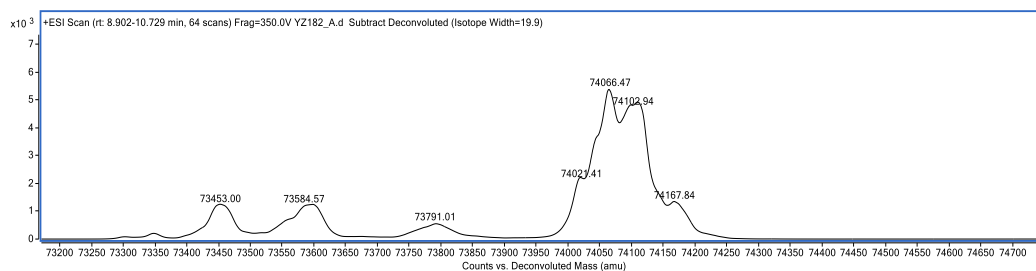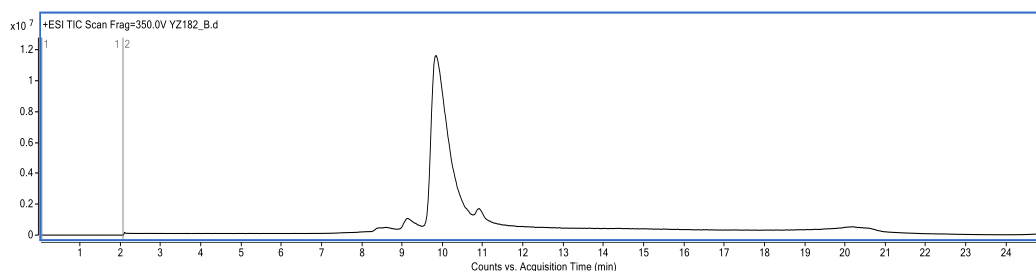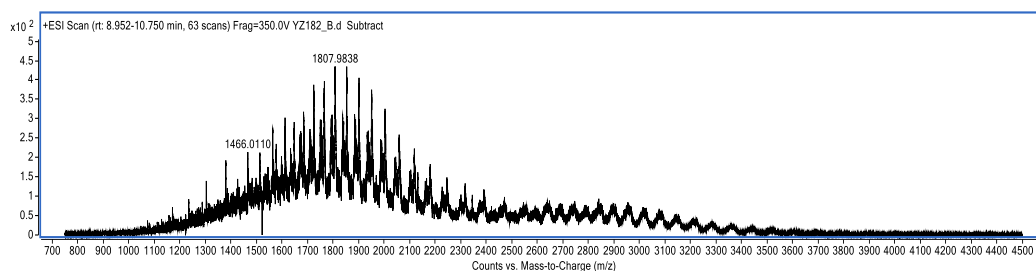**Figure S31** – LC-MS analysis of trastuzumab Ab-DBM-BCN conjugate **36** (Method A, 20 °C): a. TIC, b. non-deconvoluted ion-series, c. deconvoluted ion series mass spectrum: HL expected 73548 Da, observed 73172 Da (lost 371 Da), 73543 Da, HHLL expected 147095 Da, observed 147082 Da, d. zoomed in deconvoluted ion series mass spectrum.

Preparation of trastuzumab Ab-DBM-BCN-DFO conjugate (37)

To trastuzumab-NGM conjugate **36** (100 µL, 0.002 µmol, 20 µM) in PB (pH 7.0) was added DFO-azide (4 µL, 0.040 µmol, 10 mM solution in DMF, 20 eq.) and the resultant mixture was incubated for 16 h at 37 °C. The excess reagent was then removed *via* ultrafiltration (10 kDa MWCO) into EDTA conjugation buffer (pH 7.0). The sample was then buffer exchanged into ammonium acetate (pH 6.9) *via* ultrafiltration (10 kDa MWCO). The final trastuzumab conjugates were deglycosylated and characterised by LC-MS.

a.

b.
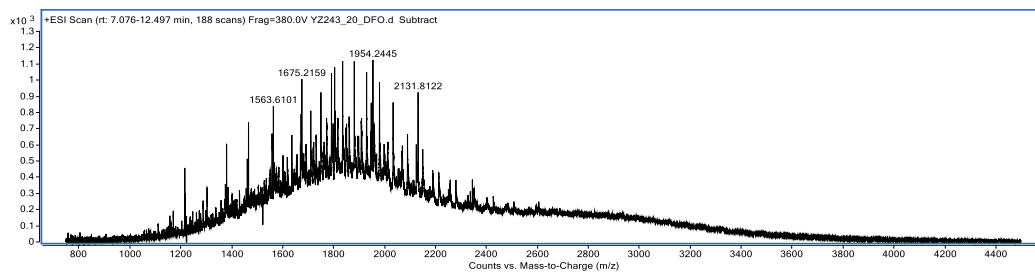
c.

d.

Figure S32 – LC-MS analysis of trastuzumab Ab-DBM-BCN-DFO conjugate **37** (Method A, 20 °C): a. TIC, b. non-deconvoluted ion-series, c. deconvoluted ion series mass spectrum: HL

expected 75215 Da, observed 70317 Da (LC*3), 74440 Da (lost 771 Da), 75211 Da, HHLL

expected 150429 Da, observed 148798 Da (lost 1627 Da), 150425 Da, d. zoomed in
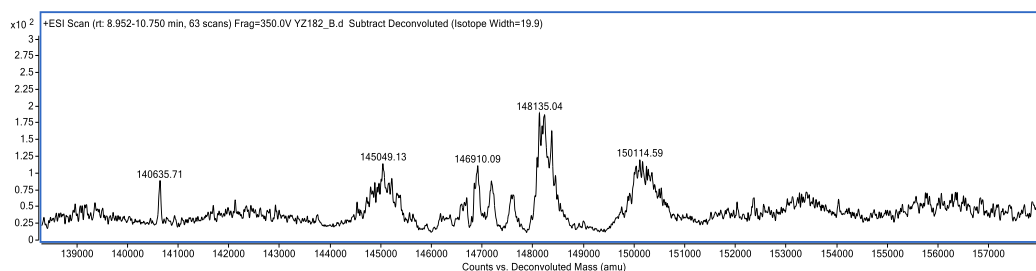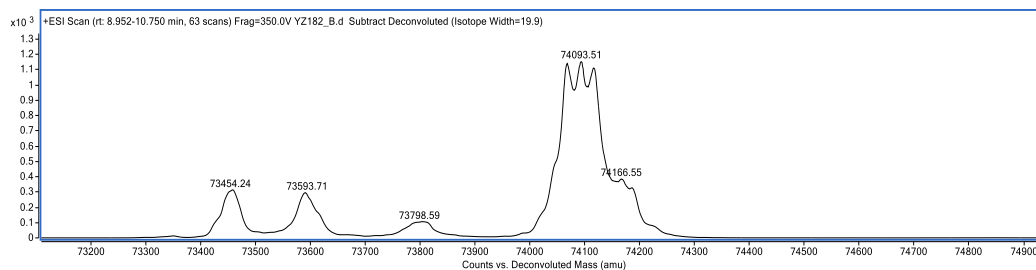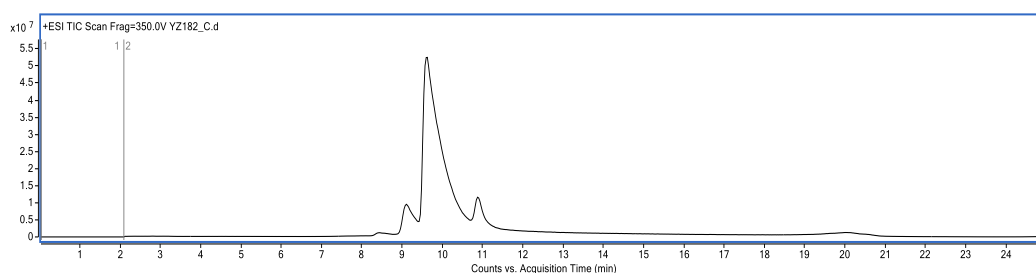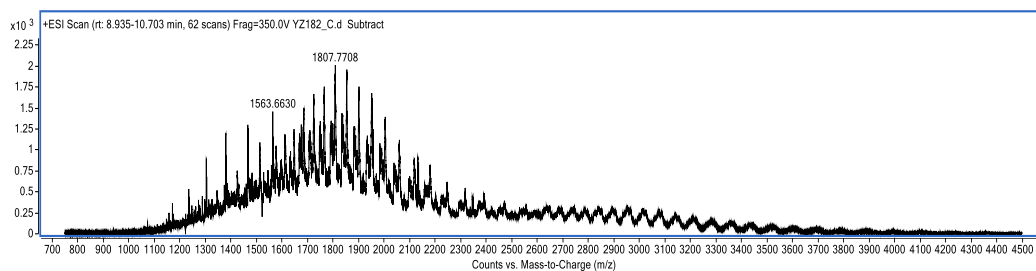
deconvoluted ion series mass spectrum.

Preparation of trastuzumab Ab-PD-BCN conjugate (38)

To trastuzumab (100 µL, 0.0023 µmol, 23 µM) in BBS buffer (pH 8.5) was added diBr Mepstra

(2.30 µL, 0.0460 µmol, 20mM solution in DMSO, 20 eq.) and TCEP.HCl (2.76 µL, 0.0276 µmol,

10mM solution in H_2O, 12 eq.). The resultant mixture was incubated for 16 h at 4 °C. The

sample was then buffer exchanged into ammonium acetate (pH 6.9) *via* ultrafiltration (10 kDa

MWCO). The final trastuzumab conjugates were deglycosylated and characterised by LC-MS.

a.

b.
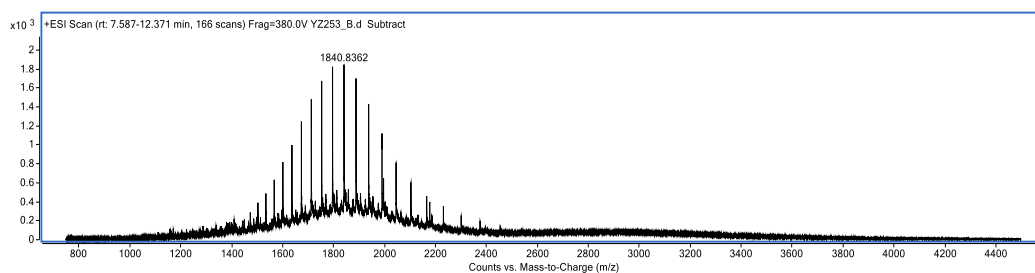
c.

d.

Figure S33 – LC-MS analysis of trastuzumab Ab-PD-BCN conjugate **38** (Method A, 20 °C): a. TIC, b. non-deconvoluted ion-series, c. deconvoluted ion series mass spectrum: HL expected 73598 Da, observed 73593 Da, HHLL expected 147195 Da, observed 147183 Da, d. zoomed in deconvoluted ion series mass spectrum.

Preparation of trastuzumab Ab-PD-BCN-DFO conjugate (39)

To trastuzumab-NGM conjugate **38** (100 μL, 0.002 μmol, 20 μM) in PB (pH 7.0) was added DFO-Azide (4 μL, 0.040 μmol, 10 mM solution in DMF, 20 eq.) and the resultant mixture was incubated for 16 h at 37 °C. The excess reagent was then removed *via* ultrafiltration (10 kDa MWCO) into EDTA conjugation buffer (pH 7.0). The sample was then buffer exchanged into ammonium acetate (pH 6.9) *via* ultrafiltration (10 kDa MWCO). The final trastuzumab conjugates were deglycosylated and characterised by LC-MS.
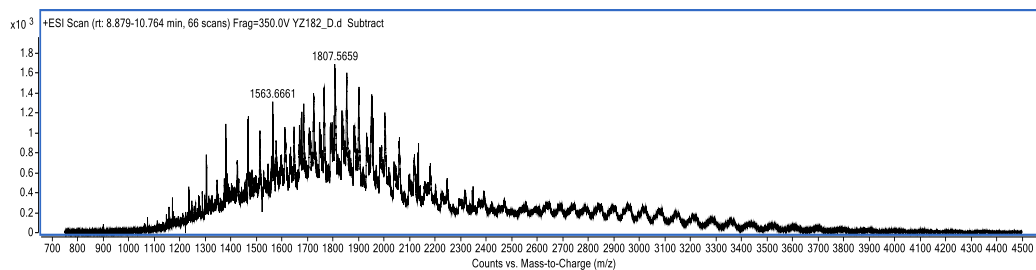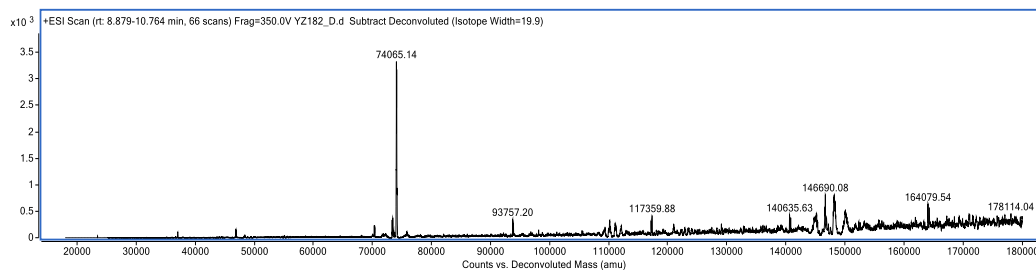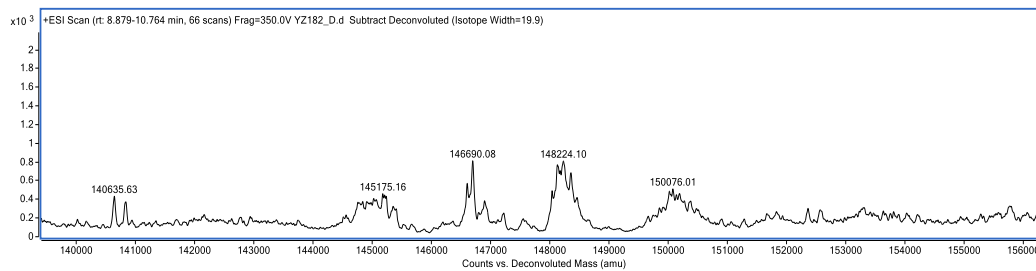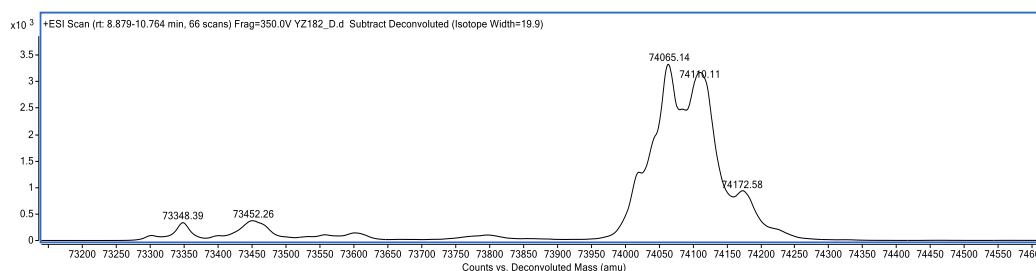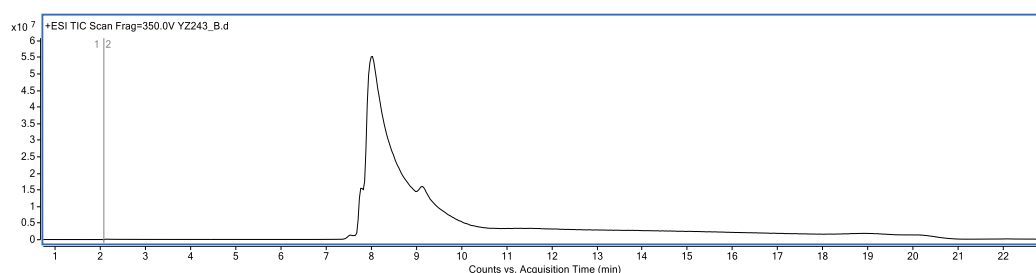
a.

b.
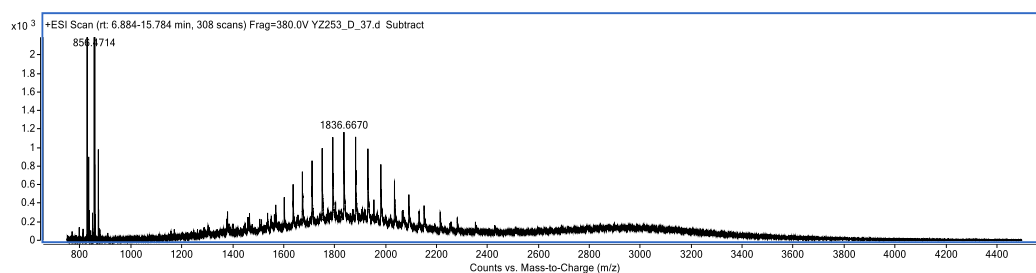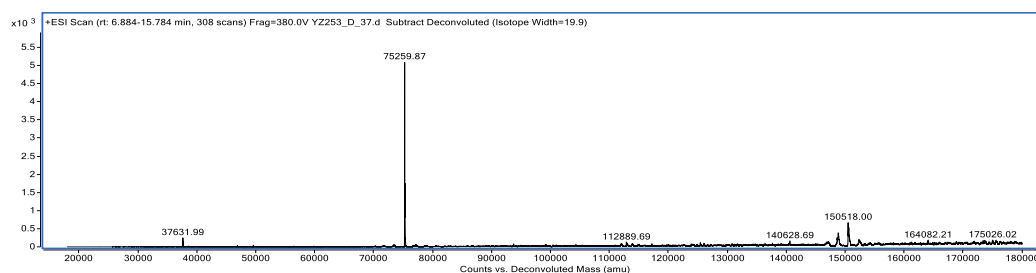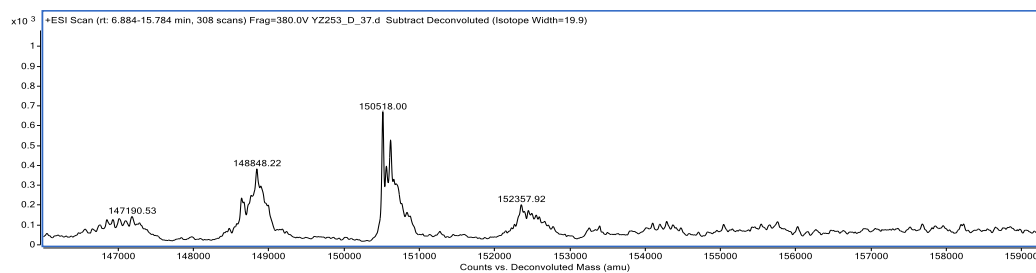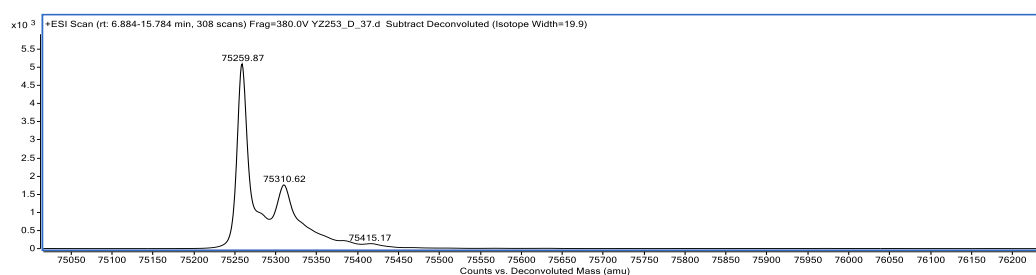
Figure S34 – LC-MS analysis of trastuzumab Ab-PD-BCN-DFO conjugate **39** (Method A, 20 °C): a. TIC, b. non-deconvoluted ion-series, c. deconvoluted ion series mass spectrum: HL expected 75265 Da, observed 75260 Da, HHLL expected 150529 Da, observed 150518 Da, d. zoomed in deconvoluted ion series mass spectrum.

## Preparation of trastuzumab Ab-DBM conjugate (65)

To trastuzumab (100 μL, 0.002 μmol, 20 μM) in BBS (pH 7.4) was added dithiophenolmaleimide **64** (8 μL, 0.080 μmol, 10 mM solution in DMF, 40 eq.), diselenide **55**

(0.2 µL, 0.002 µmol, 10 mM solution in DMF, 1 eq.), and TCEP.HCl (4 µL, 0.040 µmol, 10 mM solution in DMF, 20 eq.), the resultant mixture was incubated for 1 h at 22 °C. The excess reagents were then removed *via* ultrafiltration (10 kDa MWCO) into BBS buffer (pH 8.5). The concentration was determined by UV-Vis absorbance and adjusted to 20.0 µM. The resultant solution was incubated for 16 h at 37 °C. The sample was then buffer exchanged into ammonium acetate (pH 6.9) *via* ultrafiltration (10 kDa MWCO). The final trastuzumab conjugates were deglycosylated and characterised by LC-MS.
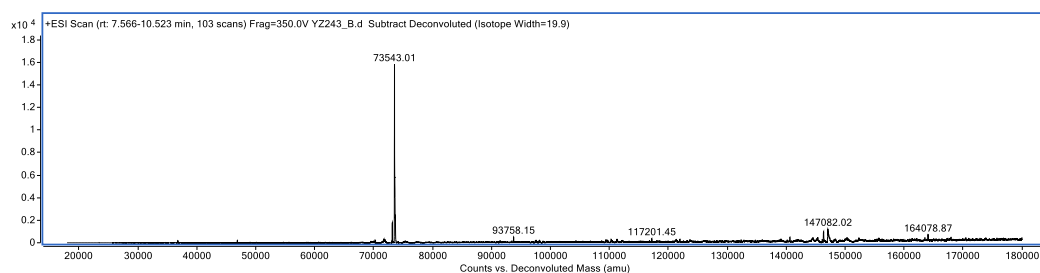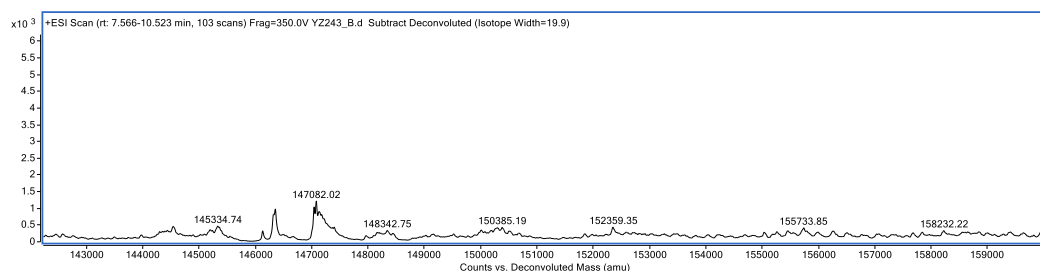
a.
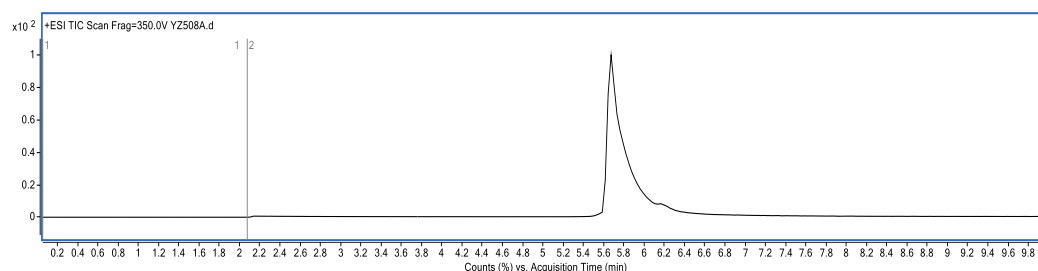
b.
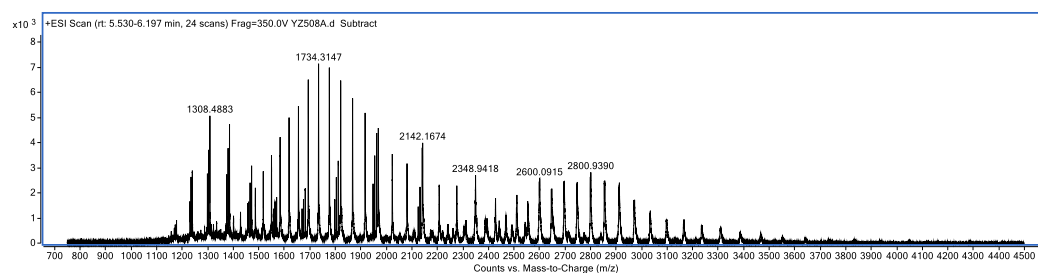
c.
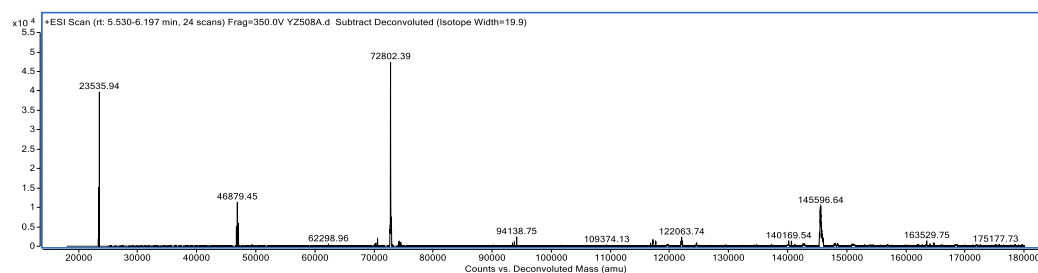
d.
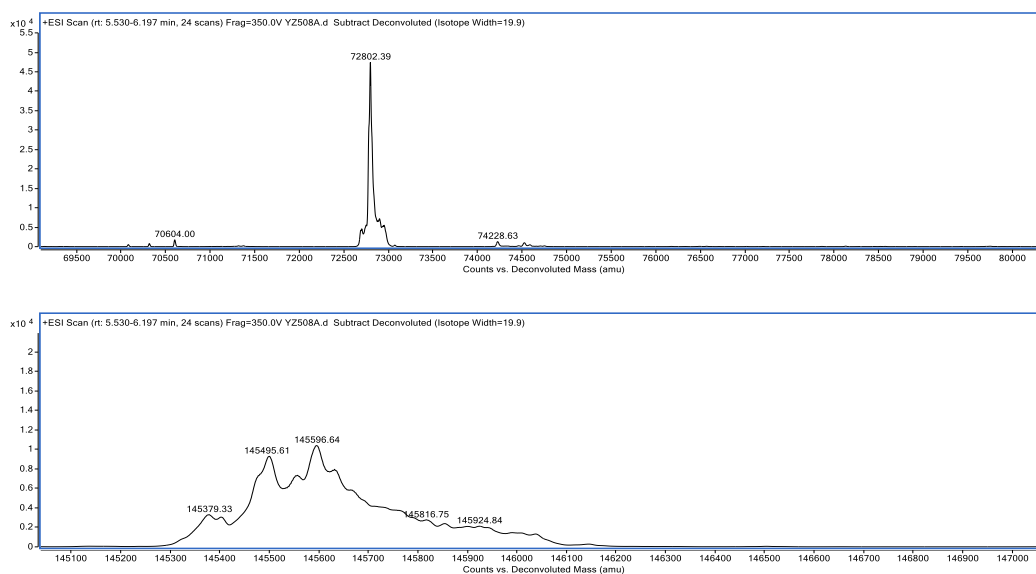
Figure S35 – LC-MS analysis of trastuzumab Ab-PD-BCN-DFO conjugate **65** (Method B): a. TIC, b. non-deconvoluted ion-series, c. deconvoluted ion series mass spectrum: HL expected 72781 Da, observed 72802 Da, HHLL expected 145559 Da, observed 145496 Da and 145597 Da, d. zoomed in deconvoluted ion series mass spectrum.

Preparation of trastuzumab Ab-DBM-Biotin-Fluor conjugate (66)

To trastuzumab Ab (50 µL, 0.005 µmol, 50 µM, 7.25 mg/mL) in BBS (pH 7.4) was added premixed diaminodiselenides (1.0 µL, 0.020 µmol, 10 mM solution in anhydrous MeOH, 4 eq.) and TCEP.HCl (7.5 µL, 0.150 µmol, 10 mM solution in dH$_2$O, 30 eq.). The resultant mixture was incubated for 4 min at 22 °C. The excess reagent was then removed *via* ultrafiltration (10 kDa MWCO) into BBS buffer (pH 8.5). To the resultant mixture, DBM **12** (5.0 µL, 0.100 µmol, 10 mM solution in anhydrous DMF, 20 eq.) was added and then incubated for 5 min at 37 °C. The excess reagent was then removed *via* ultrafiltration (10 kDa MWCO) into PB (pH 7.0). To the conjugate, TCO-Biotin (2.5 µL, 0.100 µmol, 20 mM solution in anhydrous DMF, 20 eq.) was added and then incubated for 1 min at 37 °C. To the conjugate, BCN-Fluor (3.8 µL, 0.150 µmol, 20 mM solution in anhydrous DMF, 30 eq.) was added and then incubated for 10 min at 37 °C. The excess reagent was then removed *via* PD column and ultrafiltration (10 kDa MWCO) into EDTA conjugation buffer (pH 7.0). The sample was then buffer exchanged into ammonium acetate (pH 6.9) *via* ultrafiltration (10 kDa MWCO). The final trastuzumab conjugates were deglycosylated and characterised by LC-MS.
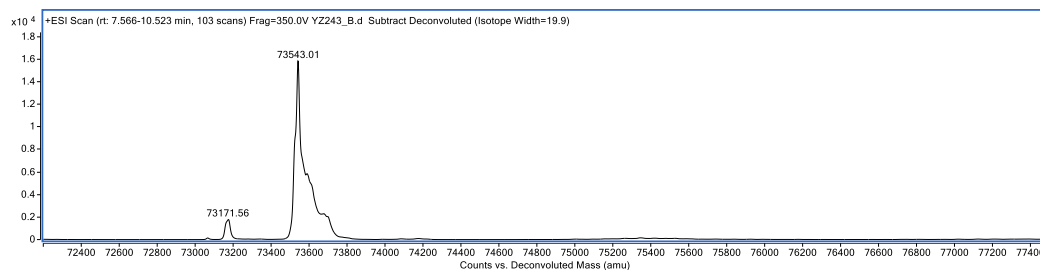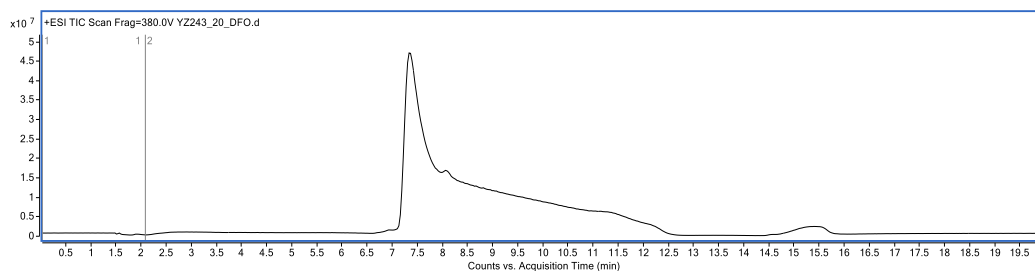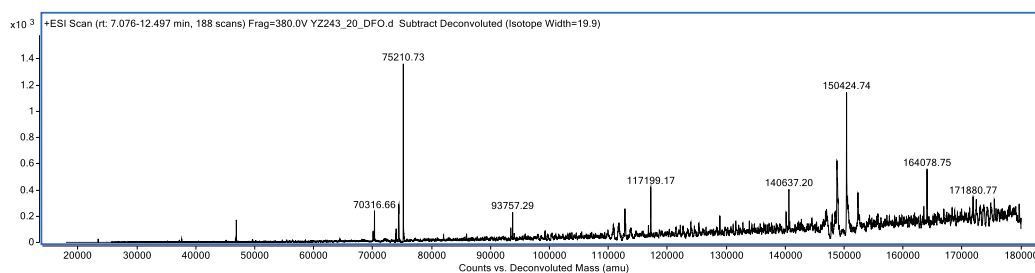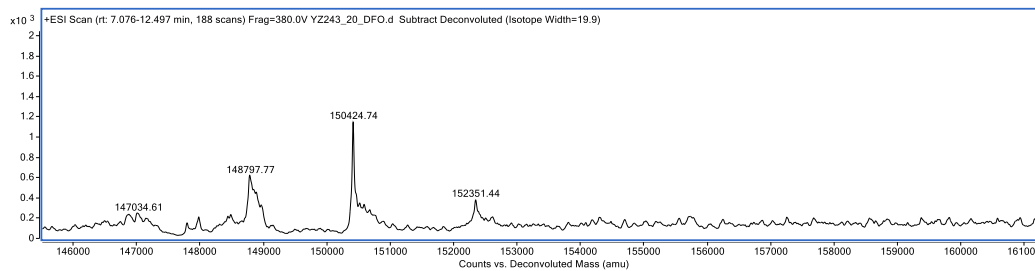
a.
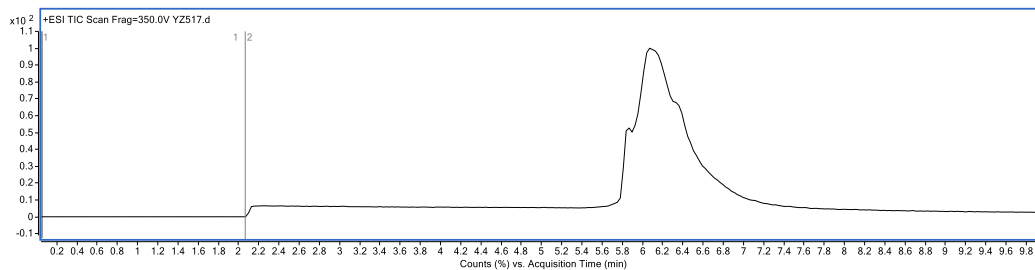
b.
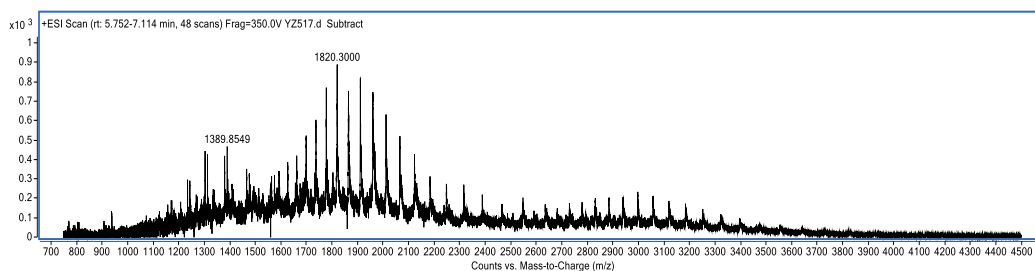
c.
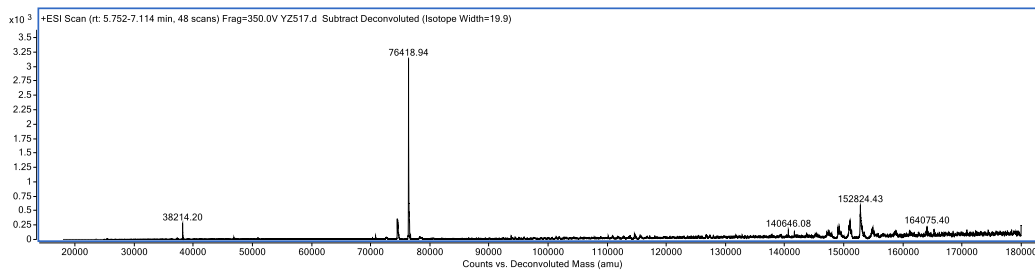
d.
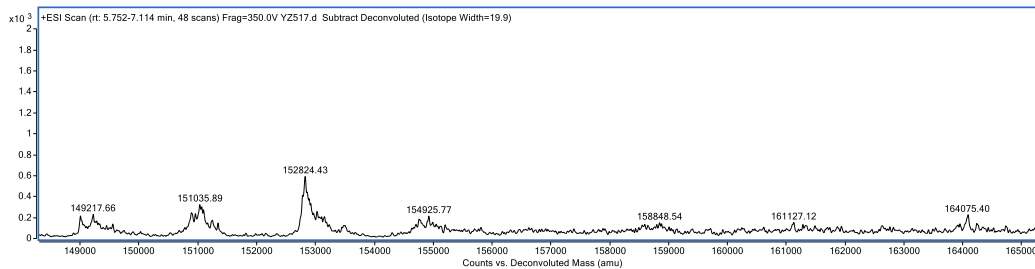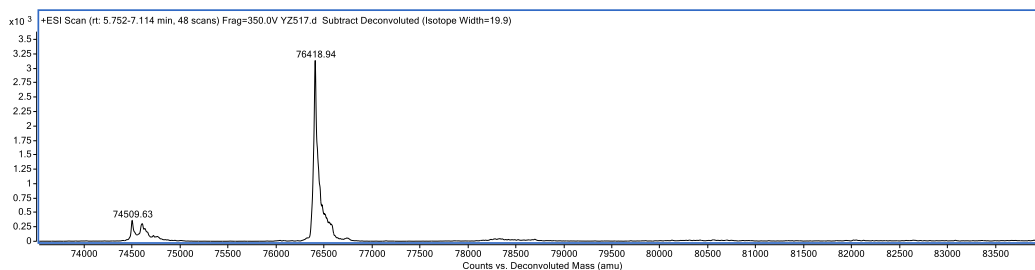
Figure S36 – LC-MS analysis of trastuzumab Ab-DBM-Biotin-Fluor conjugate **66** (Method B): a. TIC, b. non-deconvoluted ion-series, c. deconvoluted ion series mass spectrum: HL expected 76441 Da, observed 76419 Da, HHLL expected 152879 Da, observed 152824 Da, HL observed 74510 Da, HHLL observed 151036 Da (showed < 5% negligible amounts of unidentified species), d. zoomed in deconvoluted ion series mass spectrum.

Preparation of trastuzumab Ab-DBM conjugate (72)

To trastuzumab (100 µL, 0.002 µmol, 24 µM, 3.48 mg/mL) in BBS buffer (pH 8.5) was added TCEP.HCl (1.9 µL, 0.019 µmol, 10mM solution in dH$_2$O, 8 eq.). After 2 h at 37 °C, TCEP.HCl was removed and DBM **70** (2.4 µL, 0.024 µmol, 10 mM solution in anhydrous DMF, 10 eq.) was added and the resultant mixture was incubated for 1 h at 22 °C. The excess reagents were then removed *via* ultrafiltration (10 kDa MWCO) into BBS buffer (pH 8.5). The concentration was determined by UV-Vis absorbance and adjusted to 20.0 µM. The resultant solution was incubated for 16 h at 37 °C. The sample was then buffer exchanged into ammonium acetate (pH 6.9) *via* ultrafiltration (10 kDa MWCO). The final trastuzumab conjugates were deglycosylated and characterised by LC-MS.
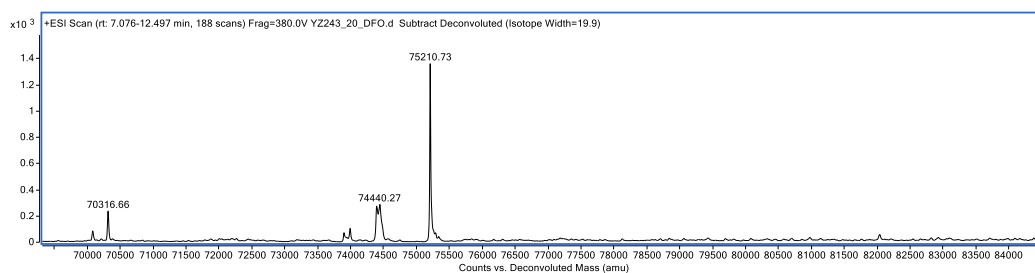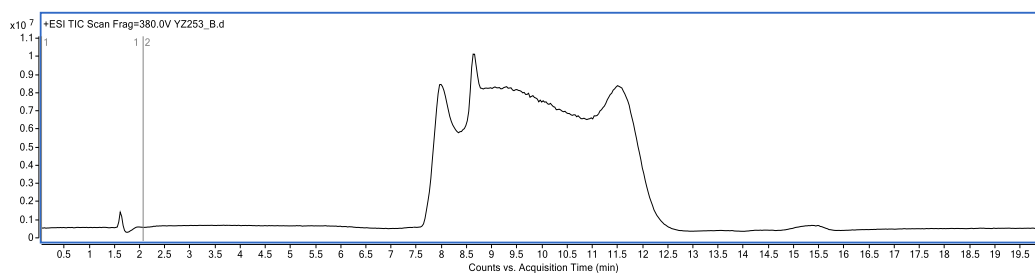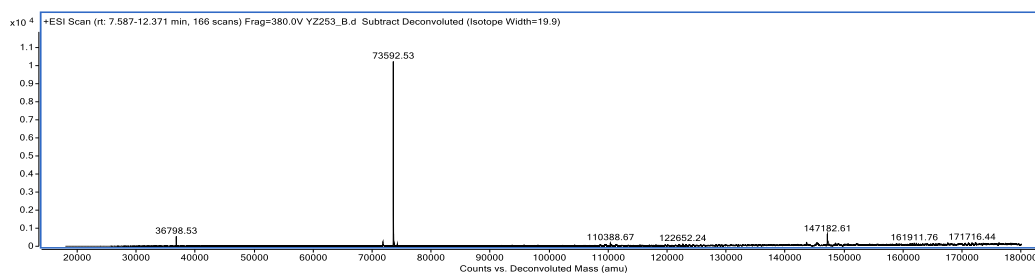
a.
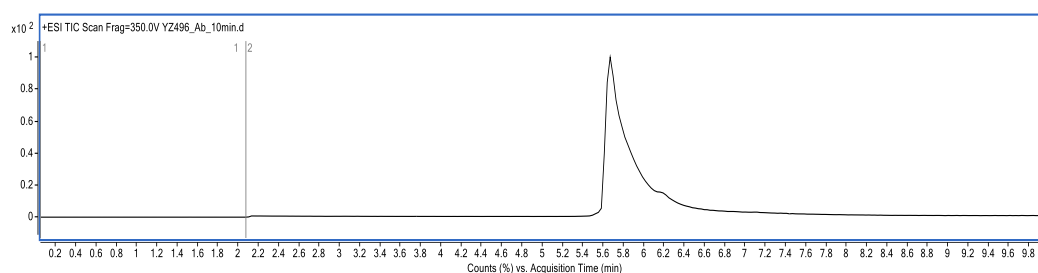
b.

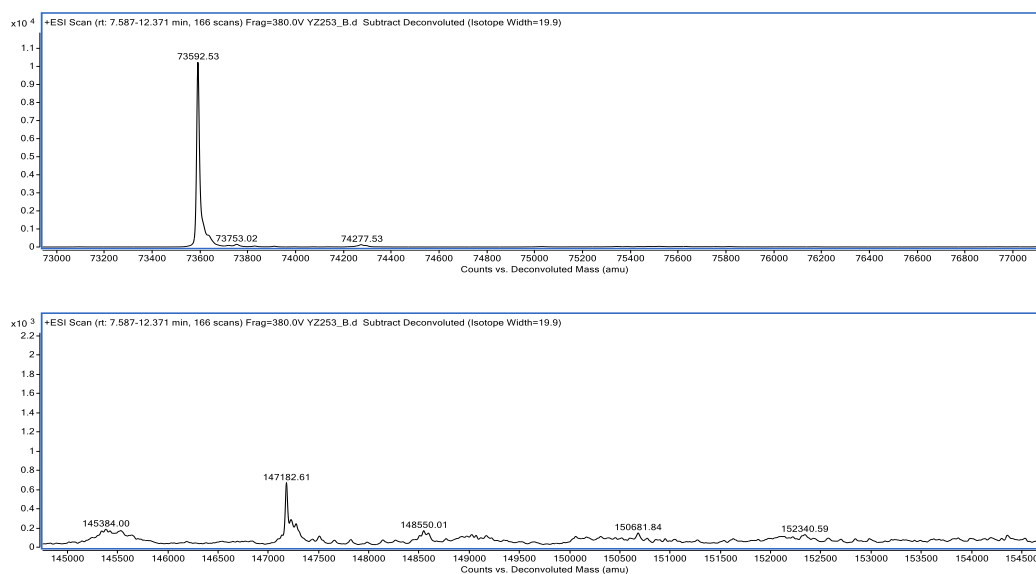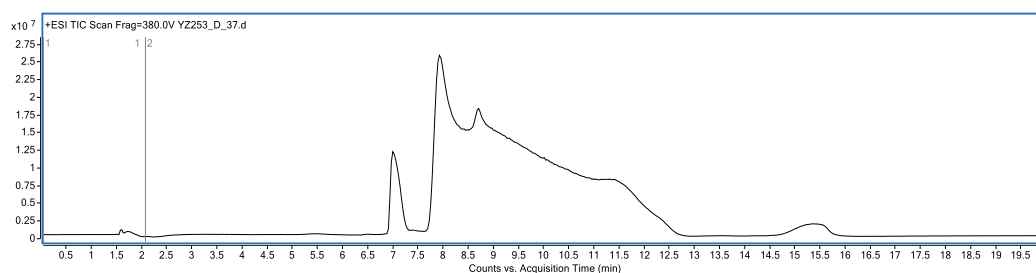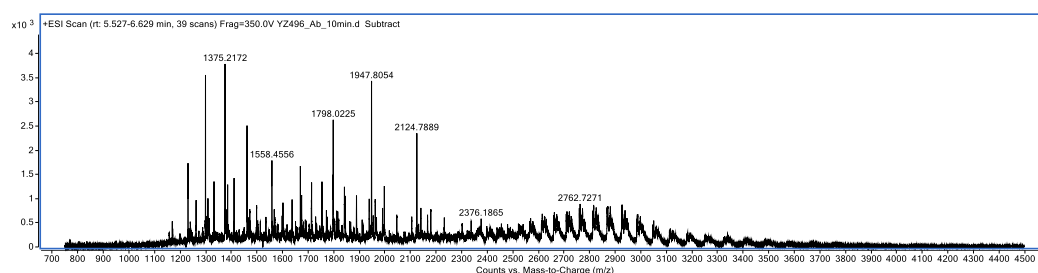c.
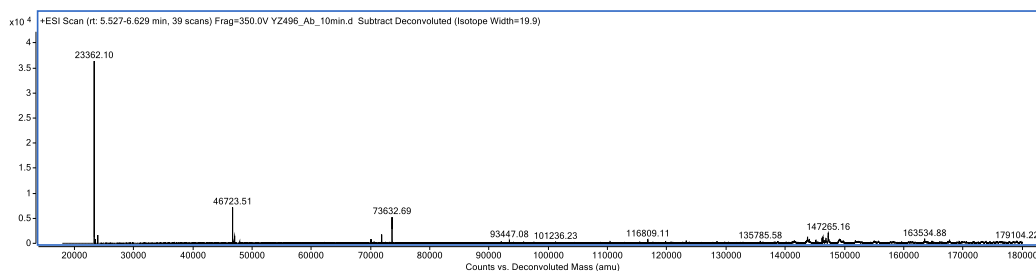
d.
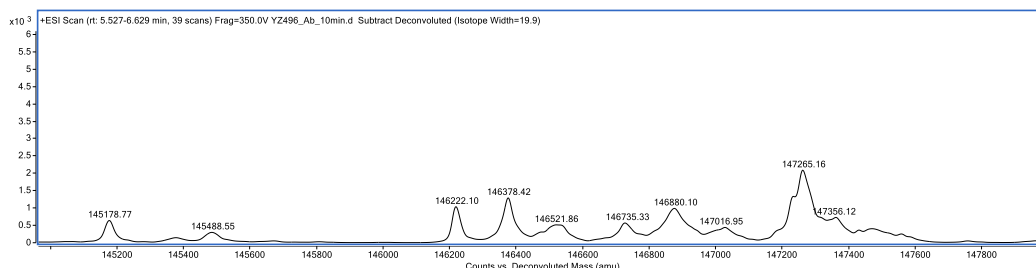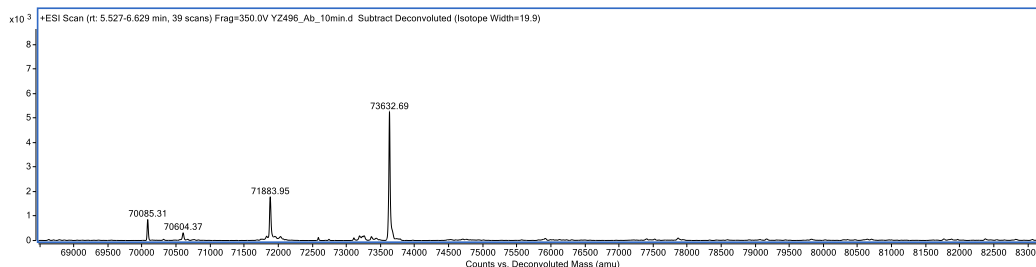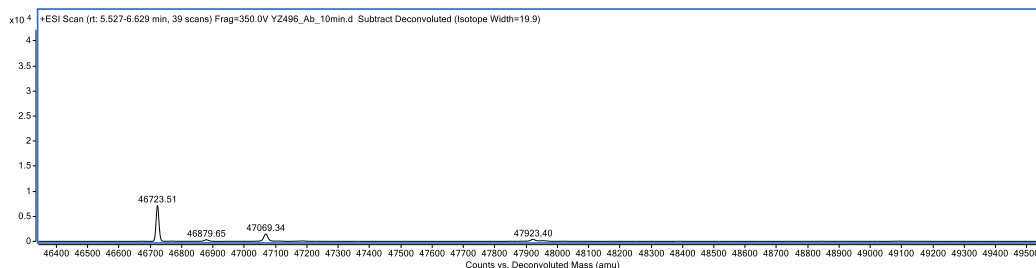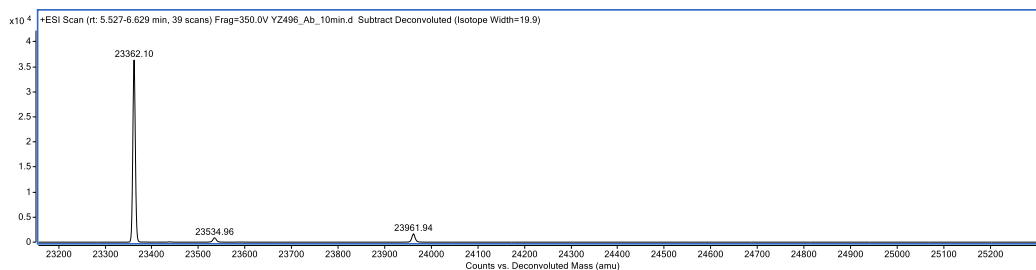
Figure S37 – LC-MS analysis of trastuzumab Ab-DBM-PEG-disulfide conjugate **72** (Method B): a. TIC, b. non-deconvoluted ion-series, c. deconvoluted ion series mass spectrum: HL expected 73113 Da, 73635 Da, observed 71884 Da, 73633 Da, HHLL expected 146223 Da, observed 145179 Da, 146222 Da, 146378 Da and 146880 Da, 147266 Da, d. zoomed in deconvoluted ion series mass spectrum.

5.6. NMR results of DTM-TCEP reactivity tests

Fresh TCEP.HCl stock (20 mM) was made by dissolving 5.8 mg TCEP.HCl in 1 mL BBS buffer (pH 8.5). DTM stock (20 mM) was made by dissolving 20 mmol of DTM in 1 mL CD$_3$CN. Each NMR sample was made by mixing 360 μL of BBS buffer and 240 μL of CD$_3$CN (buffer: CD$_3$CN = 3:2). Each NMR reaction was monitored at 0 h, 1 h, 2 h and 24 h whilst TCEP control was monitored at 0 h, 1 h, and 24 h by Bruker AMX400 (400 MHz).
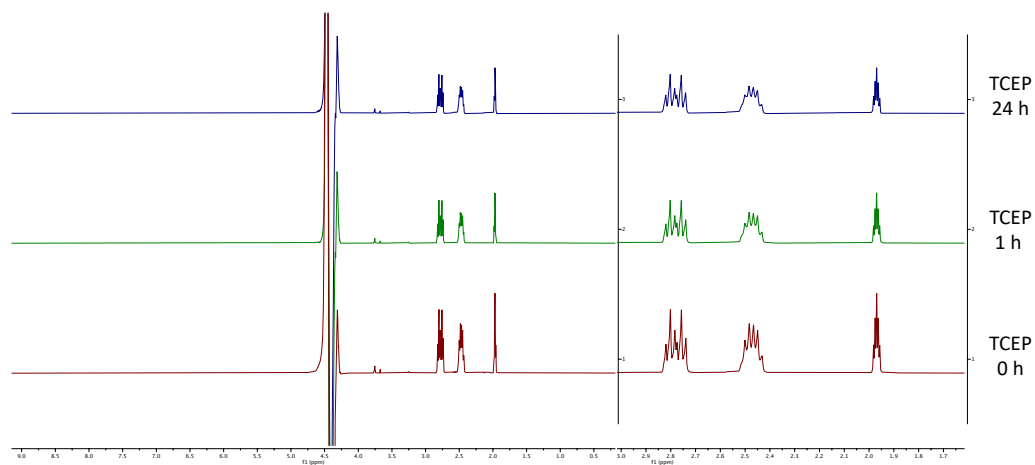
Figure S38 – NMR reactions of TCEP control.
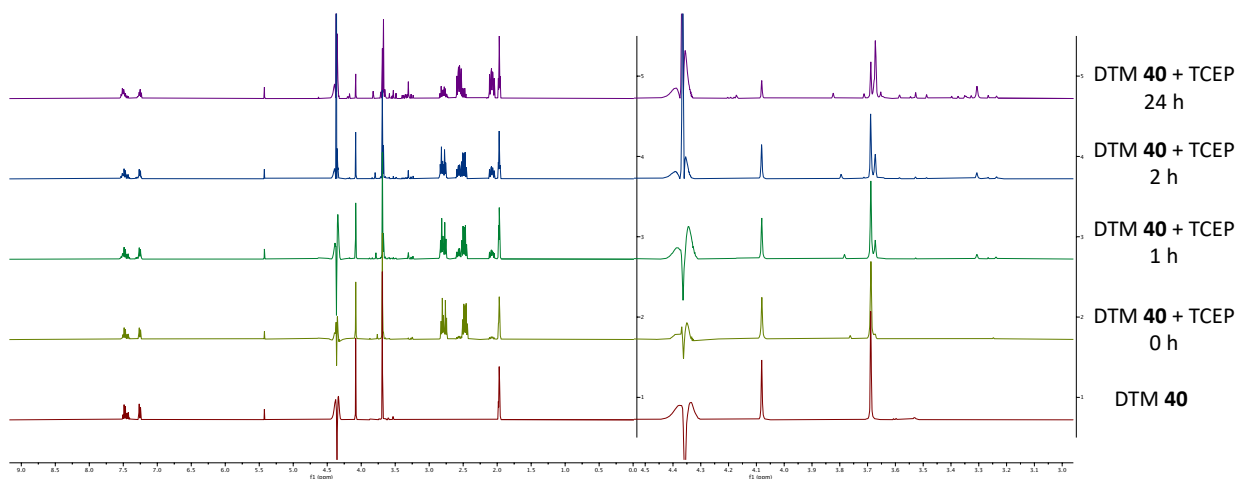
Figure S39 – NMR reactions of DTM **40**.
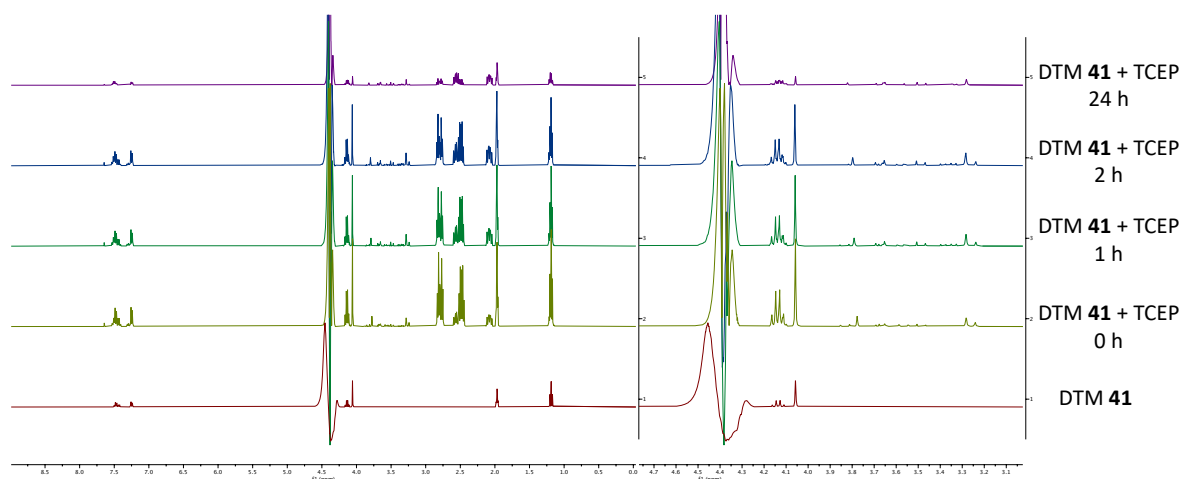
Figure S40 – NMR reactions of DTM **41**.
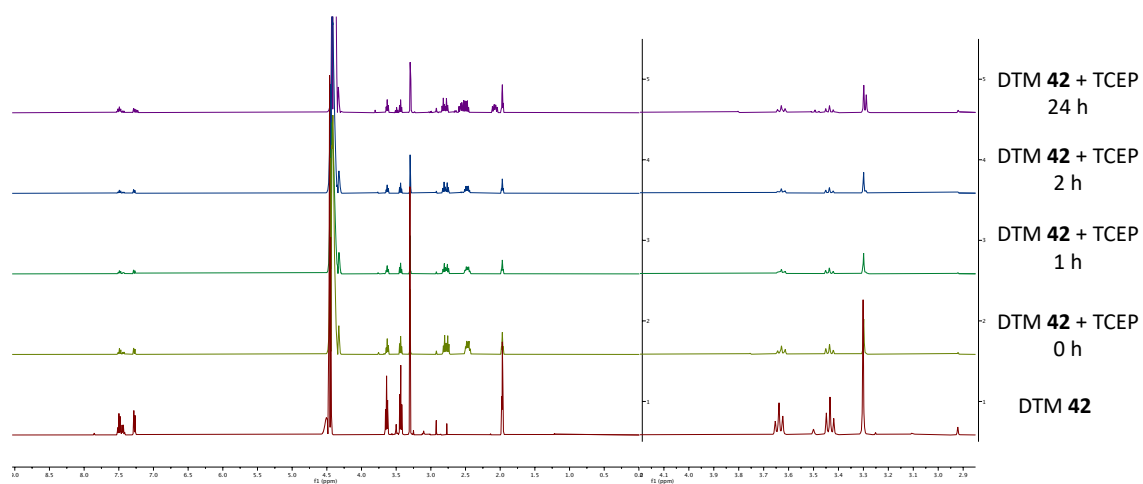
Figure S41 – NMR reactions of DTM **42**.
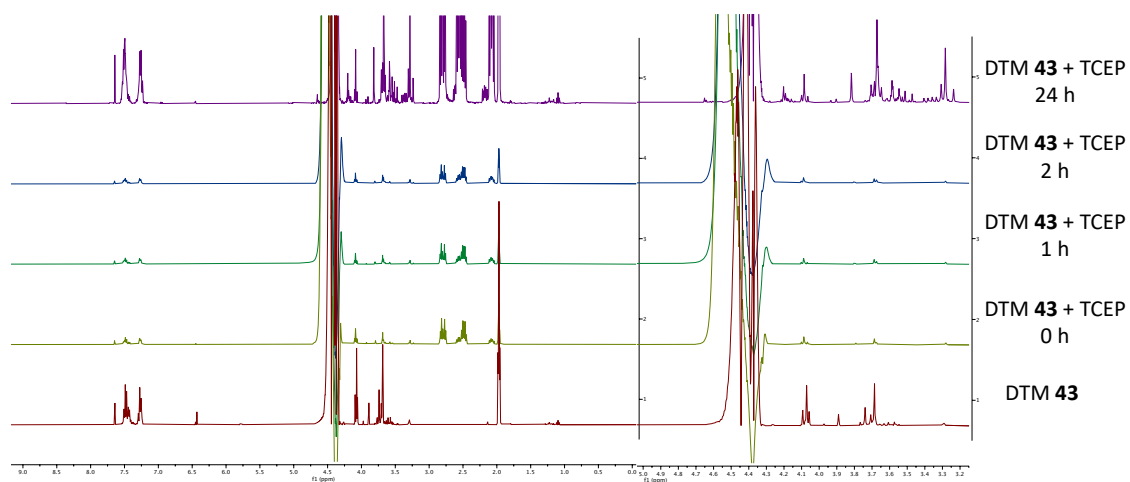
Figure S42 – NMR reactions of DTM **43**.
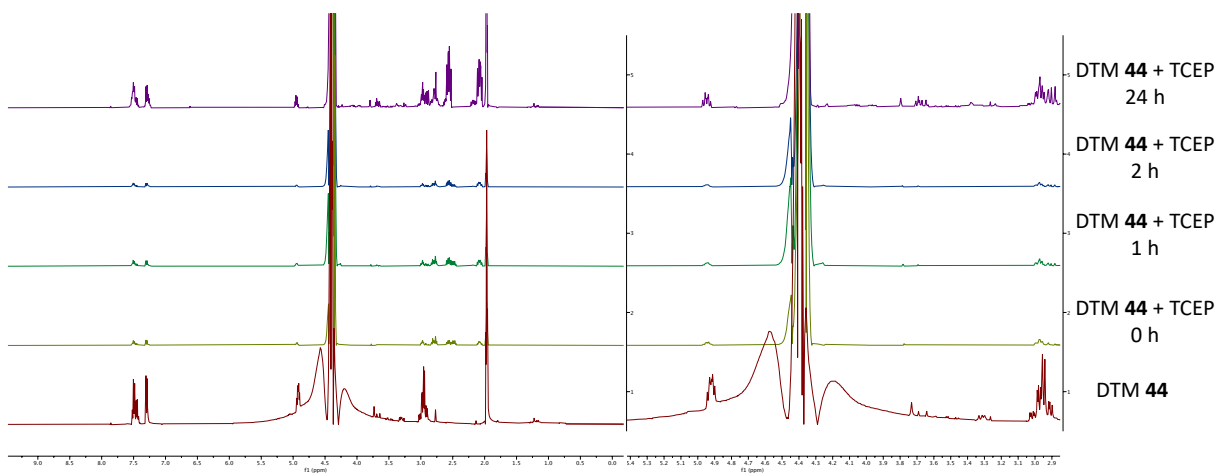
Figure S43 – NMR reactions of DTM **44**.
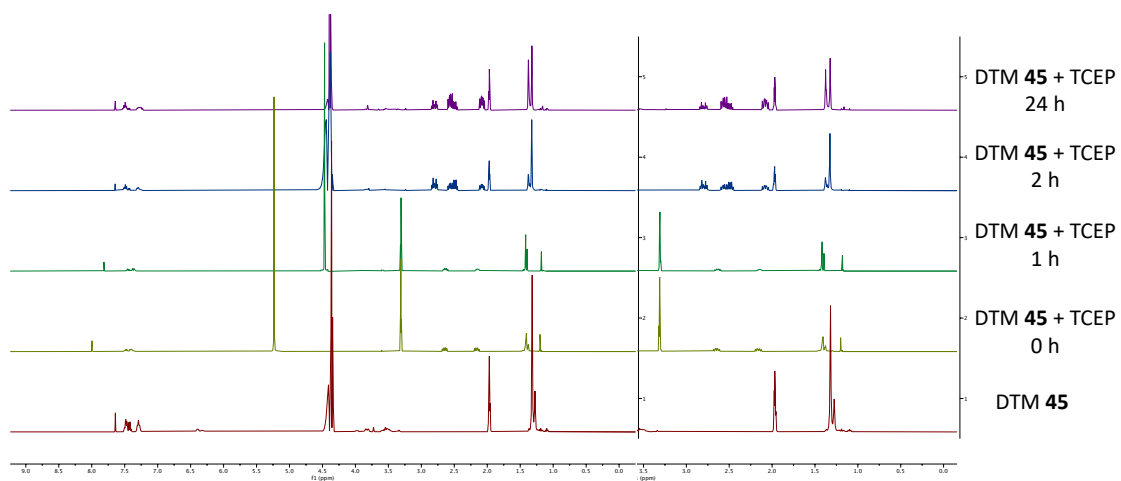
Figure S44 – NMR reactions of DTM **45**.
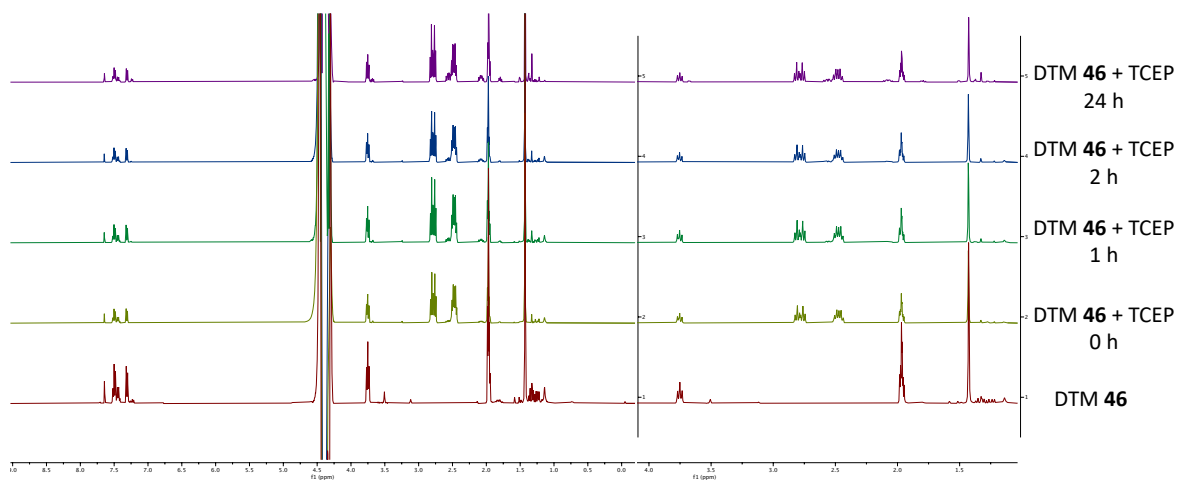
Figure S45 – NMR reactions of DTM **46**.
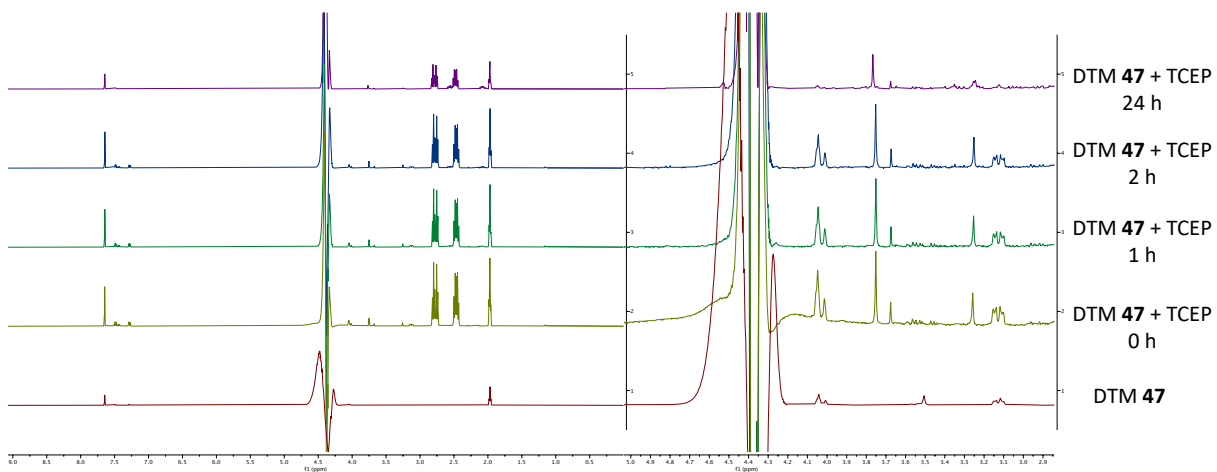
Figure S46 – NMR reactions of DTM **47**.
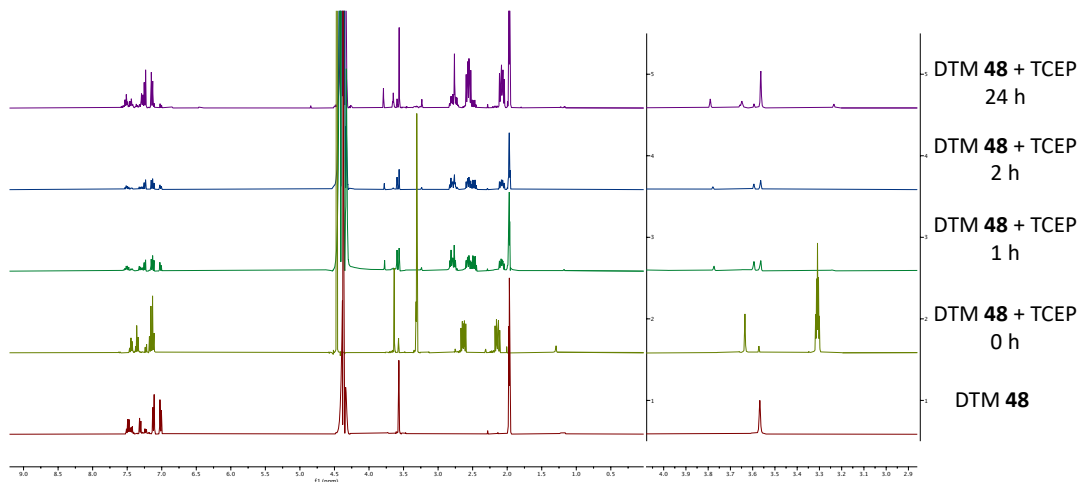
Figure S47 – NMR reactions of DTM **48**.
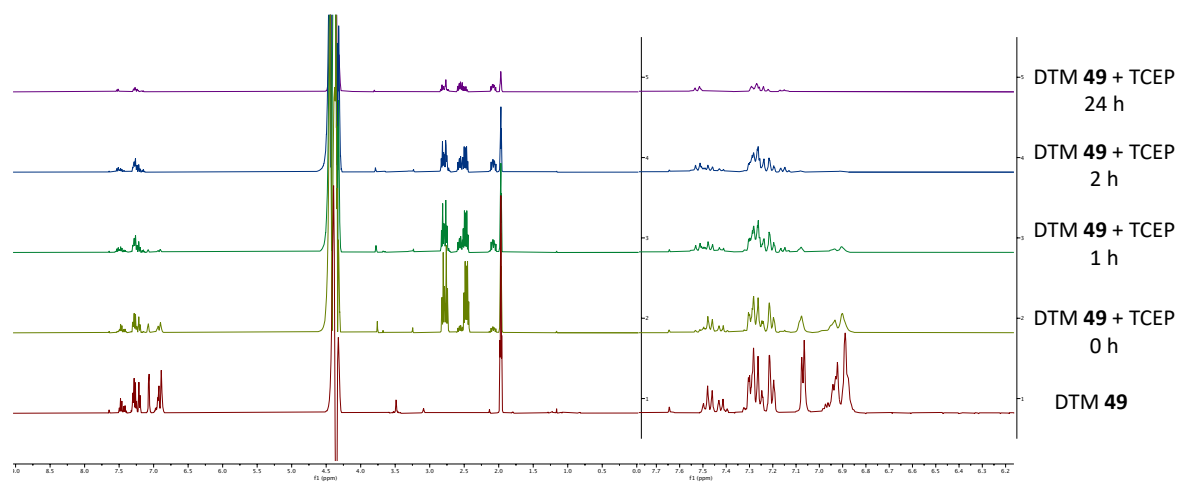
Figure S48 – NMR reactions of DTM **49**.

Chapter 6: Reference

1   G. Vidarsson, G. Dekkers and T. Rispens, *Frontiers in Immunology*, 2014, **5**, 1–17.

2   D. E. Thurston and P. J. M. Jackson, *Cytotoxic Payloads for Antibody - Drug Conjugates*, 2019, pp. 1–30.

3   H. Liu and K. May, *mAbs*, 2012, **4**, 17–23.

4   T. Suzuki, A. Ishii-Watabe, M. Tada, T. Kobayashi, T. Kanayasu-Toyoda, T. Kawanishi and T. Yamaguchi, *The Journal of Immunology*, 2010, **184**, 1968–1976.

5   E. B. Irvine and G. Alter, *Glycobiology*, 2020, **30**, 241–253.

6   G. P. Subedi and A. W. Barb, *Structure*, 2015, **23**, 1573–1583.

7   P. Holliger and P. J. Hudson, *Nature Biotechnology*, 2005, **23**, 1126–1136.

8   R. J. Flanagan and A. L. Jones, *Drug Safety*, 2004, **27**, 1115–1133.

9   M. Deonarain, G. Yahioglu, I. Stamati, A. Pomowski, J. Clarke, B. Edwards, S. Diez-Posada and A. Stewart, *Antibodies*, 2018, **7**, 16.

10 Q. Li, A. Barrett, B. Vijayakrishnan, A. Tiberghien, R. Beard, K. W. Rickert, K. L. Allen, R. J. Christie, M. Marelli, J. Harper, P. Howard, H. Wu, W. F. Dall'Acqua, P. Tsui, C. Gao and M. J. Borrok, *Bioconjugate Chemistry*, 2019, **30**, 1232–1243.

11 A. Bates and C. A. Power, *Antibodies*, 2019, **8**, 28.

12 Y. T. Lee, Y. J. Tan and C. E. Oon, *European Journal of Pharmacology*, 2018, **834**, 188–196.

13 Ansori, *Paper Knowledge . Toward a Media History of Documents*, 2015, **3**, 49–58.

14 S. Riethmiller, *Bulletin for the History of Chemistry*, 1999, **23**, 28–33.

15 A. Cambrosio and P. Keating, *Journal of the History of Biology*, 1992, **25**, 175–230.

16 K. McKeage and C. M. Perry, *Drugs*, 2002, **62**, 209–243.

17 G. L. Plosker and D. P. Figgitt, *Drugs*, 2003, **63**, 803–843.

18 S. Goswami, W. Wang, T. Arakawa and S. Ohtake, *Antibodies*, 2013, **2**, 452–500.

19 Y. Gao, X. Huang, Y. Zhu and Z. Lv, *Journal of Immunoassay and Immunochemistry*, 2018, **39**, 351–364.

20 A. M. Scott, J. D. Wolchok and L. J. Old, *Nature Reviews Cancer*, 2012, **12**, 278–287.

21 Y. V. Kovtun and V. S. Goldmacher, *Cancer Letters*, 2007, **255**, 232–240.

22 S. Ali, H.-M. Dunmore, D. Karres, J. L. Hay, T. Salmonsson, C. Gisselbrecht, S. B. Sarac, O. W. Bjerrum, D. Hovgaard, Y. Barbachano, N. Nagercoil and F. Pignatti, *The Oncologist*, 2019, **24**, 171–179.

23 P. R. Hamann, L. M. Hinman, I. Hollander, C. F. Beyer, D. Lindh, R. Holcomb, W. Hallett, H.-R. Tsou, J. Upeslacis, D. Shochat, A. Mountain, D. A. Flowers and I. Bernstein, *Bioconjugate Chemistry*, 2002, **13**, 47–58.

24 Q. Jiang, B. Patel, X. Jin, D. Di Grandi, E. Bortell, B. Czapkowski, T. F. Lerch, D. Meyer, S. Patel, J. Pegg, A. Arbuckle, J. Lagliva, V. Sriskanda, L. Letendre, H. Li, E. Thomas and D. Nadkarni, *ACS Omega*, 2019, **4**, 6468–6475.

25 J. Lu, F. Jiang, A. Lu and G. Zhang, *International Journal of Molecular Sciences*, 2016, **17**, 561.

26 J. A. Francisco, C. G. Cerveny, D. L. Meyer, B. J. Mixan, K. Klussman, D. F. Chace, S. X. Rejniak, K. A. Gordon, R. DeBlanc, B. E. Toki, C.-L. Law, S. O. Doronina, C. B. Siegall, P. D. Senter and A. F. Wahl, *Blood*, 2003, **102**, 1458–1465.

27 C. Vaklavas and A. Forero-Torres, *Therapeutic Advances in Hematology*, 2012, **3**, 209–225.

28 J. Katz, J. E. Janik and A. Younes, *Clinical Cancer Research*, 2011, **17**, 6428–6436.

29 Y. Chen, M. T. Kim, L. Zheng, G. Deperalta and F. Jacobson, *Bioconjugate Chemistry*, 2016, **27**, 2037–2047.

30 L. Amiri-Kordestani, G. M. Blumenthal, Q. C. Xu, L. Zhang, S. W. Tang, L. Ha, W. C. Weinberg, B. Chi, R. Candau-Chacon, P. Hughes, A. M. Russell, S. P. Miksinski, X. H. Chen, W. D. McGuinn, T. Palmby, S. J. Schrieber, Q. Liu, J. Wang, P. Song, N. Mehrotra, L. Skarupa, K. Clouse, A. Al-Hakim, R. Sridhara, A. Ibrahim, R. Justice, R. Pazdur and P. Cortazar, *Clinical Cancer Research*, 2014, **20**, 4436–4441.

31 E. D. Deeks, *Drugs*, 2019, **79**, 1467–1475.

32 R. Ohri, S. Bhakta, A. Fourie-O'Donohue, J. Dela Cruz-Chuh, S. P. Tsai, R. Cook, B. Wei, C. Ng, A. W. Wong, A. B. Bos, F. Farahi, J. Bhakta, T. H. Pillow, H. Raab, R. Vandlen, P. Polakis, Y. Liu, H. Erickson, J. R. Junutula and K. R. Kozak, *Bioconjugate Chemistry*, 2018, **29**, 473–485.

33 A. G. Polson, S. F. Yu, K. Elkins, B. Zheng, S. Clark, G. S. Ingle, D. S. Slaga, L. Giere, C. Du, C. Tan, J. A. Hongo, A. Gogineni, M. J. Cole, R. Vandlen, J. P. Stephan, J. Young, W. Chang, S. J. Scales, S. Ross, D. Eaton and A. Ebens, *Blood*, 2007, **110**, 616–623.

34 Z. Xu, D. Guo, Z. Jiang, R. Tong, P. Jiang, L. Bai, L. Chen, Y. Zhu, C. Guo, J. Shi and D. Yu, *European Journal of Medicinal Chemistry*, 2019, **183**, 111682.

35 S. J. Keam, *Drugs*, 2020, **80**, 501–508.

36 Y. Ogitani, T. Aida, K. Hagihara, J. Yamaguchi, C. Ishii, N. Harada, M. Soma, H. Okamoto, M. Oitate, S. Arakawa, T. Hirai, R. Atsumi, T. Nakada, I. Hayakawa, Y. Abe and T. Agatsuma, *Clinical Cancer Research*, 2016, **22**, 5097–5108.

37 P. M. Challita-Eid, D. Satpayev, P. Yang, Z. An, K. Morrison, Y. Shostak, A. Raitano, R. Nadell, W. Liu, D. R. Lortie, L. Capo, A. Verlinsky, M. Leavitt, F. Malik, H. Aviña, C. I. Guevara, N. Dinh, S. Karki, B. S. Anand, D. S. Pereira, I. B. J. Joseph, F. Doñate, K. Morrison and D. R. Stover, *Cancer Research*, 2016, **76**, 3003–3013.

38 S. Sahota and L. T. Vahdat, *Expert Opinion on Biological Therapy*, 2017, **17**, 1027–1031.

39 W. Dong, J. Shi, T. Yuan, B. Qi, J. Yu, J. Dai and L. He, *European Journal of Medicinal Chemistry*, 2019, **167**, 583–593.

40 S. Trudel, N. Lendvai, R. Popat, P. M. Voorhees, B. Reeves, E. N. Libby, P. G. Richardson, A. Hoos, I. Gupta, V. Bragulat, Z. He, J. B. Opalinska and A. D. Cohen, *Blood Cancer Journal*, 2019, **9**, 37.

41 N. Joubert, A. Beck, C. Dumontet and C. Denevault-sabourin, *Pharmaceuticals*, 2020, 1–31.

42 F. Zammarchi, S. Corbett, L. Adams, P. C. Tyrer, K. Kiakos, N. Janghra, T. Marafioti, C. E. Britten, C. E. G. Havenith, S. Chivers, F. D'Hooge, D. G. Williams, A. Tiberghien, P. W. Howard, J. A. Hartley and P. H. van Berkel, *Blood*, 2018, **131**, 1094–1105.

43 X. Zhang, Q. Li, H. Zhao, L. Ma, T. Meng, J. Qian, R. Jin, J. Shen and K. Yu, *Oncotarget*, 2017, **8**, 59086–59102.

44 C. S. B. Chia, *ChemMedChem*, 2022, **17**, e202200032.

45 A. Beck, L. Goetsch, C. Dumontet and N. Corvaïa, *Nature Reviews Drug Discovery*, 2017, **16**, 315–337.

46 R. V. J. Chari, *Accounts of Chemical Research*, 2008, **41**, 98–107.

47 P. J. Carter and P. D. Senter, *The Cancer Journal*, 2008, **14**, 154–169.

48 K. Tsuchikama and Z. An, *Protein and Cell*, 2018, **9**, 33–46.

49 N. Jain, S. W. Smith, S. Ghone and B. Tomczuk, *Pharmaceutical Research*, 2015, **32**, 3526–3540.

50 J. Z. Drago, S. Modi and S. Chandarlapaty, *Nature Reviews Clinical Oncology*, 2021, **18**, 327–344.

51 C. Selby, L. R. Yacko, and A. E. Glode, *Journal of the Advanced Practitioner in Oncology*, 2019, **10**, 68-82.

52 B. A. Kellogg, L. Garrett, Y. Kovtun, K. C. Lai, B. Leece, M. Miller, G. Payne, R. Steeves, K. R. Whiteman, W. Widdison, H. Xie, R. Singh, R. V. J. Chari, J. M. Lambert and R. J. Lutz, *Bioconjugate Chemistry*, 2011, **22**, 717–727.

53 G. M. Dubowchik and R. A. Firestone, *Bioorganic and Medicinal Chemistry Letters*, 1998, **8**, 3341–3346.

54 H. K. Erickson, G. D. Lewis Phillips, D. D. Leipold, C. A. Provenzano, E. Mai, H. A. Johnson, B. Gunter, C. A. Audette, M. Gupta, J. Pinkas and J. Tibbitts, *Molecular Cancer Therapeutics*, 2012, **11**, 1133–1142.

55 M. Cristofanilli, W. J. Bryan, L. L. Miller, A. Y. C. Chang, W. J. Gradishar, D. W. Kufe and G. N. Hortobagyi, *Anti-Cancer Drugs*, 1998, **9**, 779–782.

56 P. Zhao, Y. Zhang, W. Li, C. Jeanty, G. Xiang and Y. Dong, *Acta Pharmaceutica Sinica B*, 2020, **10**, 1589–1600.

57 F. Li, K. K. Emmerton, M. Jonas, X. Zhang, J. B. Miyamoto, J. R. Setter, N. D. Nicholas, N. M. Okeley, R. P. Lyon, D. R. Benjamin and C.-L. Law, *Cancer Research*, 2016, **76**, 2710–2719.

58 S. S. Matikonda, R. McLaughlin, P. Shrestha, C. Lipshultz and M. J. Schnermann, *Bioconjugate Chemistry*, 2022, **33**, 1241–1253.

59 J. W. Buecheler, M. Winzer, J. Tonillo, C. Weber and H. Gieseler, *Molecular Pharmaceutics*, 2018, **15**, 2656–2664.

60 R. P. Lyon, T. D. Bovee, S. O. Doronina, P. J. Burke, J. H. Hunter, H. D. Neff-LaFord, M. Jonas, M. E. Anderson, J. R. Setter and P. D. Senter, *Nature Biotechnology*, 2015, **33**, 733–735.

61 A. L. Smith and K. C. Nicolaou, *Journal of Medicinal Chemistry*, 1996, **39**, 2103–2117.

62 R. C. Elgersma, R. G. E. Coumans, T. Huijbregts, W. M. P. B. Menge, J. A. F. Joosten, H. J. Spijker, F. M. H. De Groot, M. M. C. Van Der Lee, R. Ubink, D. J. Van Den Dobbelsteen, D. F. Egging, W. H. A. Dokter, G. F. M. Verheijden, J. M. Lemmens, C. M. Timmers and P. H. Beusker, *Molecular Pharmaceutics*, 2015, **12**, 1813–1835.

63 M. S. Kung Sutherland, R. B. Walter, S. C. Jeffrey, P. J. Burke, C. Yu, H. Kostner, I. Stone, M. C. Ryan, D. Sussman, R. P. Lyon, W. Zeng, K. H. Harrington, K. Klussman, L. Westendorf, D. Meyer, I. D. Bernstein, P. D. Senter, D. R. Benjamin, J. G. Drachman and J. A. McEarchern, *Blood*, 2013, **122**, 1455–1463.

64 S. O. Doronina, B. E. Toki, M. Y. Torgov, B. A. Mendelsohn, C. G. Cerveny, D. F. Chace, R. L. DeBlanc, R. P. Gearing, T. D. Bovee, C. B. Siegall, J. A. Francisco, A. F. Wahl, D. L. Meyer and P. D. Senter, *Nature Biotechnology*, 2003, **21**, 778–784.

65 W. C. Widdison, S. D. Wilhelm, E. E. Cavanagh, K. R. Whiteman, B. A. Leece, Y. Kovtun, V. S. Goldmacher, H. Xie, R. M. Steeves, R. J. Lutz, R. Zhao, L. Wang, W. A. Blättler and R. V. J. Chari, *Journal of Medicinal Chemistry*, 2006, **49**, 4392–4408.

66 M. J. Birrer, K. N. Moore, I. Betella and R. C. Bates, *Journal of the National Cancer Institute*, 2019, **111**, 538–549.

67 P. A. Szijj, K. A. Kostadinova, R. J. Spears and V. Chudasama, *Organic and Biomolecular Chemistry*, 2020, **18**, 9018–9028.

68 H. Tagawa, K. Maruyama, K. Sasaki, N. Konoue, A. Kishimura, M. Kanai, T. Mori, K. Oisaki and Y. Katayama, *RSC Advances*, 2020, **10**, 16727–16731.

69 S. Lin, X. Yang, S. Jia, A. M. Weeks, M. Hornsby, P. S. Lee, R. V. Nichiporuk, A. T. Iavarone, J. A. Wells, F. D. Toste and C. J. Chang, *Science*, 2017, **355**, 597–602.

70 W. H. Zhang, G. Otting and C. J. Jackson, *Current Opinion in Structural Biology*, 2013, **23**, 581–587.

71 N. Forte, V. Chudasama and J. R. Baker, *Drug Discovery Today: Technologies*, 2018, **30**, 11–20.

72 L. Wang, G. Amphlett, W. A. Blättler, J. M. Lambert and W. Zhang, *Protein Science*, 2005, **14**, 2436–2446.

73 P. Dennler, E. Fischer and R. Schibli, *Antibodies*, 2015, **4**, 197–224.

74 P. D. Senter and E. L. Sievers, *Nature Biotechnology*, 2012, **30**, 631–637.

75 G. W. Anderson, J. E. Zimmerman and F. M. Callahan, *Journal of the American Chemical Society*, 1964, **86**, 1839–1842.

76 E. M. Sletten and C. R. Bertozzi, *Angewandte Chemie International Edition*, 2009, **48**, 6974–6998.

77 S. Mädler, C. Bich, D. Touboul and R. Zenobi, *Journal of Mass Spectrometry*, 2009, **44**, 694–706.

78　S. Kalkhof and A. Sinz, *Analytical and Bioanalytical Chemistry*, 2008, **392**, 305–312.

79　Y. Zhang, Y. Liang, F. Huang, Y. Zhang, X. Li and J. Xia, *Biochemistry*, 2019, **58**, 1010–1018.

80　P. M. S. D. Cal, J. B. Vicente, E. Pires, A. V. Coelho, L. F. Veiros, C. Cordeiro and P. M. P. Gois, *Journal of the American Chemical Society*, 2012, **134**, 10299–10305.

81　L. Hao, Q. Zhou, Y. Piao, Z. Zhou, J. Tang and Y. Shen, *Journal of Controlled Release*, 2021, **330**, 362–371.

82　T. Nakamura, Y. Kawai, N. Kitamoto, T. Osawa and Y. Kato, *Chemical Research in Toxicology*, 2009, **22**, 536–542.

83　A. Narayanan and L. H. Jones, *Chemical Science*, 2015, **6**, 2650–2659.

84　I. Dovgan, S. Ursuegui, S. Erb, C. Michel, S. Kolodych, S. Cianférani and A. Wagner, *Bioconjugate Chemistry*, 2017, **28**, 1452–1457.

85　S. Diethelm, M. A. Schafroth and E. M. Carreira, *Organic Letters*, 2014, **16**, 3908–3911.

86　M. Haque, N. Forte and J. R. Baker, *Chemical Communications*, 2021, **57**, 10689–10702.

87　M. E. B. Smith, M. B. Caspersen, E. Robinson, M. Morais, A. Maruani, J. P. M. Nunes, K. Nicholls, M. J. Saxton, S. Caddick, J. R. Baker and V. Chudasama, *Organic and Biomolecular Chemistry*, 2015, **13**, 7946–7949.

88　W. J. Wedemeyer, E. Welker, M. Narayan and H. A. Scheraga, *Biochemistry*, 2000, **39**, 4207–4216.

89　Z.-Y. Guo, X.-Y. Jia and Y.-M. Feng, *Biological Chemistry*, 2004, **385**, 1171–1175.

90　D. Bontempo, K. L. Heredia, B. A. Fish and H. D. Maynard, *Journal of the American Chemical Society*, 2004, **126**, 15372–15373.

91　A. J. Slezak, A. Mansurov, M. M. Raczy, K. Chang, A. T. Alpar, A. L. Lauterbach, R. P. Wallace, R. K. Weathered, J. E. G. Medellin, C. Battistella, L. T. Gray, T. M. Marchell, S. Gomes, M. A. Swartz and J. A. Hubbell, *ACS Central Science*, 2022, **8**, 1435–1446.

92　E. Calce and S. De Luca, *Chemistry - A European Journal*, 2017, **23**, 224–233.

93　M. S. Masri and M. Friedman, *Journal of Protein Chemistry*, 1988, **7**, 49–54.

94　J. T. Palmer, D. Rasnick, J. L. Klaus and D. Bromme, *Journal of Medicinal Chemistry*, 1995, **38**, 3193–3196.

95　U. Ramseier and J. Y. Chang, *Analytical Biochemistry*, 1994, **221**, 231–233.

96　S. B. Gunnoo and A. Madder, *ChemBioChem*, 2016, **17**, 529–553.

97 J. T. Patterson, S. Asano, X. Li, C. Rader and C. F. Barbas, *Bioconjugate Chemistry*, 2014, **25**, 1402–1407.

98 M. Morpurgo, F. M. Veronese, D. Kachensky and J. M. Harris, *Bioconjugate Chemistry*, 1996, **7**, 363–368.

99 J. Morales-Sanfrutos, F. J. Lopez-Jaramillo, F. Hernandez-Mateo and F. Santoyo-Gonzalez, *The Journal of Organic Chemistry*, 2010, **75**, 4039–4047.

100 M. Abo, C. Li and E. Weerapana, *Molecular Pharmaceutics*, 2018, **15**, 743–749.

101 M. S. S. Palanki, A. Bhat, B. Bolanos, F. Brunel, J. Del Rosario, D. Dettling, M. Horn, R. Lappe, R. Preston, A. Sievers, N. Stankovic, G. Woodnut and G. Chen, *Bioorganic and Medicinal Chemistry Letters*, 2013, **23**, 402–406.

102 D. P. Nair, M. Podgórski, S. Chatani, T. Gong, W. Xi, C. R. Fenoli and C. N. Bowman, *Chemistry of Materials*, 2014, **26**, 724–744.

103 E. Friedmann, D. H. Marrian and I. Simon-Reuss, *British Journal of Pharmacology and Chemotherapy*, 1949, **4**, 105–108.

104 P. Schelté, C. Boeckler, B. Frisch and F. Schuber, *Bioconjugate Chemistry*, 2000, **11**, 118–123.

105 R. P. Lyon, J. R. Setter, T. D. Bovee, S. O. Doronina, J. H. Hunter, M. E. Anderson, C. L. Balasubramanian, S. M. Duniho, C. I. Leiske, F. Li and P. D. Senter, *Nature Biotechnology*, 2014, **32**, 1059–1062.

106 M. E. B. Smith, F. F. Schumacher, C. P. Ryan, L. M. Tedaldi, D. Papaioannou, G. Waksman, S. Caddick and J. R. Baker, *Journal of the American Chemical Society*, 2010, **132**, 1960–1965.

107 C. P. Ryan, M. E. B. Smith, F. F. Schumacher, D. Grohmann, D. Papaioannou, G. Waksman, F. Werner, J. R. Baker and S. Caddick, *Chemical Communications*, 2011, **47**, 5452–5454.

108 M. W. Jones, R. A. Strickland, F. F. Schumacher, S. Caddick, James. R. Baker, M. I. Gibson and D. M. Haddleton, *Journal of the American Chemical Society*, 2012, **134**, 1847–1852.

109 A. Maruani, M. E. B. Smith, E. Miranda, K. A. Chester, V. Chudasama and S. Caddick, *Nature Communications*, 2015, **6**, 6645.

110 E. Robinson, J. P. M. Nunes, V. Vassileva, A. Maruani, J. C. F. Nogueira, M. E. B. Smith, R. B. Pedley, S. Caddick, J. R. Baker and V. Chudasama, *RSC Advances*, 2017, **7**, 9073–9077.

111 C. Bahou, P. A. Szijj, R. J. Spears, A. Wall, F. Javaid, A. Sattikar, E. A. Love, J. R. Baker and V. Chudasama, *Bioconjugate Chemistry*, 2021, **32**, 672–679.

112 S. Shaunak, A. Godwin, J.-W. Choi, S. Balan, E. Pedone, D. Vijayarangam, S. Heidelberger, I. Teo, M. Zloh and S. Brocchini, *Nature Chemical Biology*, 2006, **2**, 312–313.

113 S. Brocchini, A. Godwin, S. Balan, J. Choi, M. Zloh and S. Shaunak, *Advanced Drug Delivery Reviews*, 2008, **60**, 3–12.

114 G. Badescu, P. Bryant, M. Bird, K. Henseleit, J. Swierkosz, V. Parekh, R. Tommasi, E. Pawlisz, K. Jurlewicz, M. Farys, N. Camper, X. Sheng, M. Fisher, R. Grygorash, A. Kyle, A. Abhilash, M. Frigerio, J. Edwards and A. Godwin, *Bioconjugate Chemistry*, 2014, **25**, 1124–1136.

115 S. J. Walsh, S. Omarjee, W. R. J. D. Galloway, T. T.-L. Kwan, H. F. Sore, J. S. Parker, M. Hyvönen, J. S. Carroll and D. R. Spring, *Chemical Science*, 2019, **10**, 694–700.

116 F. M. Dannheim, S. J. Walsh, C. T. Orozco, A. H. Hansen, J. D. Bargh, S. E. Jackson, N. J. Bond, J. S. Parker, J. S. Carroll and D. R. Spring, *Chemical Science*, 2022, **13**, 8781–8790.

117 A. J. Counsell, S. J. Walsh, N. S. Robertson, H. F. Sore and D. R. Spring, *Organic and Biomolecular Chemistry*, 2020, **18**, 4739–4743.

118 O. Koniev, I. Dovgan, B. Renoux, A. Ehkirch, J. Eberova, S. Cianférani, S. Kolodych, S. Papot and A. Wagner, *Medicinal Chemistry Communications*, 2018, **9**, 827–830.

119 C. Canovas, M. Moreau, C. Bernhard, A. Oudot, M. Guillemin, F. Denat and V. Goncalves, *Angewandte Chemie International Edition*, 2018, **57**, 10646–10650.

120 N. Gupta, J. Kancharla, S. Kaushik, A. Ansari, S. Hossain, R. Goyal, M. Pandey, J. Sivaccumar, S. Hussain, A. Sarkar, A. Sengupta, S. K. Mandal, M. Roy and S. Sengupta, *Chemical Science*, 2017, **8**, 2387–2395.

121 E. Khozeimeh Sarbisheh, G. Dewaele-Le Roi, W. E. Shannon, S. Tan, Y. Xu, B. M. Zeglis and E. W. Price, *Bioconjugate Chemistry*, 2020, **31**, 2789–2806.

122 C. E. Stieger, L. Franz, F. Körlin and C. P. R. Hackenberger, *Angewandte Chemie International Edition*, 2021, **60**, 15359–15364.

123 L. Juen, C. B. Baltus, C. Gély, O. Feuillâtre, A. Desgranges, M.-C. Viaud-Massuard and C. Martin, *Bioconjugate Chemistry*, 2021, **32**, 595–606.

124 V. Chudasama, M. E. B. Smith, F. F. Schumacher, D. Papaioannou, G. Waksman, J. R. Baker and S. Caddick, *Chemical Communications*, 2011, **47**, 8781.

125 A. Maruani, M. E. B. Smith, E. Miranda, K. A. Chester, V. Chudasama and S. Caddick, *Nature Communications*, 2015, **6**, 6645.

126 A. Maruani, P. A. Szijj, C. Bahou, J. C. F. Nogueira, S. Caddick, J. R. Baker and V. Chudasama, *Bioconjugate Chemistry*, 2020, **31**, 520–529.

127 M. T. W. Lee, A. Maruani, J. R. Baker, S. Caddick and V. Chudasama, *Chemical Science*, 2016, **7**, 799–802.

128 C. Bahou, D. A. Richards, A. Maruani, E. A. Love, F. Javaid, S. Caddick, J. R. Baker and V. Chudasama, *Organic and Biomolecular Chemistry*, 2018, **16**, 1359–1366.

129 M. T. W. Lee, A. Maruani, D. A. Richards, J. R. Baker, S. Caddick and V. Chudasama, *Chemical Science*, 2017, **8**, 2056–2060.

130 M. K. Greene, D. A. Richards, J. C. F. Nogueira, K. Campbell, P. Smyth, M. Fernández, C. J. Scott and V. Chudasama, *Chemical Science*, 2018, **9**, 79–87.

131 F. A. Liberatore, R. D. Comeau, J. M. McKearin, D. A. Pearson, B. Q. Belonga, S. J. Brocchini, J. Kath, T. Phillips, K. Oswell and R. G. Lawton, *Bioconjugate Chemistry*, 1990, **1**, 36–50.

132 S. Balan, J. Choi, A. Godwin, I. Teo, C. M. Laborde, S. Heidelberger, M. Zloh, S. Shaunak and S. Brocchini, *Bioconjugate Chemistry*, 2007, **18**, 61–76.

133 A. Pfisterer, K. Eisele, X. Chen, M. Wagner, K. Müllen and T. Weil, *Chemistry - A European Journal*, 2011, **17**, 9697–9707.

134 S. Shaunak, A. Godwin, J. W. Choi, S. Balan, E. Pedone, D. Vijayarangam, S. Heidelberger, I. Teo, M. Zloh and S. Brocchini, *Nature Chemical Biology*, 2006, **2**, 312–313.

135 S. Brocchini, A. Godwin, S. Balan, J. won Choi, M. Zloh and S. Shaunak, *Advanced Drug Delivery Reviews*, 2008, **60**, 3–12.

136 G. Badescu, P. Bryant, M. Bird, K. Henseleit, J. Swierkosz, V. Parekh, R. Tommasi, E. Pawlisz, K. Jurlewicz, M. Farys, N. Camper, X. Sheng, M. Fisher, R. Grygorash, A. Kyle, A. Abhilash, M. Frigerio, J. Edwards and A. Godwin, *Bioconjugate Chemistry*, 2014, **25**, 1124–1136.

137 P. Bryant, M. Pabst, G. Badescu, M. Bird, W. McDowell, E. Jamieson, J. Swierkosz, K. Jurlewicz, R. Tommasi, K. Henseleit, X. Sheng, N. Camper, A. Manin, K. Kozakowska, K. Peciak, E. Laurine, R. Grygorash, A. Kyle, D. Morris, V. Parekh, A. Abhilash, J. W. Choi, J. Edwards, M. Frigerio, M. P. Baker and A. Godwin, *Molecular Pharmaceutics*, 2015, **12**, 1872–1879.

138 C. Bahou and V. Chudasama, *Organic and Biomolecular Chemistry*, 2022, **20**, 5879–5890.

139 C. Bahou, E. A. Love, S. Leonard, R. J. Spears, A. Maruani, K. Armour, J. R. Baker and V. Chudasama, *Bioconjugate Chemistry*, 2019, **30**, 1048–1054.

140 J. R. Junutula, K. M. Flagella, R. A. Graham, K. L. Parsons, E. Ha, H. Raab, S. Bhakta, T. Nguyen, D. L. Dugger, G. Li, E. Mai, G. D. Lewis Phillips, H. Hiraragi, R. N. Fuji, J. Tibbitts, R. Vandlen, S. D. Spencer, R. H. Scheller, P. Polakis and M. X. Sliwkowski, *Clinical Cancer Research*, 2010, **16**, 4769–4778.

141 J. R. Junutula, H. Raab, S. Clark, S. Bhakta, D. D. Leipold, S. Weir, Y. Chen, M. Simpson, S. P. Tsai, M. S. Dennis, Y. Lu, Y. G. Meng, C. Ng, J. Yang, C. C. Lee, E. Duenas, J. Gorrell, V. Katta, A. Kim, K. McDorman, K. Flagella, R. Venook, S. Ross, S. D. Spencer, W. Lee Wong, H. B. Lowman, R. Vandlen, M. X. Sliwkowski, R. H. Scheller, P. Polakis and W. Mallet, *Nature Biotechnology*, 2008, **26**, 925–932.

142 J. P. M. Nunes, V. Vassileva, E. Robinson, M. Morais, M. E. B. Smith, R. B. Pedley, S. Caddick, J. R. Baker and V. Chudasama, *RSC Advances*, 2017, **7**, 24828–24832.

143 N. Zacharias, V. N. Podust, K. K. Kajihara, D. Leipold, G. Del Rosario, D. Thayer, E. Dong, M. Paluch, D. Fischer, K. Zheng, C. Lei, J. He, C. Ng, D. Su, L. Liu, S. Masih, W. Sawyer, J. Tinianow, J. Marik, V. Yip, G. Li, J. Chuh, J. H. Morisaki, S. Park, B. Zheng, H. Hernandez-Barry, K. M. Loyet, M. Xu, K. R. Kozak, G. L. Phillips, B.-Q. Shen, C. Wu, K. Xu, S.-F. Yu, A. Kamath, R. K. Rowntree, D. Reilly, T. Pillow, A. Polson, V. Schellenberger, W. L. W. Hazenbos and J. Sadowsky, *Chemical Science*, 2022, **13**, 3147–3160.

144 X. Li, J. T. Patterson, M. Sarkar, L. Pedzisa, T. Kodadek, W. R. Roush and C. Rader, *Bioconjugate Chemistry*, 2015, **26**, 2243–2248.

145 T. J. Hallam and V. V. Smider, *Future Medicinal Chemistry*, 2014, **6**, 1309–1324.

146 T. J. Hallam, E. Wold, A. Wahl and V. V. Smider, *Molecular Pharmaceutics*, 2015, **12**, 1848–1862.

147 A. Deiters, T. A. Cropp, D. Summerer, M. Mukherji and P. G. Schultz, *Bioorganic and Medicinal Chemistry Letters*, 2004, **14**, 5743–5745.

148 J. Y. Axup, K. M. Bajjuri, M. Ritland, B. M. Hutchins, C. H. Kim, S. A. Kazane, R. Halder, J. S. Forsyth, A. F. Santidrian, K. Stafin, Y. Lu, H. Tran, A. J. Seller, S. L. Biroc, A. Szydlik, J. K. Pinkstaff, F. Tian, S. C. Sinha, B. Felding-Habermann, V. V. Smider and P. G. Schultz, *Proceedings of the National Academy of Sciences of the United States of America*, 2012, **109**, 16101–16106.

149 L. Zhang, Z. Wang, Z. Wang, F. Luo, M. Guan, M. Xu, Y. Li, Y. Zhang, Z. Wang and W. Wang, *Bioconjugate Chemistry*, 2021, **32**, 1094–1104.

150 S. Jeger, K. Zimmermann, A. Blanc, J. Grünberg, M. Honer, P. Hunziker, H. Struthers and R. Schibli, *Angewandte Chemie International Edition*, 2010, **49**, 9995–9997.

151 P. M. Drake, A. E. Albers, J. Baker, S. Banas, R. M. Barfield, A. S. Bhat, G. W. de Hart, A. W. Garofalo, P. Holder, L. C. Jones, R. Kudirka, J. McFarland, W. Zmolek and D. Rabuka, *Bioconjugate Chemistry*, 2014, **25**, 1331–1341.

152 R. R. Beerli, T. Hell, A. S. Merkel and U. Grawunder, *PLOS ONE*, 2015, **10**, e0131177.

153 Q. Zhou, J. E. Stefano, C. Manning, J. Kyazike, B. Chen, D. A. Gianolio, A. Park, M. Busch, J. Bird, X. Zheng, H. Simonds-Mannes, J. Kim, R. C. Gregory, R. J. Miller, W. H. Brondyk, P. K. Dhal and C. Q. Pan, *Bioconjugate Chemistry*, 2014, **25**, 510–520.

154 R. van Geel, M. A. Wijdeven, R. Heesbeen, J. M. M. Verkade, A. A. Wasiel, S. S. van Berkel and F. L. van Delft, *Bioconjugate Chemistry*, 2015, **26**, 2233–2242.

155 L. M. Tedaldi, M. E. B. Smith, R. I. Nathani and J. R. Baker, *Chemical Communications*, 2009, 6583–6585.

156 C. Marculescu, H. Kossen, R. E. Morgan, P. Mayer, S. A. Fletcher, B. Tolner, K. A. Chester, L. H. Jones and J. R. Baker, *Chemical Communications*, 2014, **50**, 7139–7142.

157 A. Wall, K. Nicholls, M. B. Caspersen, S. Skrivergaard, K. A. Howard, K. Karu, V. Chudasama and J. R. Baker, *Organic and Biomolecular Chemistry*, 2019, **17**, 7870–7873.

158 A. Wall, A. G. Wills, N. Forte, C. Bahou, L. Bonin, K. Nicholls, M. T. Ma, V. Chudasama and J. R. Baker, *Chemical Science*, 2020, **11**, 11455–11460.

159 J. Youziel, A. R. Akhbar, Q. Aziz, M. E. B. Smith, S. Caddick, A. Tinker and J. R. Baker, *Organic and Biomolecular Chemistry*, 2014, **12**, 557–560.

160 M. Morais, J. P. M. Nunes, K. Karu, N. Forte, I. Benni, M. E. B. Smith, S. Caddick, V. Chudasama and J. R. Baker, *Organic and Biomolecular Chemistry*, 2017, **15**, 2947–2952.

161 M. Maneiro, N. Forte, M. M. Shchepinova, C. S. Kounde, V. Chudasama, J. R. Baker and E. W. Tate, *ACS Chemical Biology*, 2020, **15**, 1306–1312.

162 L. Castañeda, A. Maruani, F. F. Schumacher, E. Miranda, V. Chudasama, K. A. Chester, J. R. Baker, M. E. B. Smith and S. Caddick, *Chemical Communications*, 2013, **49**, 8187.

163 F. F. Schumacher, M. Nobles, C. P. Ryan, M. E. B. Smith, A. Tinker, S. Caddick and J. R. Baker, *Bioconjugate Chemistry*, 2011, **22**, 132–136.

164 F. F. Schumacher, J. P. M. Nunes, A. Maruani, V. Chudasama, M. E. B. Smith, K. A. Chester, J. R. Baker and S. Caddick, *Organic and Biomolecular Chemistry*, 2014, **12**, 7261–7269.

165 E. A. Hull, M. Livanos, E. Miranda, M. E. B. Smith, K. A. Chester and J. R. Baker, *Bioconjugate Chemistry*, 2014, **25**, 1395–1401.

166 N. Forte, M. Livanos, E. Miranda, M. Morais, X. Yang, V. S. Rajkumar, K. A. Chester, V. Chudasama and J. R. Baker, *Bioconjugate Chemistry*, 2018, **29**, 486–492.

167 D. A. Richards, S. A. Fletcher, M. Nobles, H. Kossen, L. Tedaldi, V. Chudasama, A. Tinker and J. R. Baker, *Organic and Biomolecular Chemistry*, 2016, **14**, 455–459.

168 R. Malde, M. A. Parkes, M. Staniforth, J. M. Woolley, V. G. Stavros, V. Chudasama, H. H. Fielding and J. R. Baker, *Chemical Science*, 2022, **13**, 2909–2918.

169 N. K. Devaraj and M. G. Finn, *Chemical Reviews*, 2021, **121**, 6697–6698.

170 H. C. Kolb, M. G. Finn and K. B. Sharpless, *Angewandte Chemie International Edition*, 2001, **40**, 2004–2021.

171 M. F. Debets, S. S. van Berkel, J. Dommerholt, A. (Ton) J. Dirks, F. P. J. T. Rutjes and F. L. van Delft, *Accounts of Chemical Research*, 2011, **44**, 805–815.

172 J. E. Hein and V. V. Fokin, *Chemical Society Reviews*, 2010, **39**, 1302.

173 R. Huisgen, *Angewandte Chemie International Edition in English*, 1963, **2**, 565–598.

174 S. S. Matikonda, D. L. Orsi, V. Staudacher, I. A. Jenkins, F. Fiedler, J. Chen and A. B. Gamble, *Chemical Science*, 2015, **6**, 1212–1218.

175 L. Liang and D. Astruc, *Coordination Chemistry Reviews*, 2011, **255**, 2933–2945.

176 V. Hong, S. I. Presolski, C. Ma and M. G. Finn, *Angewandte Chemie International Edition*, 2009, **48**, 9879–9883.

177 L. Carroll, H. L. Evans, E. O. Aboagye and A. C. Spivey, *Organic and Biomolecular Chemistry*, 2013, **11**, 5772.

178 E. M. Sletten and C. R. Bertozzi, *Accounts of Chemical Research*, 2011, **44**, 666–676.

179 J. C. Jewett and C. R. Bertozzi, *Chemical Society Reviews*, 2010, **39**, 1272.

180 J. Dommerholt, F. P. J. T. Rutjes and F. L. van Delft, *Topics in Current Chemistry*, 2016, **374**, 1–20.

181 J. M. Baskin, J. A. Prescher, S. T. Laughlin, N. J. Agard, P. V. Chang, I. A. Miller, A. Lo, J. A. Codelli and C. R. Bertozzi, *Proceedings of the National Academy of Sciences*, 2007, **104**, 16793–16797.

182 X. Ning, J. Guo, M. A. Wolfert and G.-J. Boons, *Angewandte Chemie International Edition*, 2008, **120**, 2285–2287.

183 P. V. Chang, J. A. Prescher, E. M. Sletten, J. M. Baskin, I. A. Miller, N. J. Agard, A. Lo and C. R. Bertozzi, *Proceedings of the National Academy of Sciences*, 2010, **107**, 1821–1826.

184 S. M. van den Bosch, R. Rossin, P. Renart Verkerk, W. ten Hoeve, H. M. Janssen, J. Lub and M. S. Robillard, *Nuclear Medicine and Biology*, 2013, **40**, 415–423.

185 J. M. Baskin, K. W. Dehnert, S. T. Laughlin, S. L. Amacher and C. R. Bertozzi, *Proceedings of the National Academy of Sciences*, 2010, **107**, 10360–10365.

186 R. R. Ramsubhag and G. B. Dudley, *Organic and Biomolecular Chemistry*, 2016, **14**, 5028–5031.

187 R. A. Carboni and R. V. Lindsey, *Journal of the American Chemical Society*, 1959, **81**, 4342–4346.

188 M. L. Blackman, M. Royzen and J. M. Fox, *Journal of the American Chemical Society*, 2008, **130**, 13518–13519.

189 R. D. Bach, *Journal of the American Chemical Society*, 2009, **131**, 5233–5243.

190 R. Selvaraj and J. M. Fox, *Current Opinion in Chemical Biology*, 2013, **17**, 753–760.

191 R. Rossin, S. M. van den Bosch, W. ten Hoeve, M. Carvelli, R. M. Versteegen, J. Lub and M. S. Robillard, *Bioconjugate Chemistry*, 2013, **24**, 1210–1217.

192 R. Rossin, P. Renart Verkerk, S. M. van den Bosch, R. C. M. Vulders, I. Verel, J. Lub and M. S. Robillard, *Angewandte Chemie International Edition*, 2010, **122**, 3447–3450.

193 N. K. Devaraj, R. Weissleder and S. A. Hilderbrand, *Bioconjugate Chemistry*, 2008, **19**, 2297–2299.

194 A. Maggi, E. Ruivo, J. Fissers, C. Vangestel, S. Chatterjee, J. Joossens, F. Sobott, S. Staelens, S. Stroobants, P. Van Der Veken, L. Wyffels and K. Augustyns, *Organic and Biomolecular Chemistry*, 2016, **14**, 7544–7551.

195 E. Kozma, O. Demeter and P. Kele, *ChemBioChem*, 2017, **18**, 486–501.

196 K. Kang, J. Park and E. Kim, *Proteome Science*, 2016, **15**, 15.

197 C. Santi and L. Bagnoli, *Molecules*, 2017, **22**, 10–13.

198 K. Brown and J. Arthur, *Public Health Nutrition*, 2001, **4**, 593–599.

199 J. Pinsent, *Biochemical Journal*, 1952, 10–16.

200 K. Schwarz and C. M. Foltz, *Journal of the American Chemical Society*, 1957, **79**, 3292–3293.

201 K. Schwarz, J. G. Bieri, G. M. Briggs and M. L. Scott, *Experimental Biology and Medicine*, 1957, **95**, 621–625.

202 J. E. Cone, R. Martin Del Rio, J. N. Davis and T. C. Stadtman, *Proceedings of the National Academy of Sciences of the United States of America*, 1976, **73**, 2659–2663.

203 J. W. Forstrom, J. J. Zakowski and A. L. Tappel, *Biochemistry*, 1978, **17**, 2639–2644.

204 H. Lindmark-Mansson and B. Akesson, *International Dairy Journal*, 2001, **11**, 649–655.

205 W. A. Günzler, G. J. Steffens, A. Grossmann, S.-M. A. Kim, F. Ötting, A. Wendel and L. Flohé, *Hoppe-Seyler´s Zeitschrift für physiologische Chemie*, 1984, **365**, 195–212.

206 E. Clementi and D. L. Raimondi, *The Journal of Chemical Physics*, 1963, **38**, 2686–2689.

207 C. N. Singman, *Journal of Chemical Education*, 1984, **61**, 137.

208 F. H. Allen, *Acta Crystallographica Section B: Structural Science*, 2002, **58**, 380–388.

209 L. Pauling and G. W. Wheland, *Journal of Chemical Physics*, 1934, **2**, 482.

210 A. Louis Allred, *Journal of Inorganic and Nuclear Chemistry*, 1961, **17**, 215–221.

211 R. E. J. Huber and R. S. Criddle, *Archives of Biochemistry and Biophysics*, 1967, **122**, 164–173.

212 H. J. Reich and R. J. Hondal, *ACS Chemical Biology*, 2016, **11**, 821–841.

213 J. C. Pleasants, W. Guo and D. L. Rabenstein, *Journal of the American Chemical Society*, 1989, **111**, 6553–6558.

214 R. Singh and G. M.Whitesides, *Journal of the American Chemical Society*, 1990, **112**, 6304–6309.

215 R. Singh and G. M. Whitesides, *The Journal of Organic Chemistry*, 1991, **56**, 6931–6933.

216 R. Singh and L. Kats, *Analytical Biochemistry*, 1995, **232**, 86–91.

217 M. L. Handel, C. K. W. Watts, A. DeFazio, R. O. Day and R. L. Sutherland, *Proceedings of the National Academy of Sciences*, 1995, **92**, 4497–4501.

218 C.-Y. Shi, Y.-C. Hew and C.-N. Ong, *Human and Experimental Toxicology*, 1995, **14**, 55–60.

219 G. F. Combs and W. P. Gray, *Pharmacology and Therapeutics*, 1998, **79**, 179–192.

220 Y. Chen and W. Maret, *European Journal of Biochemistry*, 2001, **268**, 3346–3353.

221 J. C. Lukesh, B. VanVeller and R. T. Raines, *Angewandte Chemie International Edition*, 2013, **125**, 13139–13142.

222 R. Singh, in *Techniques in Protein Chemistry*, 1996, **7**, 221–230.

223 R. Singh and E. K. Maloney, *Analytical Biochemistry*, 2002, **304**, 147–156.

224 F. F. Schumacher, M. Nobles, C. P. Ryan, M. E. B. Smith, A. Tinker, S. Caddick and J. R. Baker, *Bioconjugate Chemistry*, 2011, **22**, 132–136.

225 K.-L. Wu, C. Yu, C. Lee, C. Zuo, Z. T. Ball and H. Xiao, *Bioconjugate Chemistry*, 2021, **32**, 1947–1959.

226 M. Werner, J. Pampel, T. L. Pham and F. Thomas, *Chemistry - A European Journal*, 2022, **28**, e202201339.

227 R. P. Lyon, T. D. Bovee, S. O. Doronina, P. J. Burke, J. H. Hunter, H. D. Neff-Laford, M. Jonas, M. E. Anderson, J. R. Setter and P. D. Senter, *Nature Biotechnology*, 2015, **33**, 733–735.

228 M. J. Roberts, M. D. Bentley and J. M. Harris, *Advanced Drug Delivery Reviews*, 2012, **64**, 116–127.

229 F. M. Veronese and A. Mero, *BioDrugs*, 2008, **22**, 315–329.

230 E. D. Goddard-Borger and R. V. Stick, *Organic Letters*, 2011, **13**, 2514–2514.

231 W. X. Ren, J. Han, S. Uhm, Y. J. Jang, C. Kang, J. H. Kim and J. S. Kim, *Chemical Communications*, 2015, **51**, 10403–10418.

232 S. Maiti and P. Paira, *European Journal of Medicinal Chemistry*, 2018, **145**, 206–223.

233 A. Maruani, P. A. Szijj, C. Bahou, J. C. F. Nogueira, S. Caddick, J. R. Baker and V. Chudasama, *Bioconjugate Chemistry*, 2020, **31**, 520–529.

234 V. Hong, S. I. Presolski, C. Ma and M. G. Finn, *Angewandte Chemie International Edition*, 2009, **121**, 10063–10067.

235 M. Morais, J. P. M. Nunes, K. Karu, N. Forte, I. Benni, M. E. B. Smith, S. Caddick, V. Chudasama and J. R. Baker, *Organic and Biomolecular Chemistry*, 2017, **15**, 2947–2952.

236 R. W. Chambers, T. Kajiwara and D. R. Kearns, *The Journal of Physical Chemistry A*, 1974, **78**, 380–387.

237 C. Bahou, E. A. Love, S. Leonard, R. J. Spears, A. Maruani, K. Armour, J. R. Baker and V. Chudasama, *Bioconjugate Chemistry*, 2019, **30**, 1048–1054.

238 H. Liu, G. Gaza-Bulseco, C. Chumsae and A. Newby-Kew, *Biotechnology Letters*, 2007, **29**, 1611–1622.

239 L. Ettlinger, R. Corbaz and R. Hütter, *Archives of Microbiology*, 1958, **31**, 326–358.

240 R. Codd, T. Richardson-Sanchez, T. J. Telfer and M. P. Gotsbacher, *ACS Chemical Biology*, 2018, **13**, 11–25.

241 Y. Toporivska and E. Gumienna-Kontecka, *Journal of Inorganic Biochemistry*, 2019, **198**, 110753.

242 D. L. Bailey, D. W. Townsend, P. E. Valk and M. N. Maisey, *Positron emission tomography*, 2005, **2**, 22.

243 M. Farleigh, T. T. Pham, Z. Yu, J. Kim, K. Sunassee, G. Firth, N. Forte, V. Chudasama, J. R. Baker, N. J. Long, C. Rivas and M. T. Ma, *Bioconjugate Chemistry*, 2021, **32**, 1214–1222.

244 M. Morais, N. Forte, V. Chudasama and J. R. Baker, *Bioconjugation*, 2019, **2033**, 15–24.

245 M. Csávás, A. Miskovics, Z. Szűcs, E. Rőth, Z. L. Nagy, I. Bereczki, M. Herczeg, G. Batta, É. Nemes-Nikodém, E. Ostorházi, F. Rozgonyi, A. Borbás and P. Herczegh, *The Journal of Antibiotics*, 2015, **68**, 579–585.

246 F. F. Schumacher, V. A. Sanchania, B. Tolner, Z. V. F. Wright, C. P. Ryan, M. E. B. Smith, J. M. Ward, S. Caddick, C. W. M. Kay, G. Aeppli, K. A. Chester and J. R. Baker, *Scientific Reports*, 2013, **3**, 1525.

247 C. Jacob, W. Maret and B. L. Vallee, *Proceedings of the National Academy of Sciences of the United States of America*, 1999, **96**, 1910–1914.

248 N. Sonoda, A. Ogawa and F. Recupero, *Encyclopedia of Reagents for Organic Synthesis*, 2005, 1–7.

249 D. Kommula, Q. Li, S. Ning, W. Liu, Q. Wang and Z. K. Zhao, *Synthetic Communications*, 2020, **50**, 1026–1034.

250 C. Zhu and J. R. Falck, *Advanced Synthesis and Catalysis*, 2014, **356**, 2395–2410.

251 R. H. Tale, G. K. Toradmal and V. B. Gopula, *RSC Advances*, 2015, **5**, 84910–84919.

252 A. V. Kachanov, O. Yu. Slabko, O. V. Baranova, E. V. Shilova and V. A. Kaminskii, *Tetrahedron Letters*, 2004, **45**, 4461–4463.

253 C. J. Burchell, P. Kilian, A. M. Z. Slawin, J. D. Woollins, K. Tersago, C. Van Alsenoy and F. Blockhuys, *Inorganic Chemistry*, 2006, **45**, 710–716.

254 S. Goswami, A. C. Maity, N. K. Das, D. Sen and S. Maity, *Synthetic Communications*, 2009, **39**, 407–415.

255 F. Challenger, A. T. Peters and J. Halévy, *Journal of the Chemical Society*, 1926, **129**, 1648–1655.

256 E. E. Aynsley, N. N. Greenwood and M. J. Sprague, *Journal of the Chemical Society*, 1965, 2395.

257 D. Plano, Y. Baquedano, D. Moreno-Mateos, M. Font, A. Jiménez-Ruiz, J. A. Palop and C. Sanmartín, *European Journal of Medicinal Chemistry*, 2011, **46**, 3315–3323.

258 Y. Baquedano, E. Moreno, S. Espuelas, P. Nguewa, M. Font, K. J. Gutierrez, A. Jiménez-Ruiz, J. A. Palop and C. Sanmartín, *European Journal of Medicinal Chemistry*, 2014, **74**, 116–123.

259 K. K. Bhasin and J. Singh, *Journal of Organometallic Chemistry*, 2002, **658**, 71–76.

260 M. A. Rizvi, S. Guru, T. Naqvi, M. Kumar, N. Kumbhar, S. Akhoon, S. Banday, S. K. Singh, S. Bhushan, G. Mustafa Peerzada and B. A. Shah, *Bioorganic and Medicinal Chemistry Letters*, 2014, **24**, 3440–3446.

261 D. Singh, A. M. Deobald, L. R. S. Camargo, G. Tabarelli, O. E. D. Rodrigues and A. L. Braga, *Organic Letters*, 2010, **12**, 3288–3291.

262 R. Gu, X. Wang, Z. Yang and S. Han, *Tetrahedron Letters*, 2018, **59**, 2835–2838.

263 F. M. Dannheim, S. J. Walsh, C. T. Orozco, A. H. Hansen, J. D. Bargh, S. E. Jackson, N. J. Bond, J. S. Parker, J. S. Carroll and D. R. Spring, *Chemical Science*, 2022, **13**, 8781–8790.

264 R. Leino and J.-E. Lönnqvist, *Tetrahedron Letters*, 2004, **45**, 8489–8491.

265 J. Košmrlj, M. Kočevar and S. Polanc, *Journal of the Chemical Society - Perkin Transactions 1*, 1998, 3917–3920.

266 M. M. Hashemi, H. Ghafuri and Z. Karimi-Jaberi, *Journal of Sulfur Chemistry*, 2006, **27**, 165–167.

267 A. Megia-Fernandez, B. Mills, C. Michels, S. V. Chankeshwara, N. Krstajić, C. Haslett, K. Dhaliwal and M. Bradley, *Organic and Biomolecular Chemistry*, 2018, **16**, 8056–8063.

268 E. D. Goddard-Borger and R. V. Stick, *Organic Letters*, 2007, **9**, 3797–3800.

269 L. Castañeda, Z. V. F. Wright, C. Marculescu, T. M. Tran, V. Chudasama, A. Maruani, E. A. Hull, J. P. M. Nunes, R. J. Fitzmaurice, M. E. B. Smith, L. H. Jones, S. Caddick and J. R. Baker, *Tetrahedron Letters*, 2013, **54**, 3493–3495.

270 Z. Li, F. Ke, H. Deng, H. Xu, H. Xiang and X. Zhou, *Organic and Biomolecular Chemistry*, 2013, **11**, 2943.

271 F. Yang, W. Wang, K. Li, W. Zhao and X. Dong, *Tetrahedron Letters*, 2017, **58**, 218–222.

272 J. W. Papatzimas, E. Gorobets, R. Maity, M. I. Muniyat, J. L. MacCallum, P. Neri, N. J. Bahlis and D. J. Derksen, *Journal of Medicinal Chemistry*, 2019, **62**, 5522–5540.

273 L. Castañeda, A. Maruani, F. F. Schumacher, E. Miranda, V. Chudasama, K. A. Chester, J. R. Baker, M. E. B. Smith and S. Caddick, *Chemical Communications*, 2013, **49**, 8187–8189.

274 A. Maruani, H. Savoie, F. Bryden, S. Caddick, R. Boyle and V. Chudasama, *Chemical Communications*, 2015, **51**, 15304–15307.

275 F. Bryden, A. Maruani, H. Savoie, V. Chudasama, M. E. B. Smith, S. Caddick and R. W. Boyle, *Bioconjugate Chemistry*, 2014, **25**, 611–617.

276 M. T. W. Lee, A. Maruani, J. R. Baker, S. Caddick and V. Chudasama, *Chemical Science*, 2016, **7**, 799–802.